Studies on Synthesis and Properties of Molecular Assemblies of Ligand-based Mixed-valence Metal Complexes

Ho-Chol Chang

Department of Synthetic Chemistry and Biological Chemistry,

Graduate School of Engineering, Kyoto University

2001

Studies on Synthesis and Properties of Molecular Assemblies of Ligand-based Mixed-valence Metal Complexes

Ho-Chol Chang

Department of Synthetic Chemistry and Biological Chemistry,

Graduate School of Engineering, Kyoto University

2001

Acknowledgment

The presented thesis is the summary of the author's studies from 1996 to 1998 at the Department of Chemistry, Graduate School of Science, Tokyo Metropolitan University and from 1998 to 2000 at the Department of Synthetic Chemistry and Biological Chemistry, Graduate School of Engineering, Kyoto University.

The present work has been conducted under the guidance of Professor Susumu Kitagawa. The author wishes to thank him for his fruitful advice, valuable discussion, and warm-hearted encouragement.

The author is sincerely grateful to Associate Professor Tadashi Mizutani (Kyoto University) and Assistant Professor Mitsuru Kondo (Kyoto University) for their suggestive discussion and encouragement.

The author wishes to express his gratitude to Associate Professor Hiroyuki Matsuzaka (Tokyo Metropolitan University), Associate Professor Satoshi Kawata (Sizuoka University), Assistant Professor Tomohiko Ishi (Tokyo Metropolitan University) for their excellent discussion, useful technical advice, and encouragement. The author is deeply grateful to Assistant Professor Hitoshi Miyasaka (Tokyo Metropolitan University) for his important contribution to the studies of the complexes described in Chapter 6.

The author is also indebted to Dr. Hitoshi Kumagai (University of Strasbourg, France), Assistant Professor Takashi Okubo (Japan Advanced Institute of Science and Technology), and Dr. Yutaka Hitomi (Northwestern University, USA) for their fruitful discussion and encouragement.

The author grateful acknowledges Professor Cortland G. Pierpont (Colorado University, USA) for his helpful discussion about the transition metal *o*-quinone chemistry. The author thanks to Associate Professor Yohji Misaki for the X-ray diffraction measurements. The author wishes to express his gratitude to Professor Motomi Katada (Tokyo Metropolitan University) for the measurement of Mösbauer spectra. The author wishes to thank to Assistant Professors Hiroyuki Nishikawa (Tokyo Metropolitan University) and Dr. Christopher J. Nuttal (Japan Advanced Institute of Science and Technology) collaborating in the electrical conductivity

measurements. The author acknowledges Professor Toshiaki Enoki (Tokyo Institute of Technology) and Assistant Professor Akihiro Otsuka (Kyoto University) for the SQUID measurements. The author is sincerely grateful to the staffs of Department of Chemistry, Tokyo Metropolitan University for the elemental analyses.

The author wishes to thanks to his classmates, Ms. Mayami Hamatani (Toyo Ink Mfg. Co., Ltd.), Ms. Yoko Shimada (Research Institute of System Planning, Inc.), Mr. Hiroshi Tobita (Fujikura), and Mr. Masanori Umeya (Dai Nippon Printing Co., Ltd.) for their valuable discussion, kind experimental supports, and encouragement.

The author wishes to express appreciation to Mr. Shin-ichiro Noro for the thermogravimetric analyses. The author appreciates Mr. Katsunori Mochizuki (Kyoto University) for his contribution to the studies of the complexes described in Chapters 5 and 6. The author is grateful to all of the members of Kitagawa laboratory and to the secretary Mrs. Hiroko Hirohata for doing office works.

The author is grateful to Korean Scholarship for their financial supports from 1997 to 1998. The author also wishes to thanks to Kim Man-Yu Foundation for their financial support in 2000.

The author greatly appreciate to all the Professors of Faculty of Science, Korea University. The author is indebted to the printing office of Korea University for the printing his thesis.

The author wishes to thanks to his grandmother Cyung-Nam Ryu, all relatives, and friends for their continuous encouragement and supports.

Finally, the author wishes to offer special thanks to his parents Byong-Tae Chang and Sang-Jyo Lee and his sisters He-Sung Chang and He-Yong Chang for all their patience, warm-hearted encouragement, and both material and spiritual supports.

Ho-Chol Chang

Department of Synthetic Chemistry and Biological Chemistry,
Graduate School of Engineering, Kyoto University

Kyoto, January 2001

Contents

General Introduction

Transition Metal *o*-Quinone Complexes.

Quinones are an important class of molecules in many disciplines ranging from biophysics to organic chemistry.[1] The main focus of research has been on derivatives of *p*-quinone (i. e. 1,4-benzoquinone) due to their roles as electron acceptors in photosynthetic assemblies as well as their presence in a large number of enzymes and proteins.[2]

In contrast to *p*-quinones, *o*-quinones (i. e. 1,2-benzoquinone) have received far less attention. Although *o*-quinones are not as widespread in biological systems as *p*-quinones, they play a much larger role as ligands in transition metal coordination chemistry.[3] Much of the interest in these molecules stems from their redox activity, providing access three different oxidation states of the ligand. *o*-Quinones may be reduced to semiquinonate (SQ) and catecholate (Cat) by one- and two-electron reduction (Scheme 1), respectively, while remaining bound to metal ion.

Scheme 1

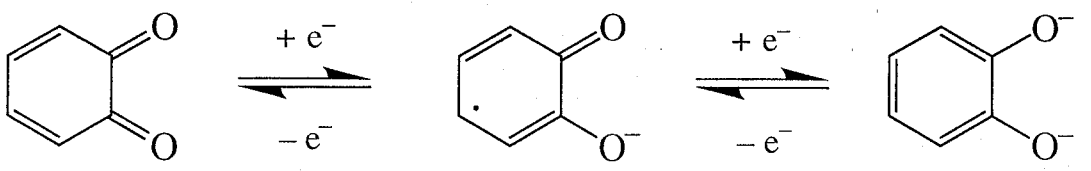

benzoquinone (BQ) $S = 0$ | **semiquinone (SQ)** $S = 1/2$ | **catechol (Cat)** $S = 0$

Transition metal complexes with the *o*-quinone ligands have been the subject of intensive research in the last few decades, and a large number of SQ and Cat complexes of first-, second-, and third-row metals have been synthesized by coordination chemists. Most of fundamental studies on the synthesis and crystal and electronic structures of the complexes have been made by Pierpont and co-workers.[4] They have developed the synthetic methods of the complexes and revealed their characteristic localized electronic structures in contrast to the delocalized electronic structures that have appeared for reduced 1,2-diimine and oxidized 1,2-dithiolene complexes. Charge distribution in the *o*-quinone complexes is related to the balance in energy

between frontier quinone and metal orbitals. In situations where metal *d* orbital energy is high relative to the quinone π^* level, ligands bond as reduced Cat form to an oxidized form of the metal. When metal *d* orbital energy is low, charge resides in metal-localized level with ligands coordinated as partially reduced SQ form.[4(b)]

Valence Tautomerism.

Interestingly, a redox active *o*-quinone ligand coordinated to a redox active metal ion can lead to a molecule that exhibit valence tautomerism, which is one of the most intriguing property of the complexes derived from bistable electronic structures. The concept of valence tautomerism was introduced to define properties of a molecular adduct $A–D^+$ (A = acceptor and D = donor) whose electronic ground state is described by two or more isomers with different charge distribution. The interconversion between different valence tautomers is accomplished by an intramolecular electron transfer according to eq. (1).

$$A–(D^+) \rightleftarrows (A^+)–D \qquad (1)$$

To obatain a molecular adduct which shows valence tautomerism, two conditions must be simultaneusly satisfied: the degree of covalency in the interaction between A and D must be low, and the energy of the frontier orbitals of the two counterparts must be similar. The coexistence of both conditions is hard to achieve, and only *o*-quinone complex exhibits this unusual property. Transition metal complexes of Co,[5] Mn,[6] Fe,[7] Rh, Ir,[8] and Cu[9] with *o*-quinone ligands have been shown to exhibit valence tautomerism. In recent years, especially for heteroleptic cobalt and manganese complexes, M^{III}(SQ)(Cat)(N-N) (N-N = nitrogen chelate ligand), have been studied extensively. For the cobalt complexes, temperature dependent equilibrium shown in Figure 1 was observed between two tautomers, which are related by an intramolecular one-electron transfer between the Cat ligand and the Co(III) ion as well as a spin change low-spin $S = 0 \rightarrow$ high-spin $S = 3/2$ at the cobalt center. In addition, the valence tautomeric conversion was also observed in a polymeric extended system, so-called "bending polymer" $[Co(pz)(3,6\text{-}DTBQ)_2]_n$, where pz is pyrazine.[5(g)] The single crystal of the compoundshows a reversible distortion upon irradiation with tungsten-halogen lamp, which is

(a)

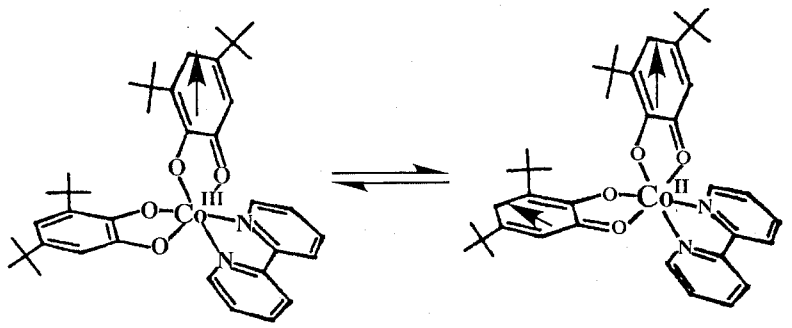

Co^{III}(3,5-DTBSQ)(3,5-DTBCat)(bpy)

Co^{III} (Low Spin, $S = 0$)

$Co^{II}(3,5\text{-DTBSQ})_2(bpy)$

Co^{II} (High Spin, $S = 3/2$)

(b)

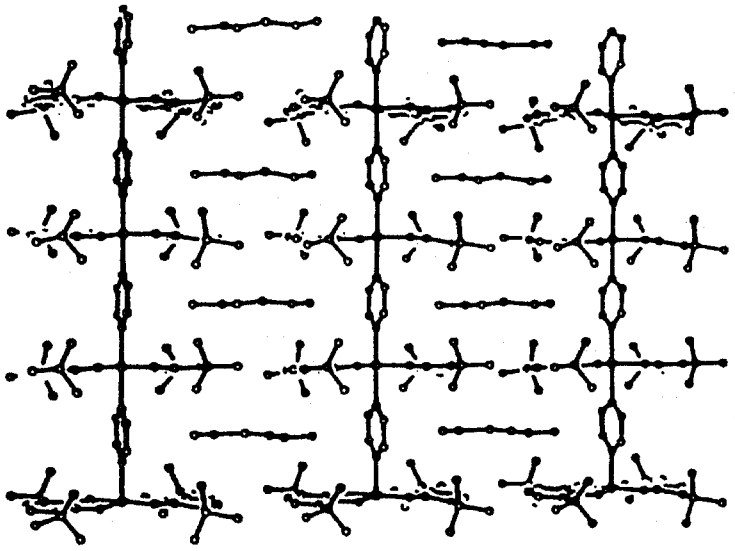

Figure 1. (a) Intramolecular electron transfer process for a valence tautomeric cobalt complex and (b) view of the $[Co(3,6\text{-DTBQ})_2(pz)]_n$ polymer.

caused by the difference of the Co–N bond distances in two tautomers.

Chromium Complexes with *o*-Quinone Ligands.

In contrast to the above mentioned complexes showing the valence tautomerism, few examples have been reported for the chromium complexes. These are listed in Table 1. Although no chromium complexes have been known to show the valence tautomerism, these are classified into another category because of their unusual and unique redox,[4] magnetic,[10(f)] and optical properties[10(b)] that appear to be governed by strong interactions between unpaired electrons localized on the metal center and the ligands. These properties are correlated with the electronic configuration of the Cr^{III} ($d^3(t_{2g}{}^3)$) ion which brings strong electron exchange interaction

Table 1. Previously Reported Mono-, Bis-, and Tris(*o*-quinone) Chromium Complexes

Mono	Bis[e]	Tris
$[Cr^{III}(L^1)(3,6\text{-DTBSQ})]^{2+}$[a]	$Cr^{III}(Cl_4SQ)(Cl_4Cat)(L^3)$	$Cr^{III}(Cl_4SQ)_3$[b,f]
$[Cr^{III}(L^2)(3,5\text{-DTBSQ})]^{2+}$[a,b]	$Cr^{III}(phenSQ)(phenCat)(L^3)$	$Cr^{III}(phenSQ)_3$[g]
$[Cr^{III}(L^1)(3,6\text{-DTBCat})]^{+}$[a]	$Cr^{III}(3,5\text{-DTBSQ})(3,5\text{-DTBCat})(L^3)$	$Cr^{III}(3,5\text{-DTBSQ})_3$[a,h]
$[Cr^{III}(L^2)(Cl_4Cat)]^{+}$[a,b]		$[Cr^{III}(Cat)_3]^{3-}$[d]
$Cr(CO)_3(Cat)$[c]		
$[Cr(CO)_3(3,5\text{-DTBCat})]^{2-}$[d]		

[a] Reference 10(a): 3,5(6)-DTBSQ/Cat = 3,5(6)-di-*tert*-butylsemiquinonate/catecholate, L^1 = tris(2-aminoethyl)amine. [b] Reference 10(b): L^2 = *rac*-5,7,7,12,14,14-hexamethyl-1,4,8,11-tetraazacyclotetradecane: Cl_4SQ/Cat = tetrachlorosemiquinonate/catecholate. [c] Reference 10(c). [d] Reference 10(d). [e] Reference 10(c): L^3 = 2,2'-bipyridine. [f] References 10(f),(g). [g] References 10(h),(i): phenSQ/Cat = 9,10-phenanthrenesemiquinone/catecholate. [h] References 10(h),(j). [i] References 10(k),(l).

between the coordinated SQ and/or Cat ligands through their π orbitals.[10(a),(b),12]

The most characteristic property of the complexes is ligand-based redox activity. Pioneering synthetic work has been carried out on the series of tris(*o*-semiquinonate) chromium complexes by Pierpont et al.. The complexes have synthesized by reaction of $Cr(CO)_6$ with corresponding

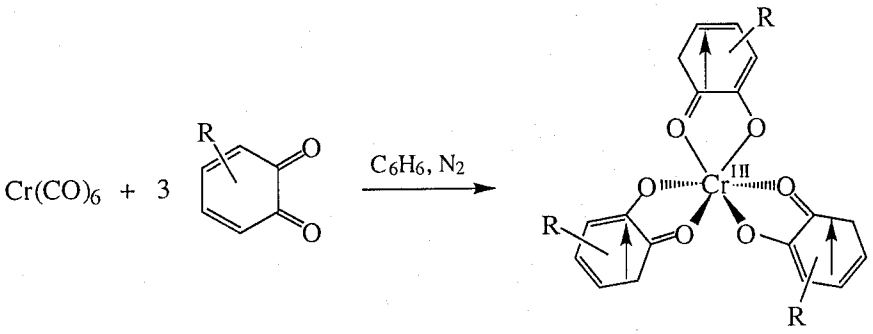

BQ derivatives. Figure 2 illustrates cyclic voltammograms of $Cr^{III}(Cl_4SQ)_3$[10(f),(g)] $Cr^{III}(phenSQ)_3$ (phenSQ = 9,10-phenanthrenesemiquinonate),[10(h),(i),13] and $Cr^{III}(3,5\text{-DTBSQ})_3$ (3,5-DTBSQ = 3,5-di-*tert*-butyl-*o*-semiquinonate).[10(j)] All the complexes undergo both oxidation and reduction reactions to afford seven-membered redox isomers as shown in Scheme 2. The BQ ligands are expected to be poor donors, but kinetic stability of Cr(III) ion allows highly oxidized members of this series exist even in solution, dissimilar to more labile metal ions. It is noteworthy that the chromium ion retains its oxidation state of +3 during the redox process.

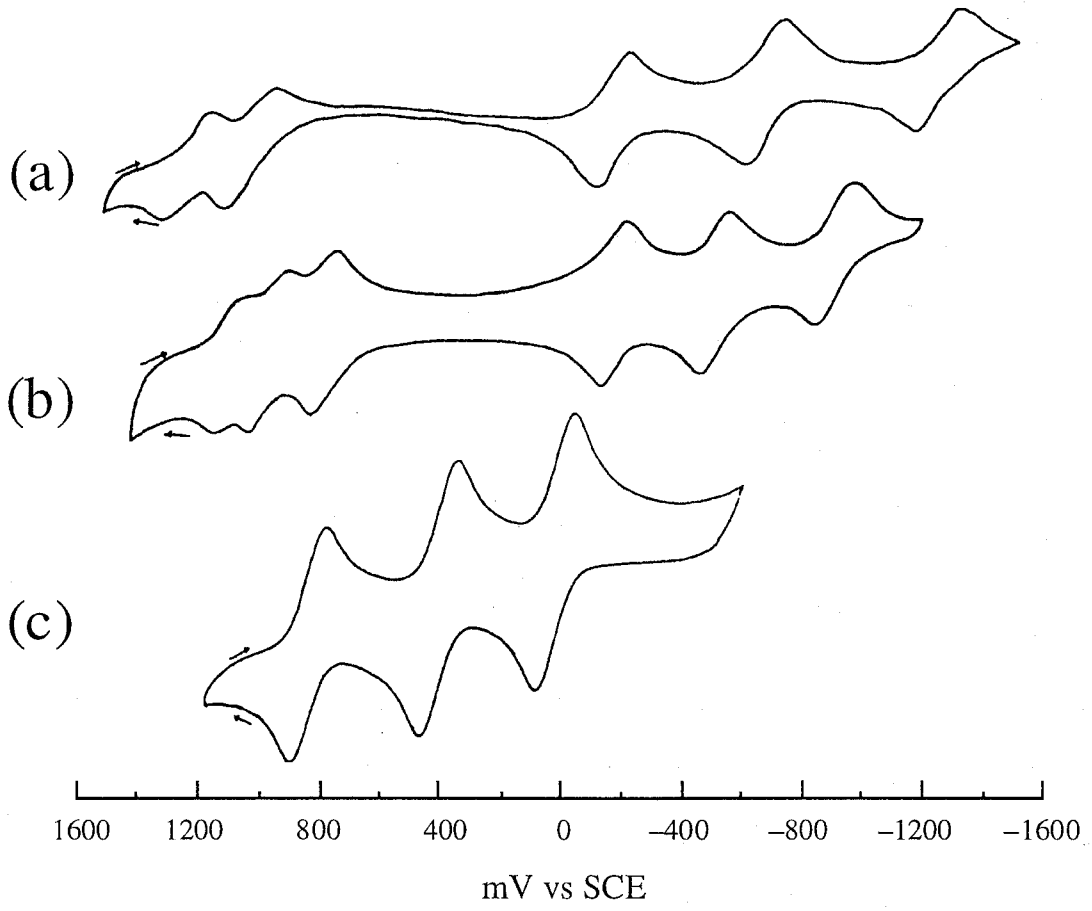

Figure 2. Cyclic voltammograms for (a) $Cr^{III}(3,5\text{-DTBSQ})_3$, (b) $Cr^{III}(phenSQ)_3$, and (c) $Cr^{III}(Cl_4SQ)_3$.

Scheme 2

$$[Cr^{III}(BQ)_3]^{3+} \underset{-e^-}{\overset{+e^-}{\rightleftharpoons}} [Cr^{III}(BQ)_2(SQ)]^{2+} \underset{-e^-}{\overset{+e^-}{\rightleftharpoons}} [Cr^{III}(BQ)(SQ)_2]^{+}$$

$$\underset{-e^-}{\overset{+e^-}{\rightleftharpoons}} \quad Cr^{III}(SQ)_3 \quad \underset{-e^-}{\overset{+e^-}{\rightleftharpoons}}$$

$$[Cr^{III}(SQ)_2(Cat)]^{-} \underset{-e^-}{\overset{+e^-}{\rightleftharpoons}} [Cr^{III}(SQ)(Cat)_2]^{2-} \underset{-e^-}{\overset{+e^-}{\rightleftharpoons}} [Cr^{III}(Cat)_3]^{3-}$$

Mixed-valency on the Ligands.

A large number of complexes with a mixed-valence state on the metal centers have long been used to study electron transfer reactions due to the availability of well-defined complexes with favorable spectroscopic properties. The Creutz-Taube ion, $[(NH_3)_5Ru^{II}(pz)Ru^{III}(NH_3)_5]^{5+}$, that burst on the scene in 1969,[14] and whose physical properties and electronic structure absorbed the energies of an army of theorists and experimentalists for several years. In the decade following the publication describing the Creutz-Taube ion this area of coordination chemistry mushroomed with a large number of complexes being prepared comprising two metal fragments attached to either end of a bridging ligand.[15] On the other hand, to date, extremely little attention to mixed-valence state on the ligand moieties has been paid.

Among the above mentioned seven-membered redox isomers, the structural and physical properties of homoleptic complexes, $Cr^{III}(Cl_4SQ)_3$,[10(f),(g),(i),11,12(a),13,16] $Cr^{III}(3,5\text{-}DTBSQ)_3$,[10(h),(j),11] and $[Cr^{III}(Cat)_3]^{3-}$[10(k),(l)] have been structurally and spectroscopically characterized in detail, whereas the redox isomers, generally written as $[Cr^{III}(SQ)_2(Cat)]^-$ and

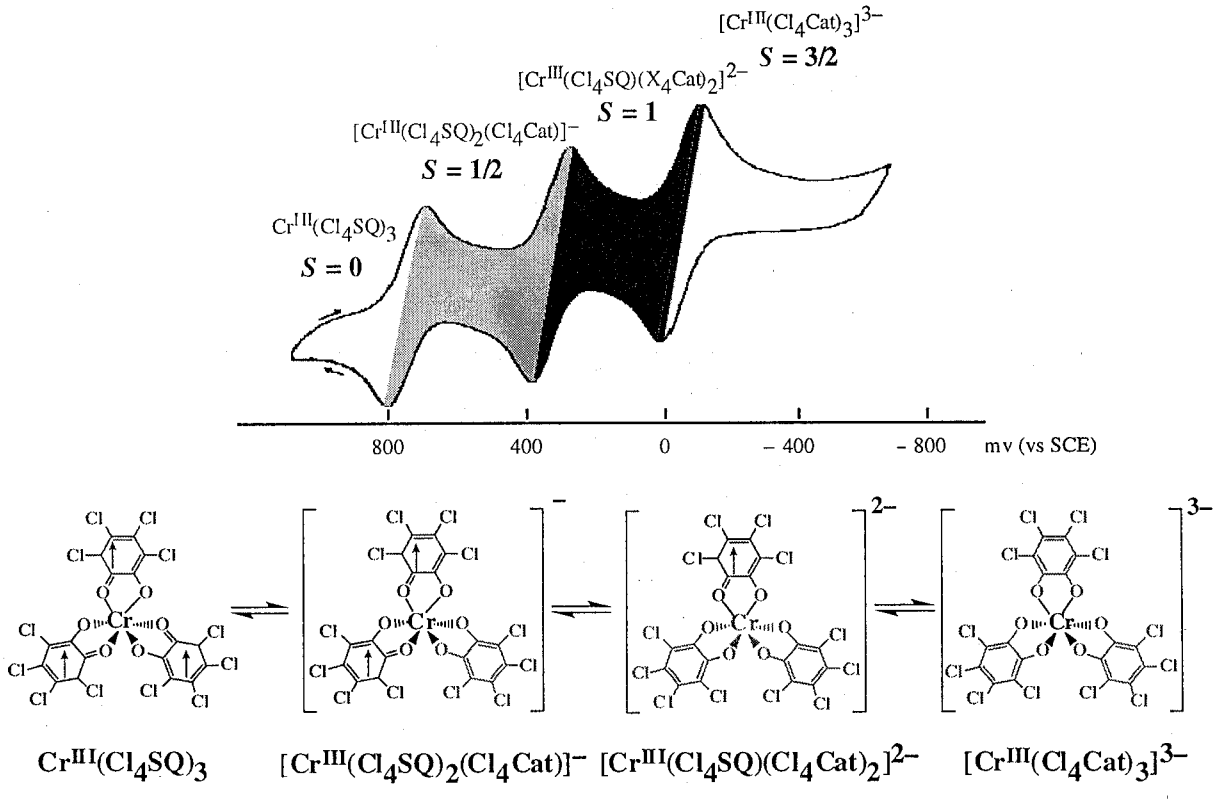

Figure 3. Cyclic voltammogram for $Cr^{III}(Cl_4SQ)_3$ and the corresponding redox isomers.

$[Cr^{III}(SQ)(Cat)_2]^{2-}$, have not been isolated and characterized X-ray crystallographically. These belong to a class of ligand-based mixed-valence complexes with two different ligands linked by a chromium (III) ion.

Of the reported complexes, $Cr^{III}(Cl_4SQ)_3$ shows stepwise ligand-based reductions at extremely high potentials of 0.80, 0.42, and –0.02 V vs SCE (Figure 3). The electron withdrawing effect of the chlorine atoms makes the complex behaves as a strong electron acceptor. Thus, the mixed-valence redox isomers would be isolated by charge-transfer (CT) reaction with reducing reagents. The CT reaction has been utilized for the synthesis of a large number of molecular conductors[17] and magnets[18] derived from the combination of the donor and acceptor molecules.

The Use of Tris(*o*-quinone) Complexes as a Molecular Module toward New Dimension to Supramolecular Assemblies.

Octahedral tris(chelate) transition metal complexes, $[M(L\text{-}L)_3]^m$, have been widely used for the development of supramolecular assemblies. Many of them have been constructed by a spontaneous self-assembly of well-defined molecular modules with coordination bonds.[19] On the other hand, noncovalent $\pi\cdots\pi$ stacking interaction between the planar ligands has been known to serves as another useful means for the construction of one-dimensional chain[20] and two-dimensional layered frameworks.[21]

Two main subjects of the present study arise from the earlier studies on the mixed-valence complexes and supramolecular chemistry described above. At first, the generation of anisotropic environments around the metal ions is one of the intriguing target giving an opportunity to investigate electronic perturbation to the interactions between the molecular modules. In contras to the octahedral modules with a uniform ligand, a ununiformity of the electronic and spin states of the ligands would give a flexibility to the module and intermolecular interactions with the adjacent module when it forms molecular assemblies.

In this context, the class of homoleptic chromium complexes, $Cr^{III}(SQ)_3$, provides a valuable set of the ligand-based mixed-valence redox isomers with alterable oxidation states of the ligands. These electronically non-innocent complexes can afford relevant modules with the

same shape but different charges on the ligand moieties. Consequently, the use of these modules could lead to a construction of new-type molecular mixed-valence assemblies in which intra- and intermolecular SQ···SQ radical type and/or SQ···Cat CT type interactions could be expected. Some of extended arrays of the *o*-quinone complexes have been found, where the direct stacking interaction of the ligand moieties occurs between the adjacent complexes.[22] The physical properties ascribed to the assemblies, however, have not been reported, while the reduced and oxidized forms of metal-free *p*-benzoquinones (BQ) molecules are well-known for their ability to form stacking structures and to give conductive donor-acceptor compounds.[23] The properties arising from the coexistence of the intra- and/or intermolecular CT interactions together with local spins on the metal ions are an intriguing target when the transition metal complexes are utilized.[24]

Secondly, the *o*-quinone complexes have a large potential ability as a trigger for the bi- or metastable molecular assemblies where the assemblies are evolved from a stable state to another stable state in a reversible and detectable fashion in response to controllable external perturbations. In addition to the valence tautomeric complexes, there are several different types of transition metal complexes that exhibit bistability: Jahn-Teller distorted complexes,[25(a)] metal-centered mixed-valence complexes,[25(b)] thermochromic complexes,[25(c)] and spin-crossover complexes.[25(d)] In all the systems listed the complexes could exist in one of two states for the same values of external parameters such as pressure, temperature, electric and magnetic fields. Application of these bistable modules to the molecular assemblies could generate a new field of assembled coordination chemistry, although such molecular- and- crystal engineering has not been established yet.

For the purposes of this thesis, the advantage of using a ligand-based redox active *o*-quinone complex lies in the ability to control the electronic structures of the ligand moieties and physical properties of the assemblies as the trigger based on their bistablity. Thus the main subject of this thesis is focused on the synthesis, crystal structures, and properties of the ligand-based mixed-valence complexes and their molecular assemblies.

Survey of This Thesis

Chapter 1 deals with the preparation and properties of tris(tetrahalogeno-*o*-semiquinonate) chromium (III) complexes, $Cr^{III}(X_4SQ)_3 \cdot 4C_6H_6$ (X = Cl and Br), synthesized by the reaction of $Cr(CO)_6$ with tetrahalogeno-*o*-benzoquinone, X_4BQ (X = Cl and Br) (Scheme 3). Two complexes crystallize in an isostructural form and the X-ray crystal structural and spectroscopic data clearly demonstrated that the ligand moieties coordinate to the chromium ion as paramagnetic SQ form. In the crystal phases, both complexes show strong $\pi \cdots \pi$ interaction between the three SQ ligands and the four solvate benzene molecules, resulting the formation of two-dimensional $\pi \cdots \pi$ stacking array. The effect of the interaction was evaluated by means of thermogravimetric and differential scanning calorimetric analysis. The weigh loss corresponding to the four benzene molecules observed up to near 470 K indicative of strong interactions between the ligand moieties and solvated benzene molecules in the crystal phases.

The complexes show three quasi-reversible redox waves corresponding to the stepwise

Scheme 3

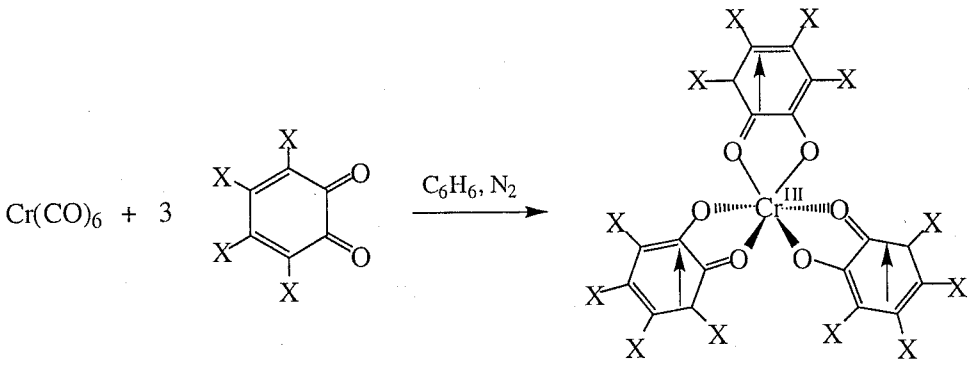

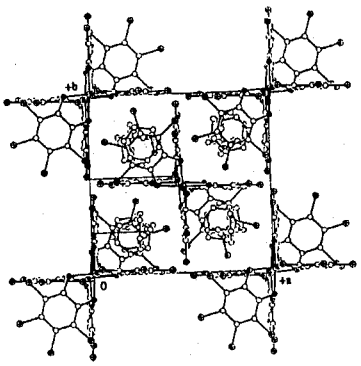

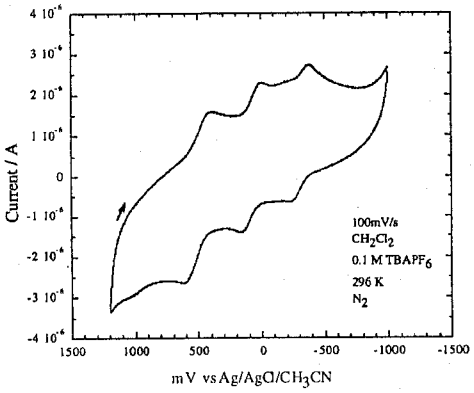

reduction of the SQ ligands to the Cat ligands to give a $[Cr^{III}(X_4SQ)_{3-n}(X_4Cat)_n]^{n-}$ (n = 1–3) redox isomers. The coordination of the paramagnetic SQ ligands was also examined by using SQUID which reveals diamagnetic ground states of the complexes derived from the intramolecular antiferromagnetic interaction between the chromium ion (Cr^{III} d^3, S = 3/2) and three SQ ligands (S = 1/2).

Chapter 2 describes the reaction of $Cr^{III}(X_4SQ)_3$ (X = Cl and Br) with tetrakis(methylsulfanyl)tetrathiafulvalene (TMT-TTF), tetramethyltetraselenafulvalene (TMTSF), and bis(propylenedithio)tetrathiafulvalene (BPDT-TTF) (Scheme 4). Six CT compounds generally written as $(D^{\bullet+})[Cr^{III}(X_4SQ)_2(X_4Cat)]$ ($D^{\bullet+}$ = TMT-TTF$^{\bullet+}$, TMTSF$^{\bullet+}$, and BPDT-TTF$^{\bullet+}$) were synthesized and X-ray crystallographically characterized. The one-electron reduced complexes, $[Cr^{III}(X_4SQ)_2(X_4Cat)]^-$, are commonly formed by cocrystallization with paramagnetic cations. The redox isomers, $[Cr^{III}(X_4SQ)_2(X_4Cat)]^-$, with two SQ and one Cat ligands were firstly isolated and crystallographically characterized. Interestingly, the isomers form one-dimensional chain, two-dimensional brick-wall, and hexagonal honeycomb networks with the aid of intermolecular π···π stacking interactions of the mixed-valence ligand moieties.

Scheme 4

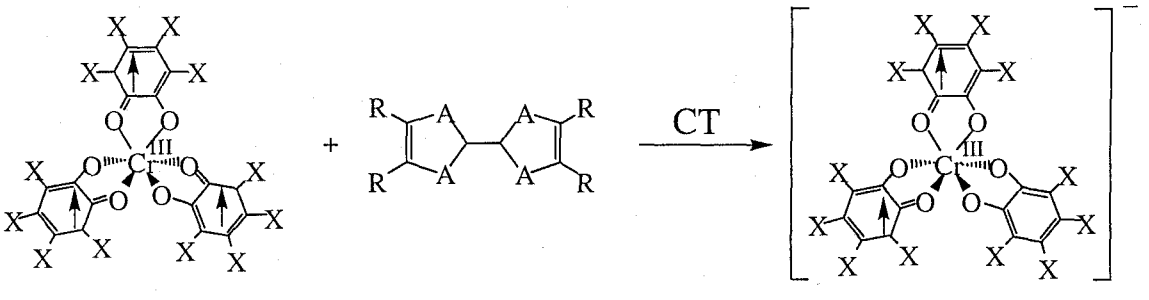

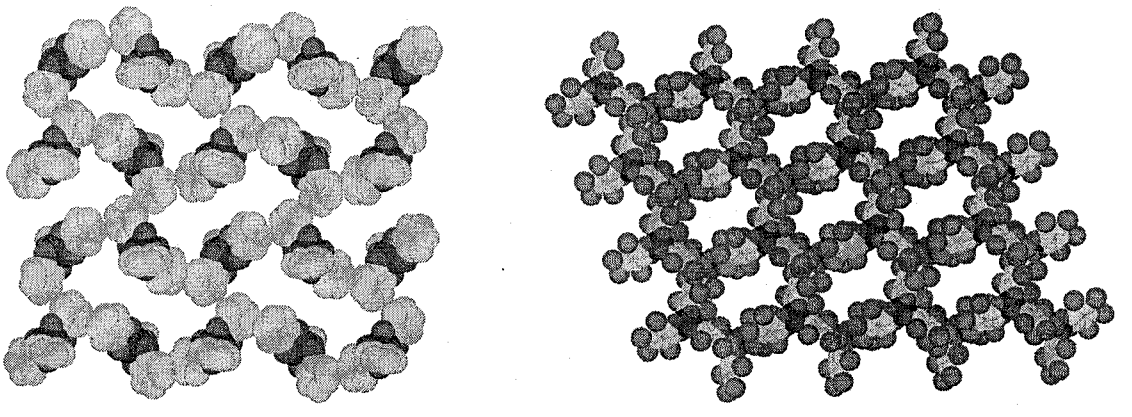

The solid state absorption spectra of the compounds clearly demonstrate the mixed-valence states of the isomers where intramolecular intervalence CT (IVCT) transitions between the SQ and Cat are observed near 4170 cm^{-1}. The temperature dependence of the magnetic susceptibilities reveals that all the $[Cr^{III}(X_4SQ)_2(X_4Cat)]^-$ isomers are in a ground state of S = 1/2, which results from the intramolecular antiferromagnetic interaction between $Cr^{III}(d^3)$ and two SQ ligands. In addition, the compounds have a contribution of the paramagnetic TMT-$TTF^{\bullet+}$, $TMTSF^{\bullet+}$, and BPDT-$TTF^{\bullet+}$ cations, and weak intermolecular magnetic interactions were recognized from the decrease of $\chi_m T$ values at low temperature.

Chapter 3 demonstrates the synthesis, crystal structure, and physicochemical properties of intra- and intermolecular mixed-valence CT compounds, (BEDT-$TTF)_3[Cr^{III}(X_4SQ)_2(X_4Cat)][Cr^{III}(X_4SQ)(X_4Cat)_2]$ (X = Cl and Br), with the paramagnetic BEDT-TTF^+ cations (Scheme 5). The compounds include two kinds of mixed-valence redox isomers, thus, could be described another type of mixed-valence supramolecular assemblies compared with those described in Chapter 2. With the characteristic three-dimensional crystal structure, the compounds show dominant ferromagnetic interaction with semiconducting behaviors. Their characteristic electronic structures and properties will be shown in this Chapter.

Scheme 5

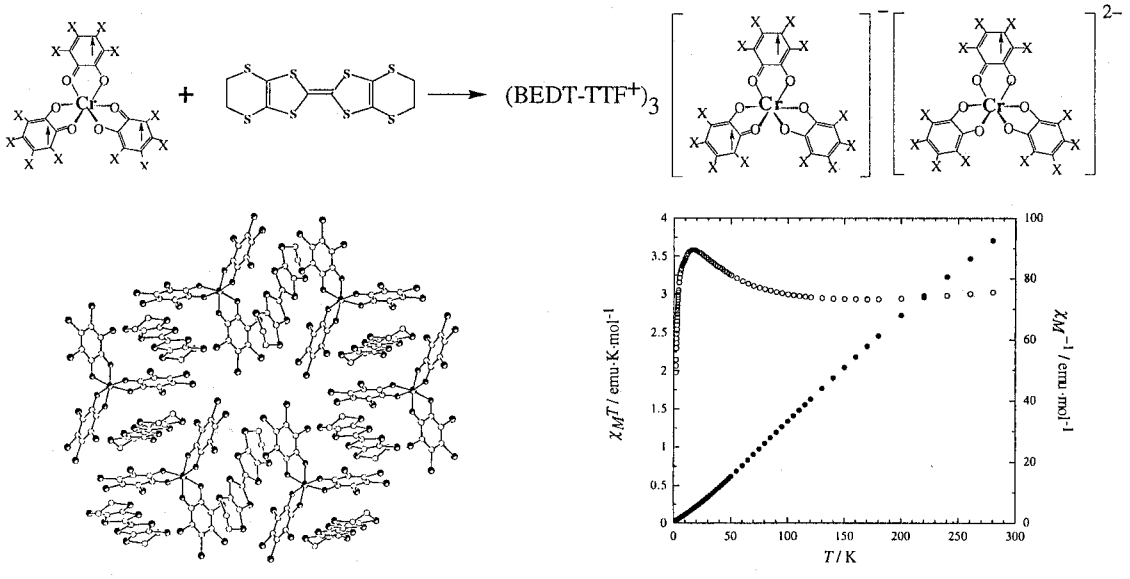

Chapter 4 describes the isolation and the detailed studied on the crystal and spectroscopic properties of the series of $[Cr^{III}(X_4SQ)_{3-n}(X_4Cat)_n]^{n-}$ (n = 0, 1, and 2) isomers with the metallocenium cations, $[M^{III}Cp_2]^+$ (M = Fe and Co) (Scheme 6). The $[Cr^{III}(X_4SQ)(X_4Cat)_2]^{2-}$ isomers have firstly isolated and X-ray crystallographically and spectroscopically characterized both in the solution and in the solid state. The use of metallocenium cation provides an opportunity to investigate not only the correlation between the charged states and assembled structures of $[Cr^{III}(X_4SQ)_{3-n}(X_4Cat)_n]^{n-}$ (n = 0, 1, and 2) isomers but also the quantitative analysis of mixed-valence states in the solution. Interestingly, the intra- and intermolecular mixed-valence states have been found in these compounds. The former could be found in CT compound including $[Cr^{III}(X_4SQ)_{3-n}(X_4Cat)_n]^{n-}$ (n = 1 and 2) isomers, while the latter is realized in $[Fe^{III}Cp_2][Cr^{III}(Cl_4SQ)_2(Cl_4Cat)][Cr^{III}(Cl_4SQ)_3]$ where the two kinds of chromium complexes differing in the oxidation states are involved.

Scheme 6

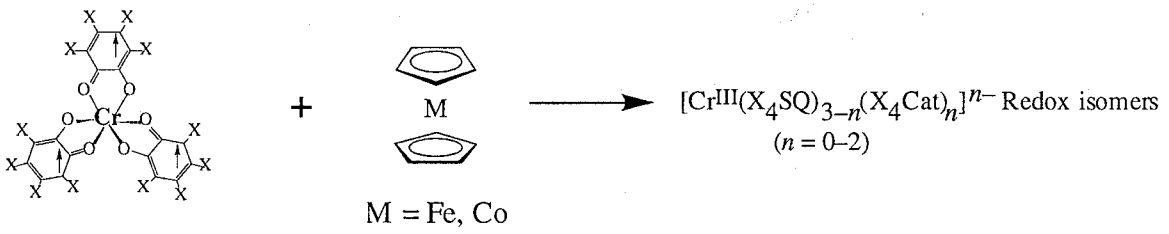

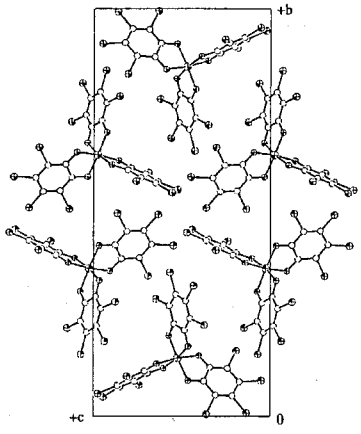

***n* = 2**

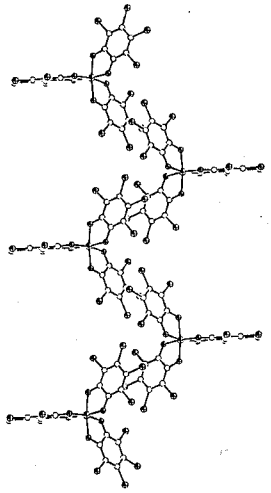

***n* = 1**

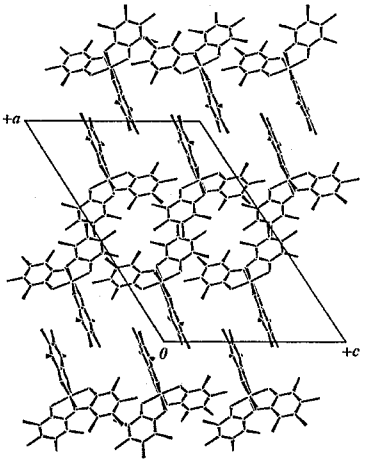

***n* = 1 and 0**

Chapter 5 deals with the synthesis and mixed-valence properties of bis(*o*-quinone) chromium complexes with nitrogen co-ligands; *trans*-$Cr^{III}(X_4SQ)(X_4Cat)(CH_3CN)_2$ and *cis*-$Cr^{III}(X_4SQ)(X_4Cat)(L)$ (L = 2,2'-bipyridine (bpy) and 3,4,7,8-tetramethylphenanthrene (TMphen)) (Scheme 7). X-ray crystal structure analyses reveal that the acetonitrile ligands coordinate to the chromium ion in *trans*-fashion making two *o*-quinone ligands being coplanar. On the other hand, the bpy or TMphen ligand coordinates to the chromium ion in *cis*-fashion so that two *o*-quinone ligands locate in the orthogonal planes. All the compounds show a mixed-valence state on the ligand moieties with two kinds of ligands, SQ and Cat. This is confirmed from the presence of the IVCT transition near 4000 cm^{-1} both in the solution and in the solid state. Thermogravimetric analyses demonstrate that the coordinated acetonitrile ligands can be thermally eliminated up to 520 K. All the complexes show electrochemically quasi-reversible one-electron reduction and oxidation reaction corresponding to $[Cr^{III}(X_4Cat)_2(L)_n]^-$ /$[Cr^{III}(X_4SQ)(X_4Cat)(L)_n]$ and $[Cr^{III}(X_4SQ)(X_4Cat)(L)_n]$/$[Cr^{III}(X_4SQ)_2(L)_n]^+$ couples. The temperature dependence of magnetic susceptibilities demonstrates a ground state of $S = 1$ for all the complexes, which resulting from the intramolecular antiferromagnetic interaction between the Cr^{III}(d^3, $S = 3/2$) ion and the X_4SQ ($S = 1/2$) ligand. The conversion of $Cr^{III}(X_4SQ)_3$ to the bis(*o*-quinone) complexes in the polar solvents could be explained by assuming the formation of $Cr^{III}(X_4BQ)(X_4SQ)(X_4Cat)$ complex as intermediate species. This implies a solvent-induced valence tautomeric conversion of $Cr^{III}(X_4SQ)_3$ to $Cr^{III}(X_4BQ)(X_4SQ)(X_4Cat)$. The first observation of the valence tautomerism for the chromium complexes was made.

Scheme 7

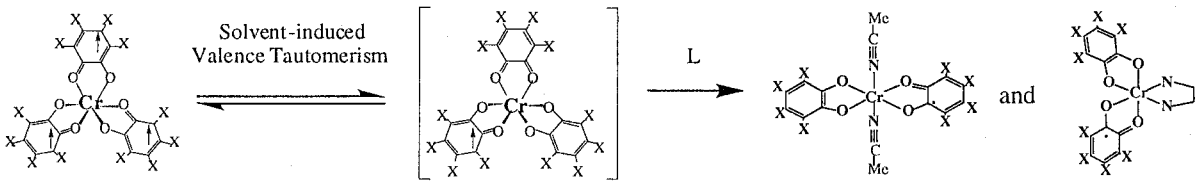

$[Cr^{III}(X_4BQ)(X_4SQ)(X_4Cat)]$ *trans*- and *cis*-$Cr^{III}(X_4SQ)(X_4Cat)(L)_n$

Chapter 6 demonstrates the synthesis, crystal structures, and physicochemical properties of homo- and mixed-valence diruthenium complexes with tetrachlorocatecholates, $[(Cl_4Cat)_2Ru^{n+}(\mu\text{-}OR)_2Ru^{n+}(Cl_4Cat)_2]^{m-}$ (n = 3 or 3.5; m = 4 or 3; R = CH_3 or C_2H_5; Cl_4Cat = tetrachlorocatecholate) (Scheme 8). Na^+/Crown ether or Ph_4P^+ cation promote the selective isolation of several compounds, including the compound with an infinite link of the ruthenium units with the aid of hydrogen bonds.

Scheme 8

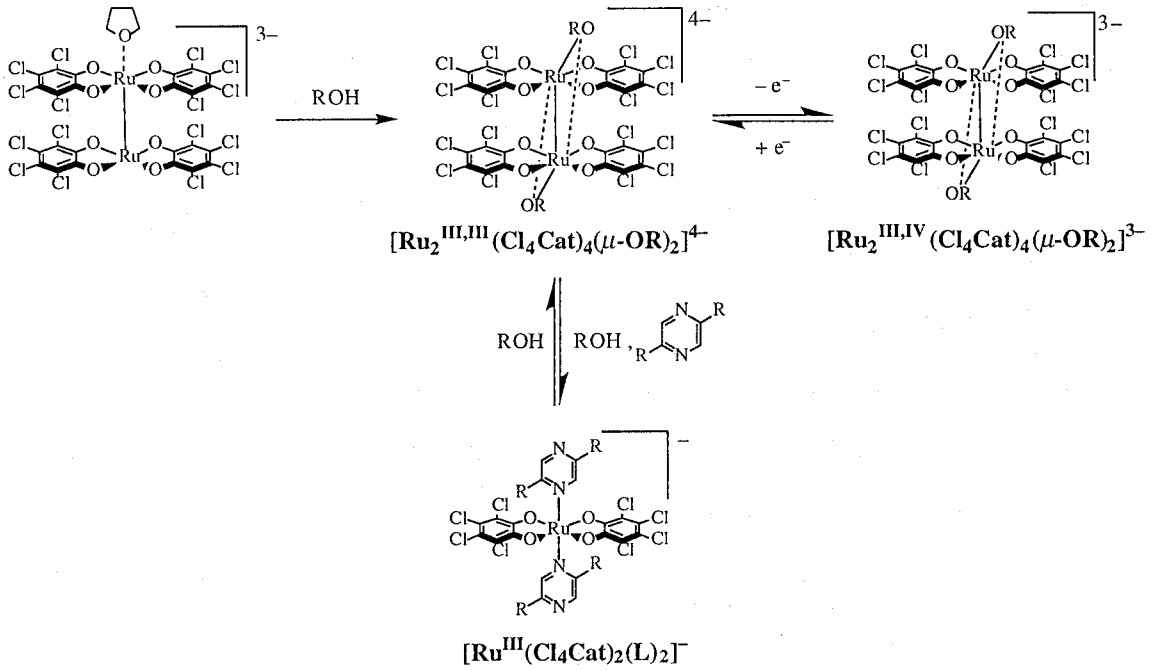

References

(1) Patai, S. *The Chemistry of the Quinoid Compounds, Parts 1 and 2*; Wiley: New York, 1974.

(2) (a) Trumpower, B. L. *Functions of Quinones in Energy Converting Systems*; Academic Press: New York, 1982. (b) Okumura, M. Y.; Feher, G. *Annu. Rev. Biochem.* **1992**, *61*, 881. (c) Klinman, J. P.; David, M. *Annu. Rev. Biochem.* **1994**, *63*, 299.

(3) Thompson, R. H. *Naturally Occurring Quinones, 2nd edn.*; Academic Press: New York, 1971.

(4) (a) Pierpont, C. G.; Buchanan, R. M. *Coord. Chem. Rev.* **1981**, *38*, 45. (b) Pierpont, C. G.; Lange, C. W. *Prog. Inorg. Chem.* **1994**, *41*, 381.

(5) (a) Buchanan, R. M.; Pierpont, C. G. *J. Am. Chem. Soc.* **1980**, *102*, 4951. (b) Adams, D. M.; Dei, A.; Rheingold, A. L.; Hendrickson, D. N. *J. Am. Chem. Soc.* **1993**, *115*, 8221. (c) Adams, D. M.; Hendrickson, D. N. *J. Am. Chem. Soc.* **1996**, *118*, 11515. (d) Adams, D. M.; Noodleman, L.; Hendrickson, D. N. *Inorg. Chem.* **1997**, *36*, 3966. (e) Abakumov, G. A.; Cherkasov, V. K.; Bubnov, M. P.; Ellert, O. G.; Dobrokhotova, Z. B.; Zakharov, L. N.; Struchkov, Y. T. *Dokl. Chem. (Engl. Transl.)* **1993**, *328*, 12. (f) Jung, O. -S.; Pierpont, C. G. *Inorg. Chem.* **1994**, *33*, 2227. (g) Jung, O. -S.; Pierpont, C. G. *J. Am. Chem. Soc.* **1994**, *116*, 2229.

(6) (a) Lynch, M. W.; Hendrickson, D. N.; Fitzgerald, B. J.; Pierpont, C. G. *J. Am. Chem. Soc.* **1984**, *106*, 2041. (b) Attia, A. S.; Pierpont, C. G. *Inorg. Chem.* **1995**, *34*, 1172.

(7) (a) Lynch, M. W.; Valentine, M.; Hendrickson, D. N. *J. Am. Chem. Soc.* **1982**, *104*, 6982. (b) Attia, A. S.; Bhattacharya, S.; Pierpont, C. G. *Inorg. Chem.* **1995**, *34*, 4427. (c) Attia, A. S.; Jung, O. -S.; Pierpont, C. G. *Inorg. Chim. Acta* **1994**, *226*, 91.

(8) (a) Abakumov, G. A.; Razuvaev, G. A.; Nevodchikov, V. I.; Cherkasov, V. K. *J. Organomet. Chem.* **1988**, *341*, 485. (b) Abakumov, G. A.; Nevodchikov, V. I.; Cherkasov, V. K. *Dokl. Chem. (Engl. Transl.)* **1985**, 814. (c) Lange, C. W.; Foldeaki, M.; Nevodchikov, V. I.; Cherkasov, V. K.; Abakumov, G. A.; Pierpont, C. G. *J. Am. Chem. Soc.* **1992**, *114*, 4220.

(9) Hendrickson, D. N.; Adams, D. M.; Wu, C. C. *Magnetism: Supramolecular Function*; Kluwer Publishing Co.: The Netherlands.

(11) Downs, H. H.; Buchanan, R. M.; Pierpont, C. G. *Inorg. Chem.* **1979**, *18*, 1736.

(10) (a) Wheeler, D. E.; McCusker, J. K. *Inorg. Chem.* **1998**, *37*, 2296. (b) Benelli, C.; Dei, A.; Gatteschi, D.; Güdel, H. U.; Pardi, D. *Inorg. Chem.* **1989**, *28*, 3089. (c) Darensbourg, D. J.; Klausmeyer, K. K.; Reibenspies, J. H. *Inorg. Chem.* **1996**, *35*, 1529. (d) Darensbourg, D. J.; Klausmeyer, K. K.; Reibenspies, J. H. *Inorg. Chem.* **1995**, *34*, 4676. (e) Buchanan, R. M.; Claflin, J.; Pierpont, C. G. *Inorg. Chem.* **1983**, *22*, 2552. (f) Pierpont, C. G.; Downs, H. H. *J. Am. Chem. Soc.* **1976**, *98*, 4834. (g) Pierpont, C. G.; Downs, H. H.; Rukavina, T. G. *J. Am. Chem. Soc.* **1974**, *96*, 5573. (h) Lobanov, A. V.; Abakumov, G. A.; Razuvaeve, G. A. *Proc. Acad. Sci. USSR (Engl. Transl.)* **1977**, 441. (i) Buchanan, R. M.; Downs, H. H.; Shorthill, W. B.; Pierpont, C. G.; Kessel, S. L.; Hendrickson, D. N. *J. Am. Chem. Soc.* **1978**, *100*, 4318. (j) Sofen, S. R.; Ware, D. C.; Cooper, S. R.; Raymond, K. N. *Inorg. Chem.* **1979**, *18*, 234. (k) Raymond, K. N.; Isied, S. S.; Brown, L. D.; Fronczek, F. R.; Nibert, J. H. *J. Am. Chem. Soc.* **1976**, *98*, 1767. (l) Isied, S. S.; Kuo, G.; Raymond, K. N. *J. Am. Chem. Soc.* **1976**, *98*, 1763.

(12) (a) Lynch, M. W.; Buchanan, R. M.; Pierpont, C. G.; Hendrickson, D. N. *Inorg. Chem.* **1981**, *20*, 1038. (b) Rodrigues, J. H.; Wheeler, D. E.; McCusker, J. K. *J. Am. Chem. Soc.* **1998**, *120*, 12051.

(13) Buchanan, R. M.; Kessel, S. L.; Downs, H. H.; Pierpont, C. G.; Hendrickson, D. N. *J. Am. Chem. Soc.* **1978**, *100*, 7894.

(14) Creutz, C.; Taube, H. *J. Am. Chem. Soc.* **1969**, *91*, 3988.

(15) (a) Robin, M. B.; Day, P. *Adv. Inog. Chem. Radiochem.* **1967**, *10*, 247. (b) Hush, N. S. *Coord. Chem. Rev.* **1985**, *64*, 135. (c) Richardson, D. E.; Taube, H. *Coord. Chem. Rev.* **1984**, *60*, 107. (d) Creutz, C. *Prog. Inorg. Chem.* **1983**, *30*, 1. (e) Kalyanasundaram, K.; Nazzeruddin, M. K. *Inorg. Chim. Acta* **1994**, *226*, 213. (f) Woitellier, S.; Launay, J.-P.; Spangler, C. W. *Inorg. Chem.* **1989**, *28*, 758. (g) Ribou, A.-C.; Launay, J.-P.; Takahashi, K.; Nihira, T.; Tarutani, S.; Spangler, C. W. **1994**, *33*, 1325. (h) Reimers, J. R.; Hush, N. S. **1990**, *29*, 3990. (i) Ward, M. D. *Chem. Soc. Rev.* **1995**, 121.

(16) (a) Vléck, J., A. *J. Organomet. Chem.* **1986**, *306*, 63. (b) Vlckova, B.; Snoeck, T. L.; Stufkens, D. J. *J. Mol. Struct.* **1990**, *218*, 7.

(17) (a) Akamatsu, H.; Inokuchi, H.; Matsunaga, Y. *Nature* **1954**, *173*, 168. (b) Acker, D. S.; Harder, R. J.; Hertler, W. R.; Mahler, W.; Melby, L. R.; Benson, R. E.; Mochel, W.-E. *J. Am. Chem. Soc.* **1960**, *95*, 948. (c) Ferraris, J.; Cowan, D. O.; Walatka, V. Jr.; H., Perlstein, J. H. *J. Am. Chem. Soc.* **1973**, *95*, 948. (d) Jerome, J.; Mozaud, A.; Ribault, M.; Bechgaard, K. *J. Phys. Lett.* **1980**, *41*, L95. (e) Williams, J. M.; Kini, A. M.; Wang, H. H.; Carlson, K. D.; Geiser, U.; Montgomery, L. K.; Phyka, G. J.; Watkins, D. M.; Kommers, J. M.; Boryschunk, S. J.; Crouch, A. V. S.; Kwok, W. K.; Chirber, J. E.; Overmyer, D. L.; Jung, D.; Whangbo, M.-H. *Inorg. Chem.* **1990**, *29*, 3272.

(18) (a) Candela, G. A.; Swartzendruber, L.; Miller, J. S.; Rice, M. J. *J. Am. Chem. Soc.* **1979**, *101*, 2755. (b) Miller, J. S.; Zhang, J. H.; Reiff, W. M.; Preston, L. D.; Reis, A. H.; Gerbert, J. E.; Extine, M.; Troup, J.; Ward, M. D. **1987**, *91*, 4344. (c) Miller, J. S.; Epstein, A. J. *Angew. Chem. Int. Ed. Engl.* **1994**, *33*, 385. (d) Miller, J. S.; Epstein, A. J.; Reiff, W. M. *Chem. Rev.* **1988**, *88*, 201.

(19) (a) Fyfe, M. C. T.; Stoddart, J. F. *Acc. Chem. Res.* **1997**, *30*, 393. (b) Simard, M.; Wuest, J. D. *J. Am. Chem. Soc.*, *113*, 4696. (c) Hanan, G. S.; Volkmer, D.; Schubert, U. S.; Lehn, J. -M.; Baum, G.; Fenske, D. *Angew. Chem., Int. Ed. Engl.* **1997**, *36*, 1842. (d) Waldmann, O.; Hassmann, J.; Müller, P.; Hanan, G. S.; Volkmer, D.; Schubert, U. S.; Lehn, J. -M. *Phys. Rev. Lett.* **1997**, *79*, 3390. (e) Rojo, J.; Lehn, J. -M.; Baum, G.; Fenske, D.; Waldmann, O.; Müller, P. *Eur. J. Inorg. Chem.* **1999**, 517. (f) Waldemann, O.; Hassmann, J.; Müller, P.; Volkmer, D.; Schubert, U. S.; Lehn, J. -M. *Phys. Rev. B Cond. Matter* **1998**, *58*, 3277. (g) Hasenknopf, B.; Lehn, J. -M.; Boumediene, N.; Dupont-Gervais, A.; van Dorsselaer, A.; Kneisel, B.; Fenske, D. *J. Am. Chem. Soc.* **1997**, *119*, 10956. (h) Swiegers, G.; Malefetse, T. J. *Chem. Rev.* **2000**, *100*, 3483.

(20) (a) Dance, I. G.; Scudder, M. L. *J. Chem. Soc., Dalton Trans.* **1998**, 1341. (b) Lewis, G.; Dance, I. *J. Chem. Soc., Dalton Trans.* **2000**, 3176.

(21) (a) Scudder, M. L.; Goodwin, H. A.; Dance, I. G. *New J. Chem.* **1999**, *23*, 695. (b) Breu, J.; Domel, H.; Stoll, A. *Eur. J. Inorg. Chem.* **2000**, 2401. (c) Breu, J.; Domel, H.;

Norrby, P. *Eur. J. Inorg. Chem.* **2000**, 2409.

(22) (a) Pierpont, C. G.; Buchanan, R. M. *J. Am. Chem. Soc.* **1975**, *97*, 6450. (b) Simpson, C. L.; Pierpont, C. G. *Inorg. Chem.* **1992**, *31*, 4308. (c) Pierpont, C. G.; Buchanan, R. M. *J. Am. Chem. Soc.* **1975**, *97*, 4912.

(23) (a) Mayerle, J. J.; Torrance, J. B. *Acta Crystallogr., Sec. B* **1981**, *B37*, 2030. (b) Nakasuji, K.; Sasaki, M.; Kotani, T.; Murata, I.; Enoki, T.; Imaeda, K.; Inokuchi, H.; Kawamoto, A.; Tanaka, J. *J. Am. Chem. Soc.* **1987**, *109*, 6970.

(24) (a) Ogawa, M. Y.; Martinsen, J.; Palmer, S. M.; Stanton, J. L.; Tanaka, J.; Greene, R. L.; Hoffman, B. M.; Ibers, J. A. *J. Am. Chem. Soc.* **1987**, *109*, 1115. (b) Kurmoo, M.; Graham, A. W.; Day, P.; Coles, S. J.; Hurstouse, M. B.; Caulfield, J. L.; Singleton, J.; Pratt, F. L.; Hayes, W.; Ducasse, L.; Guinneau, P. *J. Am. Chem. Soc.* **1995**, *117*, 12209. (c) Day, P.; Kurmoo, M.; Mallah, T.; Marsden, R.; Triend, R. H.; Pratt, F. L.; Hayes, W.; Chasseau, J.; Bravic, G.; Ducasse, L. *J. Am. Chem. Soc.* **1992**, *114*, 10722. (d) Kobayashi, A.; Udagawa, T.; Tomita, H.; Naito, T.; Kobayashi, H. *Chem. Lett.* **1993**, 1993. (e) Kobayashi, H.; Tomita, H.; Naito, T.; Kobayashi, A.; Sakai, F.; Watanabe, T.; Cassoux, P. *J. Am. Chem. Soc.* **1996**, *118*, 368.

(25) (a) Bersuker, I. B.; Polinger, V. Z. *Vibronic Interactions in Molecules and Crystals*; Springer-Verlag: Berlin, 1989. (b) *Mixed-Valency System: Applications in Chemistry, Physics, and Biology: NATO ASI Series C: Mathematical and Physical Sciences*; Kliwer Academic: Dordrecht, 1991; Vol. 343. (c) Sone, K.; Fukuda, Y. *Inorganic Thermochromism*; Springer-Verlag: Berlin, 1987. (d) Gütlich, P.; Hauser, A.; Spiering, H. *Angew. Chem., Int. Ed. Engl.* **1994**, *33*, 2024.

Chapter 1

Synthesis, X-ray Crystal Structures, and Physical Properties of Tris(tetrahalogeno-*o*-semiquinonate) Chromium (III) Complexes, $Cr^{III}(X_4SQ)_3 \cdot 4C_6H_6$ (X = Cl and Br)

Abstract

Thermal reaction of $Cr(CO)_6$ with tetrahalogeno-*o*-benzoquinone, X_4BQ (X = Cl and Br), affords tris(tetrahalogeno-*o*-semiquinonate) chromium (III) complexes,

$Cr^{III}(Cl_4SQ)_3 \cdot 4C_6H_6$ (**1**)
$Cr^{III}(Br_4SQ)_3 \cdot 4C_6H_6$ (**2**)

Two complexes crystallize in an isostructural form; tetragonal, space group $P4_12_12$ with a = 13.452(2) Å, c = 24.78(2) Å, V = 4484(3) Å^3 and a = 13.7465 (7) Å, c = 25.680 (1) Å, V = 4852.6(4) Å^3 for **1** and **2**, respectively. The X-ray crystal structural and spectroscopic data clearly demonstrated that the ligand moieties coordinate to the chromium ion as paramagnetic SQ form both in **1** and **2**. The inner coordination environments of the complex molecules are similar to those of previously reported crystal, $Cr^{III}(Cl_4SQ)_3 \cdot CS_2 \cdot 1/2C_6H_6$, while both complexes show strong $\pi \cdots \pi$ interaction between the three SQ ligands and the four solvate benzene molecules, resulting the formation of two-dimensional $\pi \cdots \pi$ stacking array. The separations between the ligands and benzene molecules are found to be 3.36(1) and 3.61(2) Å for two kinds of stacks. The effect of $\pi \cdots \pi$ interactions was evaluated by thermogravimetric and differential scanning calorimetric analysis where the weigh loss corresponding to the four benzene molecules observed up to near 470 K indicative of strong interactions between the ligand moieties and solvated benzene molecules in the crystal phases.

The complexes show three quasi-reversible redox waves near 510, 100, and –300 mV vs Ag/AgCl/CH_3CN, which are attributable to the stepwise reduction of the SQ ligands to the Cat ligands. The coordination of the paramagnetic SQ ligands was also examined by using SQUID and diamagnetic ground states derived from the intramolecular antiferromagnetic interaction between the chromium ion (Cr^{III} d^3, S = 3/2) and three SQ ligands (S = 1/2) were examined.

Introduction

The chemistry and physical properties of complexes containing "non-innocent" ligands have attracted considerable interest. The most widely encountered class of these molecules are the quinoids whose "non-innocent" nature rests largely in their reversible redox chemistry: A large number of semiquinonate (SQ) and catecholate (Cat) complexes of first-, second-, and third-row metals are known to date.[1]

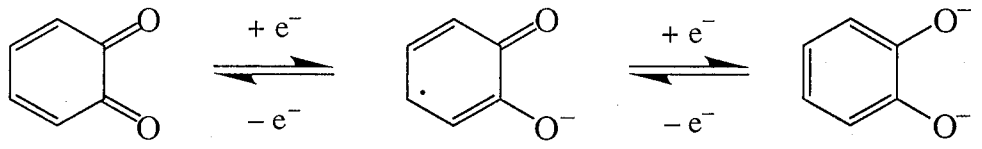

benzoquinone (BQ) **semiquinone (SQ)** **catechol (Cat)**

$S = 0$ $S = 1/2$ $S = 0$

Among them, chromium complexes with paramagnetic SQ ligands are of particular interest because these show unusual and unique redox,[2] magnetic,[3] and optical properties[4] that appear to be governed by strong interactions between the unpaired electrons and the corresponding spins localized on the metal center and the ligands.

Tris(tetrachloro-*o*-semiquinonate) chromium (III), $Cr^{III}(Cl_4SQ)_3 \cdot 4C_6H_6$, has been thermally synthesized by the reaction of $Cr(CO)_6$ with tetrachloro-*o*-benzoquinone (Cl_4BQ) in benzene for the first time by Pierpont et al. in 1974.[5] They have also reported the electro- and magnetochemical properties of the complex together with the crystal structure of $Cr^{III}(Cl_4SQ)_3 \cdot CS_2 \cdot 1/2C_6H_6$. In fact, the complex was obtained as $Cr^{III}(Cl_4SQ)_3 \cdot 4C_6H_6$ with four solvated benzene molecules under the synthetic condition they used,[2,3,6] however, only the cell dimension and space group are known to date.[7] There are some of complexes cocrystallized with aromatic solvates exhibiting $\pi \cdots \pi$ stacking interactions with the ligand moieties of the complexes.[8,9] The interaction could involve net charge-transfer (CT) between the donor and acceptor molecules, which often plays an important role in molecular-based conducting materials.

Although the thermal synthesis of the complex was reported by Pierpont et al., in 1982, Vlcek et al. pointed out the reproducibility of the synthesis under the reported condition. Furthermore, they have demonstrated that the complex could be successfully synthesized by photochemical synthesis,[10] and successful synthesis has been carried out by irradiation of mercury-arc light to the mixture of $Cr(CO)_6$ and Cl_4BQ for two hours (60–70 % yield).

In this Chapter, to begin with, the thermal synthesis of the complexes has been reinvestigated with two tetrahalogeno-*o*-benzoquinone derivatives, Cl_4BQ and Br_4BQ. In addition, the crystal phases of $Cr^{III}(X_4SQ)_3 \cdot 4C_6H_6$ have been determined by single crystal X-ray crystal analyses for the first time. Finally, the substituent effects on the crystal structure and physical properties of complexes have been studied to collect the fundamental data for the synthesis of novel molecular assemblies derived from $Cr^{III}(X_4SQ)_3 \cdot 4C_6H_6$.

Experimental Section

Materials.

All chemicals were reagent grade. $Cr(CO)_6$, Cl_4BQ, and Br_4BQ were obtained from Aldrich. Syntheses of complexes were carried out under a dry nitrogen atmosphere by use of standard Schlenk techniques with freshly distilled solvents.

Preparation of the Complexes.

$Cr^{III}(Cl_4SQ)_3 \cdot 4C_6H_6$ (1) A 150 ml benzene suspension containing $Cr(CO)_6$ (4.550 g, 20.70 mmol) and Cl_4BQ (25.425 g, 103.4 mmol) was refluxed for seventeen days under a nitrogen atmosphere. The microcrystals were washed with cold benzene several times, then dried under vacuum. Yield 12.894 g (43 %). Found: C, 45.48; H, 2.05. $C_{42}H_{24}O_6Cl_{12}Cr$ requires C, 45.77, H, 2.19. Single crystals were obtained by recrystallization from hot benzene/dichloromethane. Violet prismatic crystal was obtained and used for X-ray diffraction experiments. IR (KBr): 3085w, 3066w, 3030w, 1475m, 1460s, 1447s, 1416w, 1384w, 1343m, 1277m, 1252w, 1219s, 1034w, 1014w, 993s, 822s, 805s, 693m, 678s, 579w, 542w, 533w, 516w, 505w, 490w, 458w, 432w, and 401w cm^{-1}.

$Cr^{III}(Br_4SQ)_3 \cdot 4C_6H_6$ (2) The complex was prepared by a similar procedure to that for **1**. A 100 ml benzene suspension containing $Cr(CO)_6$ (1.01 g, 4.59 mmol) and Br_4BQ (9.75 g, 23.0 mmol) was refluxed for three days under a nitrogen atmosphere. The suspension was filtered, and the powder obtained washed with benzene several times. Yield 7.03 g (94%). Found: C, 30.61; H, 1.47. $C_{42}H_{24}Br_{12}CrO_6$ requires C, 30.84; H, 1.48. Single crystals were obtained by recrystallization from hot benzene/dichloromethane. Violet prismatic crystal was obtained and used for X-ray diffraction experiments. IR (KBr): 3083w, 3064w, 3027w, 1475m, 1454s, 1433s, 1394w, 1329w, 1255m, 1178m, 1033w, 937m, 754m, 679s, 623w, 561w, and 526w cm^{-1}.

Physical Measurements.

Infrared spectra for KBr pellets were recorded on a Perkin-Elmer system 2000 FT-IR spectrometer over the range of 350–7000 cm^{-1} and absorption spectra on a Hitachi U-3500 spectrophotometer over the range of 3130–33000 cm^{-1} at 296 K. Electrochemical

measurements were carried out by a BAS CV-50W polarographic analyzer. A standard three-electrode system was used with a glassy carbon working electrode, platinum-wire counter electrode and Ag/AgCl/CH_3CN electrode as reference. Magnetic susceptibilities were recorded over the temperature range 1.9–350 K at 1 T with a superconducting quantum interference device (SQUID) susceptometer (Quantum Design, San Diego, CA) interfaced with a HP Vectra computer system. All the values were corrected for diamagnetism that were calculated from Pascal's table.[11] Thermogravimetric analyses were made on Rigaku Thermo Plus 2 TG8120 over the temperature range of 295–773 K.

Crystallographic Data Collection and Refinement of Structures.

Diffraction measurements were performed on a Rigaku mercury diffractometer with CCD two-dimensional detector with Mo Kα radiation employing a graphite monochromator. The sizes of the unit cells were calculated from the reflections collected on the setting angles of four frames by changing ω by 0.5° for each frame. Two different χ settings were used and w was changed by 0.5° per frame. Intensity data were collected in 480 frames with an ω scan width of 0.5° and exposure times 40 and 100 s for **1** and **2**, respectively. Empirical absorption correction using the program REQABA[12] was performed for all the data. All the crystal data are summarized in Table 1. The structures were solved by direct methods[13] and expanded using Fourier techniques.[14] The final cycles of the full-matrix least-squares refinements were based on the observed reflections ($I > 3\sigma(I)$ (**1**) and $4\sigma(I)$ (**2**)). In complex **2** the disorder of the benzene molecules was found at the final stage, thus, its atom positions were refined under a rigid condition. All the calculations were performed using the teXsan crystallographic software package of Molecular Structure Corporation.[15]

Table 1. Crystallographic and Refinement Data for **1** and **2**

	1	**2**
Formula	$C_{42}H_{24}O_6Cl_{12}Cr$	$C_{42}H_{24}O_6Br_{12}Cr$
Formula weight	1102.08	1635.49
Color	reddish violet	violet
Crystal size, mm	0.30×0.10×0.06	0.30×0.28×0.075
Crystal system	tetragonal	tetragonal
Space group	$P4_12_12$	$P4_12_12$
a, Å	13.452(2)	13.7465(7)
c, Å	24.78(2)	25.680(1)
Z	4	4
V, Å^3	4484(3)	4852.6(4)
ρ_{calcd}, g/cm^3	1.632	2.238
μ, cm^{-1}	10.17	101.91
T, K	296	223
λ (Mo Kα), Å	0.71069	0.71069
No. observations	1914[a]	1229[b]
No. parameters	277	182
Refls./para. ratio	6.91	6.75
GOF	1.86	2.32
R_{int}	0.030	0.036
R, R_w[a]	0.052, 0.059	0.059, 0.063

[a] $I > 3\sigma(I)$. [b] $I > 4\sigma(I)$. [c] $R = \Sigma||F_0|-|F_0||/\Sigma|F_0|$, $R_w = [\Sigma(|F_0|-|F_0|)^2/\Sigma w|F_0|^2)]^{1/2}$.

Results and Discussion

Thermal synthesis of $Cr^{III}(Cl_4SQ)_3$ under the conditions reported by Pierpont et al. has been failed in accordance with Vlcek's report. On the other hand, Vlcek et al. have proposed that the reaction of $Cr(CO)_6$ with Cl_4BQ is a photochemical process which occurs readily even at laboratory temperature. The author has carried out the thermal synthesis of the complexes under the several reaction times based on these alternative reports. The experiments show that the yields of complex are increased by the reaction time; Yield/% (reaction time, hour) 0 (10), 1.7 (45), 9.1 (92), 28 (120), 33 (143), and 43 (408). Furthermore, the thermal reaction has been applied for the synthesis of $Cr^{III}(Br_4SQ)_3$ and the product was obtained in satisfactory yield 94 % with refluxing for three days. From these results it is concluded that the complexes could be thermally synthesized without irradiation.

Crystal Structures.

Complexes **1** and **2** crystallize by recrystallization from dichloromethane/benzene solution in an isostructural form. Figure 1 show ORTEP drawing of **1** with the atom numbering schemes. As shown in Figure 1 only one-half of ligands are crystallographically independent. The geometry of the chromium ion is distorted octahedron with six oxygen atoms from the three

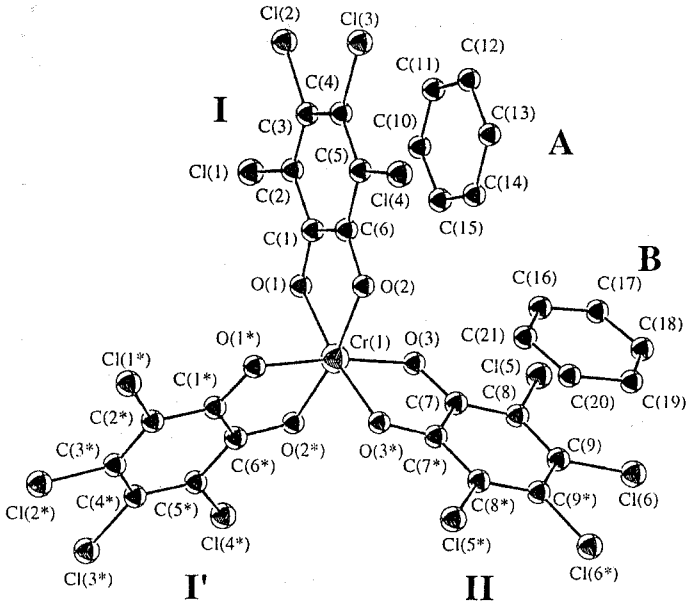

Figure 1. An ORTEP drawing of **1** with hydrogen atoms omitted (showing 30% isotropic thermal ellipsoids). Crystallographically independent ligands and benzene molecules are designated **I** and **II** and **A** and **B**, respectively. The atomic numbering scheme for **2** is the same as that for **1**.

bidentate ligands **I**, **II**, and **I'**. Table 2 lists average bond distances and angles of **1** and **2** compared with those of complexes reported previously. The average Cr–O distances are 1.956(5) and 1.95(1) Å for **1** and **2**, respectively. These distances are similar to that of $Cr^{III}(Cl_4SQ)_3 \cdot CS_2 \cdot 1/2C_6H_6$ and compare well with distances for typical Cr(III) complexes with O_6 coordination environments; 1.942–1.959(7) and 1.96 Å for $Cr^{III}(acac)_3$[16] and $Cr^{III}(C_2O_4)^{3-}$,[17] respectively. It has been found that typical C–O bond distances for BQ, SQ, and Cat are 1.23, 1.29, and 1.35 Å, respectively.[1] The C–O bond distances in general increase with the reduction of the ligand because of antibonding nature of C–O bond in π^* orbital of the ligand.[18] The C–O bond distances of ligands **I** and **II** of **1** are found to be 1.297(9) and 1.280(8) Å, respectively, while those of **2** are 1.31(3) and 1.32(3) Å, respectively. These values indicate the SQ form of each ligand similar to $Cr^{III}(Cl_4SQ)_3 \cdot CS_2 \cdot 1/2C_6H_6$.[3] The observed O–Cr–O angles also similar to those of chromium complexes with the SQ ligands reported so far.[3,19]

Table 2. Average Bond Distances (Å) and Angles (°) of **1**, **2**, and $Cr^{III}(Cl_4SQ)_3 \cdot CS_2 \cdot 1/2C_6H_6$

	L	**1**	**2**	$Cr^{III}(Cl_4SQ)_3 \cdot CS_2 \cdot 1/2C_6H_6$[a]
Cr–O (Å)	**I**	1.957(5)	1.95(1)	
	II	1.954(5)	1.94(1)	
total average		1.956(5)	1.95(1)	1.949(5)
C–O (Å)	**I**	1.297(9)	1.31(3)	
	II	1.280(8)	1.32(3)	
total average		1.291(8)	1.31(3)	1.280(1)
C–C (Å)	**I**	1.40(1)	1.40(4)	
	II	1.41(2)	1.40(4)	
total average		1.40(1)	1.40(4)	1.40(1)
O–Cr–O (°)	**I**	82.3(2)	82.4(6)	
	II	81.9(3)	82.4(7)	
total average		82.1(3)	82.4(7)	81.8(2)

[a] Reference 3.

Crystal Packing Structures.

The complexes were isolated from a dichloromethane/benzene solution and found to contain two crystallographically independent benzene molecules per complex. As shown in Figure 2(a), ligand **I** (**I'**) forms infinite mixed-stack chains with benzene **A** molecules along the *a*(*b*)-axis. The mean interplanar separation is 3.36(1) Å with the dihedral angle of 3.5(3)°. Figure 2(b) illustrates the overlap mode of these stacks along the normal direction of the mean plane of the ligand **I**. Six-membered rings of the ligand and the benzene molecule show well-overlap region with slight slipping. Thus, each complex molecule is linked to two adjacent molecules

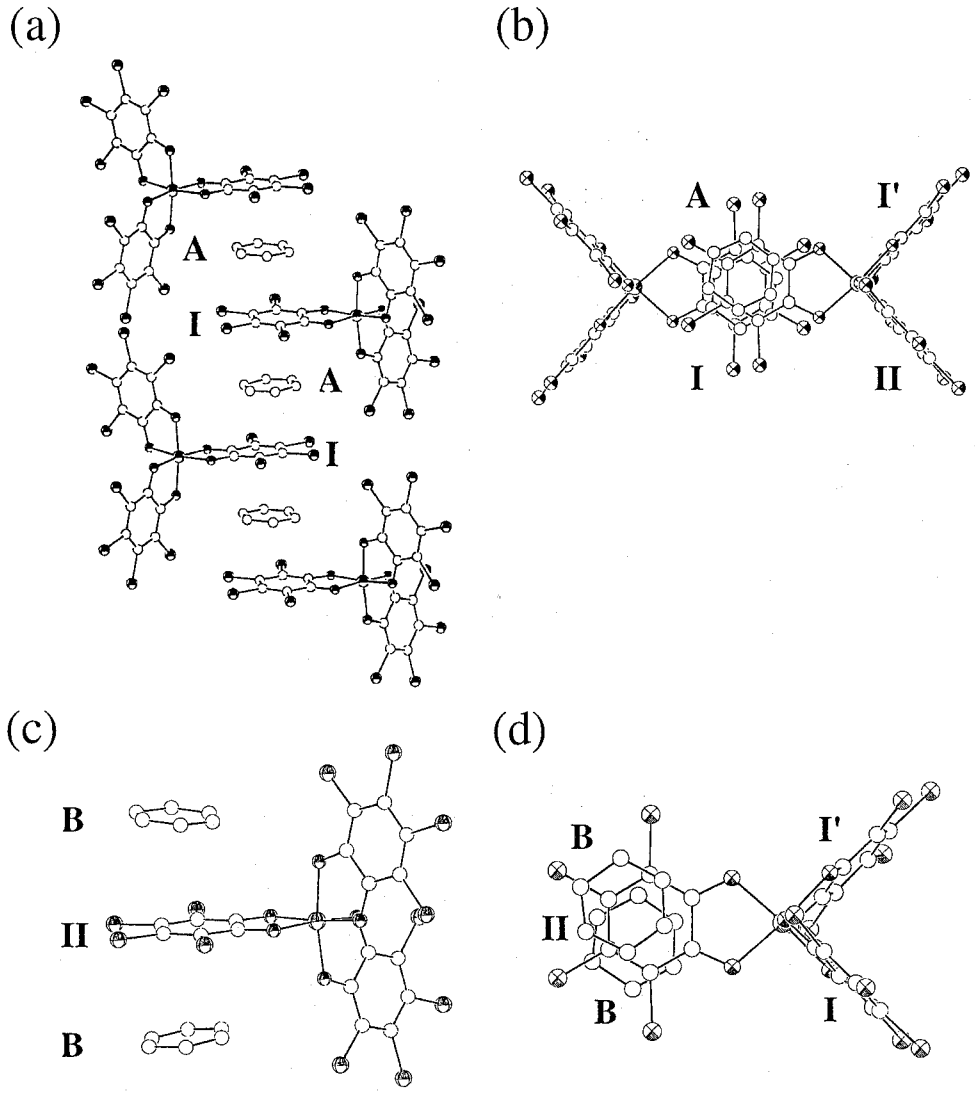

Figure 2. (a) One-dimensional mixed-stacking chain of ligand **I**···benzene **A** along the *a*(*b*)-axis and (b) projection of the chain along the normal direction of the mean plane of the ligand **I**. (c) The π··· π interactions between ligand **II**···benzene **B** and (d) projection of the stacking interaction along the normal direction of the mean plane of the ligand **II**.

through benzene solvate bridges, resulting in the formation of a two-dimensional polymeric array in the *ab*-plane. Hydoquinones and *p*-benzoquinones are well known for their ability to form CT compounds[20,21] and the benzene···ligand separations observed are similar to the range of values observed for the compounds between hydroquinones and other quinoid molecules. Additionally, ligand **II** is sandwiched by two benzene molecules **B** along the *c*-axis making discrete-type benzene **B**···SQ···benzene **B** trimer unit (Figures (c) and (d)). The mean interplanar separation is 3.61(2) Å, which is longer than that for the ligand **I**···benzene **A**.

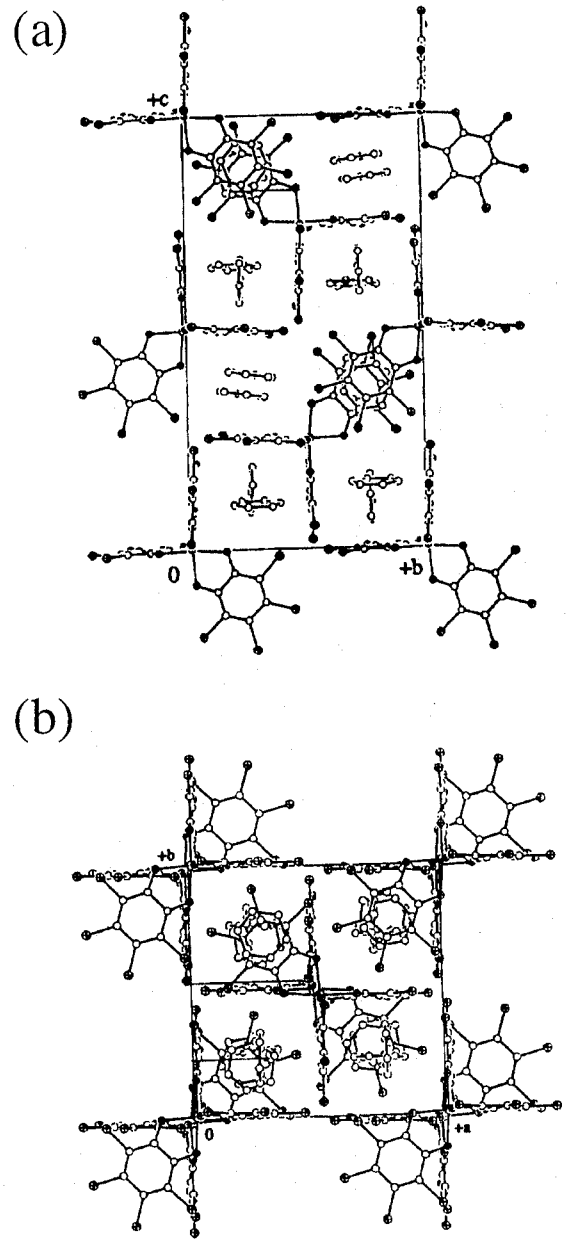

Figure 3. Projection of crystal packing diagrams of **1** (**2**) along the (a) *a*- and (b) *c*-axes.

Dihedral angle between them is found to be 5.8(4)°. The two observed mean separations are comparable to that of $Cr^{III}(Cl_4SQ)_3 \cdot CS_2 \cdot 1/2C_6H_6$, where the ligand and benzene molecules form discrete stacking interaction with the separation of 3.45 Å and the dihedral angle of 5.4°.[3]

The π···π interaction between the ligand and aromatic molecules have been also found in $[Mo(Cl_4Cat)_2]_2 \cdot 3C_6H_6$ (3.47 and 3.54 Å)[8] and $W_2(Cl_4Cat)_6 \cdot 3C_6H_6CH_3$.[9] These structural features of the transition metal SQ/Cat complexes demonstrate that the SQ/Cat ligands favor to stack with aromatic molecule to stabilize the whole crystal structures. This tendency is also found in the CT compounds of a series of $[Cr^{III}(X_4SQ)_{3-n}(X_4Cat)_n]^{3-n}$ (n = 0 and 1) redox isomers where the homoleptic and heteroleptic stacking interactions including SQ···solvent, Cat···solvent, SQ···SQ, and SQ···Cat are found. In addition to the π··· π interactions, complexes **1** and **2** show intermolecular atomic contacts between halogen atoms with the distances shorter than the sum of van der Waals radii of two halogen atoms, 3.60 (Cl) and 3.90 (Br) Å; **1**: 3.562 and 3.123(4) Å for Cl(1)···Cl(3*) (1/2–y+3, 1/2+x+3, 1/4+z+3) and Cl(4)···Cl(4*) (–y, –x, 1/2–z+1). **2**: 3.279(6) Br(1)···Br(1*) (x+6, y+6, z+6), 3.764(5) Br(1)···Br(6*) (1/2–x–1, 1/2+y, 1/4–z), 3.784(4) Br(2)···Br(4*) (1/2–y, 1/2+x–1, 1/4+z), 3.832(4) Br(2)···Br(5*) (x+3, y+3, z+3), 3.810 Br(3)···Br(4*) (1/2–y, 1/2+x, 1/4+z), 3.773(3) Br(3)···Br(5*) (x+3, y+3, z+3), and 3.772(3) Å Br(4)···Br(5*) (x+1, y, z).

Infrared Spectra.

Infrared spectroscopy has proven to be a potent probe in determing the structures of transition metal quinone complexes.[22,23] Figure 4 shows infrared spectra of **1** and **2** in the region of 400–1600 cm^{-1}. Among several sharp peaks, the bands at 1478, 1034, 678, and 458 cm^{-1} are assigned to those of benzene molecules in **1** and **2**. In general, the spectral region between 1500 and 1000 cm^{-1} contains strong bands associated with the C–O and C–C stretching modes of the ligand moieties that are sensitive to their charged state. The C=O stretching frequency for free Cl_4BQ occurs at 1681 cm^{-1}, whereas no bands were observed in this region for **1** and **2**. On the other hand, two sharp bands are found at 1460 and 1447 cm^{-1} and 1454 and 1433 cm^{-1} for **1** and **2**, respectively. These bands have been found in transition

metal complexes with the SQ ligands[22] indicative of SQ nature of the ligand moieties in both complexes.

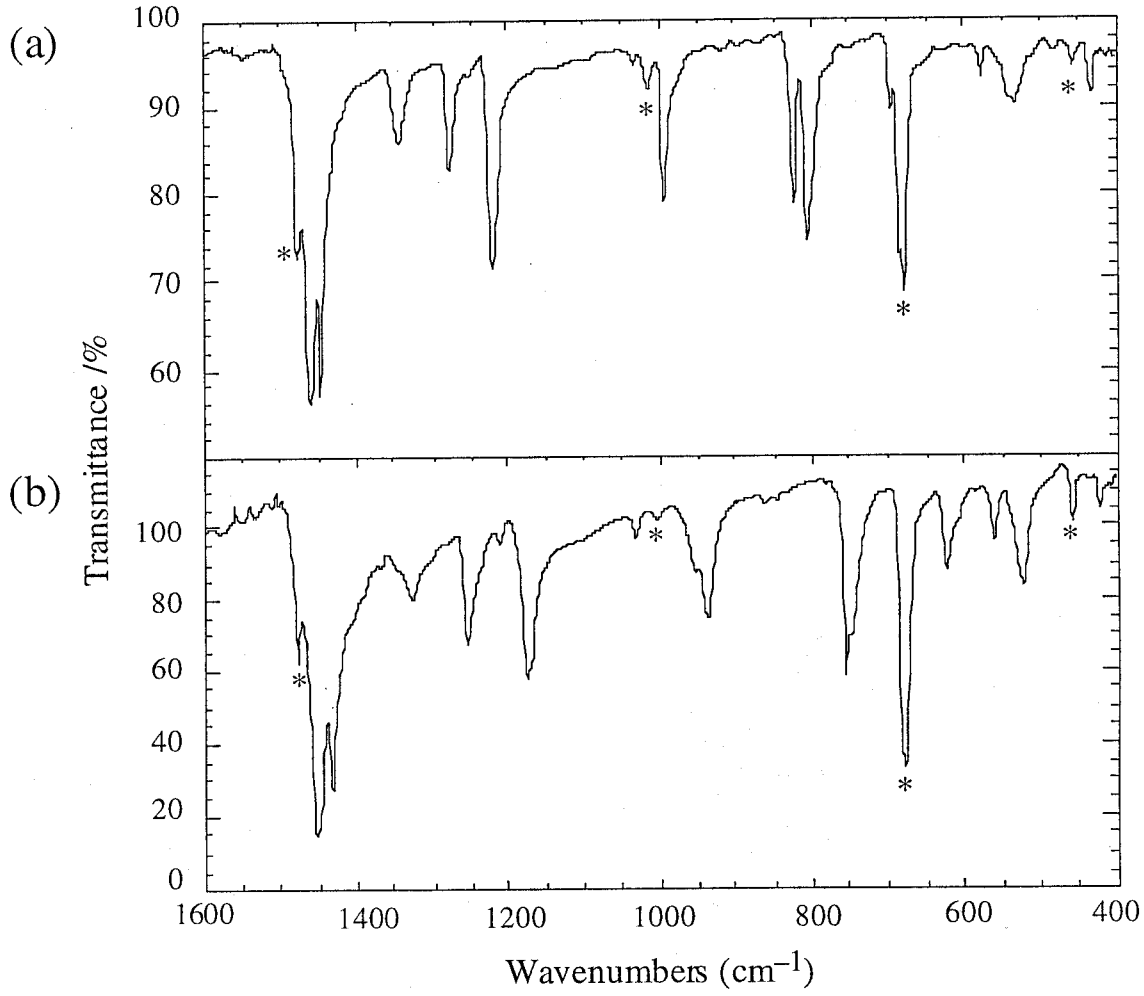

Figure 4. Infrared spectra (KBr pellets) of (a) **1** and (b) **2**. The asterisks indicate the peaks of solvate benzene molecules.

UV-vis-NIR-IR Absorption Spectra.

UV-vis-NIR-IR absorption spectra were measured in dichloromethane, carbondisulfide, and cyclohexane solution and on KBr pellets. The spectra of **1** and **2** are shown in Figures 5 and 6, respectively, and all the data are summarized in Table 3. The absorption spectra of both complexes are dominated by high-intensity CT bands mainly in the visible region, and are in good agreement each other. The band positions and absorption coefficients are similar to those of previously reported data for $Cr^{III}(Cl_4SQ)_3 \cdot 4C_6H_6$.[3]

Figures 5(b) and 6(b) show the spectra measured on KBr pellets. The spectral patterns are

similar to those of solution indicative of the similarity of the electronic structures in the solution and in the solid states. The peak maxima in the spectra of solid state tend to shift to the lower energy, especially, the bands at 18300 and 18200 cm^{-1} for **1** and **2**, respectively. These shifts reflect the solid effects derived from the $\pi\cdots\pi$ interaction between the ligands with benzene molecules. No significant solvent dependency was observed in three non-polar solvents except for the small difference between the absorption coefficients in dichloromethane and carbondisulfide and that in cyclohexane. On the other hand, in polar solvents such as acetone and acetonitrile, the spectra of the complexes show drastic changes. These changes are responsible to a valence tautomeric conversion, $Cr^{III}(X_4SQ)_3 \rightleftarrows Cr^{III}(X_4BQ)(X_4SQ)(X_4Cat)$ (Chapter 5).

Table 3. Absorption Spectral Parameters for **1** and **2**

compound	condition	ν_{max} ($10^3 \times cm^{-1}$) ($\varepsilon_{max} = 10^3 \times M^{-1}\cdot cm^{-1}$)					
1	CH_2Cl_2	8.70	10.0	13.0	19.0	20.8	22.2
		(0.887)	(1.39)	(4.85)	(20.8)	(sh, 12.9)	(sh, 8.96)
	CS_2	8.58	9.96	13.0	18.7	20.6	21.7
		(0.978)	(1.49)	(4.91)	(20.3)	(sh, 11.7)	(sh, 9.16)
	C_6H_{12}	8.40	10.1	13.1	19.2	20.8	22.2
		(0.681)	(1.06)	(3.80)	(16.9)	(sh, 10.7)	(sh, 7.46)
	KBr	7.81	9.35	12.7	18.3		
2	CH_2Cl_2	8.33	9.90	13.0	18.6	19.8	21.3
		(sh, 0.920)	(1.43)	(4.66)	(19.0)	(sh, 11.6)	(sh, 7.71)
	CS_2	8.33	9.90	12.9	18.2	19.8	21.3
		(sh, 0.904)	(1.37)	(4.50)	(19.3)	(sh, 11.2)	(sh, 7.42)
	C_6H_{12}	8.33	10.0	13.1	18.8	20.4	21.7
		(sh, 0.885)	(1.09)	(3.47)	(15.3)	(sh, 10.4)	(sh, 5.92)
	KBr	7.94	9.80	12.9	18.2		

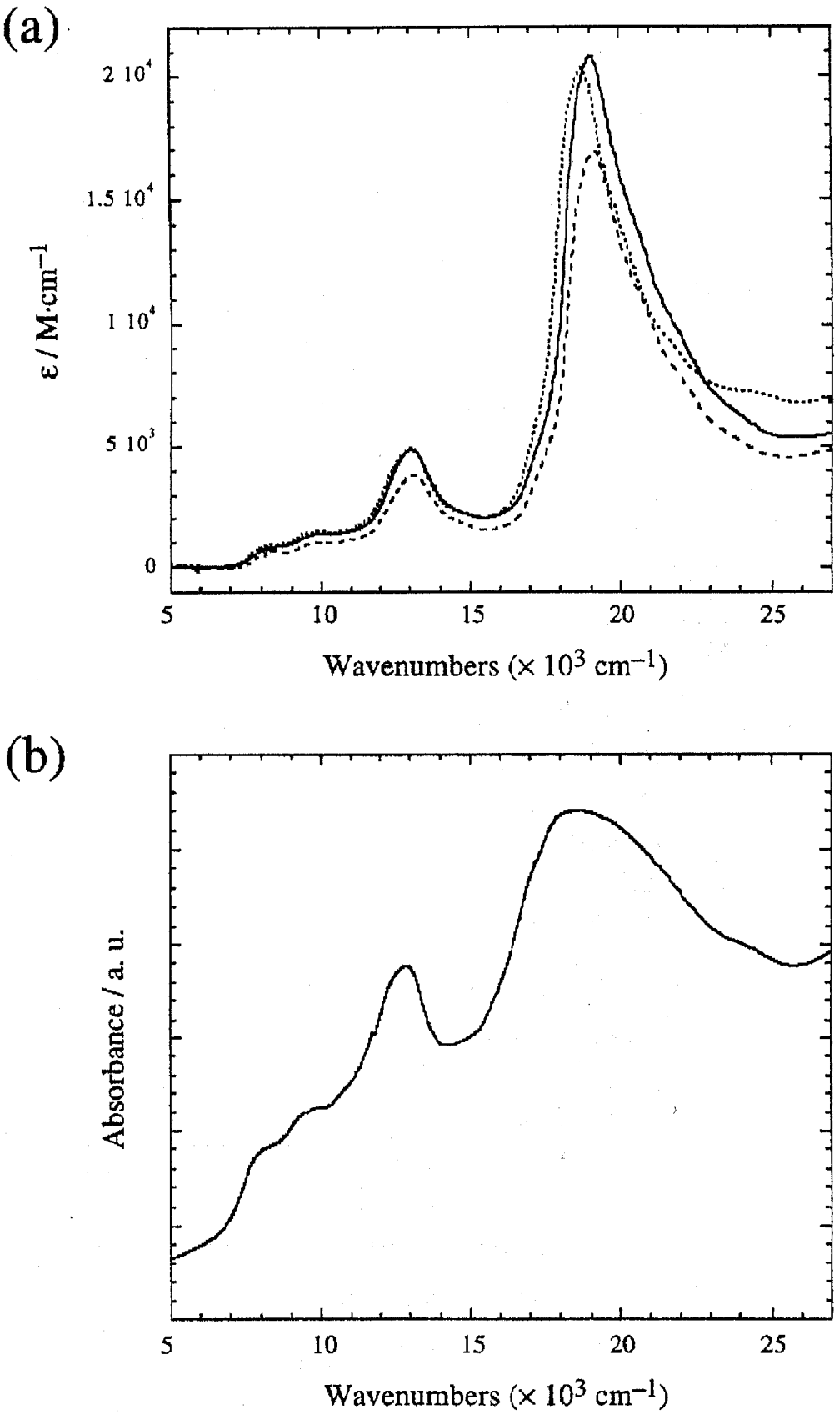

Figure 5. Electronic absorption spectra of **1** measured in (a) dichloromethane (–), carbondisulfide (···), and cyclohexane (---), and (b) on KBr pellet. The discontinuity near 12000 cm^{-1} is an instrumental artifact due to a detector change in the spectrometer.

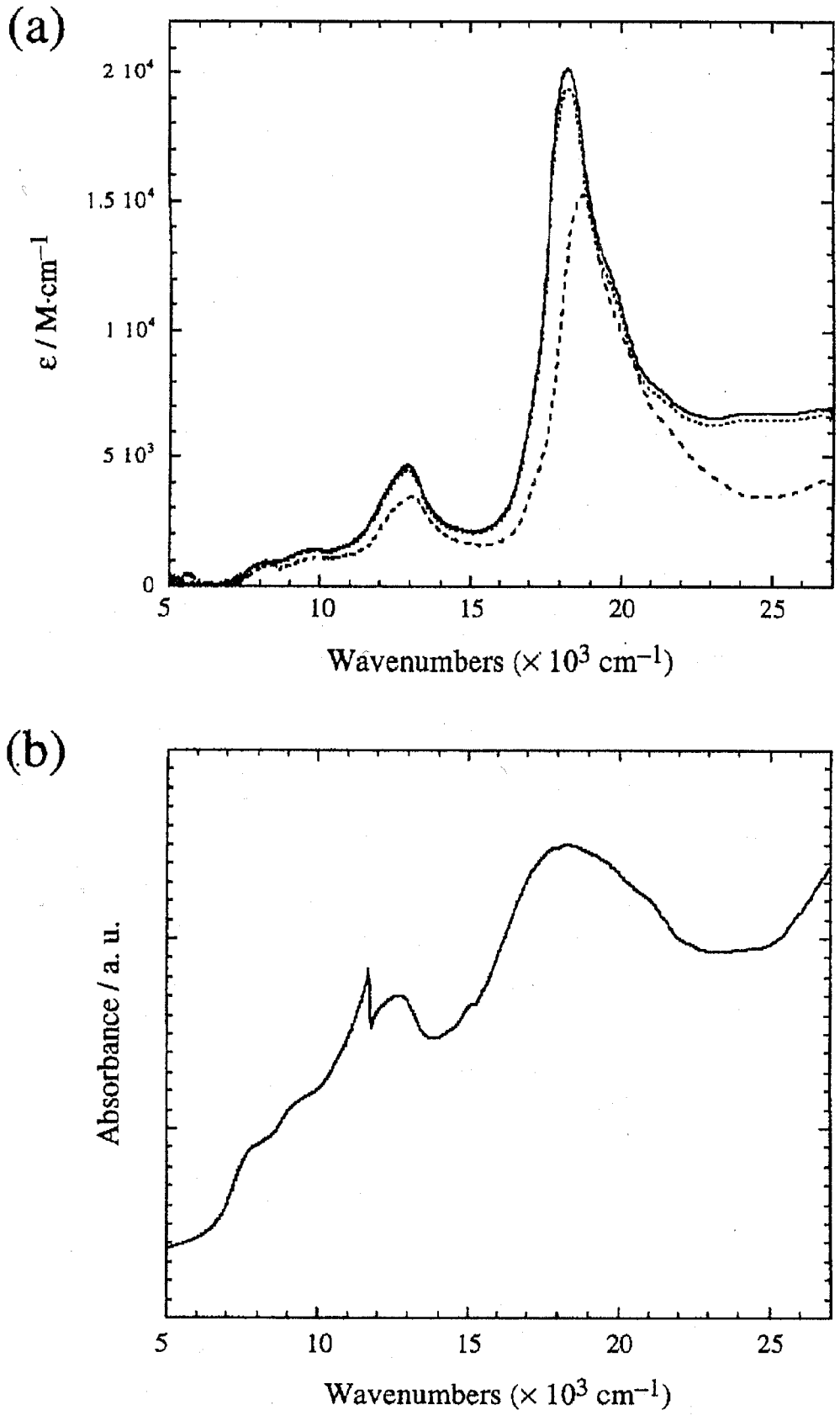

Figure 6. Electronic absorption spectra of **2** measured in (a) dichloromethane (–), carbondisulfide (···), and cyclohexane (---), and (b) on KBr pellet. The discontinuity near 12000 cm^{-1} is an instrumental artifact due to a detector change in the spectrometer.

Electrochemical Properties.

Figure 7 shows cyclic voltammograms of **1** and **2** measured in dichloromethane solution. The redox potentials are given in Table 4. Both complexes show three quasi-reversible redox couples at 522, 122, and –322 mV and at 510, 86, and –302 mV for **1** and **2**, respectively. The electrochemical behaviors are similar to the previous report for the electrochemical properties of $Cr^{III}(SQ)_3$ series.[2] The observed redox couples correspond to the stepwise reductions of three SQ ligands to the Cat form. The first, second, and third reduction of neutral $Cr^{III}(X_4SQ)_3$ afford a mono-anionic $[Cr^{III}(X_4SQ)_2(X_4Cat)]^-$, di-anionic $[Cr^{III}(X_4SQ)(X_4Cat)_2]^{2-}$, and tri-anionic $[Cr^{III}(X_4Cat)_3]^{3-}$ redox isomer respectively (Scheme 1). Relatively high redox

Scheme 1

$$Cr^{III}(X_4SQ)_3 \rightleftharpoons [Cr^{III}(X_4SQ)_2(X_4Cat)]^- \rightleftharpoons [Cr^{III}(X_4SQ)(X_4Cat)_2]^{2-} \rightleftharpoons [Cr^{III}(X_4Cat)_3]^{3-}$$

(X = Cl and Br)

potentials could be explained by electron-withdrawing effects of the halogen atoms; the redox potentials of **1** and **2** are higher by approximately 1000 mV than those of Cr^{III}(3,5-DTBSQ)$_3$ and Cr^{III}(phenSQ)$_3$ (3,5-DTBSQ = 3,5-di-tert-butyl-*o*-semiquinonate and phenSQ = 9,10-phenathrenesemiquinonate).[2] Small difference in the redox potentials between **1** and **2** indicates that the electron-withdrawing forces between chlorine and bromine atoms are not significant as to be expected. However, these data clearly shows that the multi-redox

Table 4. Cyclic Voltammetric Data for **1** and **2**[a]

couple	**1**				**2**			
	E_{ox}	E_{red}	Δ^b	$E_{1/2}{}^c$	E_{ox}	E_{red}	Δ^b	$E_{1/2}{}^c$
0/–1	554	490	64	522	391	628	237	510
–1/–2	167	57	110	112	–4	168	172	86
–2/–3	–272	–372	100	–322	–379	–225	154	–302

[a] condition: in dichloromethane, scan rate 100 mV/s, N_2, 296 K, [b] Separation between E_{ox} and E_{red} (mV). [c] mV vs Ag/AgCl/CH_3CN.

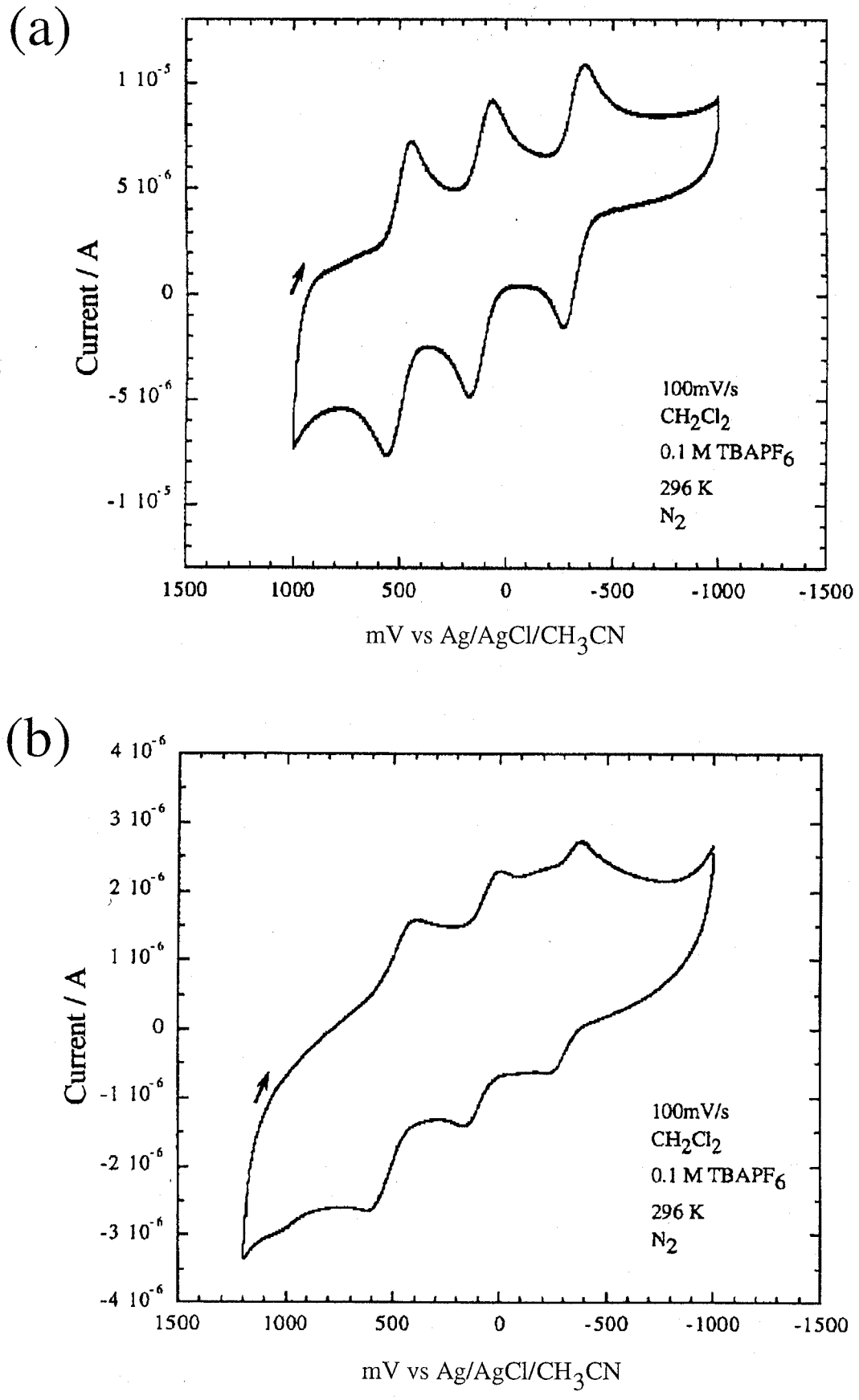

Figure 7. Cyclic voltammograms of (a) **1** and (b) **2** measured in dichloromethane.

and strong acceptor properties are maintained in the bromine-substituted complex. The isolation and physical properties of one- and two-electron reduced isomers, $[Cr^{III}(X_4SQ)_2(X_4Cat)]^-$ and $[Cr^{III}(X_4SQ)(X_4Cat)_2]^{2-}$, with mixed-charge ligands will be shown in later Chapter, and the proof of above assignments for the redox process will be shown.

Magnetic Properties.

Figure 8 shows the temperature dependent magnetic susceptibility for **1** in the forms of $\chi_m T$ and χ_m^{-1}. At 350 K, the compound shows $\chi_m T$ value of 0.154 emu·K·mol^{-1}, which drops to a value of 0.002 emu·K·mol^{-1} at 1.9 K. As reported previously, the complex has a ground state of $S = 0$ as a result of strong intramolecular antiferromagnetic interaction between three unpaired electrons of Cr^{III} ion (d^3, $S = 3/2$) and three SQ ligands ($S = 1/2$). Figure 9 illustrates the low-lying energy states for $Cr^{III}(SQ)_3$ complex resulting from an intramolecular antiferromagnetic interaction between the spins on the Cr^{III} ion and the SQ ligands. Pierpont et al. have proposed that there would be three energetically degenerate $S = 1$ excited states, three energetically degenerate $S = 2$ exited states, and one $S = 3$ excited states in $Cr^{III}(SQ)_3$ type complexes.[6]

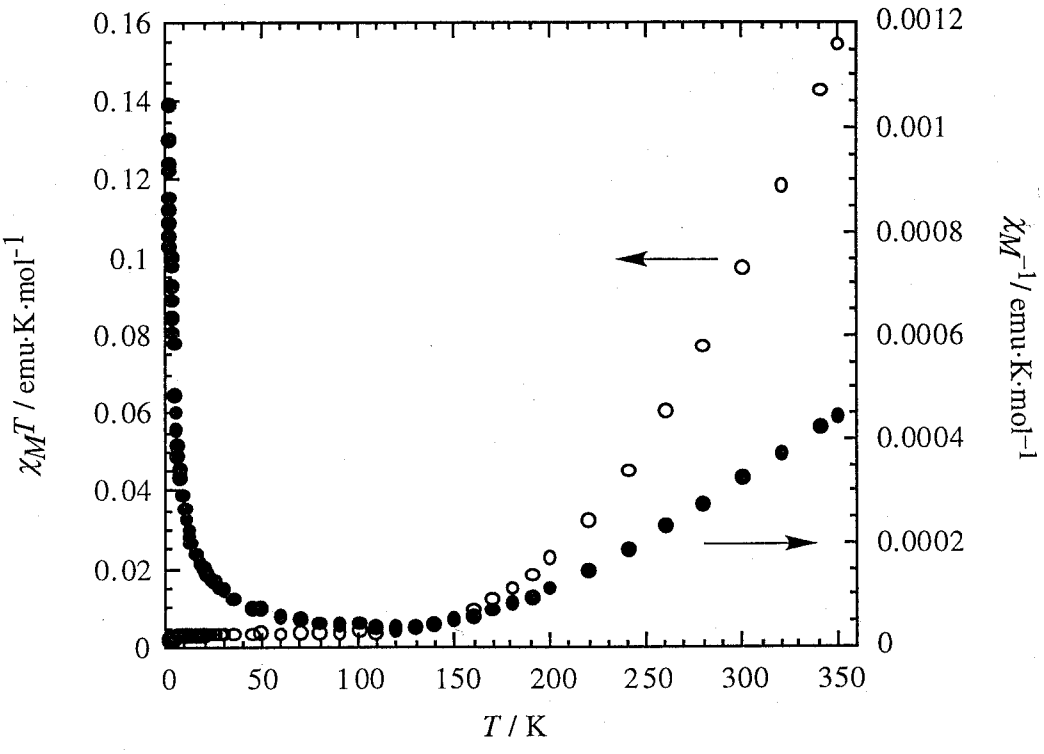

Figure 8. The plots of the temperature dependence of $\chi_m T$ (O) and χ_m^{-1} (●) measured under the field of 1 T.

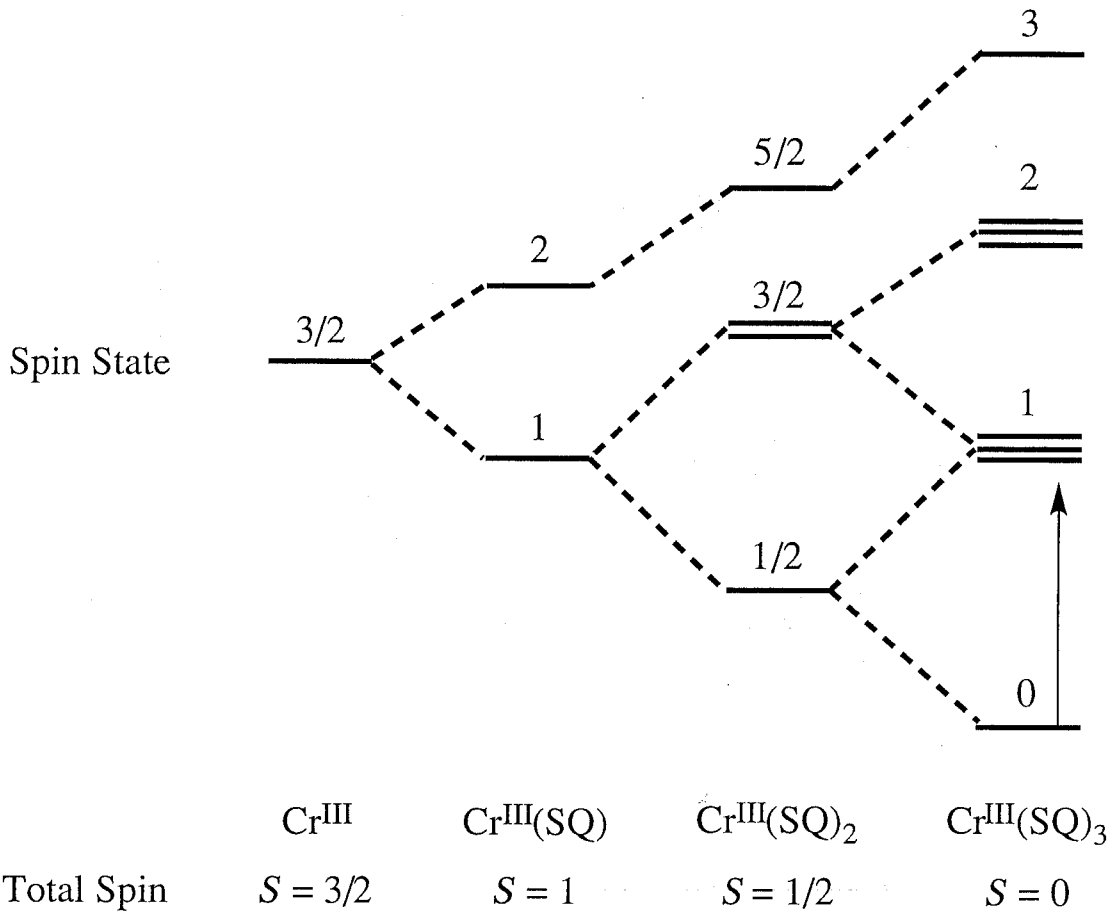

Figure 9. The low-lying energy states for $Cr^{III}(SQ)_3$ complex resulting from an intramolecular antiferromagnetic interaction between the spins on the SQ ligands and the chromium ion.

Actually, $\chi_m T$ value shows temperature dependency associated with Boltzmann distribution from the $S = 0$ ground state to the $S = 1$ exited state and, at 350 K, the $S = 1$ excited state is weakly populated.

Thermogravimetric Analyses.

To evaluate $\pi\cdots\pi$ interactions between the complex and benzene molecules, the thermogravimetric (TG) and differential scanning calorimetry (DSC) have been carried out for **1** and **2**. As shown in Figure 10, rapid weight loss take place up to 500 K. Weight loss at this temperature correspond to 28.3 and 18.8 % for **1** and **2**, respectively. The liberation of four solvate benzene molecules account for these weight loss for **1** ($4C_6H_6$, 28.3 %) and **2** ($4C_6H_6$, 19.1 %). The temperature is higher than that of boiling point of the benzene molecule under the ambient pressure (353 K), reflecting the effect of the interactions in the crystal phases.

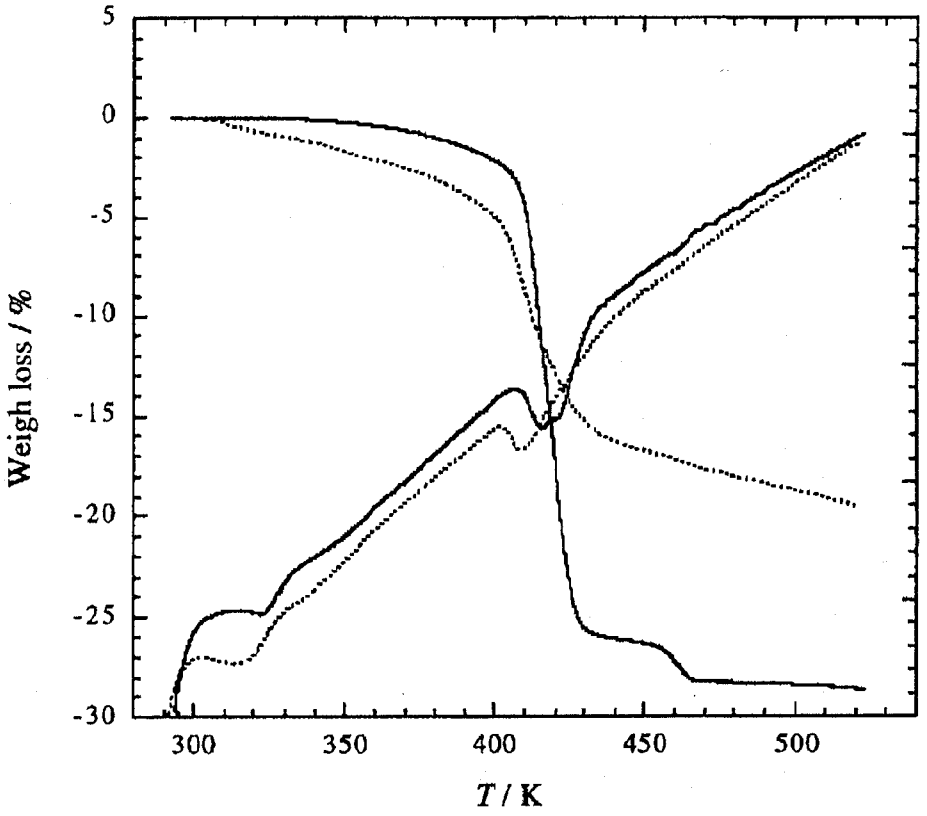

Figure 10. Thermogravimetric data for **1** (–) and **2** (···).

Conclusion

The thermal reaction of $Cr(CO)_6$ with X_4BQ was re-investigated and found to be useful for the synthesis of tris(*o*-semiquinonate) complexes even though relatively long reaction time is need. By using the reaction, bromo-substituted complex was synthesized for the first time.

In this Chapter, two fundamental and characteristic properties of the $Cr^{III}(X_4SQ)_3$ complexes were examined. Firstly, the stacking interactions of ligand moieties with solvate benzene molecules were characterized in isostructural crystals, $Cr^{III}(X_4SQ)_3 \cdot 4C_6H_6$, by the X-ray diffraction and thermogravimetric analyses. The structural analyses reveal that the $\pi \cdots \pi$ interaction of the ligand moieties is inherent nature for the *o*-quinone complexes, and this could be useful for the construction of new-type supramolecular assemblies. Secondly, the electronic structures of the complexes were examined by CV, UV-vis-NIR-IR absorption spectra, and SQUID measurements. The complexes have electronic structures in which three ligands coordinate to Cr^{III} ion as paramagnetic SQ form. The electrochemical data demonstrate that the

complexes would behave as good three-electron acceptors. Furthermore, the strong intramolecular magnetic interaction between the spins on the Cr^{III} (d^3) ion and the SQ ligands was recognized by temperature dependence of magnetic susceptibility. Combination of these structural characteristics, electrochemical, and magnetic properties of the complexes will be effected by the CT reaction between donor molecules.

References

(1) Pierpont, C. G.; Lange, C. W. *Prog. Inorg. Chem.* **1994**, *41*, 331.

(2) Downs, H. H.; Buchanan, R. M.; Pierpont, C. G. *Inorg. Chem.* **1979**, *18*, 1736.

(3) Pierpont, C. G.; Downs, H. H. *J. Am. Chem. Soc.* **1976**, *98*, 4834.

(4) Benelli, C.; Dei, A.; Gatteschi, D.; Güdel, H. U.; Pardi, D. *Inorg. Chem.* **1989**, *28*, 3089.

(5) Pierpont, C. G.; Downs, H. H.; Rukavina, T. G. *J. Am. Chem. Soc.* **1974**, *96*, 5573.

(6) Buchanan, R. M.; Kessel, S. L.; Downs, H. H.; Pierpont, C. G.; Hendrickson, D. N. *J. Am. Chem. Soc.* **1978**, *100*, 7894.

(7) Buchanan, R. M.; Downs, H. H.; Shorthill, W. B.; Pierpont, C. G.; Kessel, S. L.; Hendrickson, D. N. *J. Am. Chem. Soc.* **1978**, *100*, 4318.

(8) Pierpont, C. G.; Downs, H. H. *J. Am. Chem. Soc.* **1975**, *97*, 2123.

(9) deLearie, L. A.; Pierpont, C. G. *Inorg. Chem.* **1988**, *27*, 3842.

(10) Smídova, I.; Vleck, A. J.; Vleck, A. *Inorg. Chim. Acta* **1982**, *64*, L63.

(11) Kahn, O. *Molecular Magnetism*; VCH: New York, 1993.

(12) Jacobson, R. A. *REQABA Empirical Absorption Correction Version 1.1-03101998:* Molecular Structure Corp.: The Woodlands, TX, 1996–1998.

(13) Altomare, A.; Burla, M. C.; Camalli, M.; Cascarano, M.; Giacovazzo, C.; Guagliardi, A.; Pilidori, G. *J. Appl. Cryst.* **1994**, *27*, 435.

(14) Beurskens, P. T.; Admiraal, G.; Beurskens, G.; Bosman, W. P.; de Gelder, R.; Israel, R.; Smits, J. M. M. , The DIRDIF-94 program system, Technical Report of the Crystallography Laboratory; University of Nijmegen: Nijmegen, The Netherlands, 1994.

(15) *teXsan: Crystal Structure Analysis Package*; Molecular Structure Corporation: The Woodlands, TX, 1985, 1992.

(16) Morosin, B. *Acta Crystallogr.* **1965**, *19*, 131.

(17) van Niekerk, J. N.; Schoening, F. R. L. *Acta Crystallogr.* **1952**, *5*, 499.

(18) Gordon, D. J.; Fenske, R. F. *Inorg. Chem.* **1982**, *21*, 2907.

(19) Sofen, S. R.; Ware, D. C.; Cooper, S. R.; Raymond, K. N. *Inorg. Chem.* **1979**, *18*, 234.

(20) Mayerle, J. J.; Torrance, J. B. *Acta Crystallogr., Sec. B* **1981**, *B37*, 2030.

(21) Nakasuji, K.; Sasaki, M.; Kotani, T.; Murata, I.; Enoki, T.; Imaeda, K.; Inokuchi, H.; Kawamoto, A.; Tanaka, J. *J. Am. Chem. Soc.* **1987**, *109*, 6970.

(22) Lynch, M. W.; Valentine, M.; Hendrickson, D. N. *J. Am. Chem. Soc.* **1982**, *104*, 6982.

(23) Clowley, P. J.; Haendler, H. M. *Inorg. Chem.* **1962**, *1*, 904.

Chapter 2

Assembled Crystal Structures of Ligand-based Mixed-valence $[Cr^{III}(X_4SQ)_2(X_4Cat)]^-$ (X = Cl and Br) Complexes in Charge-transfer Compounds with Tetrathiafulvalene Derivatives Cations

Abstract

The reaction of tris(tetrahalogeno-*o*-semiquinonate) chromium (III) complexes, $Cr^{III}(X_4SQ)_3$ (X = Cl and Br), with tetrakis(methylsulfanyl)tetrathiafulvalene (TMT-TTF), tetramethyltetraselenafulvalene (TMTSF), and bis(propylenedithio)tetrathiafulvalene (BPDT-TTF), afford six charge-transfer compounds,

(TMT-TTF)$[Cr^{III}(Cl_4SQ)_2(Cl_4Cat)]$ (**1**)
(TMT-TTF)$[Cr^{III}(Br_4SQ)_2(Br_4Cat)]\cdot C_6H_5CH_3$ (**2**$\cdot C_6H_5CH_3$)
(TMTSF)$[Cr^{III}(Cl_4SQ)_2(Cl_4Cat)]\cdot 1/2CH_2Cl_2$ (**3**$\cdot 1/2CH_2Cl_2$)
(TMTSF)$[Cr^{III}(Br_4SQ)_2(Br_4Cat)]\cdot 2CH_2Cl_2$ (**4**$\cdot 2CH_2Cl_2$)
(BPDT-TTF)$[Cr^{III}(Cl_4SQ)_2(Cl_4Cat)]\cdot 1/2C_6H_6$ (**5**)
(BPDT-TTF)$[Cr^{III}(Br_4SQ)_2(Br_4Cat)]\cdot 1/2C_6H_6$ (**6**)

, where Cat is catecholate. The one-electron reduced complexes, $[Cr^{III}(X_4SQ)_2(X_4Cat)]^-$, are commonly formed by cocrystallization with paramagnetic TMT-TTF$^{\bullet+}$, TMTSF$^{\bullet+}$, and BPDT-TTF$^{\bullet+}$ cations. The complexes, $[Cr^{III}(X_4SQ)_2(X_4Cat)]^-$, with two semiquinonates and one catecholate ligands were firstly isolated and crystallographically characterized. The complexes show a mixed-valence state on the ligand moieties, where the SQ and Cat ligands simultaneously coordinated to the chromium (III) ion. Interestingly, the complexes form a one-dimensional chain (**2**$\cdot C_6H_5CH_3$), two-dimensional brick-wall (**3**$\cdot 1/2CH_2Cl_2$), and hexagonal honeycomb (**4**$\cdot 2CH_2Cl_2$) networks with the aid of intermolecular $\pi\cdots\pi$ stacking interactions of the ligand moieties.

The solid state absorption spectra of the compounds clearly demonstrate the mixed-valence states of the complexes where intramolecular intervalence charge-transfer (IVCT) transitions from Cat to SQ are observed near 4170 cm^{-1}. The temperature dependence of the magnetic

susceptibilities reveals that all the $[Cr^{III}(X_4SQ)_2(X_4Cat)]^-$ complexes are in a ground state of S = 1/2, which results from the intramolecular antiferromagnetic interaction between Cr^{III}(d^3, S = 3/2) and two SQ ligands (S = 1/2). In addition, the compounds have a contribution of the paramagnetic TMT-$TTF^{\bullet+}$ (**2**), and $TMTSF^{\bullet+}$ (**3**–**4**) cations and weak intermolecular magnetic interactions were recognized from the decrease of the $\chi_m T$ values at low temperature.

Introduction

Transition metal complexes with *o*-quinone ligands have been the subject of intensive research in the last few decades, because these complexes afford a rich redox chemistry based on a variety of formal oxidation states not only for the metal center but also for the ligand moiety.[1] In particular, most intriguing are valence tautomerism and ligand-based mixed-valence ligands, attributable to the contiguity of the frontier orbital energy of the metal center and the ligands.[2] The latter series are related, in a sense, to a class of complexes with mixed-valence metal ions linked by a bridging ligand.

The homoleptic tris(*o*-semiquinonate) chromium(III) complexes $Cr^{III}(Cl_4SQ)_3$ (Cl_4SQ = tetrachloro-*o*-semiquinonate), $Cr^{III}(phenSQ)_3$ (phenSQ = 9,10-phenanthrenesemiquinonate), and $Cr^{III}(3,5\text{-}DTBSQ)_3$ (3,5-DTBSQ = 3,5-di-*tert*-butyl-*o*-semiquinonate) undergo both oxidation and reduction reactions to afford a seven-membered redox series in which complexes having mixed-valence ligands are involved. During the redox process, the oxidation state +3 for the chromium ion is retained (Scheme 1).[3]

Scheme 1

$$[Cr^{III}(X_4BQ)_3]^{3+} \rightleftharpoons [Cr^{III}(X_4BQ)_2(X_4SQ)]^{2+} \rightleftharpoons [Cr^{III}(X_4BQ)(X_4SQ)_2]^{+}$$

(BQ = benzoquinone)

$$\rightleftharpoons \quad Cr^{III}(X_4SQ)_3 \quad \rightleftharpoons$$

(X = Cl and Br)

(Cat = catecholate)

$$[Cr^{III}(X_4SQ)_2(X_4Cat)]^{-} \rightleftharpoons [Cr^{III}(X_4SQ)(X_4Cat)_2]^{2-} \rightleftharpoons [Cr^{III}(X_4Cat)_3]^{3-}$$

Among the redox isomers, the structural and physical properties of $Cr^{III}(Cl_4SQ)_3$, $Cr^{III}(3,5\text{-}DTBSQ)_3$, and $[Cr^{III}(Cat)_3]^{3-}$ (Cat = catecholate) have been characterized in detail,[3,4] whereas the intermediate species, generally written as $[Cr^{III}(SQ)_2(Cat)]^{-}$ and $[Cr^{III}(SQ)(Cat)_2]^{2-}$, have not been isolated and characterized X-ray crystallographically. Of the reported complexes, $Cr^{III}(Cl_4SQ)_3$ shows stepwise ligand-based reductions at 0.552, 0.112, and –0.332 V (vs Ag/AgCl/CH_3CN).[5] The electron-withdrawing effect of the chlorine atoms makes the complex

behaves as a strong electron acceptor. Thus, it is possible to get the intermediate species by utilizing a reducing reagent. As the reducing reagent, the author chose organic donors, tetrakis(metylsulfanyl)tetrathiafulvalene (TMT-TTF), and tetramethyltetraselenafulvalene (TMTSF), and bis(propylenedithio)tetrathiafulvalene (BPDT-TTF), which are well known to form a number of charge-transfer (CT) compounds (Chart 1). This chapter describes crystal structures and spectroscopic and magnetic properties of ligand-based mixed-valence $[Cr^{III}(X_4SQ)_2(X_4Cat)]^-$ (X = Cl and Br) complexes isolated as CT compounds.

Chart 1

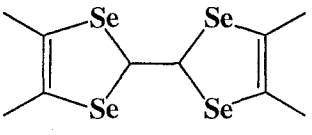

tetramethyltetraserenafulvalene
(TMTSF)

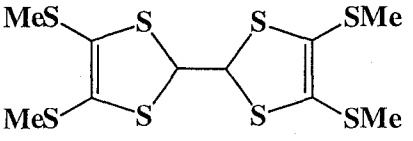

tetrakis(methylthio)tetrathiafulvalene
(TMT-TTF)

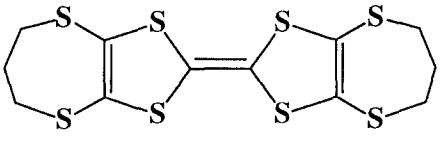

bis(propylenedithio)tetrathiafulvalene
(BPDT-TTF)

Experimental Section

Materials.

All chemicals were reagent grade. TMTSF was obtained from Aldrich. TMT-TTF and BPDT-TTF were purchased from Tokyo Chemical Industry Co., Ltd. $Cr^{III}(X_4SQ)_3 \cdot 4C_6H_6$ (X = Cl and Br) were prepared by the procedure described in Chapter 1.

Preparation of the Compounds.

(TMT-TTF)[$Cr^{III}(Cl_4SQ)_2(Cl_4Cat)$] (1) Polycrystalline sample was obtained by the direct reaction between TMT-TTF and $Cr^{III}(Cl_4SQ)_3$. A carbondisulfide solution (200 ml) of $Cr^{III}(Cl_4SQ)_3 \cdot 3.5C_6H_6$ (520 mg, 0.489 mmol) was added to a carbondisulfide solution (200 ml) of TMT-TTF (190 mg, 0.489 mmol) under the atmosphere. The mixture was allowed to stand for 3 days. The solid product was collected by filtration and washed with carbondisulfide. The powder was dried under the reduced pressure. Yield 545 mg (95 %). Found: C, 28.60; H, 0.84. $C_{28}H_{12}O_6S_8Cl_{12}Cr$ requires C, 28.54; H, 1.03. IR (KBr): 1472m, 1425m, 1399s, 1350w, 1317s, 1248m, 1201s, 1110s, 1038w, 981s, 798m, 780m, 690w, 580w, 459m, and 421w cm^{-1}.

(TMT-TTF)[$Cr^{III}(Br_4SQ)_2(Br_4Cat)$]·$C_6H_5CH_3$ (2·$C_6H_5CH_3$) Single crystals of compound **2**·$C_6H_5CH_3$ were grown from a layered solution of a carbondisulfide solution of $Cr^{III}(Br_4SQ)_3 \cdot 4C_6H_6$ (0.369 mM) and a toluene solution of TMT-TTF (0.369 mM). Black cubic crystals were obtained after two weeks. They readily loose solvate molecules under the atmosphere to give a desolvated compound (**2**) which is insoluble in common organic solvents. Found: C, 18.95; H, 0.90. $C_{28}H_{12}Br_{12}CrO_6S_8$ requires C, 18.99; H, 0.68. IR (KBr): 1472w, 1450w, 1418m, 1396s, 1315m, 1290m, 1250s, 1209m, 1159s, 1125s, 935s, 752m, 702s, 623w, 561w, 503w, and 476w cm^{-1}.

(TMTSF)[$Cr^{III}(Cl_4SQ)_2(Cl_4Cat)$]·1/2$CH_2Cl_2$ (3·1/2CH_2Cl_2) Single crystals of **3**·1/2CH_2Cl_2 were grown from a layered solution with a carbondisulfide solution of $Cr^{III}(Cl_4SQ) \cdot 4C_6H_6$ (0.200 mM) and a dichloromethane solution of TMTSF (0.200 mM). Dark green cubic crystals were obtained after two weeks. Found: C, 26.69; H, 1.14. $C_{28.5}H_{13}O_6Cl_{12}CrSe_4$ requires C, 26.74; H, 1.02. IR (KBr): 1541m, 1471m, 1437m, 1377w,

1329s, 1259s, 1116s, 981s, 920w, 796s, 739w, 690s, 576m, and 493s cm^{-1}.

(TMTSF)[$Cr^{III}(Br_4SQ)_2(Br_4Cat)$]·2$CH_2Cl_2$ (4·2CH_2Cl_2) Single crystals of compound **4**·2CH_2Cl_2 were grown from a layered solution of a carbondisulfide solution of $Cr^{III}(Br_4SQ)_3$·4C_6H_6 (0.58 mM) and a dichloromethane solution of TMTSF (0.58 mM). Dark green cubic crystals were obtained after three weeks which readily lose solvent under the atmosphere to give a desolvated compound **4** as well as **2**·$C_6H_5CH_3$. The compound is insoluble in common organic solvents. Found: C, 18.95; H, 0.90. $C_{28}H_{12}Br_{12}CrO_6Se_4$ requires C, 18.99; H, 0.68. IR (KBr): 1545m, 1474w, 1450m, 1427m, 1334m, 1282w, 1250m, 1209w, 1095s, 933s, 752m, 696s, 623w, 559w, and 501w cm^{-1}.

(BPDT-TTF)[$Cr^{III}(Cl_4SQ)_2(Cl_4Cat)$]·1/2$C_6H_6$ (5) Single crystal of **5** was grown from a layered solution of a carbondisulfide solution of $Cr^{III}(Cl_4SQ)_3$·4C_6H_6 (81 mg, 0.227 mM) and a benzene solution of BPDT-TTF (60 mg, 0.481 mM). Black plate shape crystals were obtained after a week. The powder sample was prepared by the mixing of a 200 ml hot benzene solution of BPDT-TTF (40 mg, 0.0969 mmol) and a 50 ml carbondisulfide solution of $Cr^{III}(Cl_4SQ)_3$·4C_6H_6 (107 mg, 0.0971 mmol). The mixture was stirred for a minute and allowed to stand for a day, then, filtered and washed with carbondisulfide several times. The powder was dried in vacuum. Yield 98 mg (81 %). Found: C, 32.22; H, 1.27, $C_{33}H_{15}Cl_{12}CrO_6S_8$ requires C, 31.93; H, 1.22. IR (KBr): 1472m, 1427s, 1420s, 1408s, 1392s, 1311s, 1275m, 1246w, 1122s, 985s, 904w, 898w, 861w, 797s, 690m, 678m, 623w, 580w, 548w, 525w, 506w, 460s, 421m, 417m, 387w, 368w, and 358w cm^{-1}.

(BPDT-TTF)[$Cr^{III}(Br_4SQ)_2(Br_4Cat)$]·1/2$C_6H_6$ (6) The powder sample was prepared by mixing of a 200 ml hot benzene solution of BPDT-TTF (40 mg, 0.097 mg) and a 100 ml carbondisulfide solution of $Cr^{III}(Br_4SQ)_3$·4C_6H_6 (158 mg, 0.0966 mmol). The mixture was stirred for a minute and allowed to stand for a day, then, filtered and washed with carbondisulfide several times. The powder was dried in vacuum. Yield 150 mg (87 %). Found: C, 21.90; H, 0.92. $C_{33}H_{15}Br_{12}CrO_6S_8$ requires C, 22.33; H, 0.85. IR (KBr): 1515m, 1504w, 1479w, 1450m, 1426s, 1379m, 1300m, 1276s, 1252w, 1236m, 1211w, 1157s, 1119s, 1035m, 1004w, 933s, 902w, 862w, 824w, 810w, 751m, 740m, 688m, 622w, 610w, 561w, 523w, 504w, 478w, 420w, and 407w cm^{-1}.

Physical Measurements.

For compounds **2**·$C_6H_5CH_3$ and **4**·$2CH_2Cl_2$ the desolvated samples, **2** and **4**, were used for physical measurements. Infrared spectra for KBr pellets were recorded on a Hitachi I-5040 FT-IR spectrometer over the range 350–7000 cm^{-1} at room temperature. Absorption spectra on the KBr pellets on a Hitachi U-3500 spectrophotometer over the range from 3130–30000 cm^{-1} at room temperature. The EPR spectra were recorded on finely ground powders enclosed in a quartz tube at X-band frequency with a JEOL RE-3X spectrometer operating 9.0–9.5 GHz. The resonance frequency was measured on an Anritsu MF76A microwave frequency counter. Magnetic field was calibrated by an Echo Electronics EMF-2000AX NMR field meter. Magnetic susceptibilities were recorded over the temperature range from 1.9 to 300 K at 1 T with a superconducting quantum interference device (SQUID) susceptometer (Quantum Design, San Diego, CA) interfaced with a HP Vectra computer system. All values were corrected for diamagnetism that were calculated from Pascal's table.[6]

Crystallographic Data Collection and Refinement of Structures.

Crystal structure determinations were carried out for complexes **2**·$C_6H_5CH_3$, **3**·$1/2CH_2Cl_2$, **4**·$2CH_2Cl_2$, and **5**. All measurements except for **5** were made on a Rigaku AFC7R diffractometer with graphite-monochromated Mo Kα radiation and a rotating anode generator. Unit cell constants and an orientation matrix for data collection were obtained from least-squares refinements using the setting angles of 25 carefully centered reflections in the ranges $29.14° < 2\theta < 29.98°$ (**1**·$C_6H_5CH_3$), $29.53° < 2\theta < 29.98°$ (**3**·$1/2CH_2Cl_2$), and $24.09° < 2\theta < 32.19°$ (**4**·$2CH_2Cl_2$). For compound **5**, the measurements were made on a Rigaku mercury diffractometer with CCD two-dimensional detector with Mo Kα radiation employing a graphite monochromator at 296 K. The size of the unit cell was calculated from the reflections collected on the setting angles of four frames by changing ω by 0.5° for each frame. Two different χ settings were used and ω was changed by 0.5° per frame. Intensity data were collected in 462 frames with an ω scan width of 0.5° and exposure time 150 s. Empirical absorption correction

using the program REQABA[7] was performed for all the data. All the crystal data are summarized in Table 1. The structures were solved by direct methods[8] and expanded using Fourier techniques.[9] The final cycles of the full-matrix least-squares refinements were based on the observed reflections ($I > 3\sigma$ (I)). All the calculations were performed using the teXsan crystallographic software package of Molecular Structure Corporation.[10] All hydrogen atoms were placed in the idealized positions, but their parameters were not refined. The non-hydrogen atoms were refined anisotropically except for the toluene (**2**·$C_6H_5CH_3$) and dichloromethane molecules (**3**·1/2CH_2Cl_2 and **4**·2CH_2Cl_2). In **2**·$C_6H_5CH_3$ the disorder of the toluene molecule was found at the final stage, and thus its atom positions were isotropically refined under a rigid condition. For compounds **3**·1/2CH_2Cl_2 and **4**·2CH_2Cl_2, the positions of the dichloromethane molecules, C(29), Cl(13), and Cl(14) (**3**·1/2CH_2Cl_2) and C(29), C(30), and Cl(1)–Cl(4) (**4**·2CH_2Cl_2), were determined from a Fourier map, but not refined.

Table 1. Crystallographic and Refinement data for **2**·$C_6H_5CH_3$, **3**·1/2CH_2Cl_2, **4**·2CH_2Cl_2, and **5**

	2·$C_6H_5CH_3$	**3**·1/2CH_2Cl_2	**4**·2CH_2Cl_2	**5**
Formula	$C_{35}H_{20}Br_{12}CrO_6S_8$	$C_{28.5}H_{13}Cl_{13}CrO_6Se_4$	$C_{30}H_{16}Br_{12}Cl_4CrO_6Se_4$	$C_{33}H_{15}Cl_{12}CrO_6S_8$
Formula weight	1803.86	1280.14	1940.95	1241.39
Color	black	dark green	dark green	black
Crystal size, mm	0.05×0.05×0.01	1×0.25×0.20	0.75×0.30×0.20	0.14×0.13×0.1
Crystal system	triclinic	monoclinic	triclinic	triclinic
Space group	$P\bar{1}$	$P2_1/n$	$P\bar{1}$	$P\bar{1}$
a, Å	14.303(2)	12.472(3)	13.523(6)	12.8835(5)
b, Å	15.084(3)	17.451(4)	16.177(8)	13.309(2)
c, Å	12.907(5)	18.815(5)	12.406(7)	14.538(1)
α, °	109.62 (2)		111.43(4)	88.672(3)
β, °	99.31(2)	101.80(2)	109.39(4)	84.580(2)
γ, °	91.86(2)		83.91(4)	65.580(1)
Z	2	4	2	2
V, Å^3	2577(1)	4008(1)	2382(2)	2262.5(3)
ρ_{calc}, g/cm^3	2.324	2.121	2.705	1.822
μ, cm^{-1}	99.19	48.26	136.531	13.74
T, K	296	296	296	297
No. observations	3658	4150	3232	4203
No. parameters	503	461	460	541
Refls./para. ratio	7.27	9.00	7.03	7.77
GOF	2.24	1.82	1.98	2.41
R_{int}	0.053	0.056	0.081	0.059
R, R_w [a]	0.063, 0.064	0.045, 0.033	0.057, 0.058	0.059, 0.062

[a] $R = \Sigma||F_0|-|F_0||/\Sigma|F_0|$, $R_w = [\Sigma(|F_0|-|F_0|)^2/\Sigma w|F_0|^2)]^{1/2}$.

Results and Discussion

Molecular Structures.

Figures 1–3 show ORTEP[11] drawings of **2**·$C_6H_5CH_3$, **3**·1/2CH_2Cl_2, **4**·2CH_2Cl_2, and **5** with the atom numbering schemes. Compounds **3**·1/2CH_2Cl_2 and **4**·2CH_2Cl_2 contain one crystallographically independent TMTSF molecule, while **2**·$C_6H_5CH_3$ and **5** have two crystallographically independent TMT-TTF and BPDT-TTF molecules, respectively, which are designated as **A** and **B**. Each compound contains one crystallographically independent $Cr(C_6O_2X_4)_3$ complex where the three ligands are denoted **I**, **II**, and **III**.

Cationic molecules In Tables 2–4 the bond distances of cationic molecules are compared with the corresponding distances found in other compounds. The central C–C bond distance of TTF skeleton in general is most sensitive to the oxidation state of the molecules.[12] The values are 1.38(4) and 1.42(5) Å for TMT-TTF (**A**) and TMT-TTF (**B**) molecules, respectively, longer than those of neutral molecules and comparable to those of 1:1 CT compounds, (TMT-TTF)$^+$·$[FeCl_4]^-$ and (TMT-TTF)$^+$·$[IBr_2]^-$. These features indicate that all the TMT-TTF

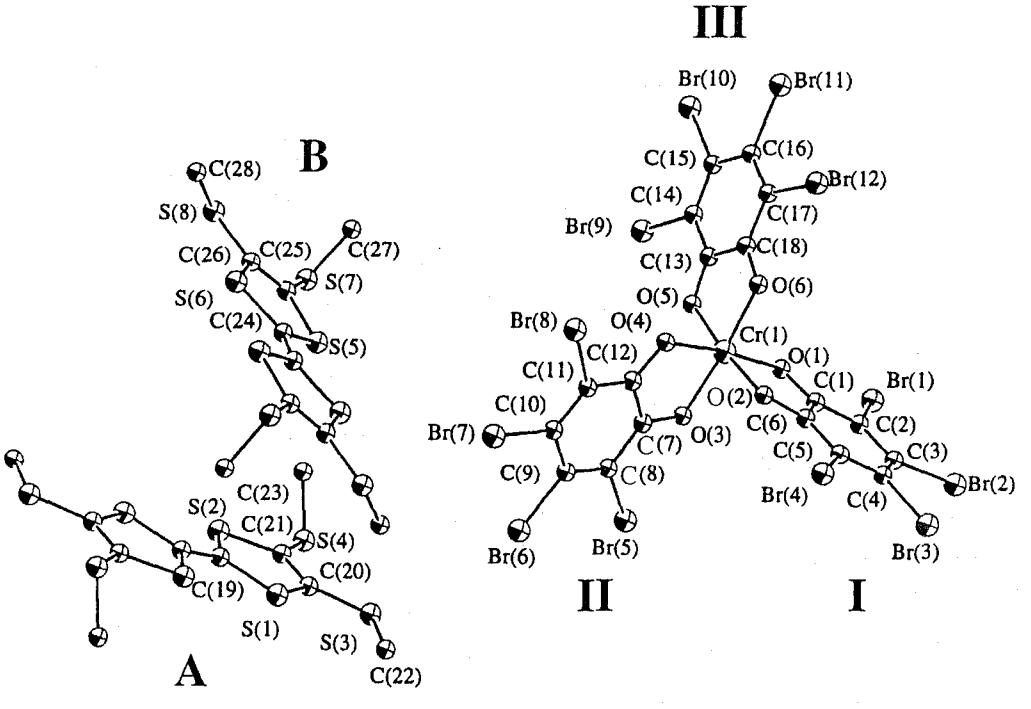

Figure 1. An ORTEP drawing of **2**·$C_6H_5CH_3$ with hydrogen atoms and solvent molecule omitted (showing 30% isotropic thermal ellipsoids). TMT-TTF molecules **A** and **B** have their centroids coincident with crystallographic symmetry. Crystallographically independent three ligands are designated **I**, **II**, and **III**.

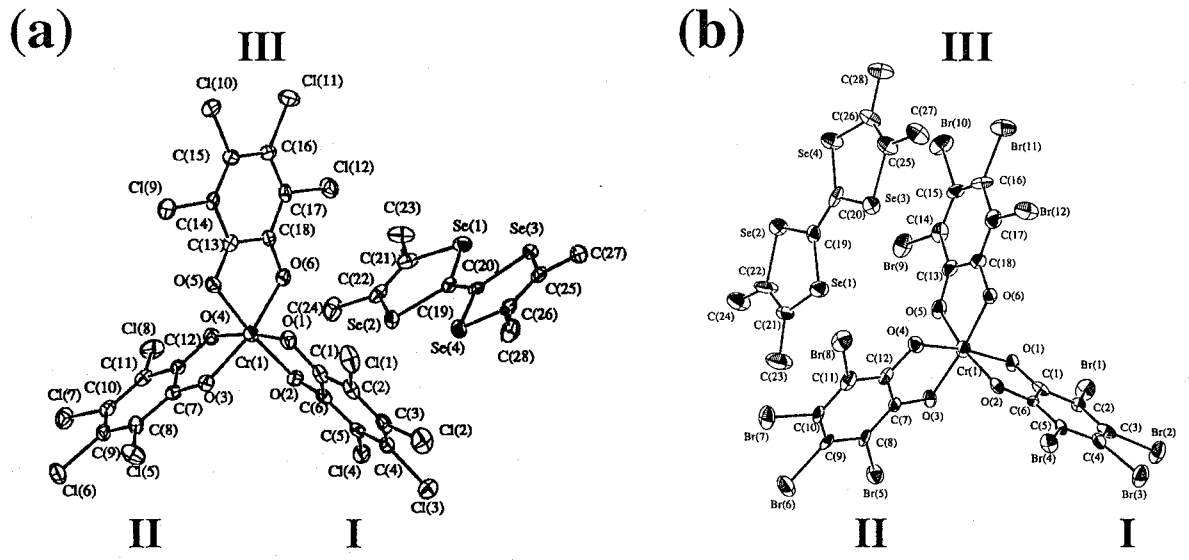

Figure 2. ORTEP drawing of (a) $3 \cdot 1/2CH_2Cl_2$ and (b) $4 \cdot 2CH_2Cl_2$ with hydrogen atoms and solvent molecules omitted (showing 30% anisotropic thermal ellipsoids). Crystallographically independent ligands are designated **I**, **II**, and **III**.

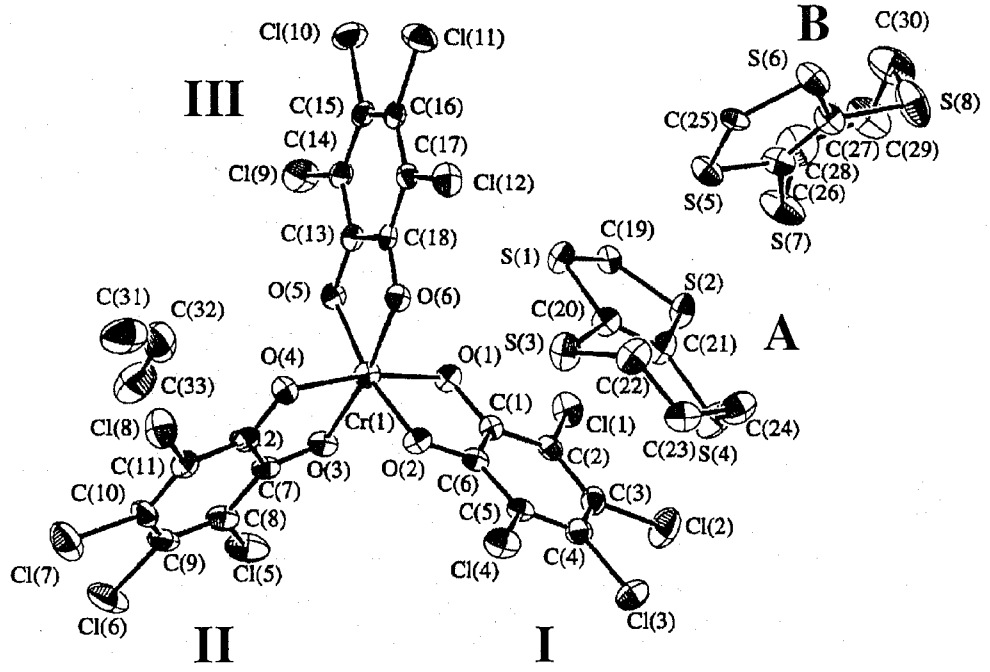

Figure 3. An ORTEP drawing of **5** with hydrogen atoms and solvent molecules omitted (showing 30% anisotropic thermal ellipsoids). Two BPDT-TTF molecules and benzene have their centroids coincident with crystallographic symmetry. Crystallographically independent ligands are designated **I**, **II**, and **III**.

Table 2. Comparison of Intramolecular Bond Distances (Å) and Estimated Charge (Q) for TMT-TTF$^{\delta+}$ Compounds and Those of **2**·$C_6H_5CH_3$

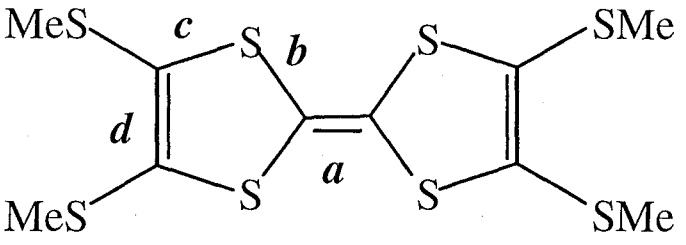

compound	*a*	*b*	*c*	*d*	*Q*
$(TMT\text{-}TTF)_2$·TCNQ[a]	1.348(4)	1.748(3)	1.749(3)	1.337(3)	+0.4
TMT-TTF·HCBD[b]	1.382(6)	1.724(4)	1.732(4)	1.364(5)	+0.4–0.6
TMT-TTF·$FeCl_4$[c]	1.380(9)	1.718(9)	1.736(8)	1.354(13)	+1
TMT-TTF·IBr_2[d]	1.392(13)	1.723(11)	1.741(10)	1.357(15)	+1
A	1.38(4)	1.72(2)	1.73(3)	1.33(3)	+1
B	1.42(5)	1.72(3)	1.72(3)	1.42(4)	+1

[a] Reference 13(a). [b] Reference 13(b), HCBD = hexacyanobutadien. [c] Reference 13(c). [d] Reference 13(d).

Table 3. Comparison of Intramolecular Bond Distances (Å) and Estimated Formal Charge (Q) for TMTSF$^{\delta+}$ Compounds and Those of **3**·1/2CH_2Cl_2 and **4**·2CH_2Cl_2

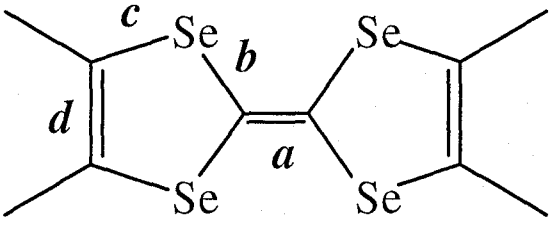

compound	*a*	*b*	*c*	*d*	*Q*
TMTSF[a]	1.352(9)	1.892	1.906	1.315	0
$(TMTSF)_3[Pt(CN)_4]$[b]	1.352(11) 1.373(11)	1.878(8) 1.859(8)	1.901(8) 1.887(8)	1.323(12) 1.346(11)	+1/3
$(TMTSF)_2PF_6$[c]	1.369(14)	1.875(10)	1.893(10)	1.329(15)	+1/2
3·1/2CH_2Cl_2	1.381(10)	1.878(8)	1.885(9)	1.32(1)	+1
4·2CH_2Cl_2	1.43(3)	1.84(2)	1.89(2)	1.35(3)	+1

[a] Reference 14(a). [b] Reference 14(b). [c] Reference 14(c).

Table 4. Comparison of Intramolecular Bond Distances (Å) and Estimated Formal Charge (Q) for BPDT-TTF$^{\delta+}$ Compounds and Those of **5**

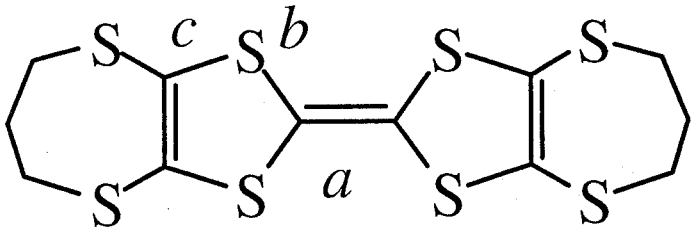

compound	*a*	*b*	*c*	*Q*
BPDT-TTF[a]	1.34	1.76	1.76	0
$[BPDT\text{-}TTF]_2[ICl_2]$[b]	1.369	1.735	1.746	+1/2
$[BPDT\text{-}TTF]_3[InCl_4]$[c]	1.38	1.72	1.73	+1
A	1.37(1)	1.720(8)	1.733(8)	+1
B	1.37(1)	1.718(8)	1.724(9)	+1

[a] Reference 15(a). [b] Reference 15(b). [c] Reference 15(c).

the TMT-TTF molecules in $\mathbf{2}\cdot C_6H_5CH_3$ exist as a mono-cation form, TMT-TTF$^{\bullet+}$. A similar trend for TMTSF (Table 3) and BPDT-TTF (Table 4) are recognized, leading to the formation of the mono-cation, TMTSF$^{\bullet+}$ and BPDT-TTF$^{\bullet+}$, respectively. These mono-cations were also confirmed by the disappearance of the C=C bond vibration modes of the neutral molecules, TMT-TTF^0, TMTSF^0, and BPDT-TTF^0 (Experimental Section). The end-group seven-membered rings of the BPDT-TTF molecules in **5** are in the extended-chair conformation, where four adjacent atoms, e. g., for molecule **A**, S(3), C(20), C(21), and S(4), are approximately in a plane, whereas the remaining three atoms, C(22)–C(24), form a plane that is displaced from but is roughly parallel to the former plane. This is typical for most BPDT-TTF compounds known to date.[15(c),16]

Chromium complexes In all the compounds the environments about the chromium ions are distorted octahedral with six oxygen atoms from the three bidentate $C_6O_2X_4$ ligands. The total oxidation numbers of the anionic complexes are responsible for the combination of SQ and Cat because of the inertness of the chromium center in the redox process.[3,17] In Table 5 the average

values of Cr–O, C–O, and C–C bond distances and O–Cr–O angles are compared with those of $Cr^{III}(Cl_4SQ)_3 \cdot CS_2 \cdot 1/2C_6H_6$. It has been demonstrated that $Cr^{III}(SQ)_3$ undergoes one-, two-, and three-electron reduction to provide the series of $[Cr^{III}(SQ)_{3-n}(Cat)_n]^{n-}$ (n = 1–3) redox isomers.[3(a)] As shown in Chapter 4, the mean C–O bond distances and O–Cr–O angles are most particularly sensitive to the charge states of the complexes, which increase with the numbers of n. Inspection of Table 5 reveals that the total average C–O distance and O–Cr–O angle of all the compounds are larger than those of $Cr^{III}(Cl_4SQ)_3$, supporting that one of the three SQ ligands is reduced to Cat form. The structural parameters of all the compounds are similar to each other indicative of the formation of the $[Cr^{III}(X_4SQ)_2(X_4Cat)]^-$ complex. This is also substantiated by spectroscopic data shown below.

There have been many mixed-ligand complexes in the series $[M^{III}(N\text{-}N)(SQ)(Cat)]$ (N-N = bidentate nitrogen co-ligand, M = Fe or Co)[18] and $[V^{V}O(3,5\text{-DTBSQ})(3,5\text{-DTBCat})]_2$,[19] (3,5-DTBCat = 3,5-di-*tert*-butylcatecholate), which show crystallographically well-distinguished mixed-charge states for the SQ and the Cat. On the other hand, two examples for homoleptic complexes, $[Ni^{II}(3,6\text{-DTBBQ})(3,6\text{-DTBSQ})_2]$[20] and $[Mn^{IV}(3,6\text{-DTBSQ})_2(3,6\text{-DTBCat})]$,[21] have been found. Of the compounds obtained in this work, $\mathbf{2}\cdot C_6H_5CH_3$ and **5** appear to show mixed-charge electronic structures between ligand **I** (Cat) and **II–III** (SQ). However, for other compounds, the distinction between the SQ and the Cat is difficult because of crystallographic disorder.[18,22] For $\mathbf{3}\cdot 1/2CH_2Cl_2$ and $\mathbf{4}\cdot 2CH_2Cl_2$ clear assignments could be made by further quantitative structural analysis with greater precision. Nevertheless, the spectroscopic and magnetic susceptibility data support the presence of two SQs and one Cat in the anionic complexes (see below). Thus, hereafter, the anionic chromium complexes are written as $[Cr^{III}(X_4SQ)_2(X_4Cat)]^-$ without the assignment of the oxidation state to the each ligand.

Table 5. Total Average Bond Distances (Å) and Angles (°) and Charge for Anionic Chromium Complexes in **2**·$C_6H_5CH_3$, **3**·1/2CH_2Cl_2, **4**·2CH_2Cl_2, and **5**

	L	**2**·$C_6H_5CH_3$	**3**·1/2CH_2Cl_2	**4**·2CH_2Cl_2	**5**	$Cr^{III}(Cl_4SQ)_3$[a]
Cr–O (Å)	**I**	1.92(1)	1.926(6)	1.93(1)	1.916(5)	
	II	1.95(2)	1.951(5)	1.96(1)	1.947(5)	
	III	1.96(2)	1.964(5)	1.93(1)	1.943(5)	
total average		1.95(2)	1.947(5)	1.94(1)	1.935(5)	1.949(5)
C–O (Å)	**I**	1.34(2)	1.315(9)	1.31(2)	1.313(9)	
	II	1.28(2)	1.298(9)	1.29(2)	1.296(9)	
	III	1.26(3)	1.288(9)	1.31(2)	1.284(8)	
total average		1.29(2)	1.300(9)	1.30(2)	1.297(9)	1.280(1)
C–C (Å)	**I**	1.39(3)	1.40(1)	1.40(3)	1.40(1)	
	II	1.40(3)	1.41(1)	1.40(3)	1.40(1)	
	III	1.42(3)	1.40(1)	1.41(3)	1.40(1)	
total average		1.40(3)	1.40(1)	1.40(3)	1.40(1)	1.40(1)
O–Cr–O (°)	**I**	84.3(6)	84.1(4)	82.3(6)	83.8(2)	
	II	82.3(5)	82.2(2)	81.7(5)	81.9(2)	
	III	81.0(6)	81.7(2)	83.4(6)	81.7(2)	
total average		82.4(6)	82.7(3)	82.5(6)	82.5(2)	81.8(2)
charge		**−1**	**−1**	**−1**	**−1**	**0**

[a] Reference 4(a).

Crystal packing.

Compound $2{\cdot}C_6H_5CH_3$ As shown in Figure 4(a) the crystal structure of compound $2{\cdot}C_6H_5CH_3$ clearly shows a two-membered alternating stack of the TMT-TTF$^{\bullet+}$ cation and the $[Cr^{III}(Br_4SQ)_2(Br_4Cat)]^-$ complex along the [110] direction, typical of 1:1 CT compounds.[23] The mean separation between the ligand **I** and the TMT-TTF$^{\bullet+}$ (**A**) and (**B**) cations is alternately 3.671 and 3.421 Å. The least-square planes of the TMT-TTF$^{\bullet+}$ cations are tilted with respect to that of ligand **I** by 10.63°(**A**) and 6.67°(**B**), respectively, and the two TMT-TTF$^{\bullet+}$ cations form staggered conformation each other. The remaining ligands (**II** and **III**) sit alternately on both sides of the chain to form an additional homoleptic one-dimensional chain structure of the $[Cr^{III}(X_4SQ)_2(X_4Cat)_2]^-$ as shown in Figure 4(b). The chain is characterized by alternating arrangements of the Δ and Λ enantiomers, indicating stacking interactions between [**II**···**II'**] and [**III**···**III'**]. The mean interplanar distances are listed in Table 6. Both pairs have a well-overlapping region regarding each six-membered ring, irrespecting of a slight slip. The mean interplanar distances are 3.507 and 3.473 Å for [**II**···**II'**] and [**III**···**III'**], respectively, which are slightly larger than 3.22 (Cl), 3.47 (Cl), and 3.37 (Br) Å found for CT compounds of *p*-X_4BQ.[24] Further, there are three types of intermolecular atomic contacts between cation···anion, cation···cation, and anion···anion pairs. Table 6 lists five cation···anion pairs between the sulfur atoms of the TMT-TTF$^{\bullet+}$ cation and the bromine atoms of the $[Cr^{III}(Br_4SQ)_2(Br_4Cat)]^-$ complex. The S···Br contacts are in the range of 3.596(7)–3.741(6) Å, which are all shorter than the sum (3.80 Å) of van der Waals radii of the two atoms. The cation···cation interaction of S(3)···S(3*) (3.23(1) Å), shorter than the sum (3.70 Å) of van der Waals radii, is found for the methylsulfanyl groups of the TMT-TTF$^{\bullet+}$ cations between the mixed-stack chain, and six anion···anion interactions between the bromine atoms are also found.

Compounds $3{\cdot}1/2CH_2Cl_2$ and $4{\cdot}2CH_2Cl_2$ In compounds $3{\cdot}1/2CH_2Cl_2$ and $4{\cdot}2CH_2Cl_2$, TMTSF molecules form face-to face dimers with the short intermolecular contacts between the selenium atoms; 3.598(1) (Se(1)-Se(4*)) and 3.582(1) Å (Se(2)-Se(3*)) and 3.697(4) (Se(1)–Se(4*)) and 3.752(4) Å (Se(2)–Se(3*)) for $3{\cdot}1/2CH_2Cl_2$ and $4{\cdot}2CH_2Cl_2$, respectively. These distances are shorter than the sum of van der Waals radii (4.00 Å) of the two selenium atoms,

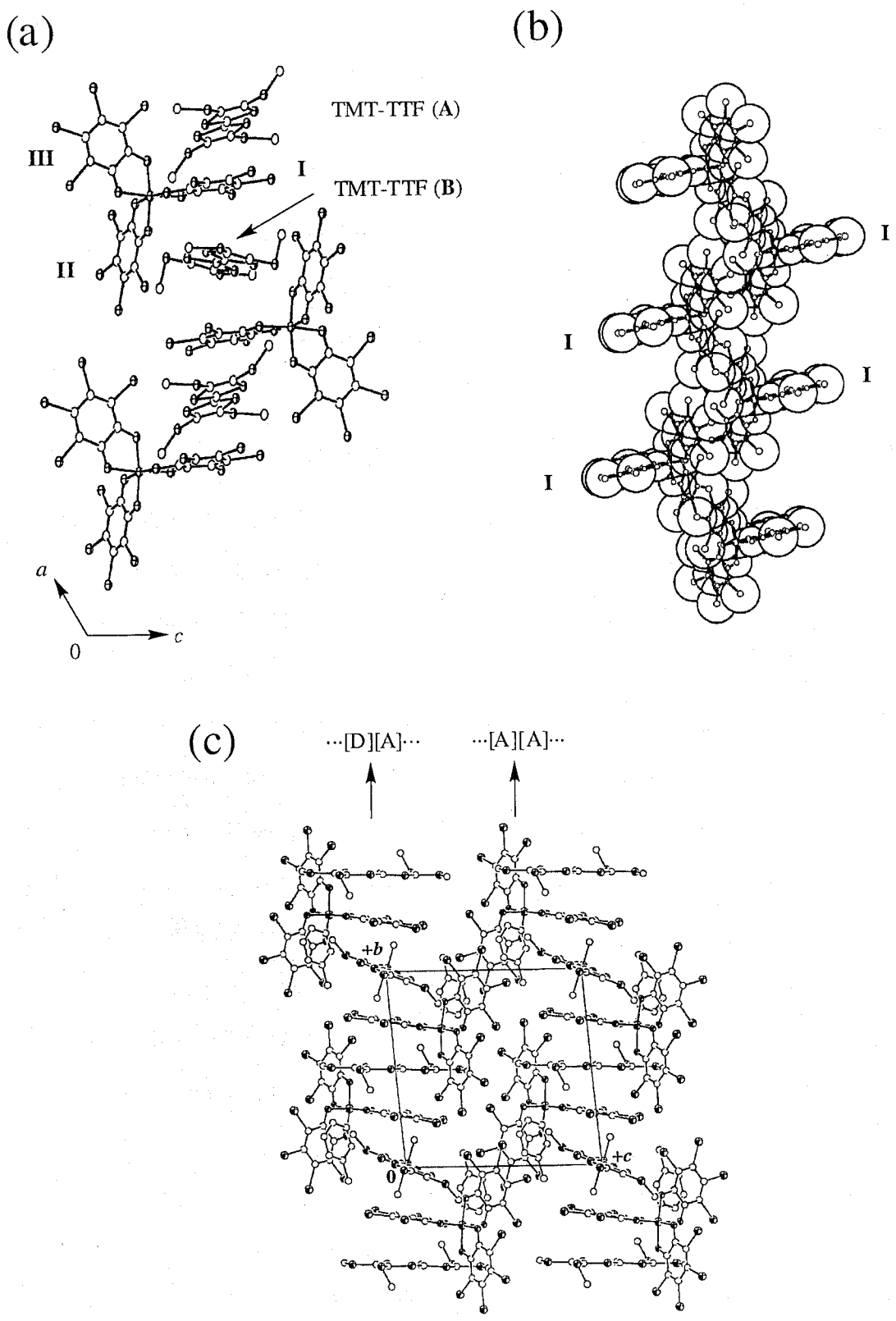

Figure 4. (a) One-dimensional two-membered alternating stacks between TMT-TTF$^{\bullet+}$ cations and $[Cr^{III}(Br_4SQ)_2(Br_4Cat)]^-$ complexes, (b) space-filling representation of one-dimensional chain structure of $[Cr^{III}(Br_4SQ)_2(Br_4Cat)]^-$ complexes, and (c) projection of whole crystal packing structure of $\mathbf{2}\cdot C_6H_5CH_3$ along the *a*-axis.

Table 6. Parameters for Intermolecular Stacking Arrangements and X···X Contacts between the Anions in **2**·$C_6H_5CH_3$, **3**·1/2CH_2Cl_2, **4**·2CH_2Cl_2, and **5**

compound		interplanar distance (Å)	intermolecular atomic contacts distance (Å)			
2·$C_6H_5CH_3$	**II···II'**	3.507	Br(1)···S(2*)[a]	3.741(6)	Br(4)···S(5*)[b]	3.698(8)
	III···III'	3.473	Br(7)···S(4*)[c]	3.596(7)	Br(8)···S(8*)[d]	3.634(8)
			Br(12)···S(6*)[b]	3.726(9)	Br(2)···Br(5*)[e]	3.508(3)
			Br(2)···Br(8*)[f]	3.789(3)	Br(2)···Br(11*)[g]	3.824(5)
			Br(5)···Br(11*)[h]	3.629(4)	Br(6)···Br(11*)[h]	3.704(4)
			Br(8)···Br(10*)[i]	3.659(5)	S(3)···S(3*)[b]	3.23(1)
3·1/2CH_2Cl_2	**I···III'**	3.60	Cl(4)···Se(1)[j]	3.600(2)	Cl(5)···Se(3)[k]	3.407(3)
	III···III'	3.44	Cl(6)···Se(2)[f]	3.712(3)	Cl(1)···Cl(6*)[f]	3.539(4)
			Cl(1)···Cl(8*)[l]	3.579(4)	Cl(4)···Cl(4*)[m]	3.473(5)
			Cl(6)···Cl(10*)[n]	3.512(3)	Cl(7)···Cl(12*)[f]	3.533(3)
			Se(1)···Se(4*)[j]	3.598(1)	Se(2)···Se(3*)[j]	3.582(1)
4·2CH_2Cl_2	**I···I'**	3.585	Br(2)···Se(2*)[o]	3.905(4)	Br(4)···Se(1*)[p]	3.681(4)
	II···II'	3.537	Br(4)···Se(4*)[a]	3.849(4)	Br(12)···Se(3*)[o]	3.813(4)
	III···III'	3.566	Br(2)···Br(5*)[q]	3.633(4)	Br(4)···Br(12*)[p]	3.542(4)
			Br(5)···Br(11*)[r]	3.782(4)	Br(6)···Br(9*)[s]	3.559(3)
			Br(6)···Br(11*)[r]	3.747(4)	Br(7)···Br(9*)[a]	3.778(3)
			Br(8)···Br(8*)[t]	3.719(5)	Br(8)···Br(10*)[u]	3.573(3)
			Br(9)···Br(11*)[u]	3.805(4)	Se(1)···Se(4*)[v]	3.697(4)
			Se(2)···Se(3*)[v]	3.752(4)		
5	**III···III'**	3.411	Cl(4)···S(6*)[w]	3.512(3)	Cl(12)···S(1*)[o]	3.438(3)
			Cl(1)···Cl(5*)[x]	3.470(3)	Cl(2)···Cl(11*)[j]	3.515(3)
			Cl(3)···Cl(9*)[y]	3.507(3)	Cl(4)···Cl(6*)[z]	3.420(3)
			Cl(4)···Cl(12*)[aa]	3.320(3)	Cl(6)···Cl(12*)[w]	3.447(3)
			S(3)···S(3*)[ab]	3.637(4)		

[a] $x, y, z-1$. [b] $-x+2, -y, -z+1$. [c] $-x+1, -y, -z+1$. [d] $x-1, y+1, z$. [e] $-x+2, -y, -z$. [f] $x+1, y, z$. [g] $-x+2, -y+1, -z$. [h] $x, y-1, z$. [i] $-x+1, -y+1, -z$. [j] $-x+1, -y, -z$. [k] $-x+1/2, y-1/2, -z+1/2$. [l] $2x, 2y, 2z$. [m] $3x, 3y, 3z$. [n] $-x, -y, -z+1$. [o] x, y, z. [p] $-x, -y+2, -z$. [q] $-x-1, -y+2, -z$. [r] $x-1, y, z-1$. [s] $-x-1, -y+1, -z-1$. [t] $-x, -y+1, -z-1$. [u] $-x, -y+1, -z$. [v] $-x, -y, -z+1$. [w] $x, y, z+1$. [x] $-x+1, y, -z+1$. [y] $x+1, y-1, z$. [z] $-x+2, -y, -z+1$. [aa] $-x+2, -y, -z$. [ab] $-x+2, -y, -z$.

showing a strong dimerization.

Figure 5 shows crystal packing structures of anionic complexes in **3**·1/2CH_2Cl_2. The two-dimensional brick-wall type layer structure of the chromium complexes is recognized. Each brick is constructed from the six complexes with the π···π interactions of the ligand moieties of adjacent molecule. The interactions are found between ligands **I**···**III'** and **III**···**III'** with mean separation of 3.60 and 3.44 Å, respectively (Table 6). As shown in Figure 5(a), two kinds of chains consist of different enantiomer are aligned alternatively along the *b*-axis. Figure 6(a) shows the side view of the layer where ligand **II** points to the direction slightly tilted to the layer. The ligands **II** stack with TMTSF dimers with mean separation of 3.50(1) Å to form three-dimensional crystal structure (Figures 5(b) and 6(b)).

As shown in Figure 7(a) the anionic complexes in **4**·2CH_2Cl_2 form an extended two-dimensional honeycomb network, whose diagonal distance is approximately 12 Å. The layer is made up of mutual stacking arrangements of three ligands with mean separations 3.585 (**I**···**I'**), 3.537 (**II**···**II'**) and 3.566 Å (**III**···**III'**) (Table 6). An analogous honeycomb network has been found in two- or three-dimensional polymeric supramolecular host-guest systems.[25] In these honeycomb layer compounds the cation molecules play an important role in the determination of not only the interlayer separation but also the packing arrangement of the crystals. As shown in Figure 7(b) each cavity is occupied by TMTSF dimer, where the cations can stack on top of each other but with a slight displacement along the long in-plane molecular axis. The molecular plane of the dimer is perpendicularly directed to that of the layer. Each dimer is associated with four anionic complexes through Se···Br contacts in the range 3.681–3.905 Å (Table 6), shorter than the sum (3.95 Å) of van der Waals radii of the two atoms. In addition, the TMTSF dimers stack with ligand **I** where mean separation and dihedral angle are 3.661 Å and 4.38°, respectively. This arrangement makes an alternating stack of the TMTSF dimers and the $[Cr^{III}(Br_4SQ)_2(Br_4Cat)]^-$ complexes ([··[A][D_2]··] type) through the [101] direction (Figure 7(b)). Each dimer is separated by distances of 11 Å through the stacking direction. With respect to the crystal stability, the TMTSF dimers seem to perform an important templating role for the construction of the anionic honeycomb layer. The stabilization is increased by the intermolecular stacking arrangement enhanced by the planarity of the TMTSF molecule and the ligands.

(a)

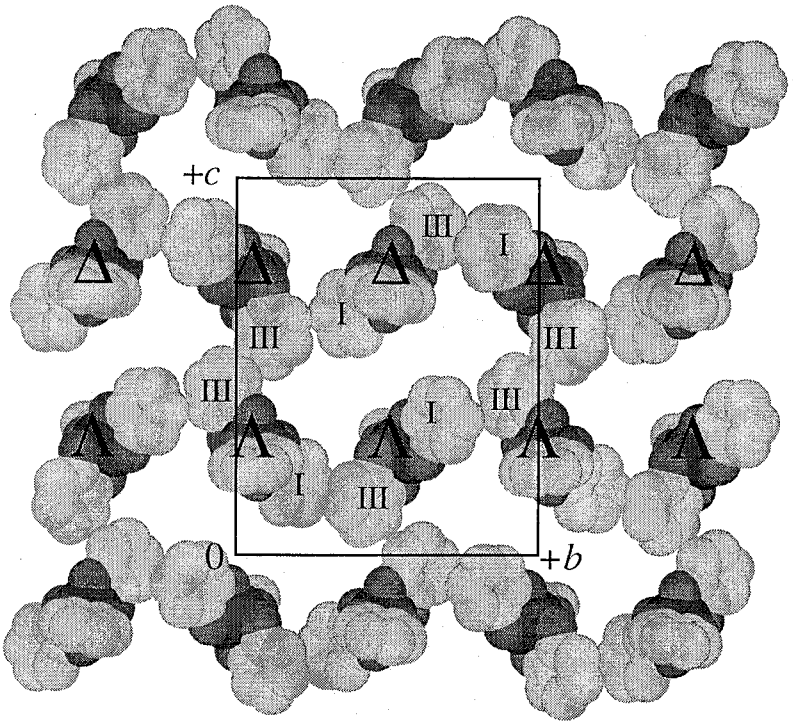

(b)

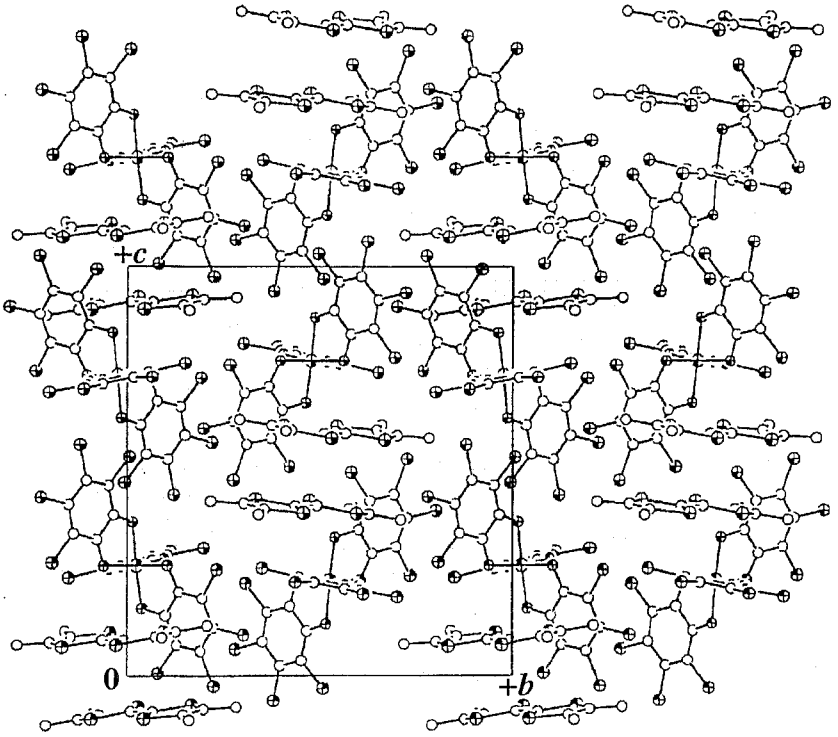

Figure 5. (a) Two-dimensional brick-wall network of $[Cr^{III}(Cl_4SQ)_2(Cl_4Cat)]^-$ anions and (b) projection of whole crystal packing structure of **3**·1/2CH_2Cl_2 along the *a*-axis.

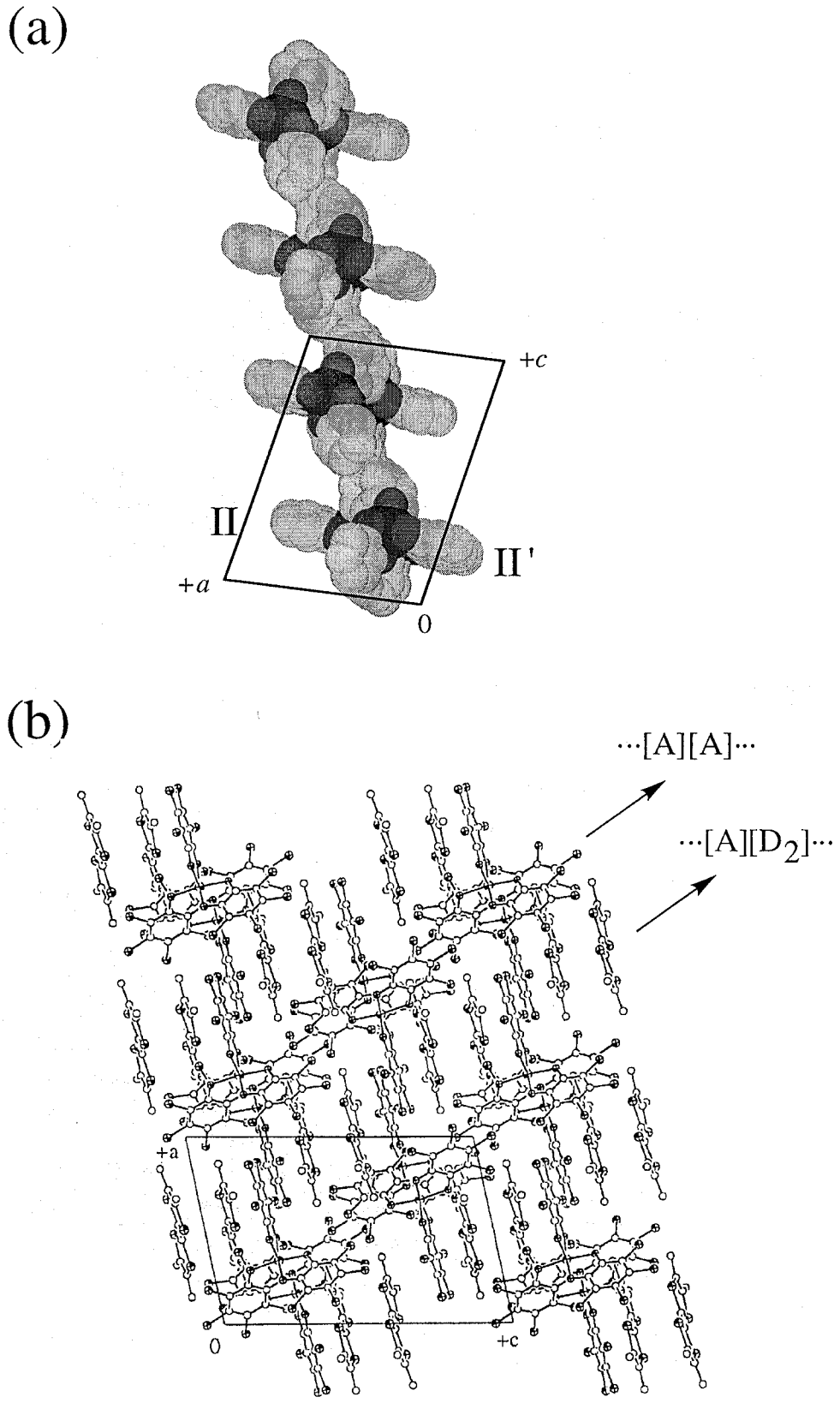

Figure 6. (a) Side view of two-dimensional brick-wall network of $[Cr^{III}(Cl_4SQ)_2(Cl_4Cat)]^-$ anions and (b) projection of whole crystal packing structure of **3**·1/2CH_2Cl_2 along the *b*-axis.

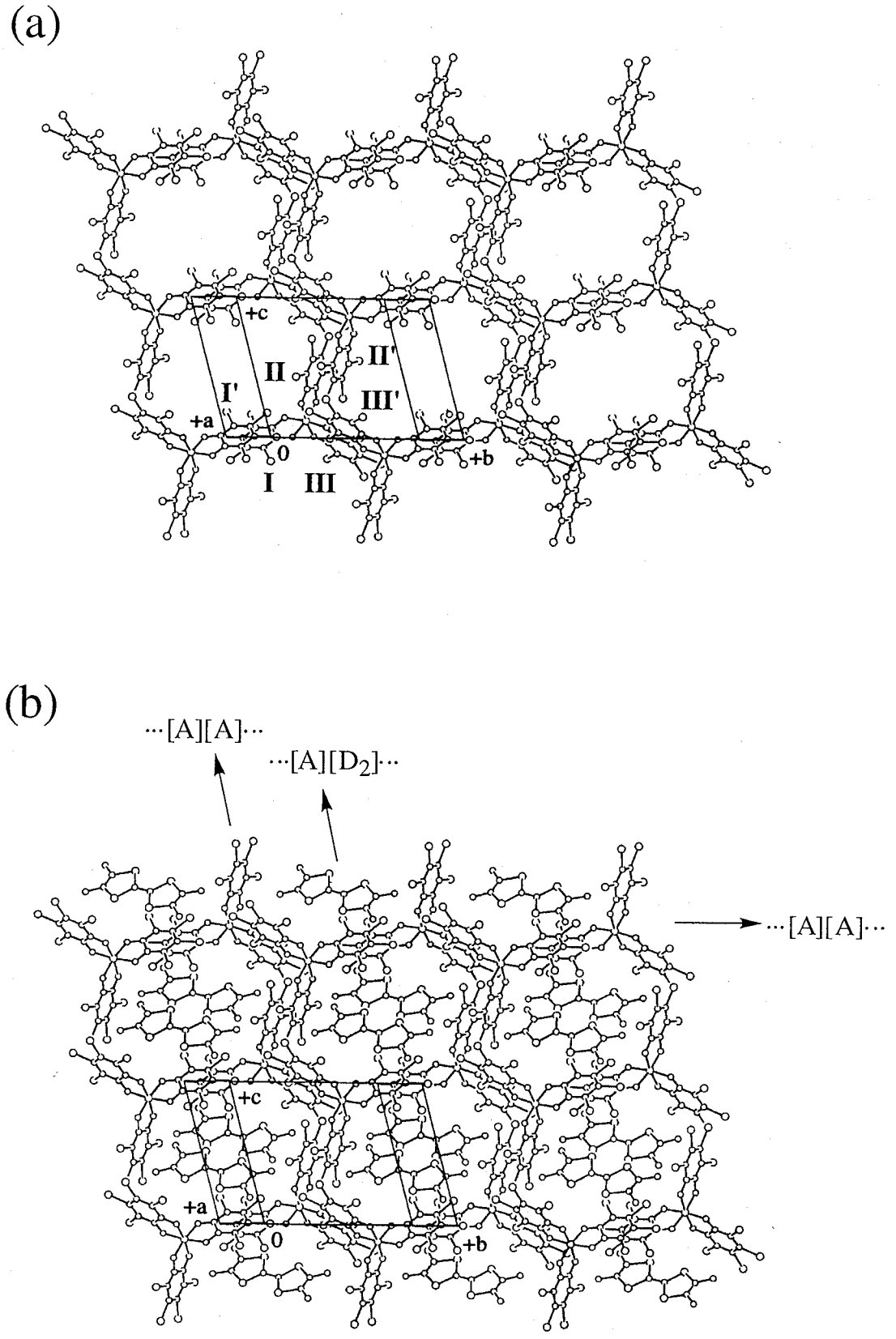

Figure 7. (a) Two-dimensional honeycomb network of $[Cr^{III}(Br_4SQ)_2(Br_4Cat)]^-$ anions and (b) whole crystal packing structure of **4**·$2CH_2Cl_2$.

Compound 5 Figure 8(a) shows crystal packing structure of **5**. A part of crystal structure is composed of two-dimensional layer constructed from two- (···[A][D]···) and three-membered (···[A][D][S]···) mixed-stacking chains, where the three independent heteroleptic π···π contacts of [**I**···BPDT-TTF **A**], [**II**···BPDT-TTF **B**], and [**II**···C_6H_6] are recognized. The dihedral angles between the best planes of them are approximately 4.7° (**I**···**A**), 5.2° (**II**···**B**), and 7.4° (**II**···C_6H_6), respectively, and the intrastack interplaner spacings are found to be 3.60(1) (**I**···**A**), 3.70(1) (**II**···**B**), and 3.41(3) (**II**···C_6H_6) Å, respectively.[26] Further, π···π interactions between the ligand **III** and ligand **III'** of adjacent molecule extend the whole intermolecular interactions two to three dimensional. However, the infinite intermolecular π···π interactions of the chromium complexes found in other compounds could not be found in this compound. This is because of steric hindrance of the seven-membered rings of BPDT-TTF molecule. In addition, the benzene molecules favor to stack with the ligands of the anions to prevent the formation of homoleptic π···π interactions. Consequently, the dimension of π···π interactions of the chromium complexes is lowered. Intermolecular Cl···S and Cl···Cl atomic contacts are also found between the BPDT-TTF and the chromium complexes and between the chromium complexes (Table 6). These contacts are shorter than the sum of van der Waals radius of 3.65 and 3.60 Å, respectively.

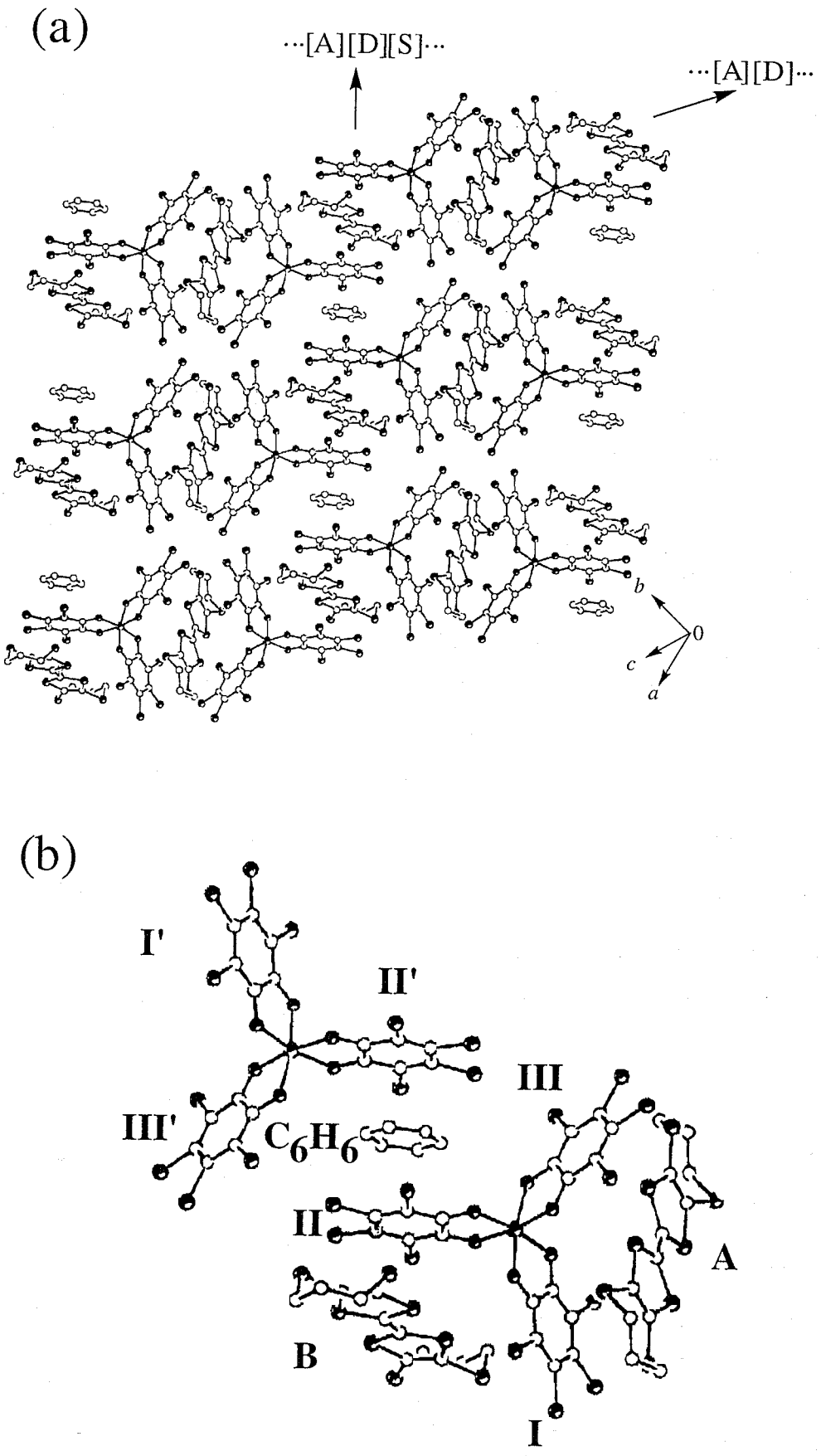

Figure 8. (a) Projection of crystal packing structures and (b) three kinds of mixed-stacks of **5**.

Infrared Spectra.

Figure 9 shows FT-IR spectra of the compounds. All the frequencies are listed in the Experimental Section. As shown in Chapter 1, complexes $Cr^{III}(X_4SQ)_3 \cdot 4C_6H_6$ show asymmetric IR bands near 1460 cm^{-1}, characteristic of SQ. Compounds **1–6** also show the corresponding bands near 1450 cm^{-1}. In addition, all the compounds have bands near 1100 cm^{-1}, which are assigned to C–O vibrational mode of Cat ligand, indicating coexistence of both ligands, SQ and Cat.[27] In the region of 1400–1500 cm^{-1}, all the compounds have bands attributed to central C=C bond vibrational modes of TTF skeleton.

UV-vis-NIR-IR Absorption Spectra.

Absorption spectral parameters for all the compounds are listed in Table 7 and the spectra are given in Figure 10. The spectral patterns of all the compounds in the visible region are similar to solution spectrum of $[Cr^{III}(3,5\text{-DTBSQ})_2(3,5\text{-DTBCat})]^-$ complex, which is electrochemically generated.[3(b)] In addition, they show characteristic absorption bands near 4000 cm^{-1}. The corresponding bands have been observed for a series of valence tautomeric complexes of manganese and cobalt ions at where the maxima of the bands are 4760[18(c),21,22] and 4170 cm^{-1},[2(b)] respectively. These bands are assigned to the intramolecular intervalence transition (IVCT) between Cat and SQ ligands,[2(a)] indicating the presence of both ligands in the complexes. Comparison of the spectra of all the compounds leads to a conclusion that **1–6** have similar electronic structures, attributed to the $[Cr^{III}(X_4SQ)_2(X_4Cat)]^-$ complexes.

EPR Spectra.

Compounds **1–6** afford single EPR signals, independent of the temperature region of 77–300 K. The isotropic g values at 77 K are summarized in Table 7. The powder sample of $(Co^{III}Cp_2)[Cr^{III}(Cl_4SQ)_2(Cl_4Cat)]$, which could be regarded as reference compound with diamagnetic cation, shows a EPR signal at g = 1.972 with a linewidth of 15 G (77 K).[28] The spectrum in a CH_2Cl_2/*n*–PrOH(1:1) glass at the same temperature consists of a signal at g = 1.972 with a linewidth of 5.6 G and hyperfine coupling (^{53}Cr, I = 3/2, 9.54% abundance) of 32.3 G. The g value is similar to that of the $[Cr^{III}(Cl_4SQ)_2(Cl_4Cat)]^-$ complex (g = 1.9701, $A^{53}(Cr)$ = 22.2 G) measured in glass matrices, which has been electrochemically synthesized.[3(a),4(a)] These results show that the unpaired electron in the $[Cr^{III}(X_4SQ)_2(X_4Cat)]^-$

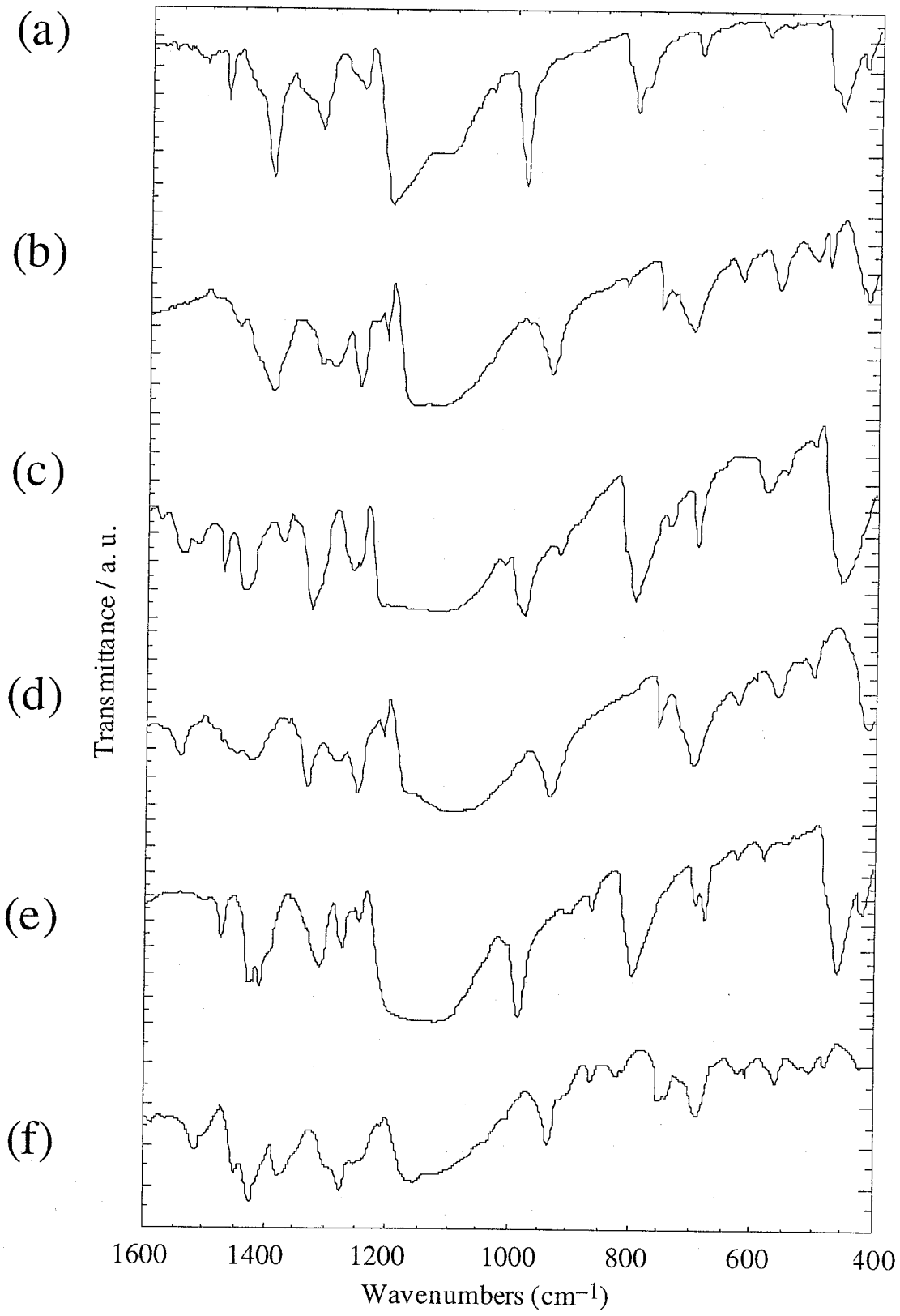

Figure 9. FT-IR spectra (KBr pellets) of (a) **1**, (b) **2**, (c) **3**, (d) **4**, (e) **5**, and (f) **6**.

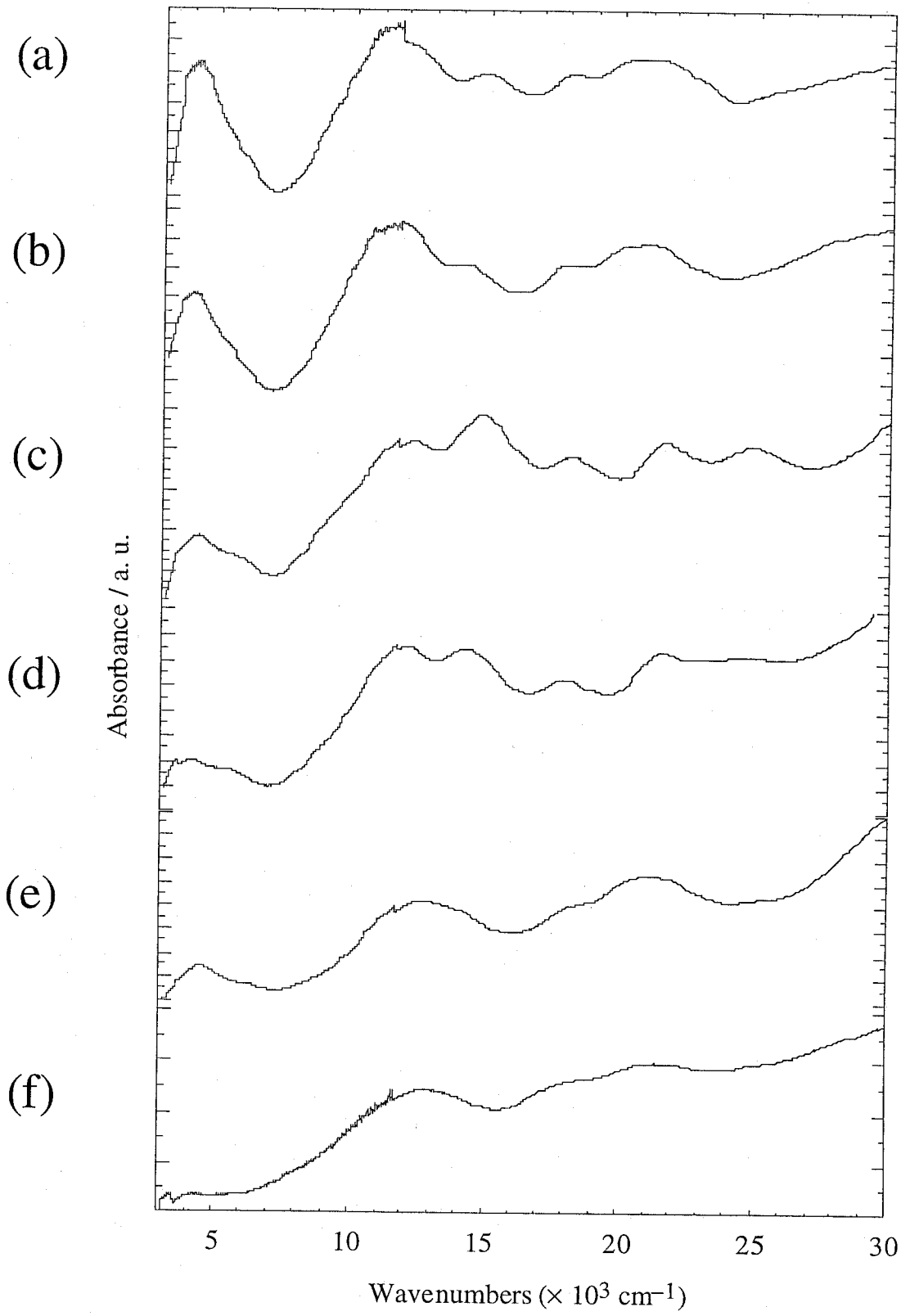

Figure 10. Solid state absorption spectra (KBr) of (a) **1**, (b) **2**, (c) **3**, (d) **4**, (e) **5**, and (f) **6**.

anion is on the chromium ion. Furthermore, the g values obtained for the solid and glass samples are identical, indicating the species in the solid and in solution have similar electronic structures.

On the other hand, all the compounds are expected to afford two types of EPR signals, attributable to the organic cations and the $[Cr^{III}(X_4SQ)_2(X_4Cat)]^-$ complex, when the two paramagnetic components are magnetically isolated. Figures 11 and 12 show EPR spectra of **1–4** in the solid state. All the compounds show a single EPR signal from room to liquid nitrogen temperature. As listed in Table 7, the g values of **1** and **2** are intermediate between those of the organic free radical (g = 2.00)[29] and 1.972 (Cl) and 1.968 (Br) for $[Cr^{III}(X_4SQ)_2(X_4Cat)]^-$ complexes. This is associated with an exchange interaction between the two paramagnetic species in the solid state. On the other hand, the g values of **3** and **4** are quite similar to that of $(Co^{III}Cp_2)[Cr^{III}(X_4SQ)_2(X_4Cat)]$, indicating that the unpaired electron is attributed only to the $[Cr^{III}(X_4SQ)_2(X_4Cat)]^-$ complex. This is because the two $TMTSF^{\bullet+}$ cations form a dimer and then spins are antiferromagnetically coupled, which is also demonstrated by bulk magnetic susceptibility measurements.

Table 7. Absorption Spectral Parameters (KBr) and g values for Compounds **1–6**

compound	ν_{max} ($10^3 \times cm^{-1}$)									g^a
1		4.20	5.88 sh		11.9	14.8	18.2	20.3	21.5	1.991
2	3.39 sh	4.08	5.88 sh	10.8 sh	11.8	14.2	18.1	20.2 sh	21.0	1.989
3	3.45 sh	4.26	5.88 sh	11.4 sh	12.3	18.2			21.7	1.974
4	3.45	4.17	5.26 sh	10.9 sh	12.2	14.3	17.9		21.5	1.968
5	3.45	4.17	5.26 s	10.9 sh	12.2	14.3	17.9		21.5	
6	3.45	4.17	5.26 sh	10.9 sh	12.2	14.3	17.9		21.5	

[a] Measured on solid samples at 77 K.

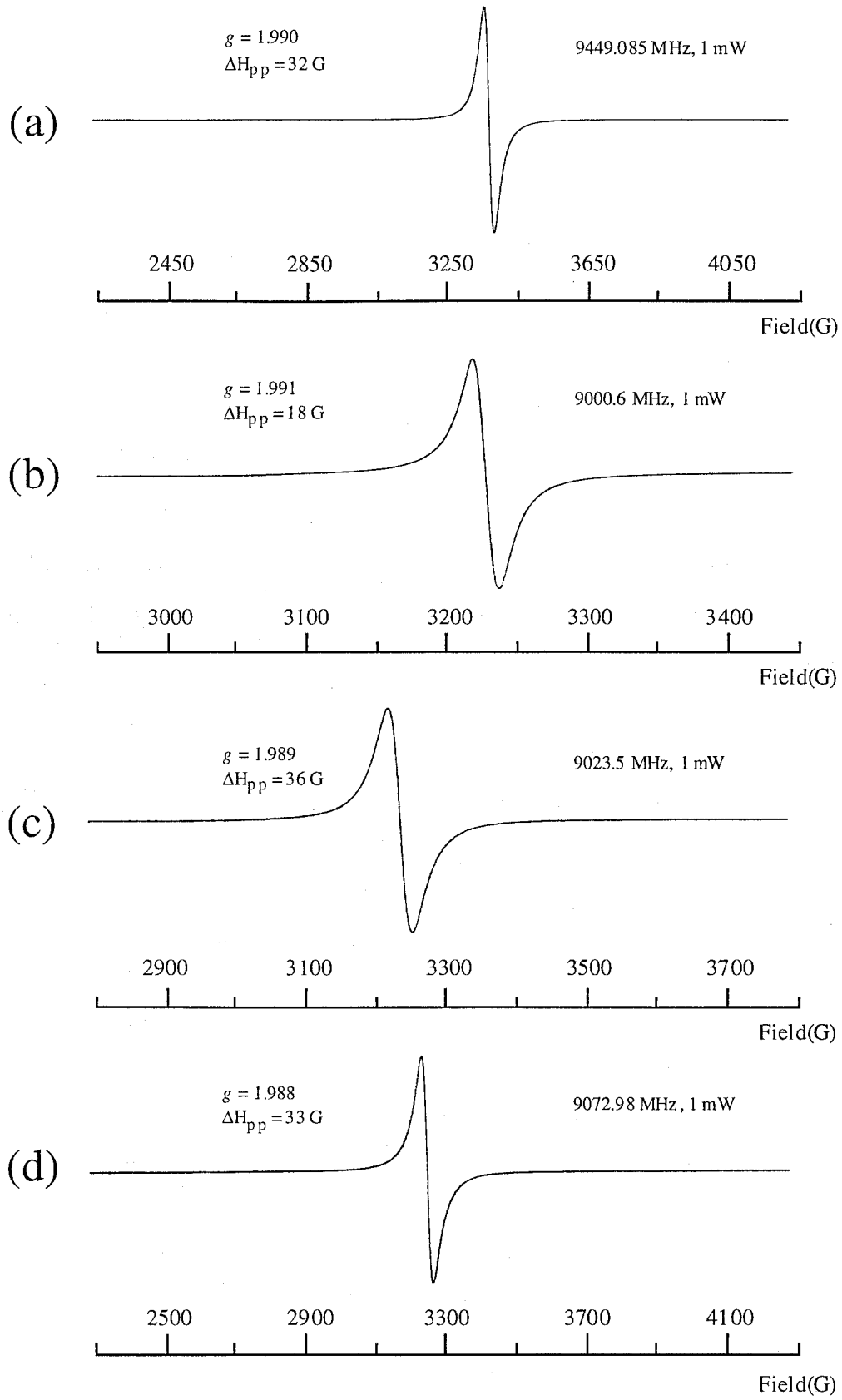

Figure 11. EPR spectra of (a) **1** and (b) **2** at room temperature and (c) **1** and (d) **2** at 77 K.

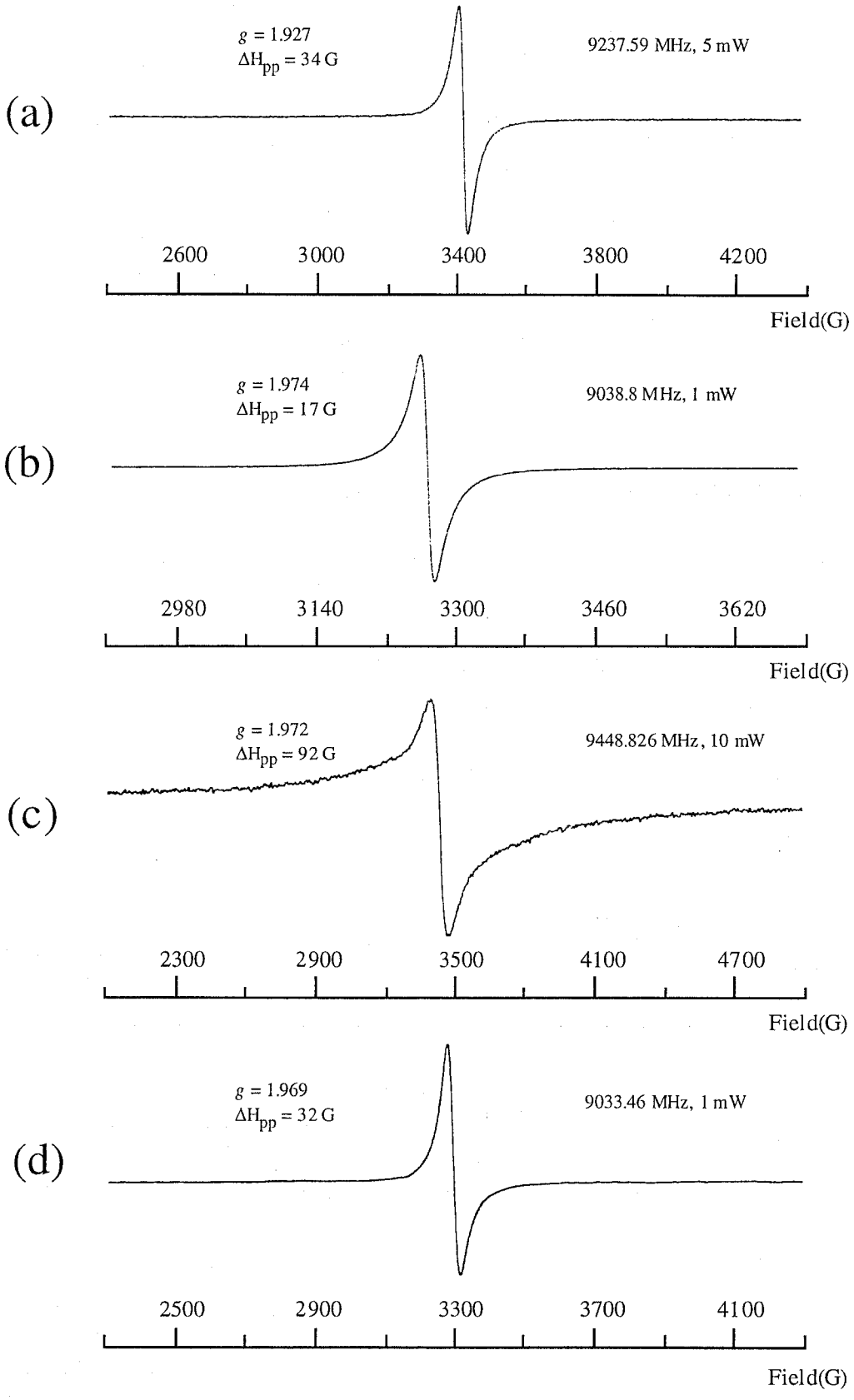

Figure 12. EPR spectra of (a) **3** and (b) **4** at room temperature and (c) **3** and (d) **4** at 77 K.

Temperature Dependence of Magnetic Susceptibilities.

Temperature dependence of $\chi_m T$ for compounds **2**, **3**, and **4** are shown in Figure 13. As mentioned above, all the compounds consist of paramagnetic cations (S = 1/2) and $[Cr^{III}(X_4SQ)_2(X_4Cat)]^-$ (S = 1/2) complexes. If there is no magnetic interaction among them, the $\chi_m T$ value can be estimated to be 0.75 emu·K·mol^{-1} by assuming an isotropic g of 2.00. For compound **2**, the observed value at 300 K is 0.847 emu·K·mol^{-1}. The large $\chi_m T$ value may be attributed to thermal population from S = 1/2 ground state to S = 3/2 excited state in the anionic complex.[5(b)] In the region 130–300 K the $\chi_m T$ value obeys the Curie–Weiss law, that is $\chi_m = C/(T - \Theta)$, with $\Theta = -2.0$ K. Below 130 K the $\chi_m T$ value decreases and reaches to 0.377 emu·K·mol^{-1} at 2 K. This suggests a weak antiferromagnetic interaction between the TMT-TTF$^{\bullet+}$ cations and the $[Cr^{III}(Br_4SQ)_2(Br_4Cat)]^-$ complexes. In fact, there are many intermolecular S···Br contacts which are shorter than the sum of the van der Waals radii of the two atoms (Table 6). In addition the crystal structure of **2**·$C_6H_5CH_3$ shows two kinds of intermolecular π···π stacking interactions of $[TMT\text{-}TTF^{\bullet}]^+$···$[Cr^{III}(Br_4SQ)_2(Br_4Cat)]^-$ and $[Cr^{III}(Br_4SQ)_2(Br_4Cat)]^-$···$[Cr^{III}(Br_4SQ)_2(Br_4Cat)]^-$ that could support such intermolecular magnetic interactions.

Compounds **3** and 2**b** shows the $\chi_m T$ values of 0.42 and 0.433 emu·K·mol^{-1} at 300 K, only 56 and 58 % of the expected values for two moles of S = 1/2 spins. Inspection of the crystal structure indicates spin cancellation in the TMTSF dimers, and is consistent with the result of the EPR measurements. Therefore, the apparent magnetic susceptibility is attributed to the $[Cr^{III}(X_4SQ)_2(X_4Cat)]^-$ complexes. The $\chi_m T$ value shows temperature independent behavior in the region 45–300 K, and below 45 K decreases to 0.0975 and 0.245 emu·K·mol^{-1} at 2 K indicative of antiferromagnetic interaction. From the crystal structures, intra- and interlayer magnetic interactions of the $[Cr^{III}(X_4SQ)_2(X_4Cat)]^-$ complexes could be expected. With regard to the intralayer magnetic interactions, the intermolecular stacks of the ligands are attributed to the magnetic interactions. On the other hand, the intermolecular X···X contacts between the

anionic complexes of the neighboring layers are responsible to the interlayer magnetic interactions.

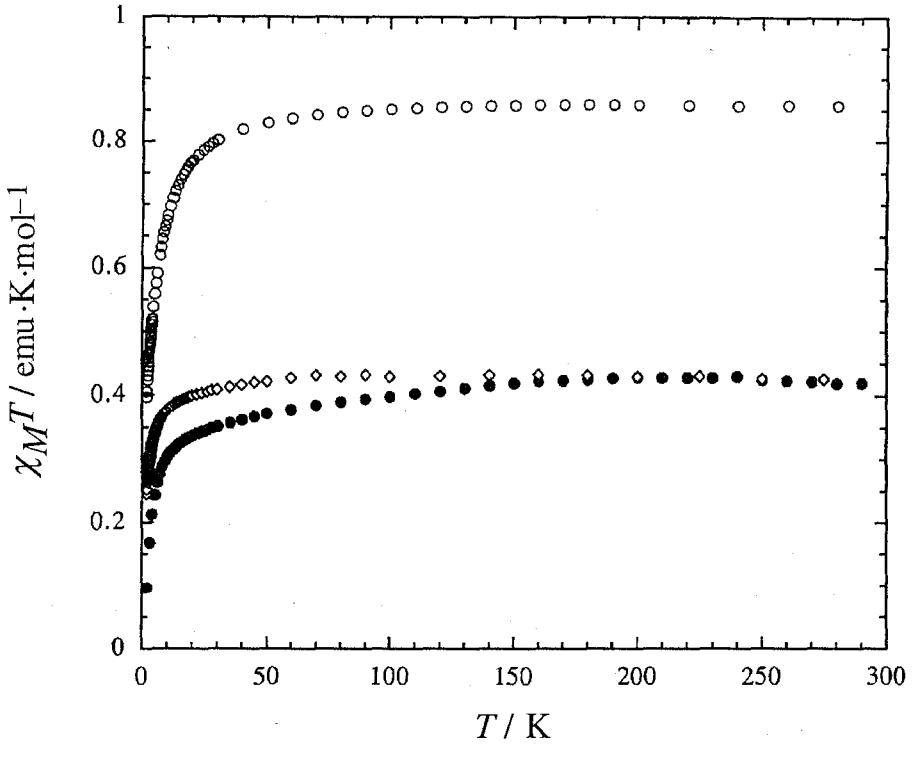

Figure 13. Temperature dependence of $\chi_m T$ for **2** (O), **3** (●), and **4** (◇).

Conclusion

In this work the author has first isolated anionic chromium complexes with mixed-valence ligands, $[Cr^{III}(X_4SQ)_2(X_4Cat)]^-$, as CT compounds with organic cations. The ligand-based mixed-valence complexes, $[Cr^{III}(X_4SQ)_2(X_4Cat)]^-$, contain two SQ and one Cat, and show the intramolecular intervalence bands in the near-infrared region characteristic of mixed-valence state. The crystal structures of the compounds are dependent on the donor molecules; **2**·$C_6H_5CH_3$ form two kinds of stacks; (i) ···[D][A]··· and (ii) ···[A][A]··· types. In compound **3**·1/2CH_2Cl_2, two-dimensional brick-wall networks of $[Cr^{III}(Cl_4SQ)_2(Cl_4Cat)]^-$ anions are found, while in **4**·2CH_2Cl_2 the intermolecular stacking arrangement of the ligands results in the formation of a two-dimensional honeycomb layer. Both structures are stabilized by the TMTSF dimers between the layers.

From studies described in this chapter, the properties of $[Cr^{III}(X_4SQ)_2(X_4Cat)]^-$ anions in the solid state have been proved, while those in the solution still remain because of the insoluble properties of **1**–**6**. Thus, these will be shown in Chapter 4.

References

(1) (a) Pierpont, C. G.; Lange, C. W. *Prog. Inorg. Chem.*, **1994**, *41*, 331. (b) Pierpont, C. G.; Buchanan, R. M. *Coord. Chem. Rev.*, **1981**, *38*, 45.

(2) (a) Adams, D. M.; Noodleman, L.; Hendrickson, D. N. *Inorg. Chem.*, **1997**, *36*, 3966. (b) Jung, O. -S.; Pierpont, C. G. *J. Am. Chem. Soc.*, **1994**, *116*, 2229. (c) Roux, C.; Adams, D. M.; Itié, J. P.; Polian, A.; Hendrickson, D. N.; Verdaguer, M. *Inorg. Chem.*, **1996**, *35*, 2846.

(3) (a) Downs, H. H.; Buchanan, R. M.; Pierpont, C. G. *Inorg. Chem.*, **1979**, *18*, 1736. (b) Sofen, S. R.; Ware, D. C.; Cooper, S. R.; Raymond, K. N. *Inorg. Chem.*, **1979**, *18*, 234.

(4) (a) Pierpont C. G.; Downs, H. H. *J. Am. Chem. Soc.*, **1976**, *98*, 4834. (b) Raymond, K. N. S.; Isied, S.; Brown, L. D.; Fronczek, F. R.; Nibert, J. H. *J. Am. Chem. Soc.*, **1976**, *98*, 1767. (c) Buchanan, R. M.; Kessel, S. L.; Downs, H. H.; Pierpont, C. G.; Hendrickson, D. N. *J. Am. Chem. Soc.*, **1978**, *100*, 7894. (d) Buchanan, R. M.; Downs, H. H.; Shorthill, W. B.; Pierpont, C. G.; Kessel, S. L.; Hendrickson, D. N. *J. Am. Chem. Soc.*, **1978**, *100*, 4318. (e) Gordon, D. J.; Fenske, R. F. *Inorg. Chem.*, **1982**, *21*, 2907.

(5) (a) Pierpont, C. G.; Downs, H. H.; Rukavina, T. G. *J. Am. Chem. Soc.*, **1974**, *96*, 5573. (b) Chapter 1 in this thesis.

(6) Kahn, O. *Molecular Magnetism*; VCH; New York, 1993.

(7) Jacobson, R. A. *REQABA Empirical Absorption Correction Version 1.1-03101998:* Molecular Structure Corp.: The Woodlands, TX, 1996–1998.

(8) Altomare, A.; Burla, M. C.; Camalli, M.; Cascarano, M.; Giacovazzo, C.; Guagliardi, A.; Pilidori, G. *J. Appl. Cryst.*, **1994**, *27*, 435.

(9) Beurskens, P. T.; Admiraal, G.; Beurskens, G.; Bosman, W. P.; de Gelder, R.; Israel, R.; Smits, J. M. M. , The DIRDIF-94 program system, Technical Report of the Crystallography Laboratory; University of Nijmegen: Nijmegen, The Netherlands, 1994.

(10) *teXsan: Crystal Structure Analysis Package*; Molecular Structure Corporation: The Woodlands, TX, 1985, 1992.

(11) Johnson, C. K. ORTEP II; Report ORNL-5138; Oak Ridge National Laboratory: Oak Ridge, TN, 1976.

(12) Guionneau, P.; Kepert, C. J.; Bravic, G.; Chasseau, D.; Truter, M. R.; Kurmoo, M.; Day, P. *Synth. Met.*, **1997**, *86*, 1973.

(13) (a) Mori, T.; Wu, P.; Imaeda, K.; Enoki, T.; Inokuchi, H. *Synth. Met.*, **1987**, *19*, 545. (b) Katayama, C.; Honda, M.; Kumagai, H.; Tanaka, K.; Saito, G.; Inokuchi, H. *Bull. Chem. Soc. Jpn.*, **1985**, *58*, 2272. (c) Endres, H. *Acta Crystallogr., Sect. C*, **1987**, *43*, 439. (d) Honda, K.; Goto, M.; Kurahashi, M.: Anzai, H.: Tokumoto, M.; Ishiguro, T. *Bull. Chem. Soc. Jpn.*, **1988**, *61*, 588.

(14) (a) Kistenmacher, T. J.; Emge, T. J.; Shu, P.; Cowan, D. O. *Acta Crystallogr., Sect. B*, **1979**, *35*, 772. (b) Ouahab, L.; Padiou, J.; Grandjean, D.; Garrigou-Lagrange, C.; Delhaes, P.; Bencharif, M. *J. Chem. Soc., Chem. Commun.*, **1989**, 1038. (c) Thorup, N.; Rindorf, G.; Soling, H. *Acta Crystallogr., Sect. B*, **1981**, *37*, 1236.

(15) (a) Porter, L. C.; Kini, A. M.; Williams, J. M. *Acta Crystallogr., Sect. C*, **1987**, *C43*, 998. (b) Williams, J. M.; Emge, T. J.; Firestone, M. A.; Wang, H. H.; Beno, M. A.; Geiser, U.; Nunez, L.; Carlson, K. D.; Nigrey, P. J.; Whangbo, M. -H. *Mol. Cryst. Liq. Cryst.*, **1987**, *148*, 233. (c) Geiser, U.; Wang, H. H.; Schlueter, J.; Chen, M. Y.; Kini, A. M.; Kao, I. H. -C.; Williams, J. M.; Whangbo, M. -H.; Evain, M. *Inorg. Chem.*, **1988**, *27*, 4284.

(16) (a) Kato, R.; Mori, T.; Kobayashi, A.; Sasaki, Y.; Kobayashi, H. *Chem. Lett.*, **1984**, 781. (b) Kobayashi, H.; Takahashi, M.; Kato, R.; Kobayashi, A.; Sasaki, Y.; *Chem. Lett.*, **1984**, 1331.

(17) Buchanan, R. M.; Claflin, J.; Pierpont, C. G. *Inorg. Chem.*, **1983**, *22*, 2552.

(18) (a) Buchanan, R. M.; Pierpont, C. G. *J. Am. Chem. Soc.*, **1980**, *102*, 4951. (b) Attia, A. S.; Bhattacharya, S.; Pierpont, C. G. *Inorg. Chem.*, **1995**, *34*, 4427. (c) Jung, O. -S.; Jo, D. H.; Lee, Y. -A.; Conklin, B. J.; Pierpont, C. G. *Inorg. Chem.*, **1997**, *36*, 19. (d) Jung, O. -S.; Pierpont, C. G. *Inorg. Chem.*, **1994**, *33*, 2227.

(19) Cass, M. E.; Greene, D. L.; Buchanan, R. M.; Pierpont, C. G. *J. Am. Chem. Soc.*, **1983**, *105*, 2680.

(20) Lange, C. W.; Pierpont, C. G. *Inorg. Chim. Acta*, **1997**, *263*, 219.

(21) Attia, A. S.; Pierpont, C. G. *Inorg. Chem.*, **1998**, *37*, 3051.

(22) Attia, A. S.; Pierpont, C. G. *Inorg. Chem.*, **1997**, *36*, 6184.

(23) (a) Underhill, A. E.; Tonge, J. S.; Clemenson, P. I.; Wang, H. -H.; Williams, J. M. *Mol. Cryst. Liq. Cryst.*, **1985**, *125*, 439. (b) Bellitto, C.; Federici, F.; Serino, P.; Day, P.; Kurmoo, M. *Synth. Met.*, **1996**, *79*, 33. (c) Pace, L. J.; Ulman, A.; Ibers, J. A. *Inorg. Chem.*, **1982**, *21*, 199. (d) Kasper, J. S.; Interrante, L. V. *Acta Crystallogr., Sect. B*, **1976**, *32*, 2914.

(24) (a) Mayerle, J. J.; Torrance, J. B. *Acta Crystallogr., Sec. B*, **1981**, *B37*, 2030. (b) Nakasuji, K.; Sasaki, M.; Kotani, T.; Murata, I.; Enoki, T.; Imaeda, K.; Inokuchi, H.; Kawamoto, A.; Tanaka, J. *J. Am. Chem. Soc.*, **1987**, *109*, 6970. (c) Konno, M.; Kobayashi, H.; Marumo, F.; Saito, Y. *Bull. Chem. Soc. Jpn.*, **1973**, *46*, 1987.

(25) (a) Decurtins, S.; Schmalle, H. W.; Oswald, H. R.; Linden, A.; Ensling, J.; Gütlich, P.; Hauser, A. *Inorg. Chim. Acta*, **1994**, *216*, 65. (b) Tamaki, H.; Zhong, Z. J.; Matsumoto, N.; Kida, S.; Koikawa, M.; Achiwa, N.; Hashimoto, Y.; Okawa, H. *J. Am. Chem. Soc.*, **1992**, *114*, 6974. (c) Nuttall, C. J.; Bellitto, C.; Day, P. *J. Chem. Soc., Chem. Commun.*, **1995**, 1513.

(26) For the [**I**···**A**], the mean plane distance was calculated between the plane of the quinone ligand defined by the $Cl_4C_6O_2$ atoms and the plane defined by the S(1)–S(4), C(19), and C(20)–C(21). For the [**II**···**B**], the $Cl_4C_6O_2$ plane and the central TTF skeleton were used. Finally, for [**II**···$\mathbf{C_6H_6}$], the distance between the $Cl_4C_6O_2$ plane and six carbon atoms of benzene molecule was calculated.

(27) (a) Lynch, M. W.; Valentine, M.; Hendrickson, D. N. *J. Am. Chem. Soc.*, **1982**, *104*, 6982. (b) Cass, M. E.; Gordon, N. R.; Pierpont, C. G. *Inorg. Chem.*, **1986**, *25*, 3962.

(28) Chang, H. -C.; Ishii, T.; Kondo, M.; Kitagawa, S. *J, Chem. Soc. Dalton Trans.*, **1999**, 2467.

(29) Williams, J. M.; Ferraro, J. R.; Thorn, R. J.; Carlson, K. D.; Geisen, U.; Wang, H. H.; Kini, A. M.; Whangbo, M. -H. *Organic Superconductors (including Fullerenes)*, Prentice Hall, Englewood Cliffs, 1992.

Chapter 3

New Mixed-Valence Supramolecular Assemblies of Redox Isomers, $(BEDT\text{-}TTF)_3[Cr^{III}(X_4SQ)_2(X_4Cat)][Cr^{III}(X_4SQ)(X_4Cat)_2]$

Abstract

Three-dimensional supramolecular charge-transfer (CT) compounds,

$(BEDT\text{-}TTF)_3[Cr^{III}(Cl_4SQ)_2(Cl_4Cat)][Cr^{III}(Cl_4SQ)(Cl_4Cat)_2]$ (**1**)
$(BEDT\text{-}TTF)_3[Cr^{III}(Br_4SQ)_2(Br_4Cat)][Cr^{III}(Br_4SQ)(Br_4Cat)_2]$ (**2**)

, where SQ and Cat is semiquinonate and catecholate, respectively, were synthesized by the reaction of tris(tetrahalogeno-*o*-semiquinonate) chromium(III) complexes, $Cr^{III}(X_4SQ)_3$, with bis(ethylenedithio)-tetrathiafulvalene (BEDT-TTF). Compound **1** crystallizes in the triclinic, space group $P\bar{1}$ with a = 12.4074(9) Å, b = 14.554(1) Å, c = 15.270(2) Å, α = 117.193(4), β = 97.7640(9), γ = 696.0637(8), V = 2386.0(3) Å^3, and Z = 2. The X-ray crystal structural and spectroscopic data reveal the oxidation states of cationic and anionic components leading a best formulation of $(BEDT\text{-}TTF^+)_3[Cr^{III}(X_4SQ)_2(X_4Cat)]^-[Cr^{III}(X_4SQ)(X_4Cat)_2]^{2-}$ for **1** and **2**. This is a first example for the coexistence of two kinds of intramolecular mixed-valence redox isomers, $[Cr^{III}(X_4SQ)_{3-n}(X_4Cat)_n]^{n-}$ (n = 1 and 2). A part of crystal structure of **1** consists of a two-dimensional mixed-stack layer of $BEDT\text{-}TTF^+$ cations and $[Cr^{III}(Cl_4SQ)_{3-n}(Cl_4Cat)_n]^{n-}$ (n = 1 and 2) isomers. Furthermore, additional intermolecular S···S contacts of $BEDT\text{-}TTF^+$ cations extend the whole crystal structure two- to three-dimensions. Temperature dependence of electric conductivity shows that compound **1** is a semiconductor with resistance $\rho = 1.32 \times 10^2$ Ω·cm at 293 K and activation energy of 0.14 eV. Interestingly, the temperature dependence of magnetic susceptibilities of the compounds shows dominant ferromagnetic interactions to which two distinctive antiferromagnetic interactions are superimposed. From the crystal structural the ferromagnetic interaction occurs between the direct π···π stacking interactions between $BEDT\text{-}TTF^+$ cations and the ligand moieties of the mixed-valence $[Cr^{III}(X_4SQ)_{3-n}(X_4Cat)_n]^{n-}$ (n = 1 and 2) isomers.

Introduction

Octahedral tris(chelate) transition metal complexes, $[M(L\text{-}L)_3]^m$, have been widely used for the development of supramolecular assemblies. Many of them have been constructed by a spontaneous self-assembly of well-defined molecular modules with coordination bonds. On the other hand, noncovalent $\pi\cdots\pi$ stacking interaction between the planar ligands has been known to serves as another useful means for the construction of one-dimensional chain[1] and two-dimensional layered frameworks.[2]

On the other hand, generation of anisotropic environments around the metal ions is one of the intriguing target giving an opportunity to investigate electronic perturbation to the interactions between the molecular modules. In contras to the octahedral modules with a uniform ligand, a ununiformity of the electronic and spin states of the ligands would give a flexibility to the module and intermolecular interactions with the adjacent module, when it forms molecular assemblies.

In this context, the class of *o*-quinone complexes provides a valuable set of the ligand-based mixed-valence redox isomers with alterable oxidation states of the ligands.[3] These electronically non-innocent complexes can afford relevant modules with the same shape but different charges on the ligand moieties. Therefor, the use of these modules could lead to a construction of new-type molecular mixed-valence assemblies.

Tris(tetrahalogeno-*o*-semiquinonate) chromium (III) complexes, $Cr^{III}(X_4SQ)_3$ (X = Cl and Br), undergo a characteristic three-step reduction on the ligand moieties at relatively high potentials to give four-membered redox isomers as shown in Scheme 1. The strong electron-acceptor properties of the complexes make easy to isolate the reduction products, $[Cr^{III}(X_4SQ)_{3-n}(X_4Cat)_n]^{n-}$ (n = 1 and 2), by the reaction with electron-donors. Using these properties, we have been studying the synthesis, crystal structures, and physical properties of charge-transfer

Scheme 1 Redox-isomers of $[Cr^{III}(X_4SQ)_{3-n}(X_4Cat)_n]^{n-}$ (X = Cl and Br)

$$Cr^{III}(X_4SQ)_3 \rightleftharpoons [Cr^{III}(X_4SQ)_2(X_4Cat)]^- \rightleftharpoons [Cr^{III}(X_4SQ)(X_4Cat)_2]^{2-} \rightleftharpoons [Cr^{III}(X_4Cat)_3]^{3-}$$

Intramolecular Mixed-valecy

(CT) compounds of $[Cr^{III}(X_4SQ)_{3-n}(X_4Cat)_n]^{n-}$ (n = 0–2) isomers with [TTF derivatives]$^+$ (TTF = tetrathiafulvalene) (Chapter 2) and $[M^{III}Cp_2]^+$ (M = Co and Fe) cations (Chapter 4). From the structural and spectroscopic studies, the intramolecular mixed-valence states of the n = 1 and 2 isomers derived from the coexistence of two kinds of ligands, SQ and Cat, have characterized. Although the n = 2 isomers show discrete crystal structures separated by the cations due to their relatively large anionic charges, the n = 1 isomers commonly associate in the crystals as one-dimensional column or two-dimensional layer structures with intermolecular homoleptic $\pi\cdots\pi$ stacks of the ligand moieties. The other aspect of this series occurs in compound, $[Fe^{III}Cp_2][Cr^{III}(Cl_4SQ)_2(Cl_4Cat)][Cr^{III}(Cl_4SQ)_3]$, in which homoleptic n = 0 and the intramolecular mixed-valence n = 1 isomer are simultaneously exist in the compound.[4] Consequently, the compound is regarded as system with both the intra- and intermolecular mixed-valence states. These examples show that the ligand-based redox activity of $Cr^{III}(X_4SQ)_3$ provides not only the intramolecular mixed-valence redox isomers, but also the intermolecular mixed-valence compound by means of controlled the synthetic condition and the donor molecules used. These molecular assemblies could be anticipated to be a new-type molecular-based compounds involving a local intermolecular SQ···SQ radical type and/or SQ···Cat CT type interactions.

In this Chapter CT compounds synthesized by the reaction of $Cr^{III}(X_4SQ)_3$ with a well-known organic π-donor, bis(ethylenedithio)tetrathiafulvalene (BEDT-TTF), which often forms mixed-stack CT compounds with planar molecules, will be presented.[5] The compounds obtained could be regarded as supramolecular mixed-valence CT compounds including both mixed-valence n = 1 and 2 redox isomers. Furthermore, the compounds show intermolecular ferromagnetic interaction and semiconducting properties with the aid of the $\pi\cdots\pi$ interaction and intermolecular mixed-valence states. The objective of this Chapter is to demonstrate the ligand-based mixed-valence octahedral modules for novel molecular assemblies such that they can then be deployed in crystal design and engineering.

Experimental Section

Materials.

All the chemicals were reagent grade. BEDT-TTF was purchased from Tokyo Kasei Kogyo Co., Ltd.. $Cr^{III}(X_4SQ)_3 \cdot 4C_6H_6$ was prepared by the procedure described in Chapter 1.

Preparation of the Compounds.

$(BEDT\text{-}TTF)_3[Cr(C_6O_2Cl_4)_3]_2$ (1) Single crystal of **1** was grown from a layered solution of a dichloromethane solution of $Cr^{III}(Cl_4SQ)_3 \cdot 4C_6H_6$ (81 mg, 0.23 mM) and a dichloromethane/acetonitrile (2:1) solution of BEDT-TTF (60 mg, 0.48 mM). Black plate crystals were obtained after a week. Found: C, 29.04; H, 0.73. $C_{66}H_{24}Cl_{24}Cr_2O_{12}S_{24}$ requires C, 29.0, H, 0.89. IR (KBr): 1397s, 1315w, 1284m, 1111s, 1024m, 977s, 925vw, 894w, 882w, 810w, 792s, 737w, 691w, 670vw, 552w, 478w, and 450m cm^{-1}.

$(BEDT\text{-}TTF)_3[Cr(C_6O_2Br_4)_3]_2$ (2) The powder sample was prepared by mixing of a 975 ml of dichloromethane/acetonitrile (2:1) solution of BEDT-TTF (100 mg, 0.256 mg) and a 500 ml dichloromethane solution of $Cr^{III}(Br_4SQ)_3 \cdot 4C_6H_6$ (204 mg, 0.128 mmol). The mixture was stirred for a minute and allowed to stand for a day. The microcrystals were collected by the filtration and washed with dichloromethane/acetonitrile (3:1) several times. Then, the powder was dried in vacuum. Yield 204 mg (84 %). Found: C, 20.55; H, 0.44. $C_{66}H_{24}Br_{24}CrO_6S_{24}$ requires C, 20.86; H, 0.64. IR (KBr): 1458m, 1394s, 1320w, 1284s, 1256s, 1207m, 1098s, 933s, 895w, 883w, 810w, 750m, 698s, 625w, 561w, 540w, 502w, 478m, and 411m cm^{-1}.

Physical Measurements.

Infrared spectra for KBr pellets was recorded on a Hitachi I-5040 FT-IR spectrometer over the range of 350–7000 cm^{-1}, absorption spectra on a Hitachi U-3500 spectrophotometer over the range of 3130–54000 cm^{-1} at 296 K. Raman spectrum was made on an ISA Confocal LABRAM System at an excitation of 632.8 nm with He-Ne laser at 296 K. The EPR spectra were recorded on finely ground powders enclosed in a quartz tube at X-band frequency with a JEOL RE-3X spectrometer operating 9.0–9.5 GHz at the temperature region of 5–296 K. The resonance frequency was measured on an Anritsu MF76A microwave frequency counter. Magnetic field was calibrated by an Echo Electronics EMF-2000AX NMR field meter.

Magnetic susceptibilities were recorded over the temperature range from 1.9 to 300 K at 1 T with a superconducting quantum interference device (SQUID) susceptometer (Quantum Design, San Diego, CA) interfaced with a HP Vectra computer system. All values were corrected for diamagnetism that were calculated from Pascal's table.[6] Electric conductivity measurements were made on the single crystal of **1** along the long crystal axis using conventional four-prove method. For compound **2**, the measurement was performed on the compacted pellet using two-prove method.

Crystallographic Data Collection and Refinement of Structures.

All the measurements were performed with Mo Kα radiation employing a graphite monochromator at 296 K on a Rigaku mercury diffractometer with CCD two-dimensional detector. The size of the unit cell was calculated from the reflections collected on the setting angles of four frames by changing ω by 0.5° for each frame. Two different χ settings were used and ω was changed by 0.5° per frame. Intensity data were collected in 462 frames with an ω scan width of 0.5° and exposure time 80 s. Empirical absorption correction using the program REQABA[7] was performed for all the data. All the crystal data are summarized in Table 1. The structure was solved by direct methods[8] and expanded using Fourier techniques.[9] The final cycles of the full-matrix least-squares refinements were based on the observed reflections ($I > 4\sigma(I)$). All the calculations were performed using the teXsan crystallographic software package of Molecular Structure Corporation.[10]

Table 1. Crystallographic and Refinement Data of **1**

	1
Formula	$C_{66}H_{24}Cl_{24}Cr_2O_{12}S_{24}$
Formula weight	2733.21
Color	black
Crystal size, mm	0.60×0.50×0.05
Crystal system	Triclinic
Space group	$P\bar{1}$
a, Å	12.4074(9)
b, Å	14.554(1)
c, Å	15.270(2)
α, °	117.193(4)
β, °	97.7640(9)
γ, °	96.0637(8)
Z	2
V, Å^3	2386.0(3)
ρ_{calcd}, g/cm^3	1.902
μ, cm^{-1}	12.81
T, K	296
λ (Mo Kα), Å	0.71069
No. observations	7092
No. parameters	577
Refls./para. ratio	12.29
R_{int}	0.040
R, R_w	0.037, 0.048

[a] $R = \Sigma||F_o|-|F_o||/\Sigma|F_o|$, $R_w = [\Sigma(|F_o|-|F_o|)^2/\Sigma w|F_o|^2)]^{1/2}$.

Results and Discussion

Crystal Structure and Spectroscopic Data.

The reaction of $Cr^{III}(X_4SQ)_3$ with BEDT-TTF gives insoluble black crystalline product which has a stoichiometry of $(BEDT\text{-}TTF)_3[Cr(X_4C_6O_2)_3]_2$. Figure 1 shows ORTEP drawing of **1** with atom numbering scheme. The unit cell contains one crystallographically independent chromium complex and three BEDT-TTF molecules. Each BEDT-TTF molecule has a crystallographically imposed center of symmetry on the central C–C bond. The symbols **I–III** and **A–C** are used to denote the three independent ligands and BEDT-TTF molecules, respectively.

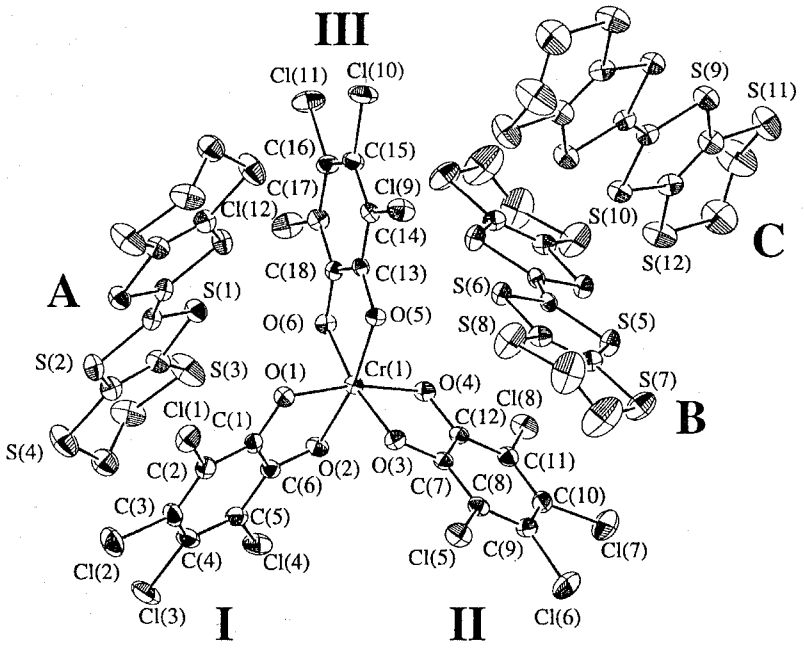

Figure 1. An ORTEP drawing of **1** with hydrogen atoms omitted (showing 30% isotropic thermal ellipsoids). Crystallographically independent ligands and BEDT-TTF molecules are designated **I–III** and **A–C**, respectively. Three BEDT-TTF molecules possess inversion center on each central C–C bond.

As shown in Figure 2(a), a part of crystal structure is composed of two-dimensional layer constructed from the mix-stacked two components, where the three independent heteroleptic $\pi\cdots\pi$ interactions of [**I**···**A**], [**I**···**C**], and [**II**···**B**] are recognized. The dihedral angles between the best planes of them are approximately 8.8° (**I**···**A**), 4.7° (**I**···**C**), and 14° (**II**···**B**),

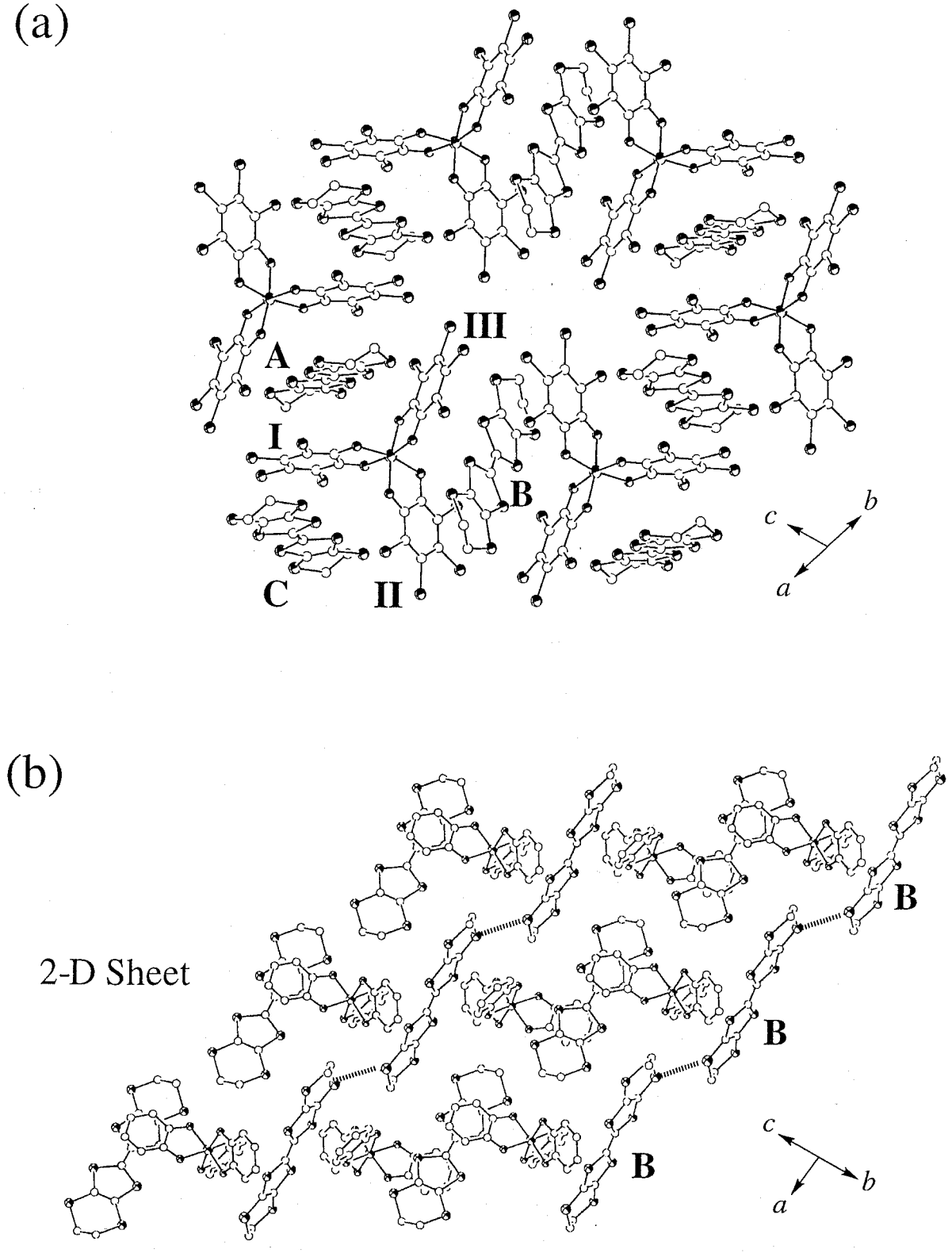

Figure 2. (a) The two dimensional mixed-stack layer and (b) the three-dimensional crystal packing structures constructed from the intermolecular S(8)···S(8*) contacts (dashed line) along the *a*-axis (chlorine atoms are omitted for clarity).

respectively. The intrastack interplaner spacings between them are found to be 3.650(3) (**I**···**A**), 3.605(3) (**I**···**C**), and 3.743(3) (**II**···**B**) Å, respectively.[11] As shown in Figure 3, the overlap modes of [**I**···**A**] and [**II**···**B**] are different with that of [**I**···**C**], namely, in the former the quinone ligand superposes upon the five- and six-membered rings of one side BEDT-TTF, while the ligand of the latter superimposes upon the central C–C bond of the BEDT-TTF molecule **C**.

In addition to the π···π contacts between the two components, atomic contacts between S(8) and S(8*) atoms of the adjacent BEDT-TTF molecules **B** results in a one-dimensional chain structure along the *a*-axis as shown in Figure 2(b). The intermolecular S···S distance is 3.323(2) Å, which is significantly shorter than the sum of van der Waals radius, 3.7 Å. The interactions extend the whole intermolecular interactions two to three dimensional. Finally, there

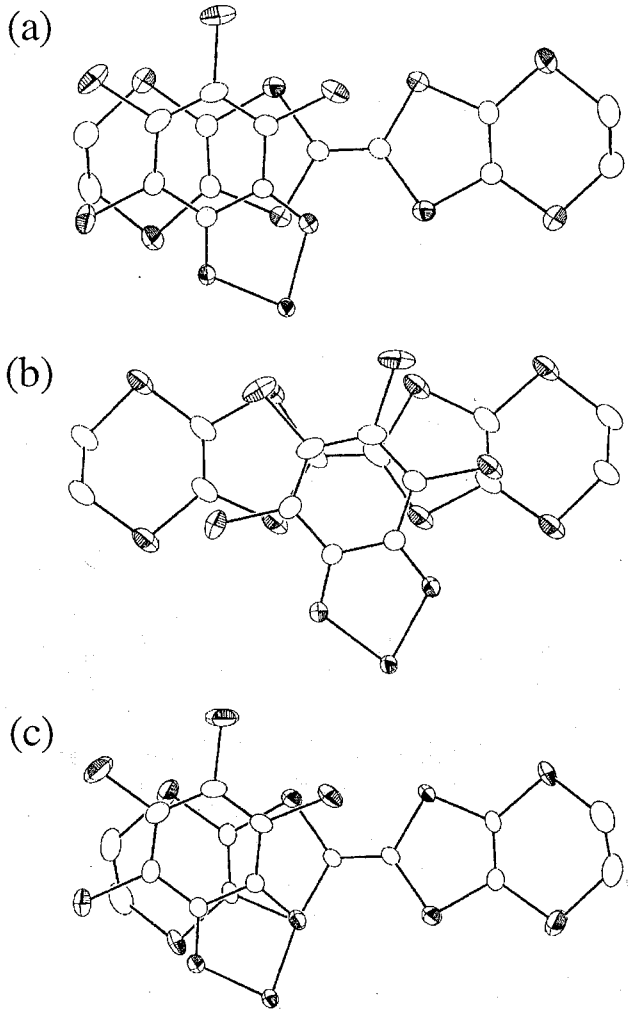

Figure 3. Projection views of the stacking interactions of (a) [**I**···**A**], (b) [**I**···**C**], and (c) [**II**···**B**] along vectors normal to the least-squares planes of the *o*-quinone ligands.

are intermolecular Cl···S atomic contacts between the chromium complexes and the BEDT-TTF; Cl(1)···S(1) 3.538(1) (**I**···**A**; $-x-2$, $-y-1$, $-z-2$), Cl(1)···S(2) 3.646(1) (**I**···**A**; $+x$, $+y$, $+z$), Cl(8)···S(5) 3.473(1) (**II**···**B**; $+x$, $+y$, $+z$), Cl(8)···S(6) 3.607(1) (**II**···**B**; $-x-1$, $-y-1$, $-z-1$), Cl(5)···S(9) 3.509(1) Å (**II**···**C**; $+x$, $+y-1$, $+z$). These contacts are shorter than the sum of van der Waals radius of 3.65 Å.

Table 2 lists the bond distances and estimated charges for BEDT-TTF molecules in **1** using a known correlation between the bond distances of the central TTF skeleton and the degree of ionicity.[12] Using the correlation, the charges on the three BEDT-TTF molecules at 296 K are calculated to be +0.981, +1.25, and +1.04 for the molecule **A**, **B**, and **C**, respectively, where the larger positive charge was estimated for the molecule **B** compared with those of the others. However, in some situations the cationic charges may be ambiguous or X-ray diffraction studies are unable to deduce the exact nature of the cation.

Table 2. Comparison of Intramolecular Bond Distances (Å) and Estimated Formal Charge (Q) for BEDT-TTF$^{\delta+}$ Compounds and Those of **1**

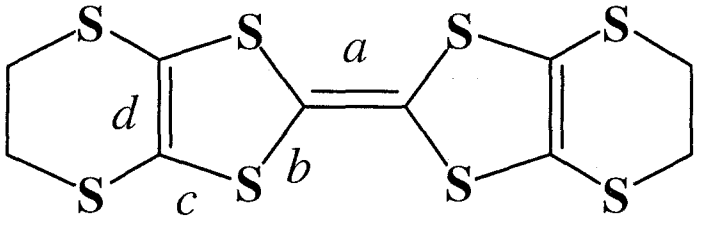

compound	*a*	*b*	*c*	*d*	Q^a
BEDT-TTF[b]	1.312(12)	1.57(7)	1.754(8)	1.322(7)	0
α-(BEDT-TTF)$_2$PF$_6$[c]	1.365(4)	1.740(2)	1.750(2)	1.345(3)	+1/2
(BEDT-TTF)$_3$[ClO$_4$]$_2$[d]	1.366(7)	1.731(7)	1.743(5)	1.345(9)	+1
BEDT-TTF(ClO$_4$)$_2$[e]	1.439(4)	1.683(3)	1.716(3)	1.379(5)	+2
A	1.378(6)	1.716(3)	1.733(4)	1.352(5)	+0.981
B	1.393(6)	1.709(3)	1.724(3)	1.357(2)	+1.25
C	1.382(6)	1.719(3)	1.731(3)	1.357(5)	+1.04

[a] Reference 12. [b] Reference 13(a). [c] Reference 13(b). [d] Reference 13(c). [d] Reference 13(d).

It has been demonstrated that Raman and infrared spectroscopy are another useful means for the determination of the oxidation states of the molecules.[14] As shown in Figure 4(a), compound **1** shows a peak at 1394 cm^{-1} and two distinctive peaks at 1416 and 1450 cm^{-1} in infrared and Raman spectrum, respectively, at 296 K. By comparison to literature values the observed frequencies indicate a charge of +1 on each BEDT-TTF molecule. From these results and the composition of the compounds, the anionic moieties should have a –3 charge per two complexes.

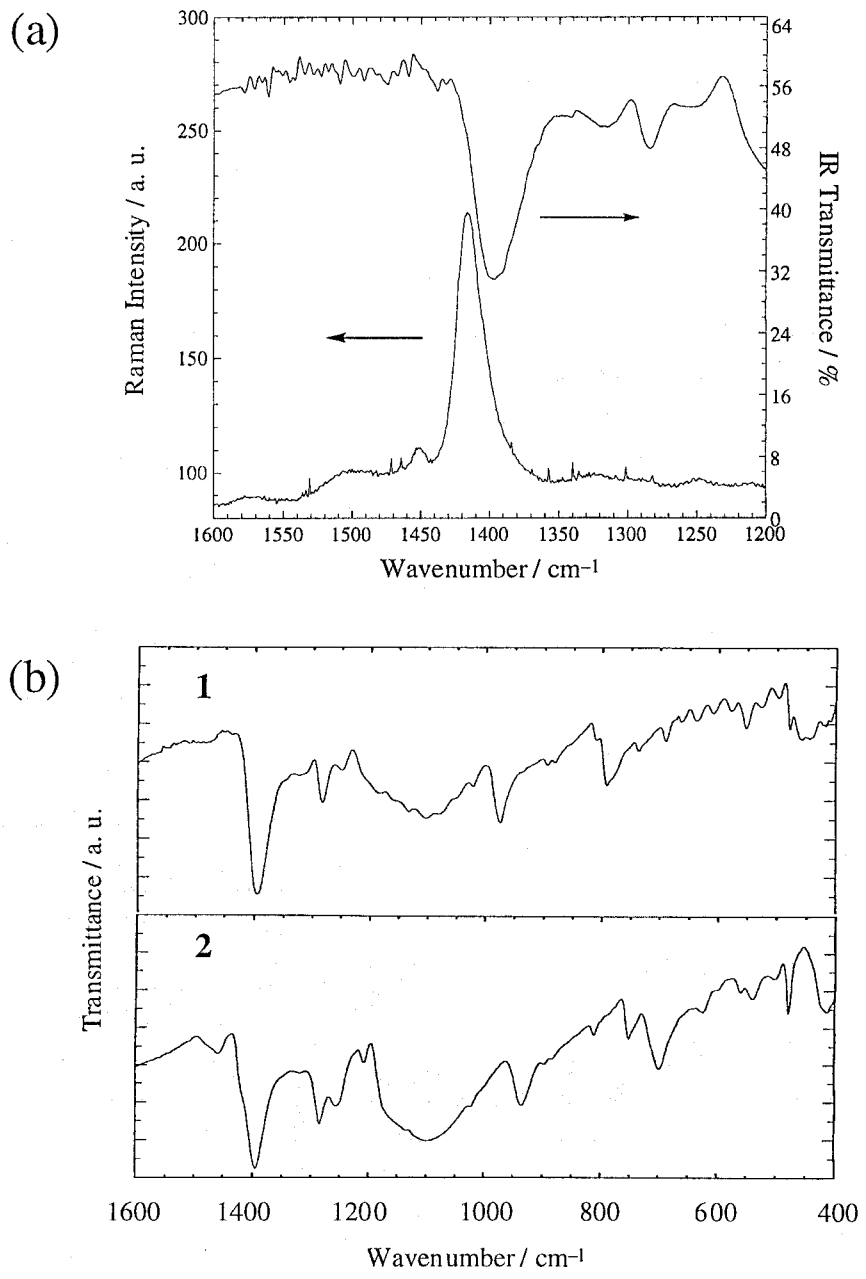

Figure 4. (a) Raman (below, pellet) and infrared (above, KBr) spectra of **1** at 296 K. (b) Infrared spectra of **1** and **2** (KBr).

Table 3 lists the mean Cr–O, C–O, and C–C bond distances and O–Cr–O angles of chromium complex of **1** together with the series of $[Cr^{III}(X_4SQ)_{3-n}(X_4Cat)_n]^{n-}$ (n = 0–3) redox isomers reported so far. It has been found that the mean C–O bond distance and O–Cr–O angle are most particularly sensitive to the charge states of the complexes, which increase with the numbers of n. In fact the observed values for compound **1** are far from those of n = 0 isomer, while intermediate between those of n = 1 and 2 isomers. The intermediate values coincident with the anionic charge of –3 expected from the structural features of the cations, however, the oxidation states of the anions will be proven by the absorption spectra (*vide infra*).

Table 3. Comparison of Average Bond Distances (Å) and Angles (°) of the Anion in **1** with the Series of $[Cr^{III}(X_4SQ)_{3-n}(X_4Cat)_n]^{n-}$ (n = 0–3) Redox Isomers

n =	0[a]	1[b]	2[c]	3[d]	**1**
X =	Cl	Cl	Br	H	Cl
Cr–O (Å)	1.949(5)	1.941(3)	1.943(6)	1.986(4)	1.942(2)
C–O (Å)	1.280(1)	1.301(5)	1.32(1)	1.349(3)	1.313(4)
C–C (Å)	1.40(1)	1.396(7)	1.40(2)	1.390(6)	1.399(4)
O–Cr–O (°)	81.8(2)	82.6(1)	83.0(2)	83.6(1)	82.92(8)

[a] Reference 15(a). [b] Reference 15(b). [c] Reference 4. [d] Reference 15(c).

Figure 5 shows a UV-vis-NIR-IR absorption spectra of **1** and **2** in the solid state (KBr) with those of n = 1 and 2 isomers. All the data are summarized in Table 4. It has been found that the most prominent spectral difference between the series of n = 0–3 isomers is the presence of an intramolecular intervalence CT (IVCT) transition from Cat to SQ[3(b)] which are found only in the intramolecular mixed-valence n = 1 and 2 isomers near 4000 and 5880 cm^{-1}, respectively.[4] From the comparison of these absorption bands to those of **1** and **2**, the bands near 4000 and 5000 cm^{-1} are assigned to the IVCT bands of the n = 1 and 2 isomers, respectively. These spectra, thus, demonstrate the coexistence of both intramolecular mixed-valence isomers, exhibiting the intermolecular mixed-valence state. In regard to the X-ray structural data the small structural differences between the n = 1 and 2 isomers (Table 3) average themselves crystallographically as shown above. Similar situation has been found in $[Fe^{III}Cp_2][Cr^{III}(Cl_4SQ)_2(Cl_4Cat)][Cr^{III}(Cl_4SQ)_3]$ where the two kinds of redox isomers, n = 0 and 1

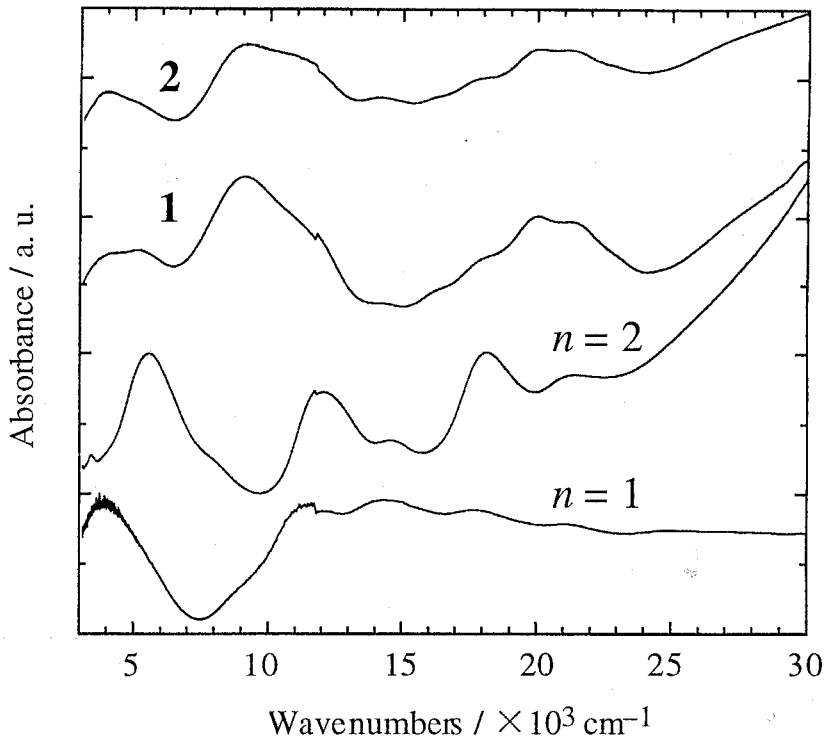

Figure 5. Electronic absorption spectra of **1** and **2** in the solid state (KBr) compared with those of $(Co^{III}Cp_2)_n[Cr^{III}(Cl_4SQ)_{3-n}(Cl_4Cat)_n]$ (n = 1 and 2).

Table 4. Comparison of Absorption Spectral Parameters of **1** and **2** with those of n = 1 and 2 redox isomers.

compound	ν_{max} ($10^3 \times cm^{-1}$) ($\varepsilon_{max} = 10^3 \times M^{-1} \cdot cm^{-1}$)									
1	4.17	5.13 (sh)	9.17	11.8		14.1	16.3	17.9	19.8	21.3
2	4.00	5.00 (sh)	9.14	11.1 (sh)		14.1	16.0 (sh)	17.8 (sh)	20.1	21.1
n = 1	3.92	5.88 (sh)	8.70 (sh)	10.8 (sh)	12.1	14.3		17.7		21.1
n = 2		5.56	8.00 (sh)		12.0	14.6		18.2		21.5

isomers, could be distinguishable only by the absorption spectra.[4]

The bands near 11500, 14100, 17900, and 21000 cm^{-1} are assigned to the intramolecular electronic transition of the n = 1 and 2 isomers,[4] while the band near 9100 cm^{-1} could be

attributed to intermolecular CT transition between the adjacent BEDT-TTF^{+} cations. The intramolecular electronic transitions in the BEDT-TTF^{+} cations are found near 16000 (sh) and 20000 cm^{-1}.[16] From these structural and spectroscopic data, compounds **1** and **2** are best formulated as $(BEDT\text{-}TTF^{+})_3[Cr^{III}(X_4SQ)_2(X_4Cat)]^{-}[Cr^{III}(X_4SQ)(X_4Cat)_2]^{2-}$.

Electric and Magnetic Properties.

Single crystal of compound **1** and compacted pellet of **2** show resistance of $\rho = 1.32 \times 10^2$ and 4.16×10^2 Ω·cm at 293 K, respectively. Temperature dependence of the resistance of **1** is shown in Figure 6. As the temperature is lowered the resistance increases monotonously and reaches to 6.4×10^6 Ω·cm at 100 K, indicating semiconductor with activation energy of 0.14 eV. These results are consistent with the structural feature of **1** where the compound does not have conduction column and each BEDT-TTF molecule shows completely ionized form.

Figure 7 shows temperature dependence of EPR spectra of **1** and the spectrum of **2** at 296 K. At room temperature, compounds **1** and **2** show isotropic EPR signal at $g = 1.990$ (1) and

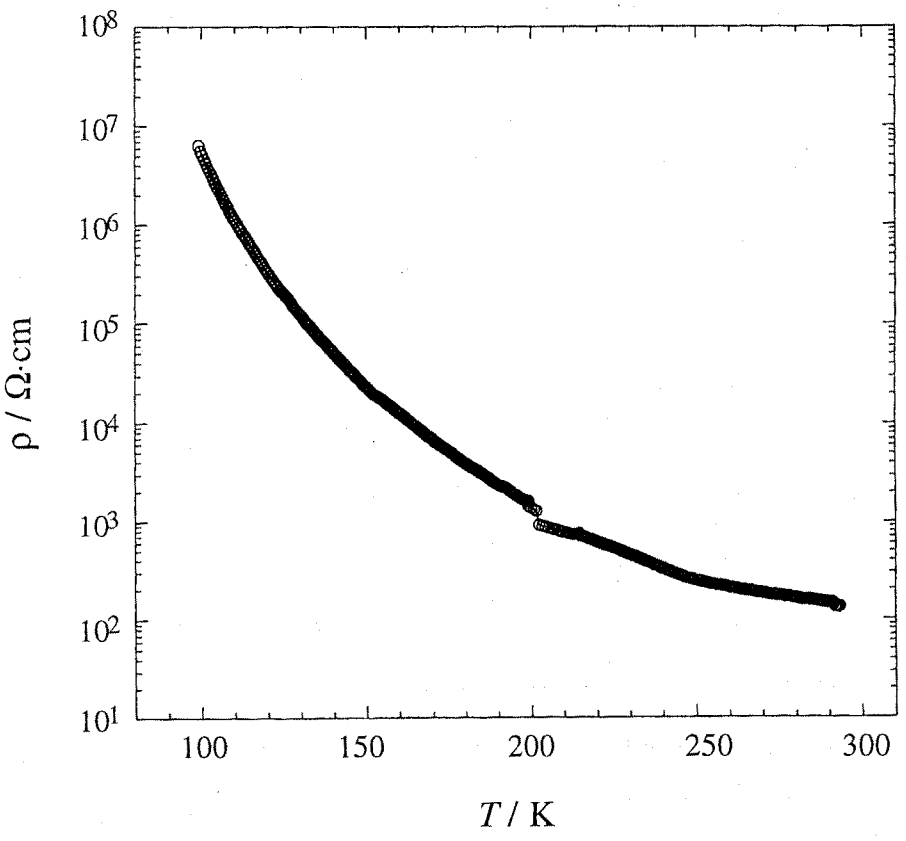

Figure 6. Temperature dependence of the resistance of **1** in the region of 99–293 K.

1.989 (**2**) with line-width 34.8 (**1**) and 92.5 G (**2**). For compound **1**, as temperature decreases to 30 K the signal split into two signals centered at g_1 = 1.990 and g_2 = 1.986. These values show slight change up to 5 K and at that temperature the signals are observed at g_1 = 1.988 and g_2 = 1.984. The observed g values are intermediate between those of n = 1 isomer (g = 1.972, line-width = 15 G (77 K))[15(a),(b),17] and conventional organic radical (g = 2.00),[18] indicating the exchange interaction between the two paramagnetic centers.

The magnetic properties of compound **1** are shown in Figure 8 in the forms of $\chi_M T$ and χ_M^{-1} versus T curves. At 300 K, $\chi_M T$ is equal to 3.05 emu·K·mol^{-1}, decreases first very slowly, then gradually increases as the temperature is lowered down to 17 K and reaches a maximum at that temperature with $\chi_M T$ = 3.58 emu·K·mol^{-1}. When the temperature is lowered further below 17 K, $\chi_M T$ decreases to 1.98 emu·K·mol^{-1} at 1.9 K. This data clearly indicates the presence of dominant ferromagnetic interactions to which two distinctive antiferromagnetic interactions are superimposed. The maximum is not observed in the χ_M versus T curve in all the temperature regions. The structural and spectroscopic data lead to three different magnetic components; (i) the n = 1 and (ii) the n = 2 isomers with S = 1/2 and 1 ground states, respectively, as a result of the intramolecular antiferromagnetic interaction between the Cr^{III} (S = 3/2) and SQ (S = 1/2).[4] Finally, (iii) the contribution of three BEDT-TTF$^+$ cations with S = 1/2 spins. The observed value at 300 K is similar to the theoretical value of 2.75 emu·K·mol^{-1} (g = 2.00) calculated for the sum of three spin components deserved above. The decreasing of $\chi_M T$ in the region of 150–300 K might be due to thermal population from the ground state S = 1 to the excited state S = 2 in n = 2 isomer.[4] As noted above, the difficulties of the assignments for the oxidation states concerning the ligands (SQ or Cat) and complexes units (n = 1 or 2) prevent the qualitative interpretation of the intermolacular magnetic interactions, however, three kinds of intermolecular interactions within the lattice are found between [BEDT-TTF]$^+\cdots$[Cr^{III}(Cl_4SQ)(Cl_4Cat)$_2$]$^{2-}$, [BEDT-TTF]$^+\cdots$[Cr^{III}(Cl_4SQ)$_2$(Cl_4Cat)]$^-$, and [BEDT-TTF **B**]$^+\cdots$[BEDT-TTF **B**]$^+$. Although it is not obvious to see which one is responsible for

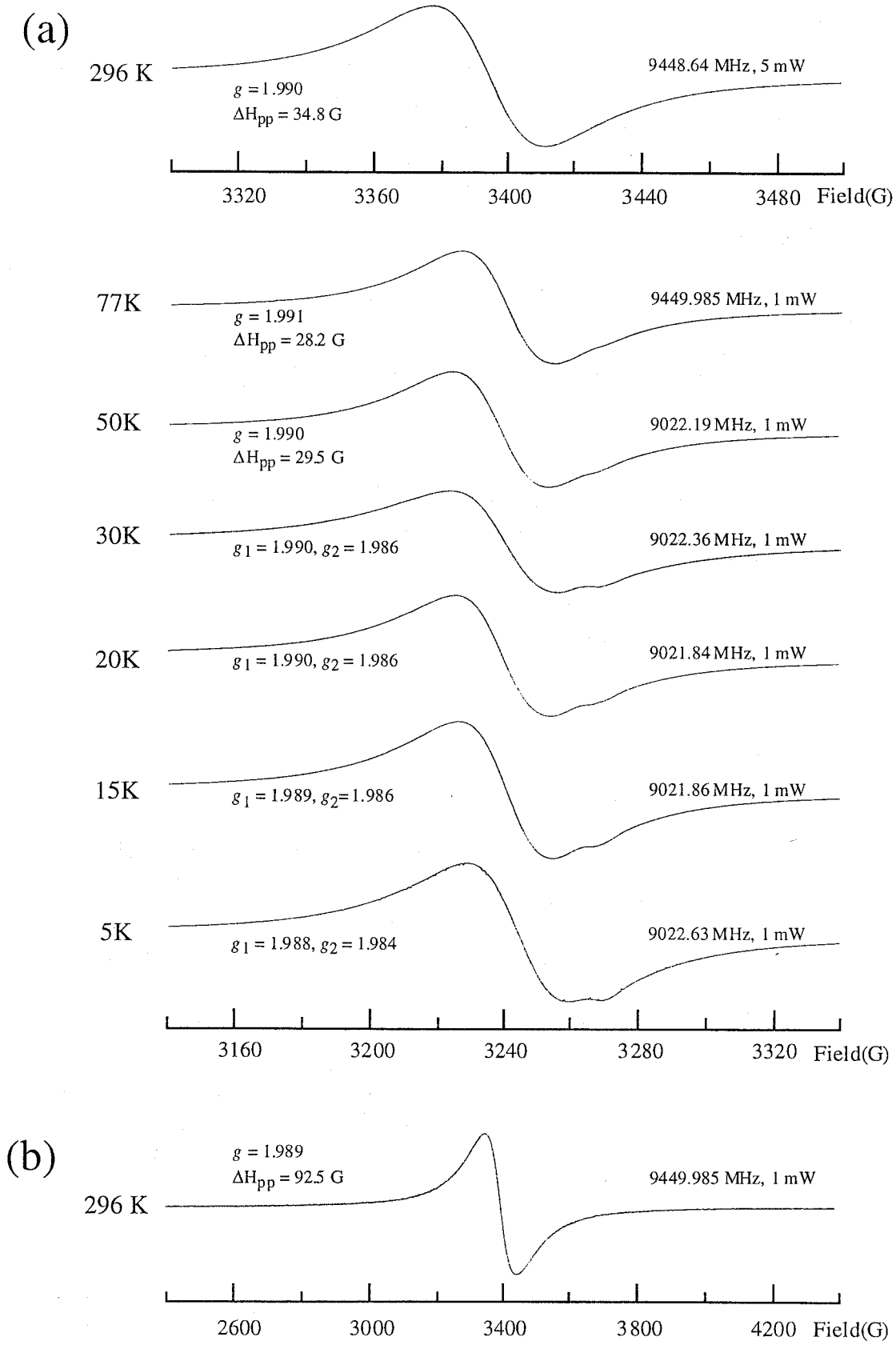

Figure 7. (a) Temperature dependence of EPR spectra of **1** and (b) the spectrum of **2** at 296 K.

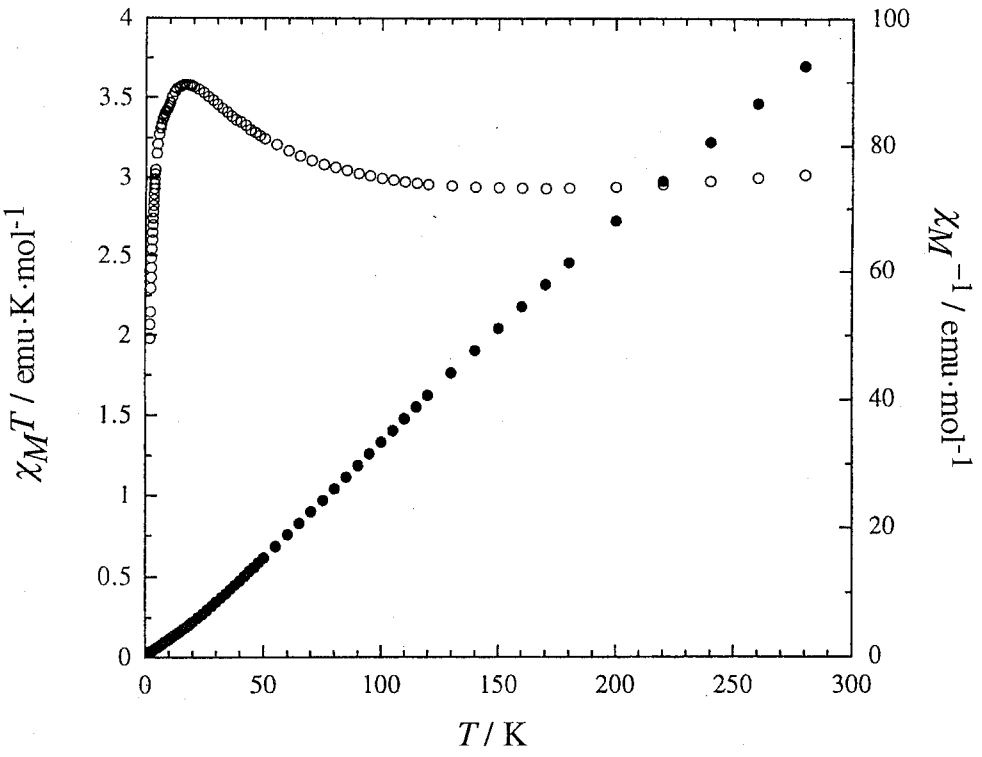

Figure 8. Temperature dependence of $\chi_m T$ (O) and χ_m^{-1} (●) of **1** under the field of 1 T.

the observed ferromagnetic coupling, the best candidate seems to be the interaction in which the BEDT–TTF$^+$ cations and the ligand moieties of the anions stacked each other. The intermolecular interactions through the ligands moieties could participate because the paramagnetic nature of the SQ ligands.[19] The through-bond intramolecular magnetic interactions between coordinated SQ ligands and paramagnetic metal ions have been well-studied.[3(a),20] On the other hand, compounds **1** and **2** regard as first examples for the intermolecular ferromagnetic interaction between the two components including the *o*-quinone metal complexes.

Conclusion

This chapter demonstrates the synthesis, crystal structure, and physicochemical properties of intra- and intermolecular mixed-valence CT compounds, **1** and **2**, with the paramagnetic BEDT-TTF^{+} cations. The compounds include two kinds of mixed-valence redox isomers, thus, could be described another type of mixed-valence supramolecular assemblies compared with those described in Chapters 2 and 4. With the characteristic three-dimensional crystal structure, the compounds show dominant ferromagnetic interaction with semiconducting behaviors. The X-ray crystal structural and spectroscopic data indicate that the 3:2 composition of the compounds arises from the preferable crystal packing with one chromium complex and three BEDT-TTF cations in the absence of aromatic solvates such as benzene. It is likely that $Cr^{III}(X_4SQ)_3$ can change their valence states depending on the preferable crystal packing to realize the coexistence of two kinds of mixed-valence redox isomers.

References

(1) (a) Dance, I. G.; Scudder, M. L. *J. Chem. Soc., Dalton Trans.* **1998**, 1341. (b) Lewis, G.; Dance, I. *J. Chem. Soc., Dalton Trans.* **2000**, 3176.

(2) (a) Scudder, M. L.; Goodwin, H. A.; Dance, I. G. *New J. Chem.* **1999**, *23*, 695. (b) Breu, J.; Domel, H.; Stoll, A. *Eur. J. Inorg. Chem.* **2000**, 2401. (c) Breu, J.; Domel, H.; Norrby, P. *Eur. J. Inorg. Chem.* **2000**, 2409.

(3) (a) Pierpont, C. G.; Lange, C. W. *Prog. Inorg. Chem.* **1994**, *41*, 331. (b) Adams, D. M.; Noodleman, L.; Hendrickson, D. N. *Inorg. Chem.* **1997**, *36*, 3966. (c) Jung, O. -S.; Pierpont, C. G. *J. Am. Chem. Soc.* **1994**, *116*, 2229.

(4) Chapter 4 in this thesis.

(5) (a) Matos, M. J.; Santos, I. C.; Henriques, R. T.; Duarte, M. T. *Synth. Met.* **1991**, *41*, 2155. (b) Mori, T.; Inokuchi, H. *Bull. Chem. Soc. Jpn.* **1987**, *60*, 402. (c) Bellitto, C.; Bonamico, M.; Fares, V.; Serino, P. *Inorg. Chem.* **1996**, *35*, 4070. (d) Hasegawa, T.; Kagoshima, S.; Mochida, T.; Sugiura, S.; Iwasa, Y. *Solid State Commun.* **1997**, *103*, 489.

(6) Kahn, O. *Molecular Magnetism*; VCH: New York, 1993.

(7) Jacobson, R. A. *REQABA Empirical Absorption Correction Version 1.1-03101998:* Molecular Structure Corp.: The Woodlands, TX, 1996–1998.

(8) Altomare, A.; Burla, M. C.; Camalli, M.; Cascarano, M.; Giacovazzo, C.; Guagliardi, A.; Pilidori, G. *J. Appl. Crystallogr.* **1994**, *27*, 435.

(9) Beurskens, P. T.; Admiraal, G.; Beurskens, G.; Bosman, W. P.; de Gelder, R.; Israel, R.; Smits, J. M. M. , The DIRDIF-94 program system, Technical Report of the Crystallography Laboratory; University of Nijmegen: Nijmegen, The Netherlands, 1994.

(10) *teXsan: Crystal Structure Analysis Package*; Molecular Structure Corporation: The Woodlands, TX, 1985, 1992.

(11) For the [**I**···**A**] and [**II**···**B**] sets, the mean plane distances were calculated between the planes of the quinone ligands, defined by the $Cl_4C_6O_2$ atoms, and the five- and six-membered rings of one side of BEDT-TTF molecules **A** and **B**, respectively. For the [**I**···**C**] set, the $Cl_4C_6O_2$ atoms and the central two five-membered rings of the BEDT-TTF molecules were

used.

(12) Guionneau, P.; Kepert, C. J.; Bravic, G.; Chasseau, D.; Truter, M. R.; Kurmoo, M.; Day, P. *Synth. Met.* **1997**, *86*, 1973.

(13) (a) Kobayashi, H.; Kobayashi, A.; Sasaki, Y.; Saito, G.; Inokuchi, H. *Bull. Chem. Soc. Jpn.* **1986**, *59*, 301. (b) Kobayashi, H.; Kato, R.; Mori, T.; Kobayashi, A.; Sasaki, Y.; Saito, G.; Enoki, T.; Inokuchi, H. *Chem. Lett.* **1984**, 759. (c) Kobayashi, H.; Kato, R.; Mori, T.; Kobayashi, A.; Sasaki, Y.; Saito, G.; Enoki, T.; Inokuchi, H. *Chem. Lett.* **1984**, 179. (d) Abboud, K. A.; Clevenger, M. B.; de Oliveira, G. F.; Talham, D. R. *J. Chem. Soc., Chem. Commun.* **1993**, 1560.

(14) (a) Kozlov, M. E.; Pokhodnia, K. I.; Yurchenko, A. A. *Spectrochim. Acta* **1987**, *43A*, 323. (b) Kozlov, M. E.; Pokhodnia, K. I.; Yurchenko, A. A. *Spectrochi. Acta* **1989**, *45A*, 437.

(15) (a) Pierpont, C. G.; Downs, H. H. *J. Am. Chem. Soc.* **1976**, *98*, 4834. (b) Chapter 2 in this thesis. (c) Raymond, K. N.; Isied, S. S.; Brown, L. D.; Fronczek, F. R.; Nibert, J. H. *J. Am. Chem. Soc.* **1976**, *98*, 1767.

(16) (a) Torrance, J. B.; Scott, B. A.; Welber, B.; Kauman, F. B.; Seiden, P. E. *Phys. Rev. B* **1979**, *19*, 730. (b) Gómez-García, C. J.; Ouahab, L.; Gimenez-Saiz, C.; Triki, S.; Coronado, E.; Delhaès, P. *Angew. Chem., Int. Ed. Engl.* **1994**, *33*, 223.

(17) Downs, H. H.; Buchanan, R. M.; Pierpont, C. G. *Inorg. Chem.* **1979**, *18*, 1736.

(18) It has been reported that the n = 2 isomer is ESR inactive. Sofen, S. R.; Ware, D. C.; Cooper, S. R.; Raymond, K. N. *Inorg. Chem.* **1979**, *18*, 234.

(19) Zirong, D.; Bhattacharya, S.; McCusker, J. K.; Hagen, P. M.; Hendrickson, D. N.; Pierpont, C. G. *Inorg. Chem.* **1992**, *31*, 870.

(20) Lynch, M. W.; Buchanan, R. M.; Pierpont, C. G.; Hendrickson, D. N. *Inorg. Chem.* **1981**, *20*, 1038.

Chapter 4

New Molecular Assemblies of Redox Isomers, $[Cr^{III}(X_4SQ)_{3-n}(X_4Cat)_n]^{-n}$ (X = Cl and Br; n = 0, 1, and 2), with Metallocenium Cations, $[M^{III}Cp_2]^+$ (M = Co and Fe)

Abstract

A series of redox isomers of $[Cr^{III}(X_4SQ)(X_4Cat)_2]^{2-}$, $[Cr^{III}(X_4SQ)_2(X_4Cat)]^-$, and $[Cr^{III}(X_4SQ)_3]^0$ (X = Cl and Br, SQ = semiquinonate, and Cat = catecholate) have been synthesized and characterized as charge-transfer (CT) compounds with metallocenium cations:

$(Co^{III}Cp_2)_2[Cr^{III}(Cl_4SQ)(Cl_4Cat)_2]$ (**1**)
$(Co^{III}Cp_2)_2[Cr^{III}(Br_4SQ)(Br_4Cat)_2]$ (**2**)
$(Co^{III}Cp_2)[Cr^{III}(Cl_4SQ)_2(Cl_4Cat)]\cdot C_6H_6$ (**3**)
$(Co^{III}Cp_2)[Cr^{III}(Br_4SQ)_2(Br_4Cat)]$ (**4**)
$(Fe^{III}Cp_2)[Cr^{III}(Cl_4SQ)_2(Cl_4Cat)]\cdot C_6H_6$ (**5**)
$(Fe^{III}Cp_2)[Cr^{III}(Br_4SQ)_2(Br_4Cat)]\cdot CS_2$ (**6**)
$(Fe^{III}Cp_2)[Cr^{III}(Cl_4SQ)_2(Cl_4Cat)][Cr^{III}(Cl_4SQ)_3]$ (**7**)

First, the oxidation states of the chromium complexes are strongly dependent on the redox potentials of the metallocenes used. The $Co^{II}Cp_2$, exhibiting stronger reduction power than $Fe^{II}Cp_2$, is useful for two-electrons reduction of the $[Cr^{III}(X_4SQ)_3]^0$, affording $[Cr^{III}(X_4SQ)(X_4Cat)_2]^{2-}$ redox isomers (**1** and **2**), which are first isolated and crystallographically characterized in the solid state. In contrast the reaction with $Fe^{II}Cp_2$ affords only $[Cr^{III}(X_4SQ)_2(X_4Cat)]^-$ redox isomers (**5**–**7**). Second, solvents influence crystal structures of these compounds. The solvent set of benzene/carbondisulfide gives 1:1:C_6H_6 compound **5** with unique charged anions, $[Cr^{III}(Cl_4SQ)_2(Cl_4Cat)]^-$, while the other set, *n*-hexane/carbondisulfide, affords 1:2 compound (**7**) including the two redox isomers, $[Cr^{III}(Cl_4SQ)_2(Cl_4Cat)]^-$ and $[Cr^{III}(Cl_4SQ)_3]^0$.

The $[Cr^{III}(X_4SQ)(X_4Cat)_2]^{2-}$ anions in **1** and **2** show no significant interconnection between them (discrete type), while the $[Cr^{III}(X_4SQ)_2(X_4Cat)]^-$ isomers in **5**–**7** form one-dimensional column type structures with the aid of intermolecular stacking interactions of the ligand moieties. The anions in **3** and **5** show additional stacking interaction with the $[M^{III}Cp_2]^+$ (M =

Co and Fe) to form one-dimensional ···[D][A][S]··· (D = $[M^{III}Cp_2]^+$, A = $[Cr^{III}(Cl_4SQ)_2(Cl_4Cat)]^-$, and S = benzene) type mixed-stack arrangements. Compound **7** forms two-dimensional layer structure where the two redox isomers, $[Cr^{III}(Cl_4SQ)_2(Cl_4Cat)]^-$ and $[Cr^{III}(Cl_4SQ)_3]^0$, are included. Consequently, the layer is regarded as an *intermolecular* mixed-valence molecular assembly.

Two types of the redox isomers, $[Cr^{III}(X_4SQ)(X_4Cat)_2]^{2-}$ (**1** and **2**) and $[Cr^{III}(X_4SQ)_2(X_4Cat)]^-$ (**3**–**7**), exhibiting an *intramolecular* mixed-valence state, show intramolecular intervalence CT transition (IVCT) from the Cat to the SQ near 5800 and 4300 cm^{-1}, respectively, both in the solution and in the solid states. The *intermolecular* mixed-valence state of **7** was characterized by absorption spectroscopy, electric conductivity, and SQUID magnetometry. Interestingly, this mixed-valence state of the chromium module is dependent on the redox active nature of the coordinated ligands.

Introduction

Transition metal complexes with *o*-quinone ligands have been one of intriguing subjects of intensive research in the last few decades due to the rich redox chemistry based on a variety of formal oxidation states not only for the metal center but also for the ligand moieties.[1] Valence tautomerism involving *o*-quinone ligands and transition metals has been discovered and increasingly studied in recent years, especially for heteroleptic cobalt and manganese complexes, $M^{III}(SQ)(Cat)(N\text{-}N)$ (SQ = semiquinonate, Cat = catecholate, N-N = nitrogen donor).[2]

The author's interest is focused on homoleptic complexes where redox isomers, SQ and Cat, are simultaneously coordinated to the metal ion to give a complex generally written as $[M(SQ)_m(Cat)_n]$ because the mixed-valence ligands are related, in a sense, to a class of complexes with mixed-valence metal ions linked by a bridging ligand. In addition, such complexes are also noted as a new type of modules for molecular assemblies because in the solid phase an intermolecular SQ···SQ radical type and/or SQ···Cat charge-transfer (CT) type interactions should be expected. Some of extended arrays of the *o*-quinone metal complexes have been found,[3] where the direct stack between the ligand moieties occurs between the adjacent complexes. The physical properties ascribed to the assembly, however, have not been reported, while the reduced and oxidized forms of metal-free *p*-benzoquinones (BQ) molecules are well-known for their ability to form stacking structures and to give conductive donor-acceptor compounds.[4] The properties arising from the coexistence of the intra- and/or intermolecular CT interactions and local spins on the metal ions are an intriguing target when the transition metal complexes are utilized.

The author presented a detailed discussion about the structural features of CT compounds derived from tris(*o*-tetrahalogenosemiquinonate) chromium(III), $Cr^{III}(X_4SQ)_3$ (X = Cl and Br), which undergo electrochemical reduction at 0.82 (Cl) and 0.44 (Cl), and 0.83 (Br) and 0.43 (Br) V (vs SCE), respectively, to afford $[Cr^{III}(X_4SQ)_2(X_4Cat)]^-$ and $[Cr^{III}(X_4SQ)(X_4Cat)_2]^{2-}$ redox isomers (Scheme 1) Using equivalent amounts of tetrathiafulvalene (TTF) derivatives and $Co^{II}Cp_2$, the author has isolated $[Cr^{III}(X_4SQ)_2(X_4Cat)]^-$ isomers as the CT compounds.[5]

Scheme 1

$$Cr^{III}(X_4SQ)_3 \rightleftharpoons [Cr^{III}(X_4SQ)_2(X_4Cat)]^- \rightleftharpoons [Cr^{III}(X_4SQ)(X_4Cat)_2]^{2-} \rightleftharpoons [Cr^{III}(X_4Cat)_3]^{3-}$$

(X = Cl and Br)

The anions include two types of ligands, SQ and Cat, and show intramolecular intervalence (IVCT) transition (SQ ← Cat) near 4000 cm^{-1} in the solid state. One of the other redox isomers with mixed-charge ligands is a two-electron-reduced complex, $[Cr^{III}(X_4SQ)(X_4Cat)_2]^{2-}$, whose structure and properties in the solid state have been still unknown. The crystal and electronic structural comparison of these two isomers is of great interest regarding their assembled structures. It has been demonstrated that the TTF derivatives could not reduce $[Cr^{III}(X_4SQ)_2(X_4Cat)]^-$ isomers to $[Cr^{III}(X_4SQ)(X_4Cat)_2]^{2-}$ one because of the restricted reduction power ($E_{1/2}$ = 0.445 (tetramethyltetraselenafulvalene, TMTSF) and 0.520 (tetrakis(methylsulfanyl)tetrathiafulvalene, TMT-TTF) V (vs. SCE)). On the other hand, $Co^{II}Cp_2$, widely used as one-electron reductant, has stronger power of the reduction ($E_{1/2}$ = – 0.86 V).[6] Based on this chemical property, the author has first succeeded in the isolation of $[Cr^{III}(X_4SQ)(X_4Cat)_2]^{2-}$ isomers as CT compounds with $[Co^{III}Cp_2]^+$. In addition, 1:2 ($[Fe^{III}Cp_2]^+$:[Cr complex]) compound containing two redox isomers, $[Cr^{III}(Cl_4SQ)_2(Cl_4Cat)]^-$ and neutral $[Cr^{III}(Cl_4SQ)_3]^0$, has been prepared using $Fe^{II}Cp_2$. The compound exhibits, in a sense, *intermolecular* mixed-valence state indicative of a new class of molecular solid.

Experimental Section

Materials.

All the chemicals were reagent grade. $Co^{II}Cp_2$ was obtained from Aldrich. Syntheses of **1–4** were carried out under a dry nitrogen atmosphere by use of standard Schlenk techniques with freshly distilled solvents. $Fe^{II}Cp_2$[7] and $Cr^{III}(X_4SQ)_3 \cdot 4C_6H_6$ (X = Cl and Br) were prepared by the procedure described previously.[5]

Preparation of the compounds.

$(Co^{III}Cp_2)_2[Cr^{III}(Cl_4SQ)(Cl_4Cat)_2]$ (1) A 200 ml dichloromethane suspension containing $Cr^{III}(Cl_4SQ)_3 \cdot 4C_6H_6$ (1212 mg, 1.100 mmol) and $Co^{II}Cp_2$ (458 mg, 2.42 mmol) was refluxed for a day under dry nitrogen. The mixture was filtered and washed with dichloromethane several times, and the bluish violet product, which is a monoanion, was completely extracted by Soxhlet extractor with 200 ml of dichloromethane for a day. The reddish violet powder was isolated in 65% yield (830 mg). The product contains 1 mol of dichloromethane molecules. Found: C, 37.02; H, 1.88. $C_{39}H_{22}O_6Cl_{13}Co_2Cr$ requires C, 37.39; H, 1.77. The single crystal was obtained by careful diffusion of *n*-hexane to the filtrate obtained above. IR (KBr): 3370m, 3108m, 3078m, 2910w, 2832w, 2706w, 2515w, 2428w, 2182w, 1829w, 1718w, 1639w, 1445s, 1415s, 1373m, 1319m, 1289w, 1250s, 1124s, 1106s, 1057s, 1009m, 973s, 858s, 847m, 806m, 790s, 740m, 689m, 555m, 501w, 457s, 440w, and 420w cm^{-1}.

$(Co^{III}Cp_2)_2[Cr^{III}(Br_4SQ)(Br_4Cat)_2]$ (2) A 150 ml dichloromethane suspension containing $Cr^{III}(Br_4SQ)_3 \cdot 4C_6H_6$ (1584 mg, 0.9690 mmol) and $Co^{II}Cp_2$ (385 mg, 2.04 mmol) was refluxed for a day under dry nitrogen. The mixture was filtered, washed with dichloromethane several times until the washings were no longer colored, and dried in a vacuum. The reddish violet microcrystals were isolated in a 88% yield (1490 mg). A single crystal was obtained by careful diffusion of diethylether to the filtrate obtained above. Found: C, 26.41; H, 1.25. $C_{38}H_{20}O_6Br_{12}Co_2Cr$ requires C, 26.83; H, 1.18. IR (KBr): 3371w, 3103m, 3089m, 2911w, 2846w, 2671w, 2509w, 2089w, 1810w, 1730w, 1632w, 1440s, 1415s, 1347w, 1297m, 1258s, 1234m, 1206w, 1134s, 1053s, 1008m, 929s, 857m, 846w, 820w, 752m, 740m, 708m, 624w, 600w, 544m, 500w, 459m, 423w, and 408w cm^{-1}.

$(Co^{III}Cp_2)[Cr^{III}(Cl_4SQ)_2(Cl_4Cat)]\cdot C_6H_6$ (3) $Co^{II}Cp_2$ (29 mg, 0.15 mmol) was added to a dichloromethane suspension (100 ml) of $Cr^{III}(Cl_4SQ)_3\cdot 4C_6H_6$ (164 mg, 0.149 mmol) under a dry nitrogen, turning from reddish purple to bluish purple in few minutes. The suspension was stirred for two days, then evaporated to a half volume. To the residue 100 ml of *n*-hexane were added. The solid product was collected by filtration and washed with small amounts of dichloromethane three times. Recrystallization from dichloromethane/benzene gave dark purple single crystals with solvated benzene (123 mg, 83%). The compound is soluble in dichloromethane and acetone. Found: C, 38.43; H, 1.57. $C_{34}H_{16}Cl_{12}CoCrO_6$ requires C, 38.64; H, 1.53. IR (KBr): 1476m, 1435m, 1416m, 1308s, 1248m, 1117s, 980m, 797s, 691m, 677m, 583w, and 450s cm^{-1}.

$(Co^{III}Cp_2)[Cr^{III}(Br_4SQ)_2(Br_4Cat)]$ (4) To a 100 ml of dichloromethane suspension containing $Cr^{III}(Br_4SQ)_3\cdot 4C_6H_6$ (154 mg, 0.0942 mmol) was added $Co^{II}Cp_2$ (18 mg, 0.0952 mmol) with stirring under a dry nitrogen. After several hours the suspension gradually turned bluish purple. It was evaporated to a half volume, and a 100 ml *n*-hexane was added. The microcrystalline solid obtained was filtered off, washed with small amounts of dichloromethane, and dried in vacuum (130 mg, 78%). The compound is soluble in dichloromethane and acetone. Found: C, 22.25; H, 1.19. $C_{28}H_{10}Br_{12}CoCrO_6$ requires C, 22.24; H, 0.67. IR (KBr): 1487w, 1449m, 1412s, 1348w, 1312m, 1244s, 1211w, 1167s, 1107s, 1061m, 1009w, 934s, 860w, 752m, 727w, 700m, 623w, 560m, and 500m cm^{-1}.

$(Fe^{III}Cp_2)[Cr^{III}(Cl_4SQ)_2(Cl_4Cat)]\cdot C_6H_6$ (5) Single crystals of the compound were grown from a layered solution of a 50 ml carbon disulfide solution containing $Cr^{III}(Cl_4SQ)_3\cdot 4C_6H_6$ (101 mg, 0.0916 mmol) and a 50 ml benzene solution containing $Fe^{II}Cp_2$ (17 mg, 0.092 mmol). Bluish violet cubic crystals were obtained after a week. Found: C, 38.71; H, 1.64. $C_{34}H_{16}O_6Cl_{12}CrFe$ requires C, 38.75; H, 1.53. IR (KBr): 3102w, 2726w, 2534w, 1476m, 1435m, 1416m, 1307m, 1248w, 1179s, 1103s, 1049s, 1011m, 980s, 847m, 797s, 785s, 691m, 677s (C_6H_6), 624w, 608w, 582w, 545w, 522w, 443s, and 417s cm^{-1}.

$(Fe^{III}Cp_2)[Cr^{III}(Br_4SQ)_2(Br_4Cat)]\cdot CS_2$ (6) Single crystals of the compound were grown from a layered solution of a 300 ml carbon disulfide solution containing $Cr^{III}(Br_4SQ)_3\cdot 4C_6H_6$ (500 mg, 0.306 mmol) and a 200 ml *n*-hexane solution containing $Fe^{II}Cp_2$ (57 mg, 0.31

mmol). Bluish violet cubic crystals were obtained after a week. Found: C, 22.09; H, 0.76. $C_{29}H_{10}O_6Br_{12}CrFeS_2$ requires C, 21.97; H, 0.64. IR (KBr): 3100w, 2458w, 1450m, 1430m, 1418m, 1349w, 1310w, 1288w, 1245m, 1232m, 1210w, 1166s, 1120s, 1106s, 1051m, 1009w, 933s, 850m, 752m, 699m, 623w, 559w, 503w, and 405 cm^{-1}.

$(Fe^{III}Cp_2)[Cr^{III}(Cl_4SQ)_2(Cl_4Cat)][Cr^{III}(Cl_4SQ)_3]_2$ (7) Single crystals of the compound were grown from a layered solution of a 80 ml carbon disulfide solution containing $Cr^{III}(Cl_4SQ)_3 \cdot 4C_6H_6$ (331 mg, 0.30 mmol) and a 80 ml *n*-hexane solution containing $Fe^{II}Cp_2$ (28 mg, 0.15 mmol). Violet crystals were obtained after 1 week. Found: C, 31.20; H, 0.74. $C_{46}H_{10}O_{12}Cl_{12}Cr_2Fe$ requires C, 31.30; H, 0.57. IR (KBr): 3109w, 2722w, 2517w, 1472m, 1456s, 1446s, 1416w, 1382w, 1337m, 1310m, 1276m, 1248w, 1216s, 1117s, 1104s, 1051w, 1013w, 990s, 979s, 856w, 824m, 799s, 786m, 693m, 581w, 529w, 447s, 433s, and 416m cm^{-1}.

Physical Measurements.

Infrared spectra for KBr pellets were recorded on a Perkin-Elmer system 2000 FT-IR spectrometer over the range of 350–7000 cm^{-1} and absorption spectra on a Hitachi U-3500 spectrophotometer over the range of 3130–33000 cm^{-1} at 296 K. Magnetic susceptibilities were recorded over the temperature range 1.9–350 K at 1 T with a superconducting quantum interference device (SQUID) susceptometer (Quantum Design, San Diego, CA) interfaced with a HP Vectra computer system. All the values were corrected for diamagnetism that were calculated from Pascal's table.[8]

Crystallographic Data Collection and Refinement of Structures.

For compounds **1** and **3**, data collection was made on a Rigaku AFC7R diffractometer with graphite-monochrometed Mo Kα radiation and a rotating anode generator at 296 K. The crystal of **1** was mounted in a thin-walled glass capillary with mother liquor. Unit cell constants and an orientation matrix for data collection were obtained from least-squares refinements using the setting angles of 25 carefully centered reflections in the ranges $6.79° < 2\theta < 14.45°$(**1**) and $28.66° < 2\theta < 29.93°$(**3**). Independent reflections of 6121(**1**) and 8945(**3**) were obtained, and 1815(**1**) and 4538(**3**) of them with $I > 2\sigma(I)$(**1**) and $I > 3\sigma(I)$(**3**) were used in the full-matrix

least-squares refinements. For compounds **2** and **5–7**, the measurements were performed on a Rigaku mercury diffractometer with CCD two-dimensional detector with Mo Kα radiation employing a graphite monochromator at 296 K. The sizes of the unit cells were calculated from the reflections collected on the setting angles of four frames by changing ω by 0.5° for each frame. Two different χ settings were used and ω was changed by 0.5° per frame. Intensity data were collected in 480 frames with an ω scan width of 0.5° and exposure times 150, 25, 60, and 120 s for **2** and **5–7**, respectively. Empirical absorption correction using the program REQABA[9] was performed for all the data. All the crystal data are summarized in Table 1. The structures were solved by direct methods[10] and expanded using Fourier techniques.[11] The final cycles of the full-matrix least-squares refinements were based on the observed reflections ($I > 3\sigma(I)$). All the calculations were performed using the teXsan crystallographic software package of Molecular Structure Corporation.[12] For compound **1**, all the atoms except for Co(1), Co(2), and Cr(1) were refined isotropically. For compounds **2**, **3**, and **5–7** the non-hydrogen atoms were refined anisotropically and all the hydrogen atoms were placed in the idealized positions, but their parameters were not refined. In compound **2** the disorder of the Cp ring containing C(34)–C(38) was found at the final stage, and thus its atom positions were isotropically refined under a rigid condition.

Table 1. Crystallographic and Refinement Data for **1–3**

	1	**2**	**3**
Formula	$C_{38}H_{20}O_6Cl_{12}Co_2Cr$	$C_{38}H_{20}O_6Br_{12}Co_2Cr$	$C_{34}H_{16}O_6Cl_{12}CoCr$
Formula weight	1167.87	1701.28	1056.86
Color	reddish violet	reddish violet	bluish violet
Crystal size, mm	0.40×0.30×0.05	0.17×0.17×0.12	0.50×0.50×0.30
Crystal system	monoclinic	monoclinic	triclinic
Space group	$P2_1/n$	$P2_1/n$	$P\bar{1}$
a, Å	9.760(5)	13.472(1)	10.950(4)
b, Å	31.535(6)	20.5443(5)	13.961(3)
c, Å	14.191(7)	17.6961(3)	14.297(3)
α, deg			104.95(2)
β, deg	108.08(4)	110.4321(4)	112.45(2)
γ, deg			81.65(2)
Z	4	4	2
V, Å^3	4152(3)	4589.8(5)	1948(1)
ρ_{calcd}, g/cm^3	1.868	2.462	
μ, cm^{-1}	18.66	114.70	15.71
T, K	296	296	296
λ(Mo Kα), Å	0.71069	0.71069	0.71069
No. observations	1815[a]	4266	4538
No. parameters	252	494	488
Refls./para. ratio	7.2	8.64	9.30
GOF	2.40	1.38	1.48
R_{int}	0.042	0.025	0.031
R, R_w[b]	0.102, 0.113	0.038, 0.041	0.042, 0.045

[a] $I > 2.00\sigma(I)$. [b] $R = \Sigma||F_0|-|F_0||/\Sigma|F_0|$, $R_w = [\Sigma(|F_0|-|F_0|)^2/\Sigma w|F_0|^2)]^{1/2}$.

Table 1(continue). Crystallographic and Refinement Data for **5–7**

	5	**6**	**7**
Formula	$C_{34}H_{16}O_6Cl_{12}CrFe$	$C_{29}H_{16}O_6Br_{12}CrFeS_2$	$C_{46}H_{10}O_{12}Cl_{24}Cr_2Fe$
Formula weight	1053.78	1585.21	1765.29
Color	bluish violet	bluish violet	violet
Crystal size, mm	0.45×0.38×0.22	0.40×0.10×0.03	0.50×0.12×0.05
Crystal system	triclinic	triclinic	monoclinic
Space group	$P\bar{1}$	$P\bar{1}$	$C2_1/c$
a, Å	10.9364(3)	11.075(1)	23.904(2)
b, Å	13.939(2)	11.2691(7)	17.807(3)
c, Å	14.3387(8)	16.899(2)	16.6538(4)
α, deg	82.036(3)	86.120(3)	
β, deg	75.470(2)	80.609(1)	123.2850(5)
γ, deg	67.498(1)	73.578(1)	
Z	2	2	4
V, Å^3	1952.2(3)	1995.3(3)	5925(1)
ρ_{calcd}, g/cm^3	1.793	2.638	1.979
μ, cm^{-1}	15.15	128.33	17.43
T, K	296	296	296
λ(Mo Kα), Å	0.71069	0.71069	0.71069
No. observations	4153	3289	3433
No. parameters	487	460	385
Refls./para. ratio	8.53	7.15	8.92
GOF	2.40	1.80	1.62
R_{int}	0.012	0.022	0.020
R, R_w[a]	0.034, 0.052	0.049, 0.054	0.042, 0.045

[a] $R = \Sigma||F_0|-|F_0||/\Sigma|F_0|$, $R_w = [\Sigma(|F_0|-|F_0|)^2/\Sigma w|F_0|^2)]^{1/2}$.

Results and Discussion

Syntheses.

Complexes $Cr^{III}(X_4SQ)_3$ undergo electrochemical reduction, capable of receiving three electrons on the ligand moieties, and afford $[Cr^{III}(X_4SQ)_2(X_4Cat)]^-$, $[Cr^{III}(X_4SQ)(X_4Cat)_2]^{2-}$, and $[Cr^{III}(X_4Cat)_3]^{3-}$ redox isomers.[13] On the other hand, $M^{II}Cp_2$ (M = Co and Fe) are oxidized to diamagnetic $[Co^{III}Cp_2]^+$ and paramagnetic $[Fe^{III}Cp_2]^+$ cations, respectively. In general, the CT reaction strongly depends on the redox potentials of the donor and the acceptor molecules used. It is worth noting that the oxidation potential of $Co^{II}Cp_2$ (–0.86 V vs SCE) is extremely low in comparison with those of $Fe^{II}Cp_2$ (0.49 V) and TTF derivatives (0.445 (TMTSF), 0.520 (TMT-TTF) V), exhibiting strong reducing power. The stoichiometric mixing of metallocene causes a CT reaction to give 1:1 (**3–6**) compounds. The second reduction of the ligand also occurs in the presence of two moles of the $Co^{II}Cp_2$ to form 2:1 compounds (**1** and **2**) (Scheme 2).

Scheme 2

$$Cr^{III}(X_4SQ)_3 \xrightarrow{M^{II}Cp_2\,(M = Co,\ Fe)} [Cr^{III}(X_4SQ)_2(X_4Cat)]^- \xrightarrow{Co^{II}Cp_2} [Cr^{III}(X_4SQ)(X_4Cat)_2]^{2-}$$

(X = Cl and Br)

Compounds **3–6** Compounds **1** and **2**

Interestingly, solvents used influence crystal structures where the stoichiometic ratios of the cation to anion are 1:1 to 1:2; a combination of benzene/carbondisulfide affords $1:1:C_6H_6$ compound (**5**), while *n*-hexane/carbondisulfide gives 1:2 compound **7**. This is associated with a stacking nature of the benzene molecule, which plays an important role into stabilizing the overall packing structures where a mixed-stack form preferentially occurs(see Figure 7(a)).

Molecular Structures.

Figures 1–3 show ORTEP[14] drawings of **1–3** and **5–7** with the atom numbering schemes. In compounds **1** and **2**, there are two crystallographically independent $CoCp_2$ molecules, while compounds **3** and **5–7** contain one crystallographically independent $FeCp_2$ molecule. At 296 K, compounds **3** and **5** are isostructural. The iron atom of **7** is located at the special position

(3/4, –1/4, 1/2), only one of the Cp ring moieties being unique. All the compounds contain one homoleptic chromium complex, $[Cr(C_6O_2X_4)_3]$ (X = Cl for **1**, **3**, **5**, and **7** and Br for **2** and **6**), where the three coordinated ligands are labeled as **I**, **II**, and **III**. Compounds **3** (**5**) and **6** are solvated with benzene and carbondisulfide, respectively.

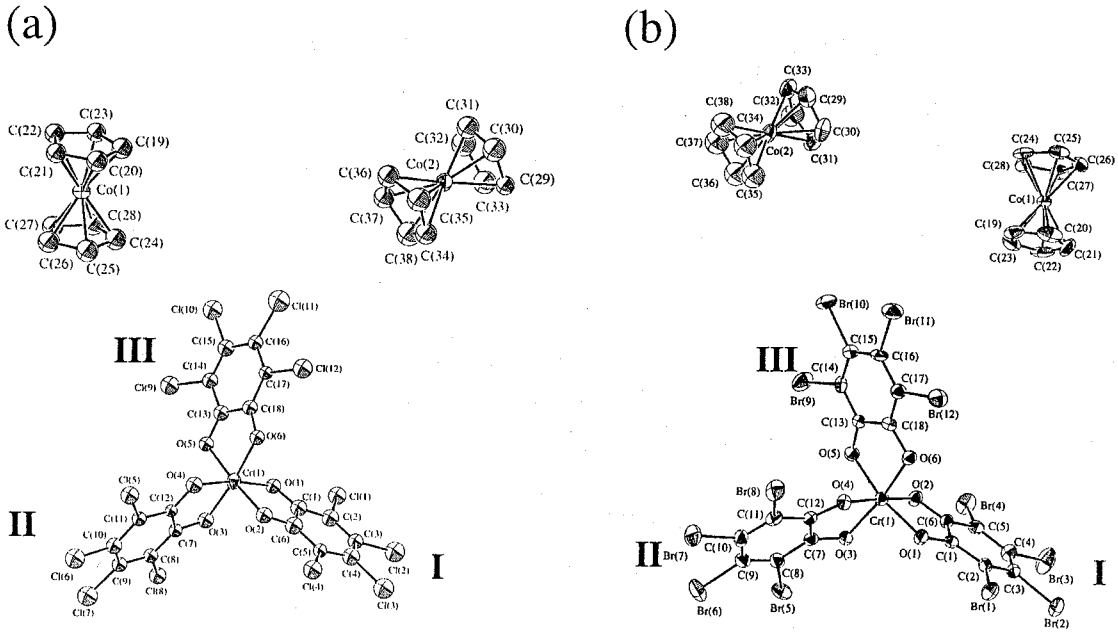

Figure 1. ORTEP drawings of (a) **1** and (b) **2** with hydrogen atoms omitted (showing 30% isotropic thermal ellipsoids). Crystallographically independent ligands are designated **I**, **II**, and **III**.

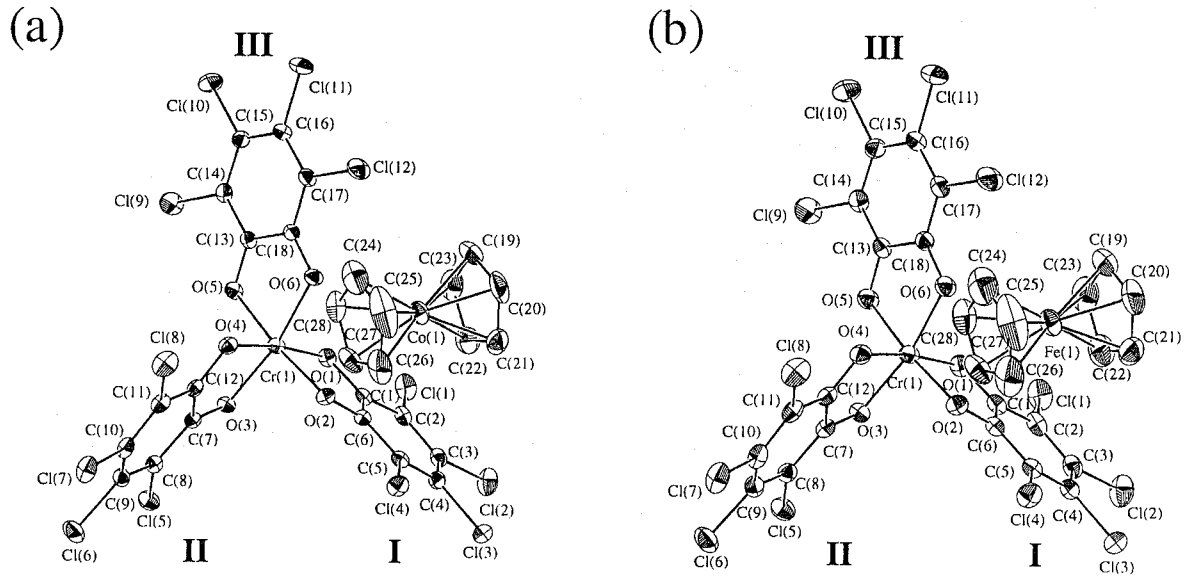

Figure 2. ORTEP drawings of (a) **3** and (b) **5** with hydrogen atoms and benzene omitted (showing 30% anisotropic thermal ellipsoids). Crystallographically independent ligands are designated **I**, **II**, and **III**.

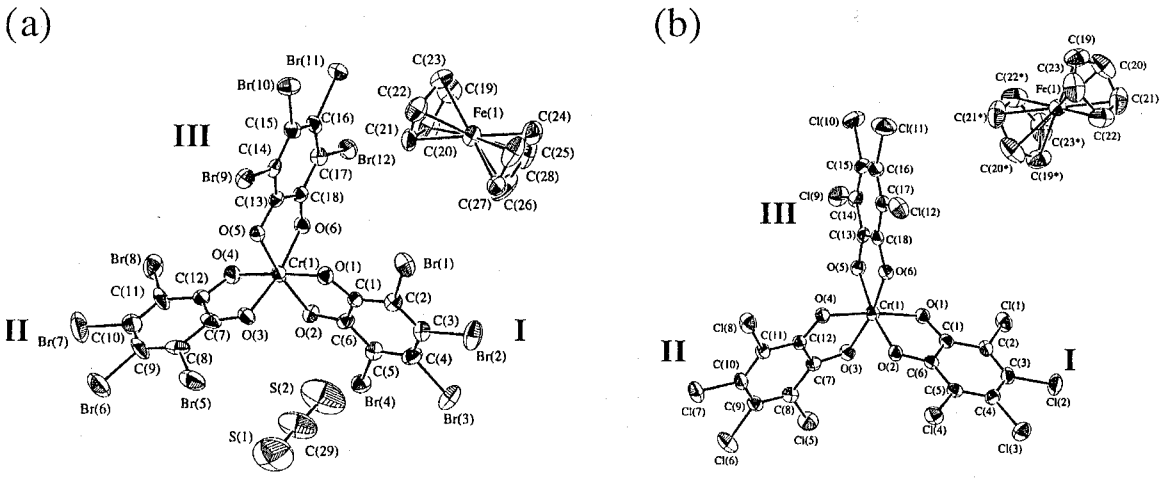

Figure 3. ORTEP drawings of **6** and **7** with hydrogen atoms omitted (showing 30% anisotropic thermal ellipsoids). The $FeCp_2$ molecule of **7** has centroids coincident with crystallographic symmetry. Three crystallographically independent ligands are designated **I**, **II**, and **III**.

$[M^{III}Cp_2]^+$ The average bond distances and angles relevant to each MCp_2 molecule in **1–3** and **5–7** are listed in Table 2 together with those of $[M^{II}Cp_2]^0$ and $[M^{III}Cp_2]^+$ (M = Co and Fe) reported so far. The Co–C bond distances of **1** and **2** range from 1.96(4) to 2.09(3) Å, averaged to 2.01(4) (**1**) and 2.01(1) (**2**) Å, respectively. The C–C bond distances range from 1.30(5) to 1.52(5) Å, averaged to 1.39(5) (**1**) and 1.39(2) (**2**) Å, respectively. These distances are shorter than those of $[Co^{II}Cp_2]^0$ (2.096(8) and 1.41(1) Å),[15(a)] and in accord with those of previously reported distances of 2.023(5) and 1.402(6) Å for $[Co^{III}Cp_2]^+$.[15(b)]

The Fe–C bond distances fall within the ranges of 2.023(6)–2.094(5), 2.03(2)–2.12(2), and 2.038(7)–2.073(6) Å for **5–7**, respectively, and the average values are slightly longer than 2.033 Å found for $[Fe^{II}Cp_2]^0$,[15(c)] showing a similar trend for $[Fe^{III}Cp_2]^+$ reported so far.[15(d)] The crystal structures of the cationic moieties clearly indicate that the $[M^{II}Cp_2]^0$ molecules are oxidized to $[M^{III}Cp_2]^+$ in all the compounds.

Chromium complexes The geometry of the chromium ion is all the distorted octahedrons with six oxygen atoms from the three bidentate ligands **I–III**. In Table 3 the Cr–O, C–C, and C–O bond distances and O–Cr–O angles are listed in comparison with those of complexes $Cr^{III}(Cl_4SQ)_3 \cdot CS_2 \cdot 1/2C_6H_6$.[3(c)] The average Cr–O and C–C bond distances for the three ligand moieties of all the compounds, hereafter called total average, show constant values of 1.94 and 1.40 Å, respectively. For each compound, the differences in bond distances among the

Table 2. Comparison of Average Intramolecular Bond Distances (Å) for $[M^{III}Cp_2]^+$ (M = Co and Fe) Found in **1–3** and **5–7** and previously reported $[M^{II}Cp_2]^0$ and $[M^{III}Cp_2]^+$

compound	M–C	C–C
1	2.00(4), 2.03(4)	1.38(4), 1.40(5)
2	2.01(1), 2.01(1)	1.38(3), 1.39(3)
3	2.005(9)	1.375(2)
$[Co^{II}Cp_2]^{0a}$	2.096(8)	1.41(1)
$[Co^{III}Cp_2]^{+b}$	2.023(5)	1.402(6)
5	2.066(6)	1.38(1)
6	2.06(2)	1.37(3)
7	2.056(7)	1.36(1)
$[Fe^{II}Cp_2]^{0c}$	2.033	1.389
$[Fe^{III}Cp_2]^{+d}$	2.08(1)	1.40(2)

[a] Reference 15(a). [b] Reference 15(b). [c] Reference 15(c). [d] Reference 15(d).

three ligands are in the ranges of 0.01-0.032 and 0.02-0.1 Å for Cr–O and C–C bond distances, respectively. In contrast, the total average C–O bond distances of **3** and **5–7** are in the range 1.292(6)-1.301(5) Å, which is elongated by approximately 0.2 Å from those of $Cr^{III}(Cl_4SQ)_3 \cdot CS_2 \cdot 1/2C_6H_6$. In particular, ligands **I** of **3**, **5**, and **6** seem to have long C–O and short Cr–O bond distances when compared with other ligands **II** and **III**. On the other hand, compound **2** has the total average C–O bond distances, 1.32(1) Å, which is longer by 0.02 Å than those of **3** and **5–7**. Similar trends are observed for the O–Cr–O angles, which are enlarged by the reduction of the SQ to the Cat,[16] that is, 81.8(2)° and 83.6(1)° for $Cr^{III}(Cl_4SQ)_3$ and $[Cr^{III}(Cat)_3]^{3-}$, respectively. In the present compounds, the total average O–Cr–O angles are larger by about 1.2° (**1–2**) and 0.6° (**3** and **5–7**) than that of $Cr^{III}(Cl_4SQ)_3$, respectively, indicating the reduction of the ligand moieties.

The oxidation numbers of the anionic complexes are responsible for the combination of SQ and Cat because of the inertness of the chromium center in the redox process.[13,16,17] On the basis of the ratio, $n[M^{III}Cp_2]^+/[Cr\ complex]$ (n = numbers of $[M^{III}Cp_2]^+$), the negative charge

Table 3. Intraligand and Total Average Bond Distances (Å) and Angles (°) and Estimated Charge for $[Cr^{III}(X_4SQ)_{3-n}(X_4Cat)_n]^{n-}$ Complexes in **1–3** and $Cr^{III}(Cl_4SQ)_3 \cdot CS_2 \cdot 1/2C_6H_6$

	L	**1**	**2**	**3**	$Cr^{III}(Cl_4SQ)_3$[a]
Cr–O (Å)	**I**	1.95(2)	1.951(6)	1.933(3)	
	II	1.96(2)	1.940(6)	1.936(3)	
	III	1.96(2)	1.939(6)	1.955(3)	
total average		1.96(2)	1.943(6)	1.941(3)	1.949(5)
C–O (Å)	**I**	1.31(3)	1.33(1)	1.311(5)	
	II	1.31(3)	1.32(1)	1.299(6)	
	III	1.29(3)	1.310(10)	1.292(2)	
total average		1.30(3)	1.32(1)	1.301(5)	1.280(1)
C–C (Å)	**I**	1.39(4)	1.39(1)	1.392(7)	
	II	1.39(4)	1.40(1)	1.397(7)	
	III	1.40 (4)	1.40(1)	1.399(7)	
total average		1.39(4)	1.40(2)	1.396(7)	1.40(1)
O–Cr–O (°)	**I**	83.2(9)	82.9(3)	83.3(1)	
	II	83.1(9)	82.6(2)	82.7(1)	
	III	82.4(8)	83.6(2)	81.9(1)	
total average		82.9(9)	83.0(2)	82.6(1)	81.8(2)
charge		–2	–2	–1	0

[a] Reference 3(e).

Table 3 (continue). Intraligand and Total Average Bond Distances (Å) and Angles (°) and Estimated Charge for $[Cr^{III}(X_4SQ)_{3-n}(X_4Cat)_n]^{n-}$ Complexes in **5**–**7** and $Cr^{III}(Cl_4SQ)_3 \cdot CS_2 \cdot 1/2C_6H_6$

	ligand	**5**	**6**	**7**	$Cr^{III}(Cl_4SQ)_3$[a]
Cr–O (Å)	**I**	1.928(2)	1.922(9)	1.938(3)	
	II	1.937(2)	1.954(10)	1.945(3)	
	III	1.957(2)	1.945(8)	1.949(3)	
total average		1.941(2)	1.940(10)	1.944(3)	1.949(5)
C–O (Å)	**I**	1.313(4)	1.31(2)	1.305(5)	
	II	1.300(4)	1.29(2)	1.286(5)	
	III	1.291(4)	1.30(1)	1.286(6)	
total average		1.301(4)	1.30(2)	1.292(6)	1.280(1)
C–C (Å)	**I**	1.394(5)	1.40(2)	1.403(7)	
	II	1.399(5)	1.41(2)	1.405(7)	
	III	1.402(5)	1.40(2)	1.405(7)	
total average		1.398(5)	1.40(2)	1.404(7)	1.40(1)
O–Cr–O (°)	**I**	83.08(9)	83.2(4)	83.0(1)	
	II	82.57(9)	81.2(4)	82.3(1)	
	III	81.66(9)	82.4(4)	81.9(1)	
total average		82.44(9)	82.3(4)	82.3(1)	81.8(2)
charge		–1	–1	–1, 0[b]	0

[a] Reference 3(e). [b] Estimated from absorption spectra and magnetic susceptibility.

of the chromium anions can be assigned to –2 and –1 for **1–2** and **3**, **5–6**, respectively. In the former, the two SQ ligands are reduced to the corresponding Cat form to provide $[Cr^{III}(X_4SQ)(X_4Cat)_2]^{2-}$ isomers while the $[Cr^{III}(X_4SQ)_2(X_4Cat)]^-$ isomers in **3**, **5–6** results from the reduction of one SQ to the Cat.

There have been many *heteroleptic o*-quinone transition metal complexes which are X-ray crystallographically well-characterized: the charged states on the ligand are well-distinguished in a series of the complexes $[M^{III}(SQ)(Cat)(N\text{-}N)]$ (M = Fe and Co, N-N = bidentate nitrogen coligand)[18] and Cu^{II}(tetramethylethyldiamine)(9,10-phenBQ)(9,10-phenCat) (9,10-phenBQ = 9,10-phenanthrenebenzoquinone).[3(d)] In the case of *homoleptic* complexes, a similar distinction has been found only for Ni^{II}(3,6-DTBBQ)(3,6-DTBSQ)$_2$[19(a)] and Mn^{IV}(3,6-DTBSQ)$_2$(3,6-DTBCat) (DTB = di-*tert*-butyl).[19(b)] On the other hand, the differences in structural parameters among the three ligand moieties for **1–3** and **5–6** are still small in comparison with the estimated standard deviations (Table 3). This is because a crystallographic disorder often takes place and prevents the distinction between the SQ and the Cat form from the structural parameters. Therefore the distinction of the charged state for the three ligands is restricted as far as X-ray crystallographic data are used. Fortunately, spectroscopic and magnetic susceptibility data show localized electronic structures of $[Cr^{III}(X_4SQ)(X_4Cat)_2]^{2-}$ and $[Cr^{III}(X_4SQ)_2(X_4Cat)]^-$ for **1–2** and **3**, **5–6**, respectively. Thus, hereafter, the anionic chromium complexes are written as $[Cr^{III}(X_4SQ)(X_4Cat)_2]^{2-}$ (**1–2**) and $[Cr^{III}(X_4SQ)_2(X_4Cat)]^-$ (**3–6**) without the assignment of the oxidation states to each ligand.

For compound **7**, the crystallographic data appears to impart the charge of –1 to the two molecules of chromium complexes. However, alternative assignment for the charge on the chromium complex could be established by absorption spectroscopy and temperature-dependence of magnetic susceptibility. The details are shown below.

Crystal packing structures.

Compounds 1 and 2 Figure 4 shows crystal packing diagrams of **1** and **2**. Each chromium complex anion is separated by $[Co^{III}Cp_2]^+$, where the planes of the Cp rings are not parallel to those of the ligands of the anion. The two (**1**) and seven (**2**) pairs of intermolecular X···X contacts between the halogen atoms of the adjacent anions are observed within the sum of van

der Waals radii (3.60 and 3.90 Å for Cl···Cl and Br···Br, respectively) (Table 4). However, both structures do not show the stacking arrangements of the $[Co^{III}Cp_2]^+$ and/or $[Cr^{III}(X_4SQ)(X_4Cat)]^{2-}$. This is associated with the large electrostatic repulsion because of their – 2 charged states. This aspect of the assemblage is quite different from those of the following compounds in which the anion makes intermolecular stacking arrangements.

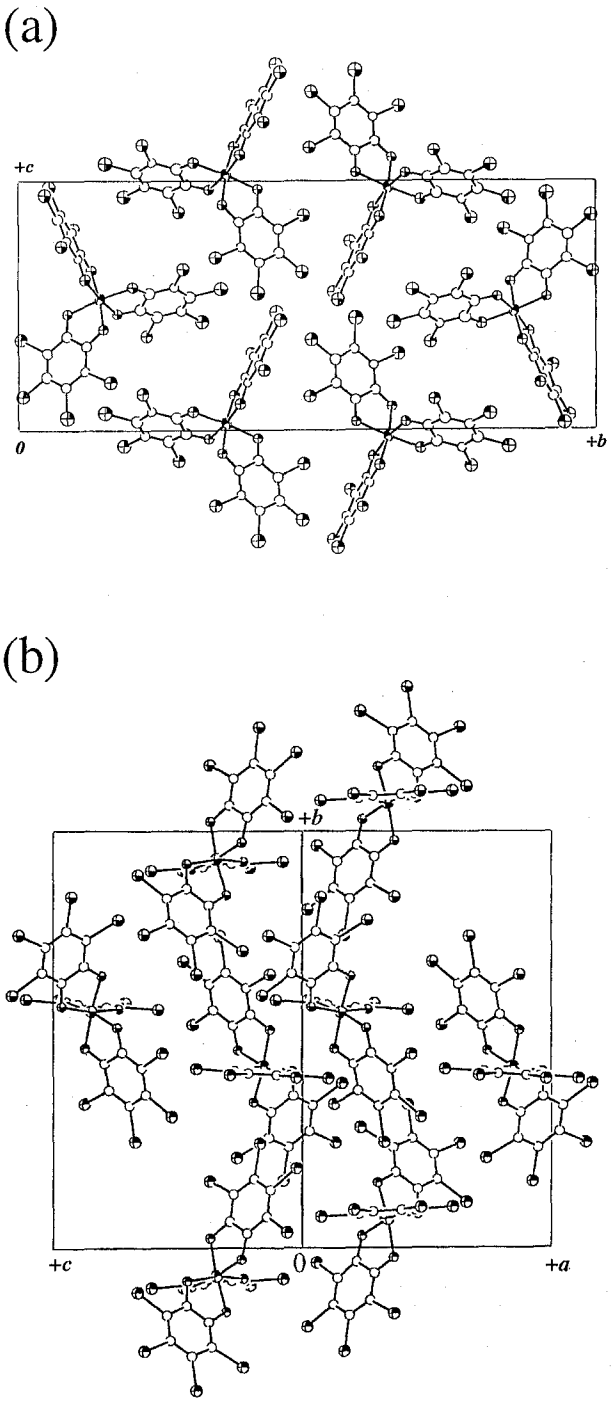

Figure 4. The crystal packing structures of $[Cr^{III}(X_4SQ)(X_4Cat)_2]^{2-}$ anions in (a) **1** and (b) **2**.

Table 4. Parameters for Intermolecular Stacking Arrangements and X···X Contacts between the Anions in **1–3** and **5–7**

compound	interplanar distance (Å)		intermolecular X···X Contacts distance (Å)			
1			Cl(2)···Cl(8*)[a]	3.47(1)	Cl(6)···Cl(10*)[b]	3.36(1)
2			Br(1)···Br(5*)[c]	3.819(2)	Br(6)···Br(10*)[d]	3.685(2)
			Br(2)···Br(7*)[c]	3.766(2)	Br(7)···Br(10*)[e]	3.897(2)
			Br(3)···Br(5*)[f]	3.873(2)	Br(8)···Br(11*)[g]	3.577(2)
			Br(6)···Br(8*)[h]	3.812(2)		
			Intracolumn (Å)		Intercolumn (Å)	
3	**I···I'**	3.473	Cl(1)···Cl(9*)[i]	3.457(2)	Cl(3)···Cl(11*)[j]	3.434(2)
	II···II'	3.507	Cl(2)···Cl(5*)[g]	3.592(2)	Cl(4)···Cl(10*)[k]	3.593(2)
			Cl(2)···Cl(7*)[l]	3.288(1)	Cl(7)···Cl(10*)[m]	3.242(2)
5	**I···I'**	3.521(4)	Cl(1)···Cl(9*)[i]	3.472(1)	Cl(3)···Cl(11*)[j]	3.454(1)
	II···II'	3.540(4)	Cl(2)···Cl(5*)[g]	3.588(2)	Cl(4)···Cl(10*)[k]	3.572(1)
			Cl(2)···Cl(7*)[l]	3.295(1)	Cl(7)···Cl(10*)[m]	3.245(1)
6	**II···II'**	3.63(2)	Br(4)···Br(7*)[c]	3.742(3)	Br(1)···Br(1*)[n]	3.513(3)
	III···III'	3.49(1)	Br(4)···Br(11*)[o]	3.699(2)	Br(2)···Br(10*)[n]	3.605(2)
			Br(8)···Br(10*)[d]	3.563(2)	Br(2)···Br(9*)[p]	3.619(2)
			Br(9)···Br(11*)[d]	3.861(2)	Br(3)···Br(5*)[p]	3.595(3)
					Br(3)···Br(11*)[o]	3.794(2)
7	**I···I'**	3.557(6)	Cl(2)···Cl(2*)[q]	3.467(3)	Cl(4)···Cl(4*)[r]	3.492(3)
	III···III'	3.583(7)	Cl(3)···Cl(12*)[s]	3.588(2)	Cl(5)···Cl(12*)[t]	3.529(2)
	I···II'	3.592(6)			Cl(6)···Cl(11*)[u]	3.189(2)
					Cl(10)···Cl(10*)[f]	3.549(7)

[a] (x, 1/2–y, 1/2+z–1). [b] (x, y, z+1). [c] (–x+1, –y, –z). [d] (–x+1, –y, –z+1). [e] (1/2–x+1, 1/2+y–*1*, –z+1). [f] (x+2, y+2, z+2). [g] (–x+2, –y, –z+1). [h] (1/2+x–1, 1/2–y–1, z). [i] (–x+1, –y+1, –z+1). [j] (–x+2, –y+1, –z+1). [k] (x+1, y–1, z). [l] (x, y, z–1). [m] (–x+1, –y+1, –z+2). [n] (–x, –y+1, –z+1). [o] (–x, –y, –z+1). [p] (x–1, y, z). [q] (–x+1, y, 1/2–z+1). [r] (–x+1, y, 1/2–z). [s] (1/2+x, 1/2–y–1, 1/2+z). [t] (x+6, y+6, z+6). [u] (x+5, y+5, z+5).

Compounds 3 and **5–7** An interesting feature of **3** and **5–7** is the one-dimensional columnar structure of the $[Cr^{III}(X_4SQ)_2(X_4Cat)_2]^-$ isomers. Figures 5(a)–(c) shows three types of one-dimensional columnar structures of **5**(**3**), **6**, and **7**, respectively. For compound **5**(**3**), each column is characterized by alternating arrangements of the Δ and Λ enantiomers, indicating stacking linkage between [**I**···**I'**] and [**II**···**II'**] for **5**(**3**). Similarly, [**II**···**II'**]/[**III**···**III'**] and

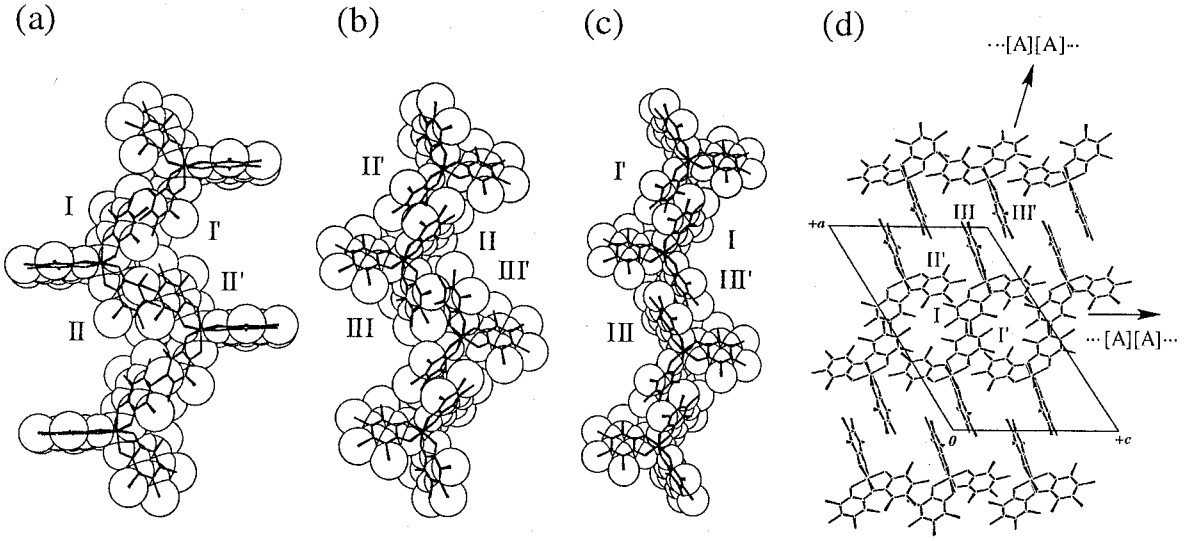

Figure 5. Space-filling representation of one-dimensional column structures of $[Cr^{III}(X_4SQ)_2(X_4Cat)]^-$ anions found in (a) **3** and **5**, (b) **6**, and (c) **7**, and (d) two-dimensional anionic layer of **7**.

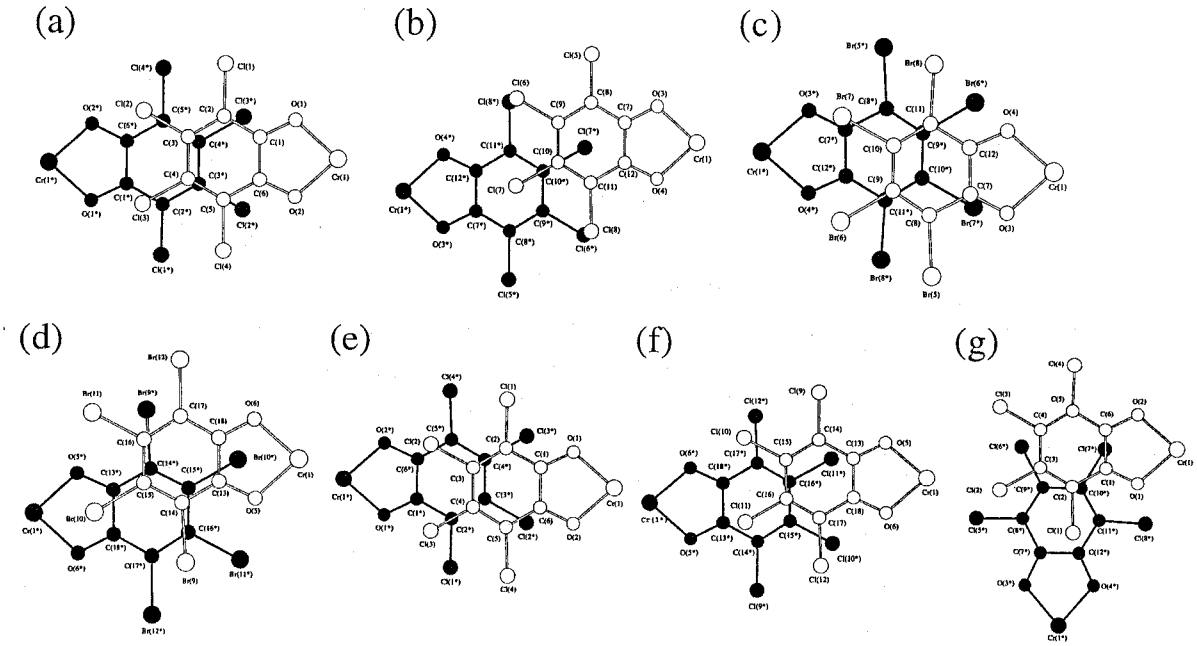

Figure 6. Views of intracolumn interactions of (a) **I···I'** (**3** and **5**), (b) **II···II'** (**3** and **5**), (c) **II···II'** (**6**), (d) **III···III'** (**6**), (e) **I···I'** (**7**), and (f) **III···III'** (**7**), and (g) intercolumn interaction **I···II'** (**7**). The stacking view projected down to a vector normal to the least-squares plane of the ligands drawn with white circles.

[**I**···**I**']/[**III**···**III**'] for **6** and **7** are found, respectively. In compound **5**(**3**), the planes of the remaining ligand (**III**) are perpendicular to the direction of the column (Figure 5(a)), while the corresponding ligands **I** and **II** for **6** and **7**, respectively, are inclined with respect to the perpendicular plane of the main axis of the column; these are the [001] (**6**) and [101] (**7**) directions. Figures 6(a)–(f) illustrates the intermolecular overlap modes of the ligand moieties where the view direction is normal to the least-squares plane of one ligand, and the mean interplanar distances are listed in Table 4. Among the six pairs, the five pairs of Figure 6(a) and Figures 6(c)–(f) have a well-overlapping region regarding each six-membered ring, irrespective of a slight slip. The mean interplanar distances are in the range 3.49(1)–3.63(2) Å (Table 4), which are slightly larger than 3.22 (Cl), 3.47 (Cl), and 3.37 (Br) Å found for CT compounds of *p*-X_4BQ.[4,20] For ligand **II** of **5** (Figure 6(b)), the adjacent ligands exhibit a poor overlap, however, the chlorine atoms sitting over the adjacent six-membered ring.

In the case of compound **7**, the neighboring columns are linked to each other through the stacking formation of the ligands **I** and **II**', forming a two-dimensional layer structure of the anions in the *ac*-plane (Figure 5(d)). The sitting mode of ligand **I** and **II**' is shown in Figure 6(g), where C(2) and C(10*) atoms of six-membered rings of each ligand are overlapped with interplanar distance 3.592(6) Å. All the stacking arrangements found in **1**–**3** and **5**–**7** occur between the crystallographically equivalent ligands except for the pair of ligands **I** and **II**' of **7**. In addition to the ligand stacking arrangements, X···X contacts between neighboring anions are found through and between the columns (Table 4).

Figure 7 shows overall crystal structures of **5**(**3**), **6**, and **7**. Compound **5**(**3**) has three-membered mixed-stack of the $[Fe^{III}Cp_2]^+$ (D), ligand **III** of the anion (A), and the benzene (S) to form an infinite column ···[D][A][S]··· along the *c*-axis. The mean separation between the least square planes is 3.51(1) (S···A), 3.56(2) (A···D), and 3.483(3) Å (S···D) with the dihedral angles of 1.1(2) (S···A), 17.4(2) (A···D), and 16.8(4)° (S···D), respectively. On the other hand, compounds **6** and **7** show two types of layers which consist of the $[Fe^{III}Cp_2]^+$ and chromium complexes (Figures 7(b) and (c)).

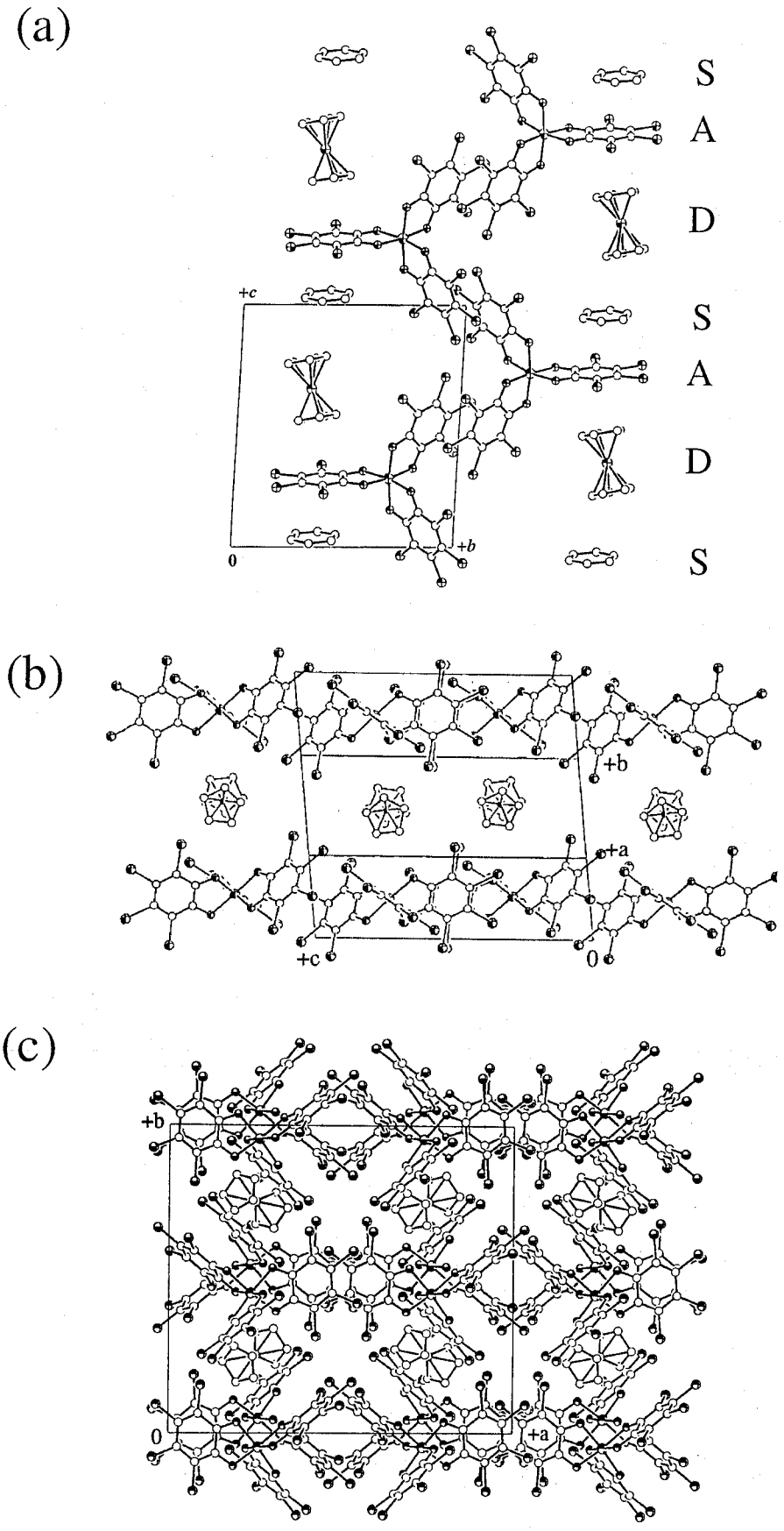

Figure 7. Projection of the whole crystal packing structures of (a) **5**(**3**), (b) **6**, and (c) **7**.

Physical Properties.

Infrared spectra and electric conductivity The spectral region between 1500 and 1000 cm^{-1} contains strong bands associated with the C–O and C–C stretching modes that are sensitive to the charge of the ligand moieties.[21] Figure 8 shows the spectra of **1**, **5**, and **7**, together with

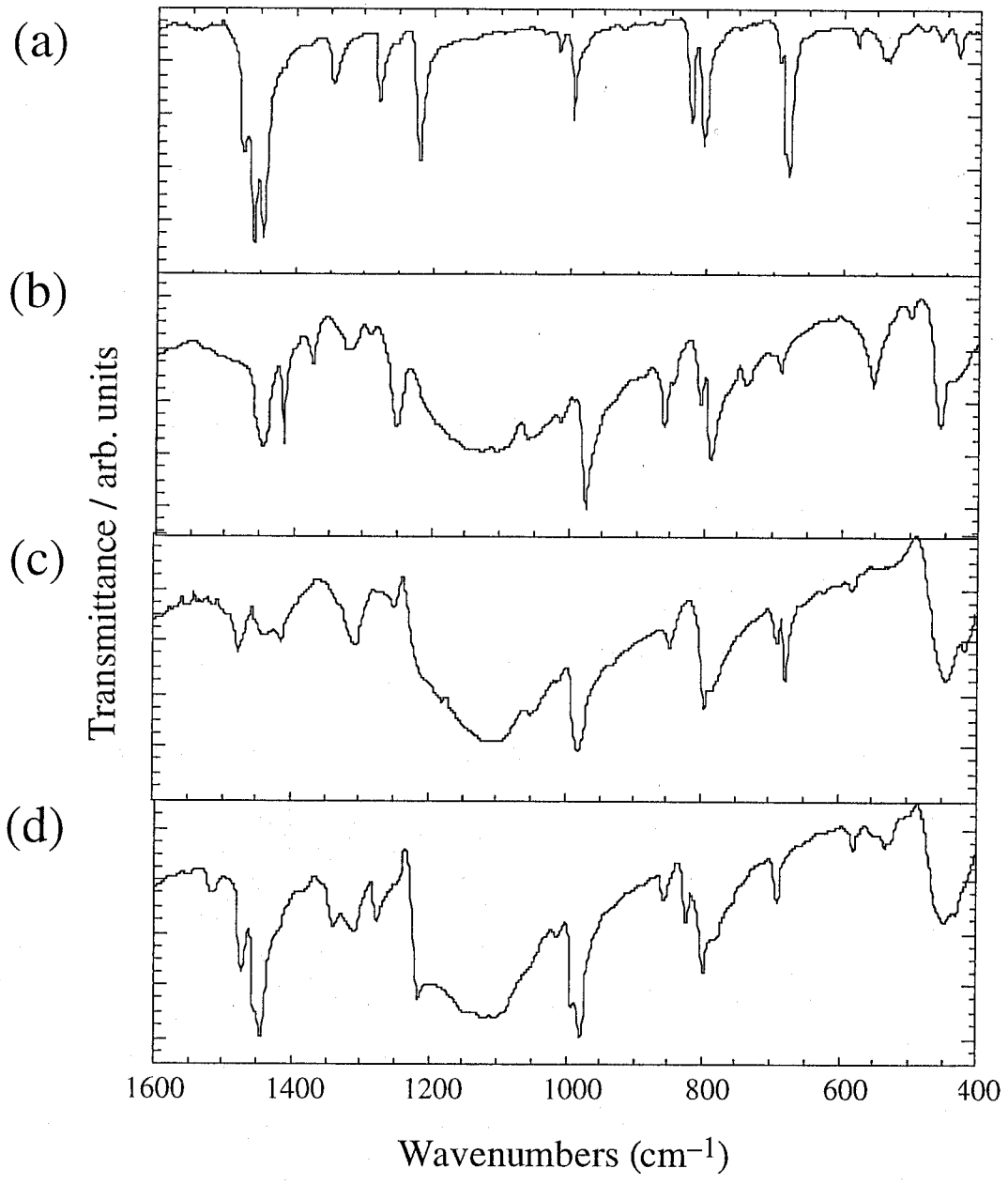

Figure 8. Infrared spectra (KBr) of (a) $Cr^{III}(Cl_4SQ)_3 \cdot 4C_6H_6$, (b) **1**, (c) **5**, and (d) **7**.

that of $Cr^{III}(Cl_4SQ)_3 \cdot 4C_6H_6$, which shows sharp bands at 1461 and 1447 cm^{-1}, characteristic for the SQ.[22] For compound **5**, two bands at 1435 and 1416 cm^{-1} are observed, indicating the presence of the SQ (Figure 8(c)). In addition, a new strong broad band appears at 1100 cm^{-1},

which is assigned to the C–O vibration mode of Cat.[23] This is consistent with the formulation of $[Cr^{III}(Cl_4SQ)_2(Cl_4Cat)]^-$ isomer. Similar bands are observed for **3–4** and **6**, indicating that both SQ and Cat forms are present (see Experimental Section), supporting $[Cr^{III}(X_4SQ)_2(X_4Cat)]^-$ representation. The spectral patterns of **1** and **2** are quite similar to those of **3–6** in which characteristic bands for the SQ and the Cat are observed (Figure 8(b)).

For compound **7**, as well as other compounds, the presence of the mixed-valence ligands could be confirmed from the bands at 1440 (SQ) and 1100 (Cat) cm^{-1} (Figure 8(d)). In addition, the spectrum for **7** is just a superposition of the spectra of $Cr^{III}(Cl_4SQ)_3 \cdot 4C_6H_6$ (Figure 8(a)) and **5** (Figure 8(c)). The bands near 1445, 1340, 1275, 990, 820, and 435 cm^{-1} are commonly found in $Cr^{III}(Cl_4SQ)_3 \cdot 4C_6H_6$ and **7**, while the bands at 1310, 1100, 1050, 980, 850, 785, 450, and 420 cm^{-1} are commonly observed in **5** and **7**. The former and latter sets indicate that the two species $[Cr^{III}(Cl_4SQ)_2(Cl_4Cat)]^-$ and $[Cr^{III}(Cl_4SQ)_3]^0$ isomers exist in **7**, though the crystallographic analysis shows one chromium species. Therefor, an *intermolecular* mixed-valence state occurs in **7** where the rate of intermolecular electron exchange is slower than the time scale of infrared spectroscopy.

Electrical conductivity is representative of physical properties for the mixed-valence molecular assemblies. Interestingly, a compacted pellet of **7** shows conductivity $\sigma_{295K} = 1.9 \times 10^{-3}$ $S \cdot cm^{-1}$ at 296 K. The conductivity could be explained by the presence of the mixed-valence chromium complexes together with their interactions in the crystal phase.

Electronic absorption spectra of solution Since all the CT compounds are soluble in dichloromethane, UV–vis–NIR–IR absorption spectroscopy could be useful to confirm the oxidation states of the chromium complexes. Figure 9 shows absorption spectra of **1**, **5**, and **7** in the two regions 10000–30000 (region A) and 3000–10000 cm^{-1} (region B). In the region A (Figure 9(a)), all the compounds commonly show the bands near 12500, 14700, and 21700 cm^{-1}, which are diagnostic of SQ/Cat chromium complexes.[16,17] The spectra can be classified into three groups from the spectral patterns, (type 1) **1** and **2**, (type 2) **3–6**, and (type 3) **7**; the spectra of type 1 are characterized by the band at 14700 (**1**) and 14500 (**2**) cm^{-1} with the intensities of $\varepsilon = 2000$ (**1**) and 3380 (**2**) $M \cdot cm^{-1}$, respectively, which are weaker than those of

types 2 and 3, ε = 4490–7130 $M \cdot cm^{-1}$. In addition, absence of the shoulder near 11400 cm^{-1} found in types 2 and 3 is also recognized. The spectra of type 1 are identical to that reported by Sofen et al.[16] for electrochemically generated $[Cr^{III}(3,5\text{-DTBSQ})(3,5\text{-DTBCat})_2]^{2-}$ anion with respect to the number and position (ν_{max}) of observed transitions, indicating the formation of $[Cr^{III}(X_4SQ)(X_4Cat)_2]^{2-}$ (X = Cl (**1**) and Br (**2**)) isomers. The characteristics of type 2 are the bands near 15900 cm^{-1} with intensities 4460–8480 $M^{-1} \cdot cm^{-1}$ together with shoulders at 11400 cm^{-1}. These features correspond to that of $[Cr^{III}(3,5\text{-DTBSQ})_2(3,5\text{-DTBCat})]^-$ anion,[28] indicating the existence of $[Cr^{III}(X_4SQ)_2(X_4Cat)]^-$ isomers for **3**–**6**. As well as compounds **3**–**6**, compound **7** (type 3) shows common absorption bands at 11400, 14800, 16000, and 22000 cm^{-1}, and the characteristic bands at 12900 and 18900 cm^{-1} are found. It is noteworthy that these two band positions are very similar to 13000 and 19000 cm^{-1} found for $Cr^{III}(Cl_4SQ)_3 \cdot 4C_6H_6$. These results exhibit that compound **7** contains two types of redox isomers, $[Cr^{III}(Cl_4SQ)_2(Cl_4Cat)]^-$ and $[Cr^{III}(Cl_4SQ)_3]^0$, and reflect the localized nature of the electronic structures of both forms in the solution.

As shown in Figure 9(b), compounds **1**–**7** show characteristic broad, intense absorption bands in the near-IR to IR region with several overtone vibrational transitions, whereas $[Cr^{III}(X_4SQ)_3]^0$ exhibits no absorption bands in this region. Upon the reduction to the mono- (**3**–**7**) and di-anions (**1** and **2**), the bands appear near 4500 (**3**–**7**) and 6000 (**1** and **2**) cm^{-1}. These bands are assigned to IVCT transitions of SQ ← Cat,[2(b)] indicating the presence of both forms of the ligand in the $[Cr^{III}(X_4SQ)_{3-n}(X_4Cat)_n]^{n-}$ (n = 2 (**1** and **2**) and 1 (**3**–**7**)) anions. The band shape data are summarized in Table 6. From the spectra the degree of electric coupling, H_{ab}, can be estimated by using the well-known Hush formula[24] for mixed-valence complexes given in eq. 1,

$$H_{ab} = (2.05 \times 10^{-2})[\varepsilon_{max}\Delta\nu_{1/2}/\nu_{max}]^{1/2}\nu_{max}/r_{oo} \qquad (1)$$

, where ε_{max} is the maximum extinction coefficient of the absorption band in $M^{-1} \cdot cm^{-1}$, $\Delta\nu_{1/2}$ is the bandwidth at half ε_{max}, ν_{max} is the energy of the absorption in cm^{-1}, and r_{oo} is the distance between donor and acceptor wave functions. Using the values of r_{oo} (shortest distances between

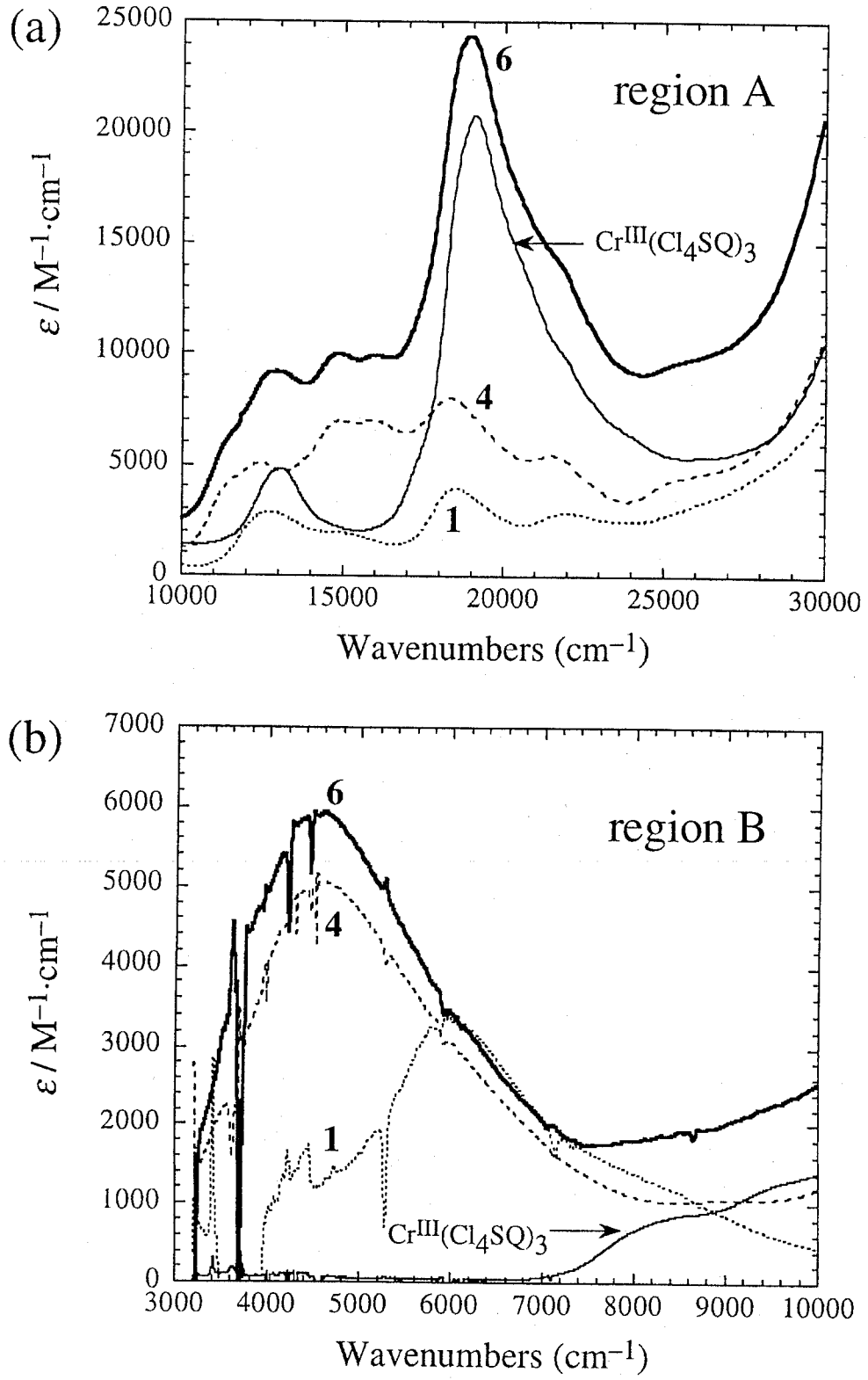

Figure 9. Electronic absorption spectra of **1** (---), **5** (– –), **7** (—), and $Cr^{III}(Cl_4SQ)_3 \cdot 4C_6H_6$ (–) in dichloromethane at 296 K. The spectrum of **2** is similar to that of **1**, while those of **3**, **4**, and **6** are similar to that of **5** (see Table 5).

Table 5. Absorption Spectral Parameters for $Cr^{III}(X_4SQ)_3 \cdot 4C_6H_6$ (X = Cl and Br) and **1–7** in Dichloromethane

compound	ν_{max} ($10^3 \times cm^{-1}$) ($\varepsilon_{max} = 10^3 \times M^{-1} \cdot cm^{-1}$)							
$Cr^{III}(Cl_4SQ)_3$		8.70	10.0	13.0			19.0	22.0
		(sh, 8.87)	(1.39)	(4.85)			(20.8)	(sh, 8.96)
$Cr^{III}(Br_4SQ)_3$		8.13	10.0	12.8			18.5	21.6
		(sh, 10.4)	(1.35)	(6.70)			(26.9)	(sh 9.60)
1	5.94	8.30		12.7	14.7		18.5	22.0
	(3.38)	(sh, 1.23)		(2.88)	(2.00)		(3.95)	(2.86)
2	6.04	8.30		12.7	14.5		18.5	21.9
	(4.66)	(sh, 1.51)		(4.24)	(3.38)		(5.40)	(4.43)
3	4.55		11.4	12.4	14.9	16.0	18.2	21.6
	(5.23)		(sh, 4.18)	(5.12)	(7.13)	(sh, 6.72)	(7.50)	(5.11)
4	4.50		11.4	12.2	14.7	15.6	18.1	21.5
	(2.36)		(sh, 2.08)	(2.43)	(3.29)	(sh, 3.13)	(3.14)	(2.20)
5	4.59		11.4	12.4	14.9	15.9	18.3	21.5
	(5.06)		(sh, 4.12)	(5.08)	(7.00)	(7.02)	(8.03)	(5.46)
6	4.55		11.4	12.3	14.7	15.7	18.3	21.3
	(5.95)		(sh, 5.37)	(6.63)	(8.69)	(8.48)	(10.7)	(6.78)
7	4.59		11.4	12.9	14.8	16.0	18.9	22.0
	(5.93)		(sh, 6.06)	(9.19)	(9.96)	(9.87)	(24.4)	(sh, 13.6)

Table 6. The IVCT Band Shape Data and Estimated Hush's Coupling Energy, H_{ab}, for **1–7** in dichloromethane at 296 K

compound	λ_{max} (nm)	ν_{max} (cm^{-1})	ε ($M^{-1} \cdot cm^{-1}$)	$\Delta\nu_{1/2}$ (cm^{-1})[a]	$r = d_{OO}$ (Å)[b]	H_{ab} (cm^{-1})
1	1690	5940	3380	2410	2.76	1630
2	1660	6040	4660	2110	2.683	1860
3	2200	4550	5230	2910	2.71	1990
4	2220	4500	2360	2180	2.71[c]	1150
5	2180	4590	5060	2830	2.709	1940
6	2200	4550	5950	2740	2.6	2150
7	2180	4590	5930	2740	2.641	2120

[a] Half-widths of bands are calculated from the higher $\nu_{1/2}$ assuming symmetric bands. [b] The shortest O···O distances obtained from crystallographic data are taken as r_{oo}. [c] The value for **3**.

oxygen atoms) listed in Table 6, H_{ab} were evaluated. The calculated values are three times greater than that of cobalt complexes,[2(a)] indicating strong coupling interaction between SQ and Cat through the chromium ion.

In conclusion, the absorption spectra clearly detect the species in different oxidation states and the spectra of redissolved samples show that even in the solution the species exist just as well as in the solid states.

Electronic absorption spectra of solid Figure 10 shows absorption spectra of $Cr^{III}(Cl_4SQ)_3 \cdot 4C_6H_6$, **1**, **5**, and **7** in the solid state (KBr pellets). The observed spectral parameters are listed in Table 5. In both regions A and B, the maximum of each peak for all the compounds tends to shift to lower energy than that of solution. In region B, compounds **1** and **2** show broad, intense bands at 5560 and 5620 cm^{-1}, respectively, while those of **3**–**7** are found in the region of 3850–4360 cm^{-1} (Figure 10(b)). As well as the solution spectra, the absorption

Table 7. Absorption Spectral Parameters for $Cr^{III}(X_4SQ)_3 \cdot 4C_6H_6$ (X = Cl and Br) and **1**–**7** in the Solid State (KBr)

compound	ν_{max} ($10^3 \times cm^{-1}$)									
$Cr^{III}(Cl_4SQ)_3$			7.81	9.35		12.7			18.3	
$Cr^{III}(Br_4SQ)_3$			7.94	9.80		12.9			18.2	
1	5.56		8.00 (sh)			12.0	14.6		18.2	21.5
2	5.62		8.33			12.1	14.5		18.5	21.3
3	3.92	5.88 (sh)	8.70 (sh)		10.8 (sh)	12.1	14.3		17.7	21.1
4	4.35	5.88 (sh)	8.70 (sh)			12.0	14.3		17.8	21.3
5	4.36	5.88 (sh)	8.70 (sh)		11.2 (sh)	12.0	14.0	15.9 (sh)	17.4	21.1
6	4.35	5.26 (sh)	8.70 (sh)		10.9 (sh)	11.8	14.0	15.6	17.4	21.1
7	3.85	5.88 (sh)	8.33 (sh)		10.9 (sh)	12.3	14.5	15.0 (sh)	18.0	21.1 (sh)

band is assigned to IVCT (SQ ← Cat) transition, indicating the presence of both forms of the ligand. The peak maxima are comparable to those for manganese (4760 cm^{-1})[25(a)] and cobalt (4170 cm^{-1})[25(b)] complexes containing 3,5-DTBSQ and 3,5-DTBCat. The isostructural compounds **3** and **5** show identical spectral patterns, reflecting the similarity of electronic structures. Compound **6** having a bromo derivative also shows a spectrum with the IVCT band at 4350 cm^{-1} as well as those of previously reported 1:1 CT compounds containing $[TMTSF]^+$ (4080 cm^{-1}) and $[TMT\text{-}TTF]^+$ (4170 cm^{-1}).[5]

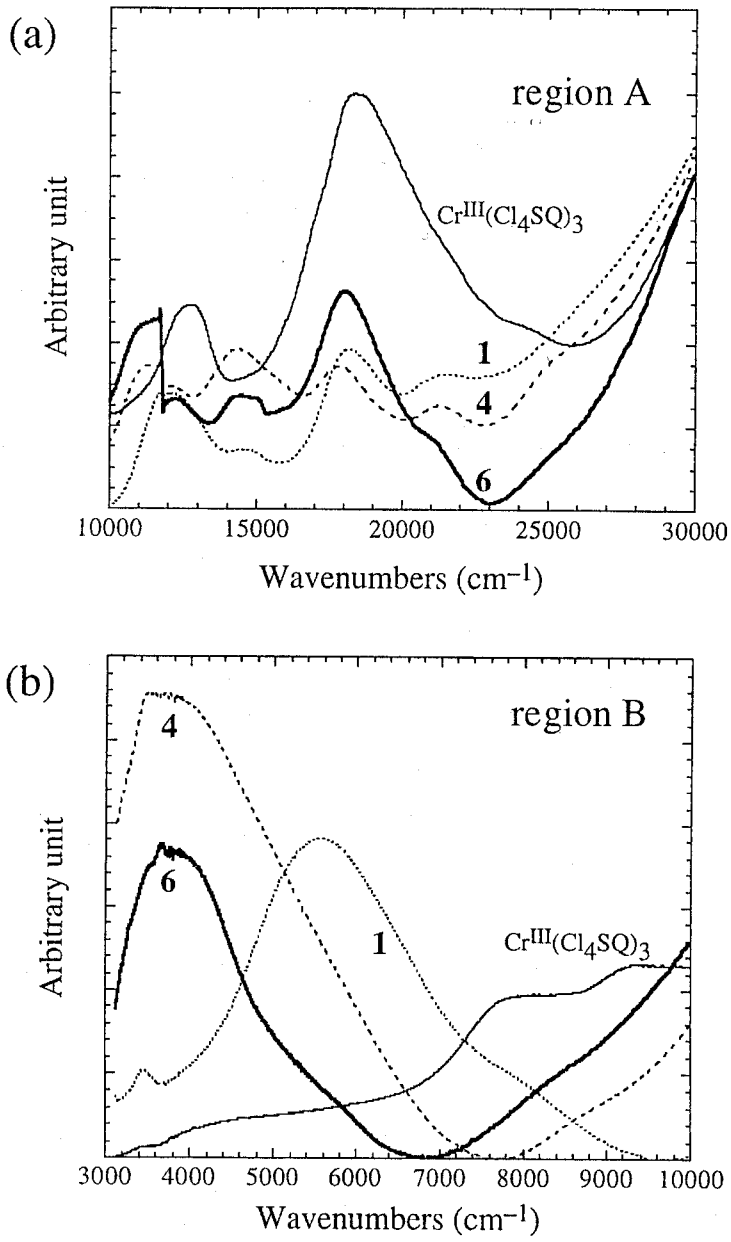

Figure 10. Electronic absorption spectra of **1** (---), **5** (– –), **7** (—), and $Cr^{III}(Cl_4SQ)_3 \cdot 4C_6H_6$ (–) in the solid state (KBr). The spectrum of **2** is similar to that of **1**, while those of **3**, **4**, and **6** are similar to that of **5** (see Table 5).

Temperature dependence of magnetic susceptibilities The temperature dependence of the molar magnetic susceptibility of **2–7** and $Cr^{III}(Cl_4SQ)_3 \cdot 4C_6H_6$ is shown in Figure 11 as plots of $\chi_m T$ vs T. For compound **2**, at 350 K, $\chi_m T$ is equal to 1.26 $cm^3 \cdot K \cdot mol^{-1}$ which is higher than 1.00 $cm^3 \cdot K \cdot mol^{-1}$ (g = 2.00) of S = 1 spin expected for antiferromagnetically coupled S = 3/2 (Cr^{III}) and 1/2 (SQ) spins, while much lower than 2.25 $cm^3 \cdot K \cdot mol^{-1}$ (g = 2.00) for two non-interacting spins.[26] As the temperature is lowered, the value gradually decreases to reach 0.684 $cm^3 \cdot K \cdot mol^{-1}$ at 2 K. The profile of this curve indicates that the Cr^{III}–SQ interaction is strongly antiferromagnetic, leading to a S = 1 ground state and a S = 2 excited state for the molecule. The exchange interaction (J) between the chromium ion and the SQ was estimated with a simple dimeric model with eq. 2,

$$\chi_M = \frac{N\mu_B{}^2 g^2}{k(T-\Theta)} \cdot \frac{2+10e^{4x}}{3+5e^{4x}} \qquad (2)$$

, where $x = J/kT$ and N, g, μ_B, k, and Θ mean Avogadro's number, isotropic g-factor, Bohr magneton, Bolztmann constant, and Curie–Weiss constant to the gauge intermolecular interactions. The best fit to eq. 2 gives g = 2.02, J = –170 cm^{-1}, and Θ = –0.9 K. The obtained J value is smaller than –400 and –350 cm^{-1} estimated for $Cr^{III}(Cl_4SQ)_3$ and $Cr^{III}(phenSQ)_3$, respectively.[27] The intramolecular antifferomagnetic interaction in **2** is weaker than those of mono-anionic species, $[Cr^{III}(X_4SQ)_2(X_4Cat)]^-$ (vide infra), which show only a small amount of thermal population to the exited state (S = 3/2), even at 350 K. The relatively weak intramolecular magnetic interaction of **2** is associated with the large energy separation of magnetic orbitals of the chromium ion and the ligands compared with those of $[Cr^{III}(X_4SQ)_2(X_4Cat)]^-$ isomers.[28] Together with this effect, the strong electron-withdrawing substituent on X_4SQ could promote the decreasing of antiferromagnetic interaction in the molecules.[3(b)] In contrast, the $\chi_m T$ value of **3** at 350 K is 0.430 emu·K·mol^{-1}, which is close to the theoretical value of 0.375 emu·K·mol^{-1} expected for S = 1/2 (g = 2.00). Therefore, the unpaired electron is consistent with strong antiferromagnetic interactions between the S = 3/2 (Cr^{III}) and two S = 1/2 spins on the SQ ligands.[29]

At 350 K, $\chi_m T$ values of **5** and **6** containing paramagnetic $[Fe^{III}Cp_2]^+$ (S =1/2) are 1.29 and 1.33 $cm^3 \cdot K \cdot mol^{-1}$, respectively. The values are larger than the sum of spins on the $[Fe^{III}Cp_2]^+$ (S = 1/2) and $[Cr^{III}(Cl_4SQ)_2(Cl_4Cat)]^-$ (S = 1/2), due to significant orbital contributions of $[Fe^{III}Cp_2]^+$ to $\chi_m T$ values over the spin only value of 0.75 $cm^3 \cdot K \cdot mol^{-1}$.[30] These values show weak temperature dependencies in the 30–350 K region and decrease rapidly under 30 K. The decreasing of $\chi_m T$ in the lower temperature region suggests the presence of zero-field splitting effect and/or intermolecular antiferromagnetic interactions between the neighboring paramagnetic centers. The interactions result from close packings of neighboring molecules in the column as found in the X-ray structure analyses. Furthermore, these are attributable to the intermolecular X···X contacts between the adjacent anionic complexes (Table 4). In the case of compound **5**, the presence of the direct stacking structure between the $[Fe^{III}Cp_2]^+$ and the $[Cr^{III}(Cl_4SQ)_2(Cl_4Cat)]^-$ causes the magnetic interactions between them.[30]

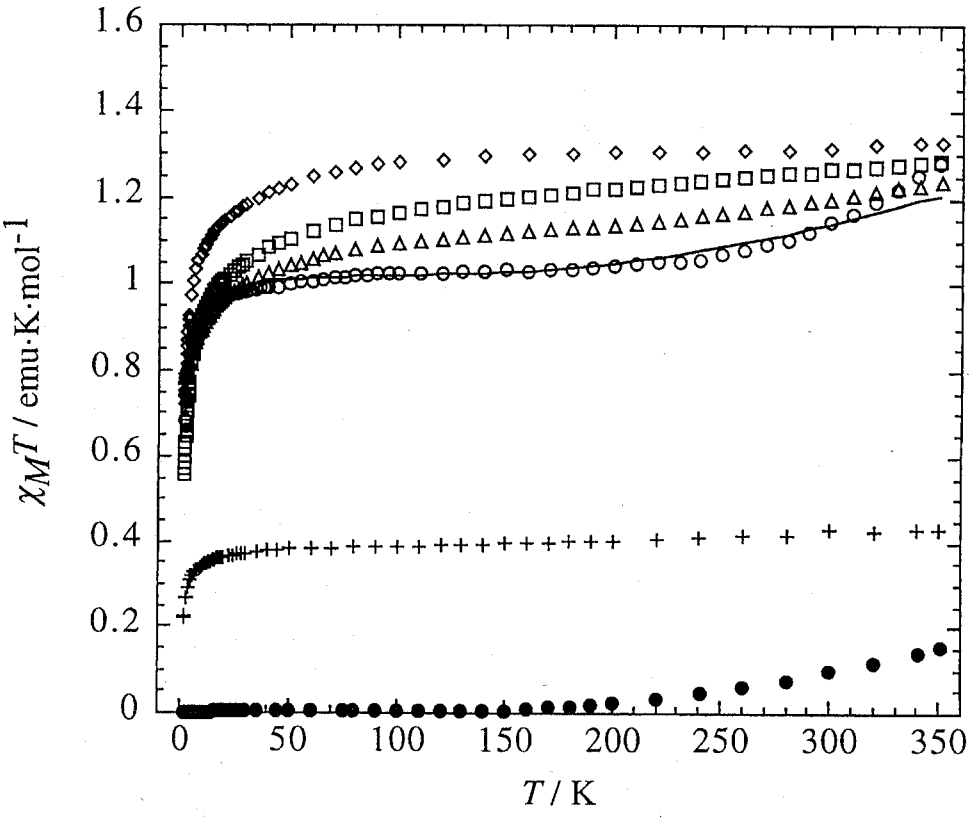

Figure 11. Temperature dependence of $\chi_m T$ plots of **2** (O), **3** (+), **4** (□), **5** (◇), **6** (Δ), and $Cr^{III}(Cl_4SQ)_3 \cdot 4C_6H_6$ (●). The solid line corresponds to the fit of the experimental data to a dimeric model (see text).

For compound **7**, $\chi_m T$ is equal to 1.24 $cm^3 \cdot K \cdot mol^{-1}$ at 350 K and, as the temperature is lowered to 200 K, gradually decreases to reach a value of 1.14 $cm^3 \cdot K \cdot mol^{-1}$. Finally, the value decreases rapidly until 0.757 $cm^3 \cdot K \cdot mol^{-1}$ at 1.9 K, followed by another decrease to 60 K. Figure 11 also shows the temperature-dependent magnetic susceptibility for $Cr^{III}(Cl_4SQ)_3 \cdot 4C_6H_6$ in the same temperature region. At 350 K, the compound has $\chi_m T$ value of 0.154 $emu \cdot K \cdot mol^{-1}$, which drops to a value of 0.002 $emu \cdot K \cdot mol^{-1}$ at 1.9 K. As reported previously,[3(b)] the complex has a ground state of $S = 0$ as a result of strong intramolecular antiferromagnetic interaction between three unpaired electrons of Cr^{III} and three SQ ligands. Actually, $\chi_m T$ value shows temperature dependency associated with Boltzmann distribution from the $S = 0$ ground state to the $S = 1$ exited state. At 350 K, the $S = 1$ excited state is weakly populated. The subtraction of this contribution from that of **7** provides a temperature dependence of the $\chi_m T$ curve similar to those of **5** and **6**. The magnetic data can be accounted for by the presence of the two redox isomers, $[Cr^{III}(Cl_4SQ)_2(Cl_4Cat)]^-$ and $[Cr^{III}(Cl_4SQ)_3]^0$, as well as infrared spectrum of the compound.

Conclusions

The CT reactions of $Cr^{III}(X_4SQ)_3$ (X = Cl and Br) with $M^{II}Cp_2$ (M = Co and Fe) give 2:1, 1:1, and 1:2 donor–acceptor CT compounds. During the reactions, $Cr^{III}(X_4SQ)_3$ complexes are reduced to $[Cr^{III}(X_4SQ)_2(X_4Cat)]^-$ and $[Cr^{III}(X_4SQ)(X_4Cat)_2]^{2-}$ redox isomers. The di-anionic form can be obtained only by use of two equivalent $Co^{II}Cp_2$, and is first structurally and spectroscopically characterized in the solid state. Both anionic forms contain the SQ and Cat, showing the bands in the region of 3130-10000 cm^{-1}, characteristic of IVCT transition between the two ligands. The crystal structures of CT compounds are dependent on the charge of the anions; the $[Cr^{III}(X_4SQ)(X_4Cat)_2]^{2-}$ isomers in **1** and **2** show discrete molecular structures, while the $[Cr^{III}(X_4SQ)_2(X_4Cat)]^-$ isomers in **3–7** form one-dimensional column structures, which are constructed from the two sets of ligand stacking interactions of chromium complexes.

The remaining ligands interacted with $[M^{III}Cp_2]^+$ and benzene in **3** and **5** to form additional one-dimensional ···[D][A][S]··· type mixed-stack arrangements. On the other hand, compound **7** forms a two-dimensional layer structure where the two redox isomers, $[Cr^{III}(Cl_4SQ)_2(Cl_4Cat)]^-$ and $[Cr^{III}(Cl_4SQ)_3]^0$ are included. Therefore, the compound is regarded as the *intermolecular* mixed-valence molecular assembly.

References

(1) (a) Pierpont, C. G.; Lange, C. W. *Prog. Inorg. Chem.* **1994**, *41*, 331. (b) Pierpont, C. G.; Buchanan, R. M. *Coord. Chem. Rev.* **1981**, *38*, 45.

(2) (a) Adams, D. M.; Hendrickson, D. N. *J. Am. Chem. Soc.* **1996**, *118*, 11515. (b) Adams, D. M.; Noodleman, L.; Hendrickson, D. N. *Inorg. Chem.* **1997**, *36*, 3966. (c) Jung, O. -S.; Pierpont, C. G. *J. Am. Chem. Soc.* **1994**, *116*, 2229.

(3) (a) Pierpont, C. G.; Buchanan, R. M. *J. Am. Chem. Soc.* **1975**, *97*, 6450. (b) Buchanan, R. M.; Kessel, S. L.; Downs, H. H.; Pierpont, C. G.; Hendrickson, D. N.; Pierpont, C. G.; Buchanan, R. M. *J. Am. Chem. Soc.* **1978**, *100*, 7894. (c) Pierpont, C. G.; Buchanan, R. M. *J. Am. Chem. Soc.* **1975**, *97*, 4912. (d) Speier, G.; Tisza, S.; Rockenbauer, A.; Boone, S. R.; Pierpont, C. G. *Inorg. Chem.* **1992**, *31*, 1017. (e) Pierpont, C. G.; Downs, H. H. *J. Am. Chem. Soc.* **1976**, *98*, 4834. (f) Simpson, C. L.; Pierpont, C. G. *Inorg. Chem.* **1992**, *31*, 4308.

(4) (a) Mayerle, J. J.; Torrance, J. B. *Acta Crystallogr., Sec. B* **1981**, *B37*, 2030. (b) Nakasuji, K.; Sasaki, M.; Kotani, T.; Murata, I.; Enoki, T.; Imaeda, K.; Inokuchi, H.; Kawamoto, A.; Tanaka, J. *J. Am. Chem. Soc.* **1987**, *109*, 6970.

(5) (a) Chapter 2 in this thesis. (b) Chang, H. -C.; Ishii, T.; Kondo, M.; Kitagawa, S. *J. Chem. Soc., Dalton Trans.* **1999**, 2467.

(6) Koelle, U.; Khouzami, F. *Angew. Chem., Int. Ed. Engl.* **1980**, *19*, 640.

(7) King, R. B.; Bisnette, M. B. *J. Organomet. Chem.* **1967**, *8*, 287.

(8) Kahn, O. *Molecular Magnetism*; VCH: New York, 1993.

(9) Jacobson, R. A. *REQABA Empirical Absorption Correction Version 1.1-03101998:* Molecular Structure Corp.: The Woodlands, TX, 1996–1998.

(10) Altomare, A.; Burla, M. C.; Camalli, M.; Cascarano, M.; Giacovazzo, C.; Guagliardi, A.; Pilidori, G. *J. Appl. Crystallogr.* **1994**, *27*, 435.

(11) Beurskens, P. T.; Admiraal, G.; Beurskens, G.; Bosman, W. P.; de Gelder, R.; Israel, R.; Smits, J. M. M. , The DIRDIF-94 program system, Technical Report of the Crystallography Laboratory; University of Nijmegen: Nijmegen, The Netherlands, 1994.

(12) *teXsan: Crystal Structure Analysis Package*; Molecular Structure Corporation: The Woodlands, TX, 1985, 1992.

(13) Downs, H. H.; Buchanan, R. M.; Pierpont, C. G. *Inorg.Chem.* **1979**, *18*, 1736.

(14) Johnson, C. K. ORTEP II; Report ORNL-5138; Oak Ridge National Laboratory: Oak Ridge, TN, 1976.

(15) (a) Kemmitt, R. D. W.; Russell, D. R. *Comprehensive Organometallic Chemistry*; Pergamon: Oxford, 1982. (b) Sens, V. I.; Ruhlandt-Senge, K.; Müller, U. *Acta Crystallogr., Sect. C* **1992**, *C48*, 742. (c) Seiler, P.; Dunitz, J. D. *Acta Crystallogr., Sect. B* **1979**, *B35*, 1068. (d) Mammano, N. J.; Zalkin, A.; Landers, A.; Rheingold, A. L. *Inorg. Chem.* **1977**, *16*, 297.

(16) Sofen, S. R.; Ware, D. C.; Cooper, S. R.; Raymond, K. N. *Inorg. Chem.* **1979**, *18*, 234.

(17) Buchanan, R. M.; Claflin, J.; Pierpont, C. G. *Inorg. Chem.* **1983**, *22*, 2552.

(18) (a) Buchanan, R. M.; Pierpont, C. G. *J. Am. Chem. Soc.* **1980**, *102*, 4951. (b) Attia, A. S.; Bhattacharya, S.; Pierpont, C. G. *Inorg. Chem.* **1995**, *34*, 4427. (c) Jung, O. -S.; Jo, D. H.; Lee, Y. -A.; J., C. B.; Pierpont, C. G. *Inorg. Chem.* **1997**, *36*, 19. (d) Jung, O. -S.; Pierpont, C. G. *Inorg. Chem.* **1994**, *33*, 2227.

(19) (a) Lange, C. W.; Pierpont, C. G. *Inorg. Chim. Acta* **1997**, *263*, 219. (b) Attia, A. S.; Pierpont, C. G. *Inorg. Chem.* **1998**, *37*, 3051.

(20) Konno, M.; Kobayashi, H.; Marumo, F.; Saito, Y. *Bull. Chem. Soc. Jpn.* **1973**, *46*, 1987.

(21) (a) Hartl, F.; Stufkens, D. J.; Vleck, J., A. *Inorg. Chem.* **1992**, *31*, 1687. (b) Hartl, F.; Vleck, J., A.; Stufkens, D. J. *Inorg. Chim. Acta* **1992**, *192*, 25.

(22) Pierpont, C. G.; Downs, H. H.; Rukavina, T. G. *J. Am. Chem. Soc.* **1974**, *96*, 5573.

(23) (a) Lynch, M. W.; Valentine, M.; Hendrickson, D. N. *J. Am. Chem. Soc.* **1982**, *104*, 6982. (b) Cass, M. E.; Gordon, N. R.; Pierpont, C. G. *Inorg. Chem.* **1986**, *25*, 3962.

(24) Hush, N. S. *Prog. Inorg. Chem.* **1967**, *8*, 357.

(25) (a)Attia, A. S.; Pierpont, C. G. *Inorg. Chem.* **1997**, *36*, 6184. (b) Jung, O. -S.; Jo, D. W.; Lee, Y. -A.; Chae, H. K.; Sohn, Y. S. *Bull. Chem. Soc. Jpn.* **1996**, *69*, 2211.

(26) The observed $\chi_m T$ for **1** is by 20% larger than those of **2**, for example, $\chi_m T$ = 1.49 (350 K), 1.46 (300 K), 1.30 (100 K), and 0.65 (2 K) emu·K·mol^{-1}. The deviation from the curve estimated for **2** (ground state is S = 1) could not be accounted for by the single crystal structure and spectroscopic data of **1**. To reproduce the observed data, the species with higher than S = 1 spin should be introduced. The used sample for the measurement was microcrystalline powder, therefore unexpected paramagnetic impurity could be one of the reason for the deviation.

(27) Lynch, M. W.; Buchanan, R. M.; Pierpont, C. G.; Hendrickson, D. N. *Inorg. Chem.* **1981**, *20*, 1038.

(28) Gordon, D. J.; Fenske, R. F. *Inorg. Chem.* **1982**, *21*, 2907.

(29) Wheeler, D. E.; McCusker, J. K. *Inorg. Chem.* **1998**, *37*, 2296.

(30) Miller, J. S.; Calabrese, J. C.; Rommelman, H.; Chittipeddi, S. R.; Zhang, J. H.; Reiff, W. M.; Epstein, A. J. *J. Am. Chem. Soc.* **1987**, *109*, 769.

Chapter 5

Synthesis of Ligand-Based Mixed-Valence $Cr^{III}(X_4SQ)(X_4Cat)(L)_n$ (X = Cl and Br, n = 1 or 2) Complexes via Solvent-induced Valence Tautomeric Conversion of $Cr^{III}(X_4SQ)_3$

Abstract

Treatment of tris(tetrahalogeno-*o*-semiquinonate) chromium(III) complexes, $Cr^{III}(X_4SQ)_3$ (X = Cl and Br), with acetonitrile gives *trans*-bis(acetonitrile)-tetrahalogenosemiquinonate-tetrahalogenocatecholate complexes, **1** and **2**. Similar treatment in the presence of 2,2'-bipyridine (bpy) and 3,4,7,8-tetramethyl-1,10-phenanthrene (TMphen) gives *cis*-chelated products, **3–6**,

trans-$Cr^{III}(Cl_4SQ)(Cl_4Cat)(CH_3CN)_2$ (**1**)
trans-$Cr^{III}(Br_4SQ)(Br_4Cat)(CH_3CN)_2$ (**2**)
cis-$Cr^{III}(Cl_4SQ)(Cl_4Cat)(bpy)\cdot CH_3CN$ (**3**)
cis-$Cr^{III}(Br_4SQ)(Br_4Cat)(bpy)\cdot 1/2CH_3CN$(**4**)
cis-$Cr^{III}(Cl_4SQ)(Cl_4Cat)(TMphen)$ (**5**)
cis-$Cr^{III}(Br_4SQ)(Br_4Cat)(TMphen)$ (**6**)

where X_4Cat is tetrahalogenocatecholate. X-ray crystal structure analyses reveal that in compounds **1** and **2**, the acetonitrile ligands coordinate to the chromium ion in *trans*-fashion making two *o*-quinone ligands being coplanar. Thermogravimetric analyses reveal that the coordinated acetonitrile ligands in complexes **1** and **2** can be thermally eliminated up to 520 K. On the other hand, the nitrogen co-ligands of **3–6** coordinate to chromium ion in *cis*-fashion so that two *o*-quinone ligands located in the orthogonal planes. All the compounds show a mixed-valence state on the ligand moieties with two kinds of ligands, SQ and Cat. This is confirmed from the presence of the interligand intervalence transition (IVCT) from π^* of X_4Cat to that of X_4SQ near 4000 cm^{-1} both in the solution and in the solid state. All the complexes show electrochemically quasi-reversible one-electron reduction and oxidation reaction corresponding to $[Cr^{III}(X_4Cat)_2(L)_n]^-/[Cr^{III}(X_4SQ)(X_4Cat)(L)_n]$ and $[Cr^{III}(X_4SQ)(X_4Cat)(L)_n]/[Cr^{III}(X_4SQ)_2(L)_n]^+$ couple, respectively. The mixed-valence nature of the complexes was also confirmed by the temperature dependence of magnetic susceptibilities where all the complexes

show a ground state of $S = 1$, which result from the intramolecular antiferromagnetic interaction between $Cr^{III}(d^3, S = 3/2)$ and X_4SQ ($S = 1/2$) radical.

The conversion of $Cr^{III}(X_4SQ)_3$ to **1–6** occurs only in polar solvents, and could be explained by assuming the formation of $Cr^{III}(X_4BQ)(X_4SQ)(X_4Cat)$ (BQ = *o*-benzoquinone) complex as intermediate species. This implies a solvent-induced valence tautomeric conversion of $Cr^{III}(X_4SQ)_3$ to $Cr^{III}(X_4BQ)(X_4SQ)(X_4Cat)$ tautomers, which is accelerated by lower coordination ability of BQ ligand. This is a first example of the observation of valence tautomerism for the chromium complexes, and the reaction could be useful for the synthesis of the series of mixed-valence bis(*o*-quinone) complexes.

Introduction

Transition metal bis(*o*-quinone) complexes have been found to show valence tautomerism and increasingly studied in recent years, especially for heteroleptic bis(*o*-quinone) cobalt and manganese complexes, M^{III}(SQ)(Cat)(N-N) (SQ = semiquinonate, Cat = catecholate, N-N = nitrogen chelate reagent).[1] A number of complexes of have been synthesized by one-pot reaction of metal carbonyl with *o*-quinone derivatives in the presence of nitrogen co-ligands.[2]

On the other hand, chromium complexes with paramagnetic SQ ligands have been a one of special interest because these show unusual and unique redox,[3] magnetic,[4] and optical properties[5] that appear to be governed by strong interactions between the unpaired electrons and the corresponding spins localized on the metal center and the ligands. Only one report for bis(*o*-quinone) chromium complex has been reported by Pierpont et al..[6] They have synthesized a series of Cr^{III}(3,5-DTBSQ)(3,5-DTBCat)(bpy), Cr^{III}(phenSQ)(phenCat)(bpy), and Cr^{III}(Cl_4SQ)(Cl_4Cat)(bpy), where 3,5-DTBSQ/Cat and phenSQ/Cat are 3,5-di-*tert*-butyl- and 9,10-phenanthrenesemiquinonate/catecholate, respectively, and bpy is 2,2'-bipyridine. The complexes are prepared by treating $Cr(CO)_4$(bpy) with corresponding quinone ligands. However, they have failed to synthesize the Cr^{III}(SQ)(Cat)(N-N) complexes by the ligand exchange reaction of $Cr^{III}(SQ)_3$ with nitrogen co-ligands, and only small quantities of product could be detected due to the kinetic inertness of Cr^{III} ion.

The author has found that the $Cr^{III}(X_4SQ)_3$ undergo the ligand exchange reaction by ligand drawn in Chart 1 only in the polar solvents to give a series of $Cr^{III}(X_4SQ)(X_4Cat)(L)_n$ (n = 2 for acetonitrile and n = 1 for bpy and 3,4,7,8-tetramethyl-1,10-phenanthrene (TMphen)) complexes. The mixed-valence state of the complexes on the ligand moieties is well-compared with those of tris(*o*-quinone) complexes described in the preceding Chapters. In addition, the formation of the complexes could be explained by assuming the presence of valence tautomerism of $Cr^{III}(X_4SQ)_3$. To date only one tris(*o*-quinone) complex, $Mn^{III}(3,6\text{-DTBSQ})_3$, has been known to show the valence tautomerism.[7] The crystal structures and mixed-valence states of the products will be shown together with the first observation of the valence tautomerism for chromium complexes.

Chart 1

L =  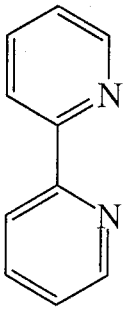 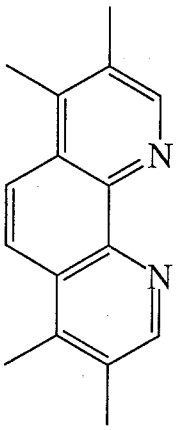

CH_3CN bpy TMphen

Experimental Section

Materials.

All chemicals were reagent grade. 3,4,7,8-tetramethyl-1,10-phenanthroline was purchased from Aldrich and 2,2'-Bipyridine from Tokyo Kasai Co., Ltd.. Preparation of $Cr^{III}(X_4SQ)_3 \cdot 4C_6H_6$ were reported in Chapter 1. The all reagents and solvents used were used without special purification.

Preparation of the Complexes.

***trans*-$Cr^{III}(Cl_4SQ)(Cl_4Cat)(CH_3CN)_2$ (1)** A carbondisulfide solution (350 ml) containing $Cr^{III}(Cl_4SQ)_3 \cdot 4C_6H_6$ (980 mg, 0.889 mmol) was added to a 150 ml acetonitrile and stirred for a day. The resulting suspension was filtered and the obtained powder was washed with carbondisulfide several times, then dried in vacuum (481 mg, 86 %). Single crystal of **1** was grown from a layered solution of carbondisulfide containing $Cr^{III}(Cl_4SQ)_3$ and acetonitrile. Found: C, 30.46; H, 1.15, N, 4.46. $C_{14}H_6Cl_8CrN_2O_4$ requires C, 30.71, H, 0.97, N, 4.48. IR (KBr): 1517w, 1472w, 1439m, 1407w, 1361w, 1314s, 1259w, 1238w, 1155s, 1037m, 981s, 952m, 813w, 794s, 691m, 669w, 585w, 549w, 524m, 444s, and 399s cm^{-1}.

***trans*-$Cr^{III}(Br_4SQ)(Br_4Cat)(CH_3CN)_2$ (2)** A carbondisulfide solution (1000 ml) containing $Cr^{III}(Br_4SQ)_3 \cdot 4C_6H_6$ (3.50 g, 2.14 mmol) was added to a 430 ml acetonitrile and stirred for a day. The resulting suspension was filtered, and the obtained powder was washed with carbondisulfide several times, then dried in vacuum (1.20 g, 57 %). Found: C, 19.60; H, 0.76, N, 2.84. $C_{14}H_6Br_8CrN_2O_4$ requires C, 19.58, H, 0.62, N, 2.85. IR (KBr): 1471w, 1464w, 1456w, 1429w, 1273s, 1199m, 1139s, 1037m, 938s, 756m, 746w, 702s, 654w, 628w, 614w, 596w, 566w, 533w, 518w, 496w, 478w, 423s, 430s, 421s, 402s, and 394s cm^{-1}.

$Cr^{III}(Cl_4SQ)(Cl_4Cat)(bpy) \cdot CH_3CN$ (3) An acetonitrile suspension (130 ml) containing $Cr^{III}(Cl_4SQ)_3 \cdot 4C_6H_6$ (98 mg, 0.090 mmol) was boiled under the atmosphere, then a 20 ml acetonitrile solution containing bpy (14 mg, 0.090 mmol) was added. The brownish violet suspension became reddish violet within few minutes. The suspension was filtered and the filtrate was allowed to stand for five days. The violet crystals were collected by filtration and

washed with acetonitrile several times, and then dried in vacuum (27 mg, 41 %). Found: C, 39.00; H, 1.61, N, 6.24. $C_{24}H_{11}Cl_8CrN_3O_4$ requires C, 38.90, H, 1.50, N, 5.67. IR (KBr): 1571w, 1566w, 1495m, 1471s, 1430s, 1376m, 1313m, 1272m, 1247s, 1216s, 1170w, 1157w, 1131w, 1104w, 1090w, 1069w, 1059w, 1045w, 1034w, 978s, 885w, 813w, 791s, 766s, 731m, 711w, 691m, 663w, 651w, 630w, 611w, 592m, 581m, 550m, 535w, 514w, 460w, 444w, and 423w cm^{-1}.

$Cr^{III}(Br_4SQ)(Br_4Cat)(bpy)\cdot 1/2CH_3CN$ (4) An acetonitrile suspension (60 ml) containing $Cr^{III}(Br_4SQ)_3\cdot 4C_6H_6$ (334 mg, 0.204 mmol) was boiled under the atmosphere, then a 10 ml acetonitrile solution containing bpy (32 mg, 0.20 mmol) was added. The brownish violet suspension turned to violet within few minutes. The microcrystalline solid was collected by the filtration and washed with acetonitrile several times, and then dried in vacuum (157 mg, 72 %). Found: C, 25.46; H, 0.94, N, 3.04. $C_{23}H_{9.5}Br_8CrN_{2.5}O_4$ requires C, 25.67, H, 0.89, N, 3.25. IR (KBr): 1564w, 1494m, 1469m, 1445s, 1425s, 1349w, 1310m, 1283m, 1249s, 1208w, 1155s, 1124s, 1105s, 1081s, 1060s, 1044s, 1035s, 1023s, 965s, 933s, 886m, 757s, 748s, 729m, 686m, 665m, 651m, 645m, 627m, 576w, 564w, 535w, 504w, 473w, 452m, 404m, and 397m cm^{-1}.

$Cr^{III}(Cl_4SQ)(Cl_4Cat)(TMphen)$ (5) The complex was synthesized by the procedure similar to that of **4** using $Cr^{III}(Cl_4SQ)_3\cdot 4C_6H_6$ (221 mg, 0.2 mmol) and TMphen (48 mg, 0.20 mmol). 87 mg (56 %). Recrystallization from chloroform affords reddish violet single crystal. Found: C, 43.40; H, 2.45, N, 3.49. $C_{28}H_{16}Cl_8CrN_2O_4$ requires C, 43.11, H, 2.07, N, 3.59. IR (KBr): 1532m, 1432m, 1402m, 1374w, 1306s, 1248m, 1101s, 1079s, 977s, 936w, 898m, 863w, 827w, 813w, 783s, 750w, 726w, 707w, 690w, 683w, 672w, 642w, 630w, 614w, 589m, 575w, 552w, 535w, 515w, 485w, 459w, 424w, and 404w cm^{-1}.

$Cr^{III}(Br_4SQ)(Br_4Cat)(TMphen)$ (6) An acetonitrile suspension (65 ml) containing $Cr^{III}(Br_4SQ)_3\cdot 4C_6H_6$ (378 mg, 0.231 mmol) was boiled under the atmosphere, then a 20 ml acetonitrile solution containing TMphen (56 mg, 0.24 mmol) was added. The brownish violet suspension turned to violet within few minutes. The suspension was filtered and the filtrate was allowed to stand for two days. The obtained powder was collected by filtration and washed with acetonitrile several times, then dried in vacuum. 147 mg (55 %). Found: C,

29.11; H, 1.49, N, 2.71. $C_{28}H_{16}Br_8CrN_2O_4$ requires C, 29.61, H, 1.42, N, 2.47. IR (KBr): 1528m, 1469m, 1427m, 1398m, 1376m, 1308w, 1284m, 1267s, 1246m, 1232w, 1198w, 1114s, 933m, 896w, 871w, 812w, 752m, 727m, 722m, 700s, 660w, 623w, 597w, 569w, 556w, 531w, 495w, 434m, and 424m cm^{-1}.

Physical Measurements.

Infrared spectra for KBr pellets were recorded on a Perkin-Elmer system 2000 FT-IR spectrometer over the range of 350–7000 cm^{-1} and absorption spectra on a Hitachi U-3500 spectrophotometer over the range of 3130–33000 cm^{-1} at 296 K. Electrochemical measurements were carried out by a BAS CV-50W polarographic analyzer. A standard three-electrode system was used with a glassy carbon working electrode, platinum-wire counter electrode, and Ag/AgCl/CH_3CN electrode as reference. Thermogravimetric analyses were made on rigaku Thermo Plus 2 TG8120 over the temperature range of 295–772 K. Magnetic susceptibilities were recorded over the temperature range 1.9–350 K at 1 T with a superconducting quantum interference device (SQUID) susceptometer (Quantum Design, San Diego, CA) interfaced with a HP Vectra computer system. All the values were corrected for diamagnetism that were calculated from Pascal's table.[8]

Crystallographic Data Collection and Refinement of Structures.

All the measurements were performed on a Rigaku mercury diffractometer with CCD two-dimensional detector with Mo Kα radiation employing a graphite monochromator at 296 K. The sizes of the unit cells were calculated from the reflections collected on the setting angles of four frames by changing ω by 0.5° for each frame. Two different χ settings were used and ω was changed by 0.5° per frame. Intensity data were collected in 480 frames with an ω scan width of 0.5° and exposure times 120, 70, and 180 s for **1**, **3** and **5**, respectively. Empirical absorption correction using the program REQABA[9] was performed for all the data. All the crystal data are summarized in Table 1. The structures were solved by direct methods[10] and expanded using Fourier techniques.[11] The final cycles of the full-matrix least-squares refinements were based on the observed reflections ($I > 3\sigma(I)$ for **1** and **3** and $I > 2\sigma(I)$ for

5). All the calculations were performed using the teXsan crystallographic software package of Molecular Structure Corporation.[12]

Table 1 Crystallographic and Refinement Data for **1**, **3**, and **5**

	1	**3**	**5**
Formula	$C_{16}H_6Cl_8N_2O_4Cr$	$C_{24}H_{11}Cl_8N_3O_4Cr$	$C_{16}H_6N_2O_4Br_8Cr$
Formula weight	625.85	740.99	625.85
Color	reddish violet	reddish violet	reddish violet
Crystal size, mm	0.22×0.10×0.05	0.50×0.08×0.05	0.35×0.08×0.05
Crystal System	triclinic	triclinic	triclinic
Space Group	$P\bar{1}$	$P\bar{1}$	$P\bar{1}$
a, Å	5.9174(8)	8.629(2)	8.571(2)
b, Å	9.4798(8)	13.739(2)	15.377(4)
c, Å	10.672(2)	14.714(3)	15.386(4)
α, °	109.517(5)	115.71(1)	116.622(5)
β, °	99.967(3)	95.706(3)	96.608(3)
γ, °	92.822(2)	92.154(4)	96.799(3)
Z	1	2	2
V, Å^3	522.0(1)	1557.6(6)	1767.4(7)
ρ_{calc}, g/cm^3	1.882	1.580	1.466
μ, cm^{-1}	15.13	10.87	9.62
T, K	296	296	296
λ (Mo Ka), Å	0.71069	0.71069	0.71069
No. observations	1610	3233	2440[a]
No. parameters	142	361	142
Refls./para. ratio	11.34	8.96	6.29
GOF	2.74	2.16	2.22
R_{int}	0.018	0.027	0.036
R, Rw[b]	0.043, 0.057	0.056, 0.065	0.068, 0.075

[a] $I > 2.0\sigma(I)$. [b] $R = \Sigma||F_o|-|F_o||/\Sigma|F_o|$, $Rw = [\Sigma(|F_o|-|F_o|)^2/\Sigma w|F_o|^2)]^{1/2}$.

Results and Discussion

Molecular and Crystal Packing Structures.

Figure 1 shows ORTEP drawings of **1**, **3**, and **5** with atom numbering scheme. Each chromium ion has octahedral coordination environment involving the four oxygen atoms from two *o*-quinone ligands and two nitrogen atoms from the acetonitrile (**1**) , bpy (**2**), and TMphen (**3**). Table 2 lists average bond distances and angles of three complexes.

In compound **1**, the acetonitrile ligands coordinate to the chromium ion in *trans*-fashion making two *o*-quinone ligands being coplanar. The chromium atom of **1** is located on a special position that averages the structural features of the two *o*-quinone ligands. The Cr–O bond distances are found to be 1.929(3) and 1.935(3) Å for Cr(1)–O(1) and Cr(1)–O(2) bonds, respectively. The average Cr–O distance is 1.932(3) Å which is similar to those of the series of

Table 2. Selected Average Bond Distances (Å) and Angles (°) of **1**, **3**, and **5**

	L	**1**	**3**			**5**		
			trans[a]	*cis*[b]	average	*trans*[a]	*cis*[b]	average
Cr–O (Å)	**I**	1.932(3)	1.909(4)	1.926(2)	1.928(4)	1.941(8)	1.893(8)	1.919(8)
	II		1.944(4)	1.952(4)	1.948(4)	1.937(8)	1.908(8)	1.923(8)
average		1.932(3)			1.938(4)			1.920(8)
Cr–N (Å)		2.038(5)			2.063(5)			2.07(1)
C–O (Å)	**I**	1.310(5)	1.326(8)	1.344(8)	1.330(8)	1.33(1)	1.33(1)	1.33(1)
	II		1.301(6)	1.314(7)	1.308(7)	1.35(1)	1.34(1)	1.35(1)
average		1.310(5)			1.319(7)			1.34(1)
C–C (Å)	**I**	1.402(6)			1.39(1)			1.40(2)
	II				1.401(1)			1.39(2)
average		1.402(6)			1.40(1)			1.49(2)
O–Cr–O (°)	**I**	83.9(1)			84.5(2)			85.0(3)
	II				82.9(2)			85.0(3)
average		83.9(1)			83.7(2)			85.0(3)
N–Cr–N		180.0(0)			78.5(2)			78.7(4)

[a] *trans* oxygen atom to the nitrogen atom. [b] *cis* oxygen atom to the nitrogen atom.

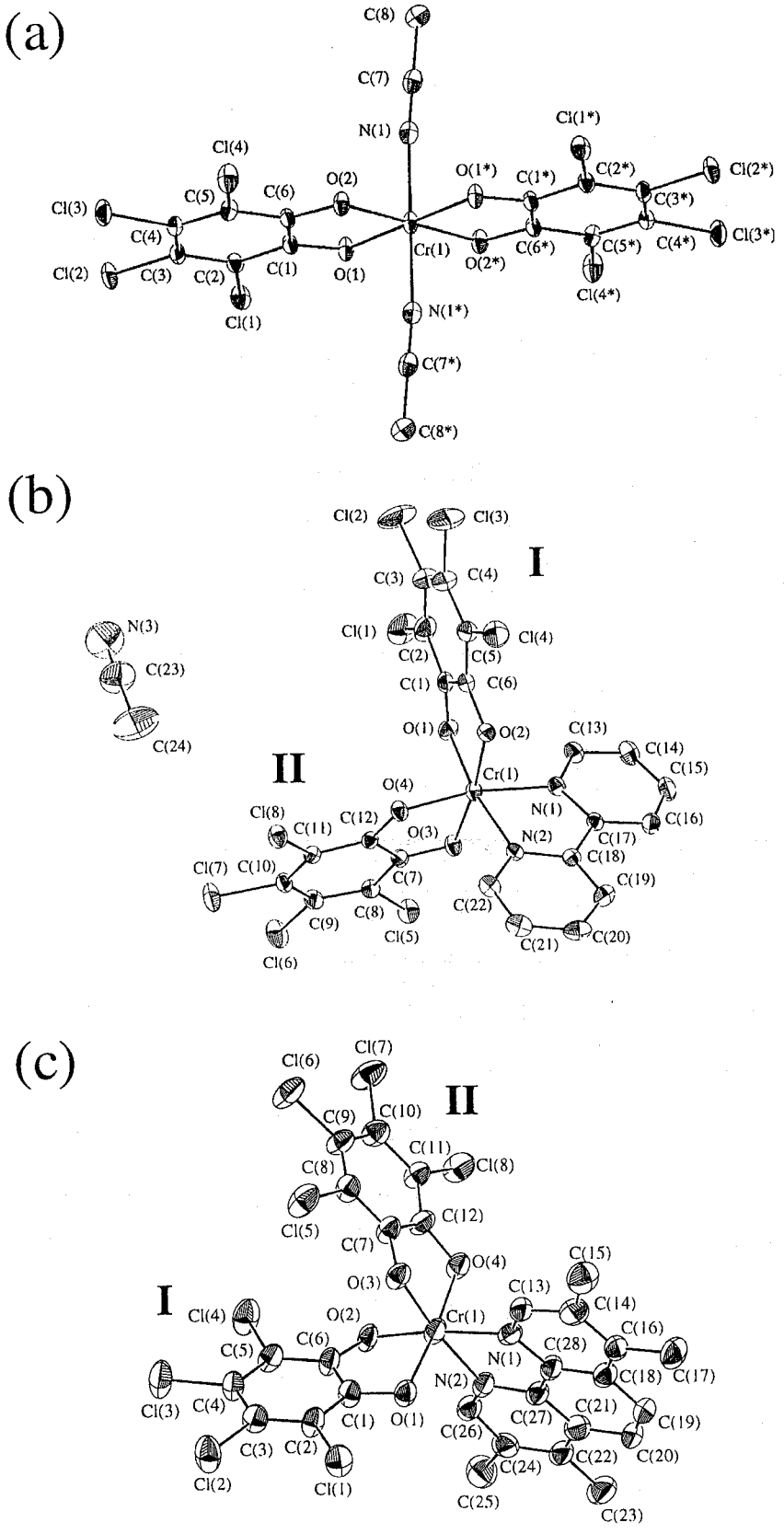

Figure 1. ORTEP drawings of (a) **1**, (b) **3**, and (c) **5** with hydrogen atoms and solvent molecule omitted (showing 30% isotropic thermal ellipsoids). Crystallographically independent ligands are designated **I** and **II**. The chromium atom of **1** has centroids coincident with crystallographic symmetry.

$[Cr^{III}(X_4SQ)_{3-n}(X_4Cat)_n]^{n-}$ isomers described in preceding Chapters. As a complex of Cr(III) the combined charge for the quinone ligands requires that one be X_4SQ other X_4Cat. In many cases, the crystallographic symmetry averages dissimilar ligands giving bond distances for the C–O bonds that are intermediate between SQ and Cat values.[7,13] The observed value for **1** is 1.310(5) Å, which is, in fact, intermediate between 1.28 and 1.34 Å for SQ and Cat forms, respectively.

For complexes **3** and **5** there are two crystallographically independent *o*-quinone ligands coordinated to the chromium ion so that two ligands located in approximately orthogonal planes. The longer C–O bond distances of 1.326(8) and 1.344(8) Å are found for the ligand **I** of **3** compared with 1.301(6) and 1.314(7) Å for ligand **II**. These values point to a localized mixed-valence electronic structure for the two independent ligands. In general, the ligand bite angle of SQ ligand is typically 2° smaller than that of the Cat ligand.[14] This tendency is also observed in complex **3** where the O(1)–Cr(1)–O(2) angle of ligand **I** (Cat) is 84.5(2)°, larger than 82.9(2)° of ligand **II** (SQ).

As shown in Figure 2(a) the crystal structure of **3** consists of weakly coupled pairs of complex molecules located about crystallographic centers of inversion. This interaction results from overlap of adjacent bpy ligands. The interplanar separation between adjacent bpy rings is 3.505(8) Å, which is shorter than 3.65 Å for $Co(3,5\text{-}DTBQ)_2(bpy)$.[14]

In contrast to complex **3**, the distinction between the SQ and Cat for complex **5** is difficult because of crystallographic disorder with relatively large standard deviation of the structural parameters (Table 2). On the other hand, the most striking feature of complex **5** is heavily distorted octahedral geometry around the chromium ion. The deviation could be attributed to the crystal packing structure of the complex. In the crystal structure of **5** there are two polymeric chains of complexes molecules. One chain consists of the stacks linked by overlapped six-membered rings of adjacent ligands **I**···**I'** and **II**···**II'** (Figure 2(b)) along the *bc*-direction. The mean separation between the ligand is found to be 3.56(2) Å. The interaction causes the distortion of the complex from the ideal octahedral geometry so that each ligand bents to the direction of the stacked chain. Additional one-dimensional chain of the complex is formed by overlapped regions of adjacent TMphen ligands along the *a*-axis. As a whole, the

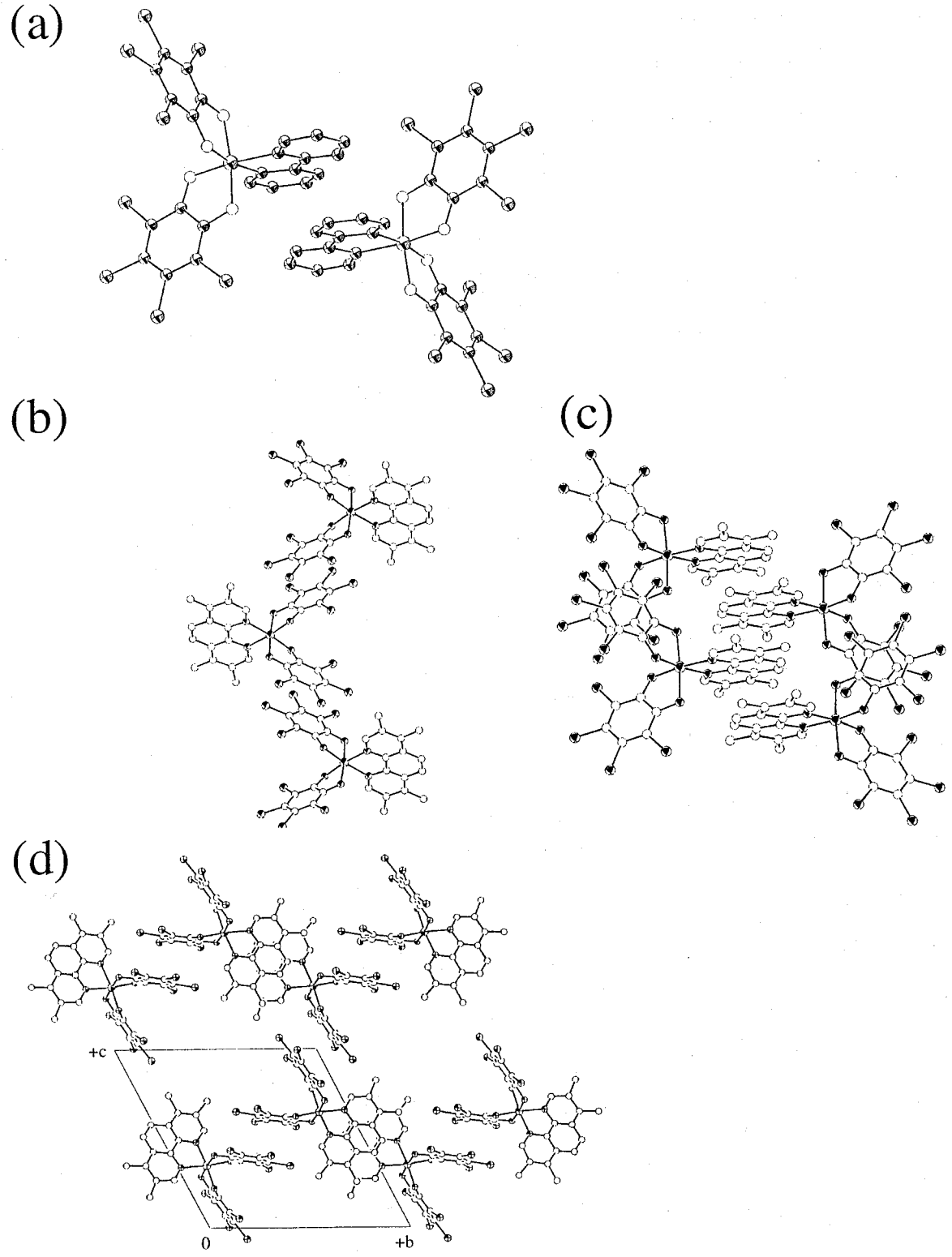

Figure 2. (a) View showing the pairing of complex **3** within unit cell. The separation between adjacent bpy ligands is 3.505(8) Å. (b) One-dimensional stacking structures of ligand **I** and **II** and (c) that of TMphen ligands in complex **5**. (d) Whole crystal packing diagram of **5** along the *a*-axis.

complex forms a three-dimensional assembled structure via two kinds of stacking interactions.

Spectroscopic Properties.

Infra-red Spectra Infra-red spectra of all the complexes are illustrated in Figure 3. The spectral features of the complexes quite similar to those of $[Cr^{III}(X_4SQ)_{3-n}(X_4Cat)_n]^{n-}$ (n = 1 and 2) redox isomers. Namely, two characteristic bands are observed near 1400 and 1100 cm^{-1}, indicating the presence of the SQ and the Cat ligands. These data demonstrate the ligand-based mixed-valence state of the complexes. Especially, for complexes **1–2** and **5–6**, the presence of two bands indicates the localized electronic structure involving the SQ and Cat ligands in contrast to the crystallographic data.

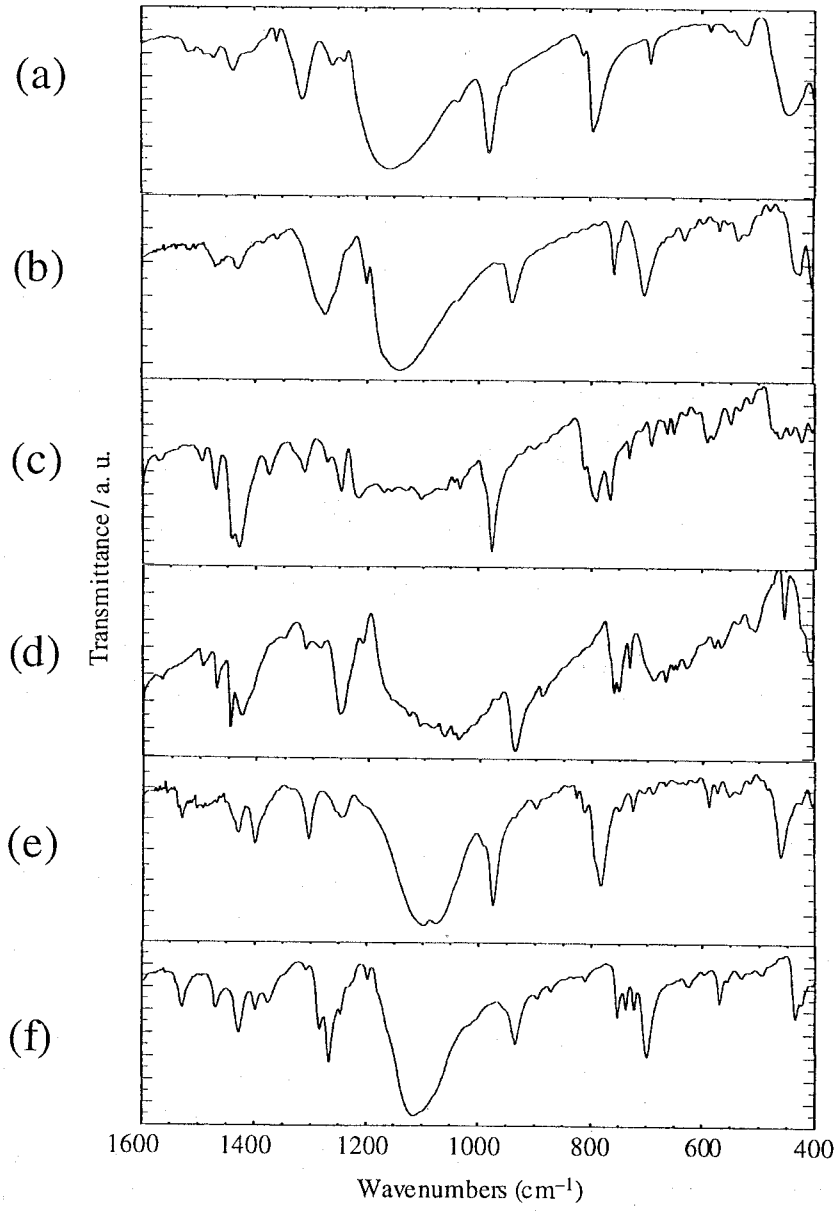

Figure 3. FT-IR spectra (KBr pellets) of complexes (a) **1** (b) **2**, (c) **3**, (d) **4**, (e) **5**, and (f) **6**.

UV-vis-NIR-IR absorption Spectra Figures 4 and 5 show absorption spectra of all the complexes measured in 1,2-dimethoxyethane and dichloromethane for **1–2** and **3–6**, respectively. All the data are summarized in Table 3. Hereafter, the spectra are discussed in two separated regions A (10000–30000 cm^{-1}) and B (3000–10000 cm^{-1}). Spectral features of complexes **1–6** are roughly similar to the $[Cr^{III}(X_4SQ)_{3-n}(X_4Cat)_n]^{n-}$ (n = 1 and 2) isomers (Chapter 4). In the region A, all the complexes commonly show several intense absorption bands. These bands could be assigned to intramolecular CT transition between the chromium ion and the ligand moieties. Among the bands, the most intense bands near 19000 cm^{-1} are commonly observed in all the complexes, and seem to be characteristic absorption band for the chromium complexes of SQ. The absorption maxima of these bands for complexes **1** and **2** are higher by 2500 cm^{-1} than those of **3–6**.

As shown in Figure 5, compounds **1–6** show characteristic broad, intense absorption bands in the region B with several overtone vibrational transitions. Similar low-energy electronic transitions have been observed in the series of $[Cr^{III}(X_4SQ)_{3-n}(X_4Cat)_n]^{n-}$ (n = 1 and 2) isomers described in Chapters 2–4. The bands are assigned to intervalence CT (IVCT) bands of SQ ← Cat, indicating the presence of both forms of the ligand in complexes **1–6**. Usually, the degree

Table 3. Absorption Spectral Parameters for Complexes **1–6** in Solution

compound	ν_{max} ($10^3 \times cm^{-1}$) ($\varepsilon_{max} = 10^3 \times M^{-1} \cdot cm^{-1}$)								
1[a]	5.08	7.41	8.47	11.0	13.6	15.9	19.0	24.8	
	(3.47)	(sh, 1.15)	(0.789)	(1.54)	(1.98)	(0.824)	(4.31)	(2.32)	
2[a]	5.05	7.46	8.38	10.9	13.4	16.0	19.0	24.2	
	(4.26)	(sh, 1.35)	(0.948)	(1.61)	(2.16)	(0.808)	(0.507)	(2.58)	
3[b]	4.32	11.2	12.7	14.0	15.6	18.1	21.6	24.8	32.9
	(2.50)	(2.42)	(2.52)	(sh, 1.95)	(1.72)	(6.50)	(sh, 2.74)	(sh, 3.07)	
4[b]	3.77	11.2	12.6	13.9	15.7	18.1	21.4	23.9	33.2
		(2.04)	(2.26)	(1.62)	(1.47)	(5.28)	(2.16)	(2.43)	(16.0)
5[b]	4.31	11.2	12.8	14.1	15.8	18.3	21.3	24.9	
	(2.12)	(2.34)	(2.47)	(sh, 1.51)	(1.41)	(5.96)	(2.68)	(2.95)	
6[b]		11.1	12.6	14.5	15.9	18.2	21.4	24.0	
		(2.77)	(3.07)	(sh, 1.51)	(1.66)	(6.91)	(3.05)	(3.50)	

[a] Measured in 1,2-dimethoxyethane. [b] Measured in dichloromethane.

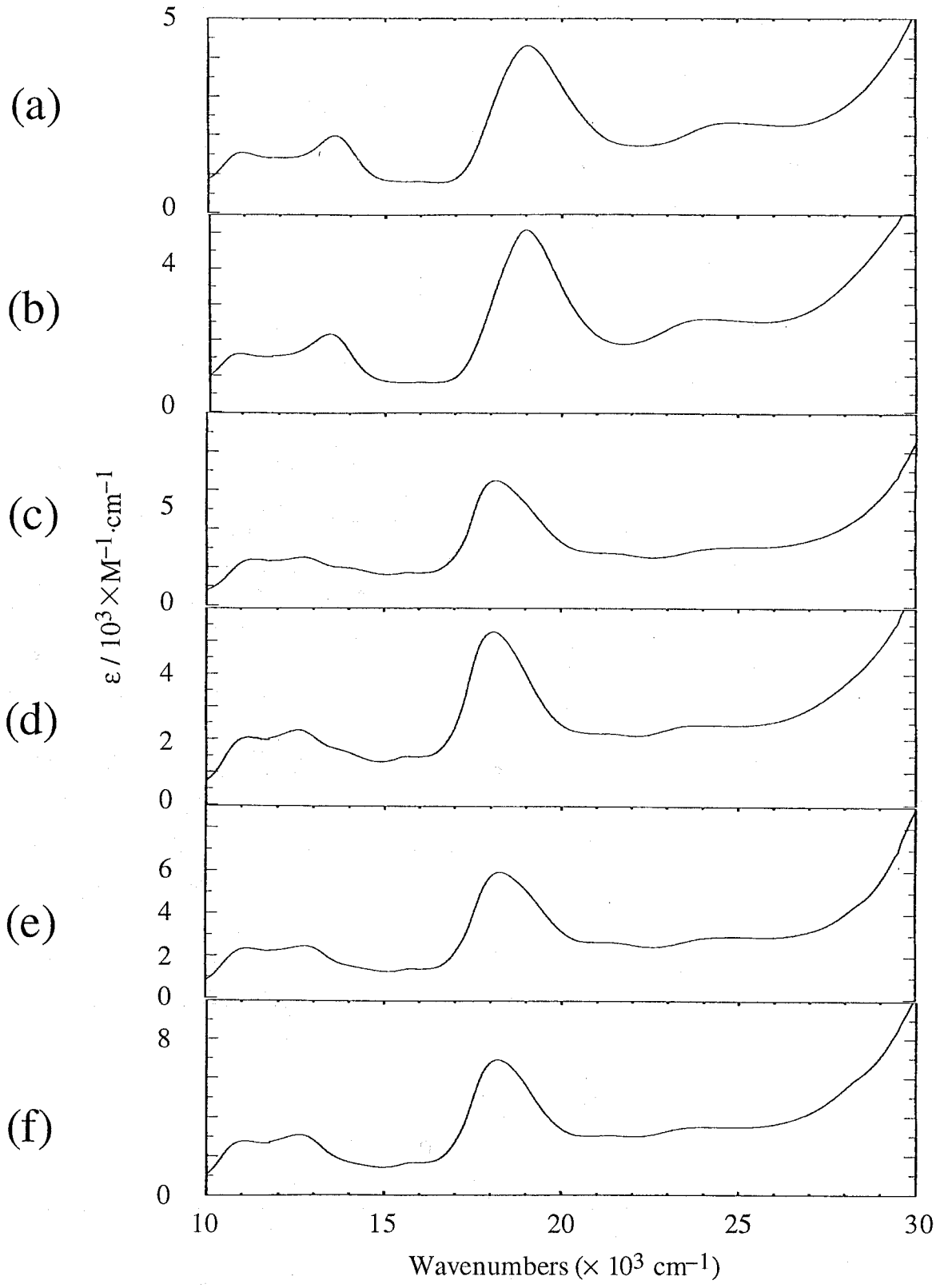

Figure 4. Electronic absorption spectra (region A) of complexes (a) **1** (b) **2**, (c) **3**, (d) **4**, (e) **5**, and (f) **6** in dichloromethane.

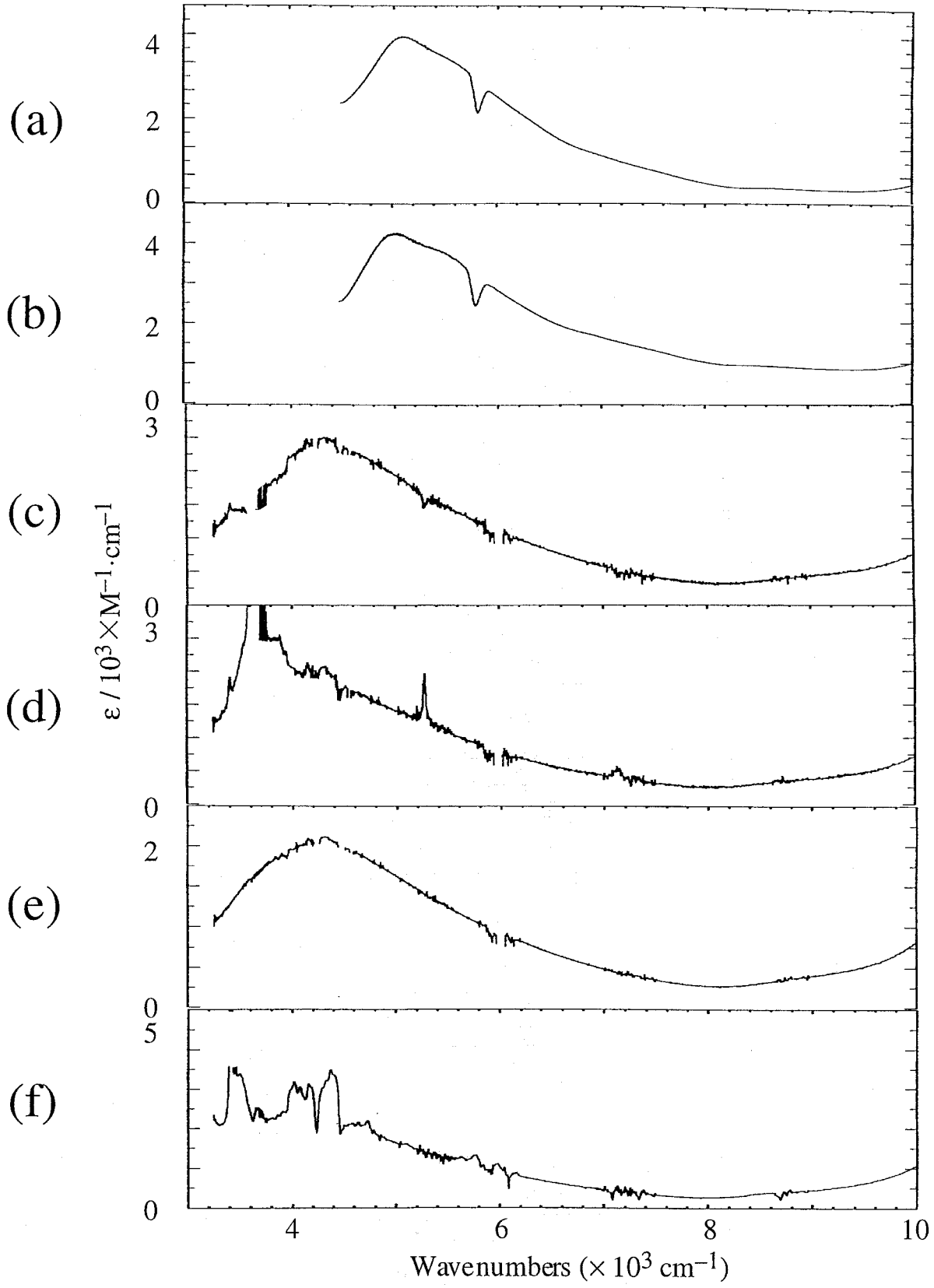

Figure 5. Electronic absorption spectra (region B) of complexes (a) **1** (b) **2**, (c) **3**, (d) **4**, (e) **5**, and (f) **6** in dichloromethane.

of electric coupling between the mixed-valence ligands, H_{ab}, can be estimated by use of Hush's formula,[16] however, in the present cases, the low symmetry of the IVCT bands prevents the quantitative analyses of the mixed-valence states. The intensities of the IVCT bands for all the complexes are nearly half compared with those of tris(*o*-quinone) chelated redox isomers. In the

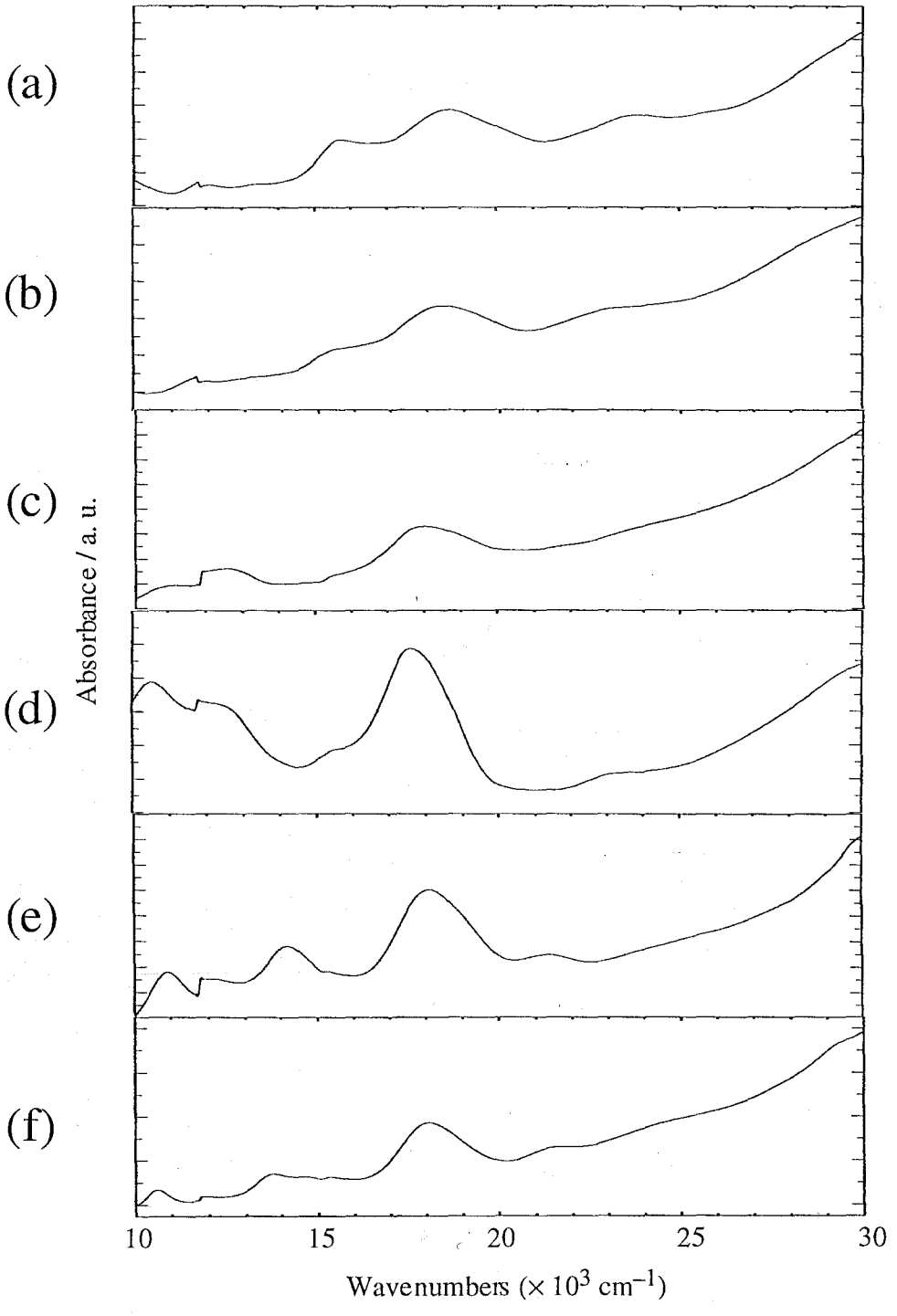

Figure 6. Electronic absorption spectra (region A) of complexes (a) **1** (b) **2**, (c) **3**, (d) **4**, (e) **5**, and (f) **6** measured on KBr pellet. The discontinuity near 12000 cm^{-1} is an instrumental artifact due to a detector change in the spectrometer.

solid state (KBr) all the complexes show similar absorption spectra as shown in Figures 6 (region A) and 7 (region B). The presence of the IVCT bands indicates that all the complexes possess the mixed-valence state in the solid state.

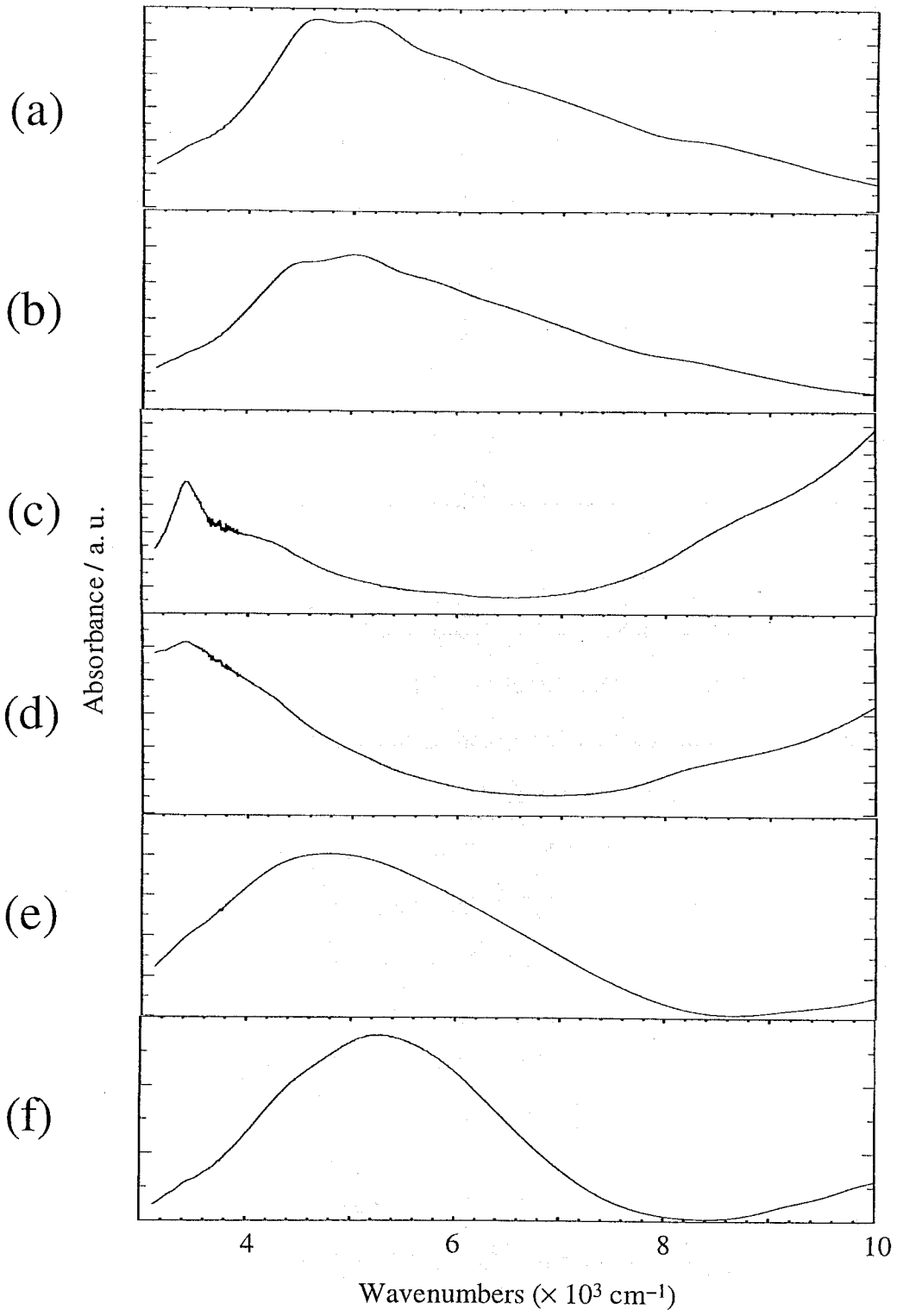

Figure 7. Electronic absorption spectra (region B) of complexes (a) **1** (b) **2**, (c) **3**, (d) **4**, (e) **5**, and (f) **6** measured on KBr pellet. The discontinuity near 12000 cm^{-1} is an instrumental artifact due to a detector change in the spectrometer.

Table 4. Absorption Spectral Parameters for Complexes **1–6** Measured on KBr Pellets

compound	ν_{max} ($10^3 \times cm^{-1}$) ($\varepsilon_{max} = 10^3 \times M^{-1} \cdot cm^{-1}$)										
1	4.62	5.10 (sh)	5.90 (sh)	6.60 (sh)	8.20 (sh)		12.1	13.5 (sh)	15.6	18.6	23.9
2	4.50 (sh)	5.00	5.70 (sh)	6.45 (sh)	8.00 (sh)		12.0	13.4 (sh)	15.6 (sh)	18.6	23.5 (sh)
3	3.43 (sh)	4.00 (sh)	5.10 (sh)	5.80	8.50 (sh)	11.1	12.5		15.3 (sh)	18.0	24.0 (sh)
4	3.42 (sh)	4.20 (sh)	5.10		8.40 (sh)	10.5	12.2 (sh)		15.7 (sh)	17.6	23.8
5	4.35 (sh)	4.73			9.40 (sh)	10.9	12.0 (sh)		14.2	15.3 18.1	21.4 25.0 (sh)
6	4.40 (sh)	5.22			9.20 (sh)	9.90 (sh)	10.6	12.0 (sh)	13.8	14.6 15.4	18.9 21.7 25.0 (sh)

Electrochemical Properties.

From the redox-active nature of the ligand moieties, ligand-based electrochemical activity would be expected for the present complexes. The electrochemical properties of the complexes were studied in 1,2-dimethoxyethane and dichloromethane solution for **1–2** and **3–6**, respectively. The results are given in Table 5 and Figure 8.

All the complexes commonly undergo quasi-reversible one-electron oxidation and reduction near 630 and 170 mV vs Ag/AgCl/CH_3CN, respectively. Since the chromium ion retains trivalent state in this potential region, both electrochemical process are corresponding to the oxidation and reduction of the ligand moieties as shown in eq. (1) . The one-electron oxidation

$$[Cr^{III}(X_4SQ)_2(L)_n]^+ \overset{e^-}{\rightleftharpoons} Cr^{III}(X_4SQ)(X_4Cat)(L)_n \overset{e^-}{\rightleftharpoons} [Cr^{III}(X_4Cat)_2(L)_n]^- \qquad (1)$$

would provide a cationic $[Cr^{III}(X_4SQ)_2(L)_n]^+$ species (left) which has two semiquinonate ligands, while the reduction affords anionic $[Cr^{III}(X_4Cat)_2(L)_n]^-$ species (right) with two catecholate ligands. A similar result was observed for $Cr^{III}(SQ)(Cat)(N\text{-}N)$ complexes reported by Pierpont et al..[8] The reduction potentials of complexes **3** and **4** are higher than those of complexes **5** and **6**, reflecting the electron donating effect of methyl groups of TMphen ligand.

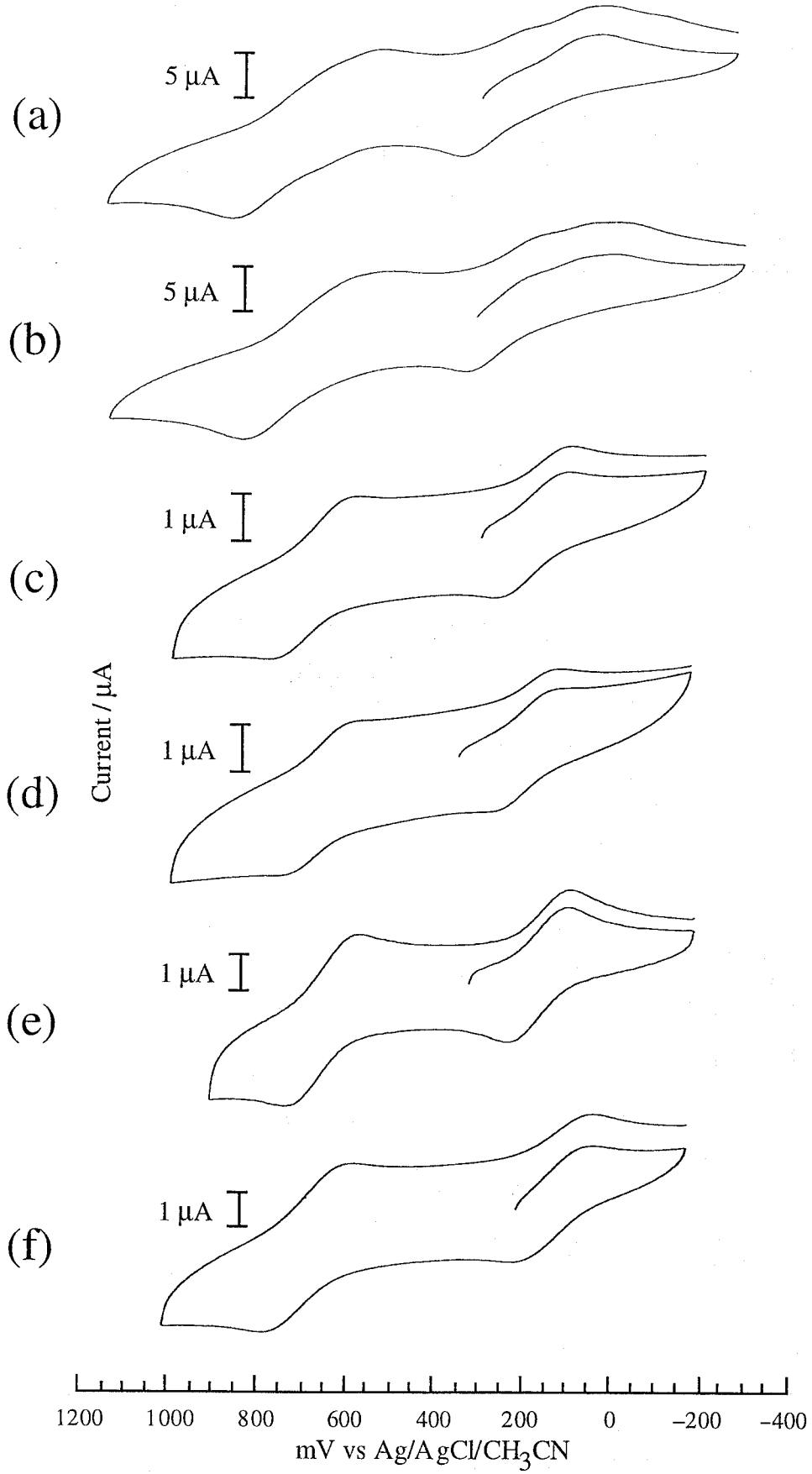

Figure 8. Cyclic voltammograms of complexes (a) **1** (b) **2**, (c) **3**, (d) **4**, (e) **5**, and (f) **6** measured in dichloromethane.

Similarly, the lower oxidation potentials are observed for complexes **3** and **4** compared with complexes **5** and **6**. The differences between the first oxidation and reduction potentials are approximately 500 mV, which is comparable to 390 mV observed for mixed-valence Creuz-Taube ion, $[(NH_3)_5Ru(py)Ru(NH_3)_5]^{5+}$ (py = pyrazine).[17]

All the complexes show irreversible reduction waves at the potentials lower than –1400 mV. The process would be attributed to the reduction of the Cr^{III} to the Cr^{II}. Finally, one (**1–4**) or two (**5–6**) irreversible reduction waves are also found. From the comparison with redox properties of tris(*o*-semiquinonate) complexes oxidation of SQ to BQ would be attributable to these redox process.[3] The irreversible electrochemical process is forced by the low coordination ability of the BQ ligand.

Table 5. Cyclic Voltammetric Data for Complexes **1–6**

complex	potential (mv)[a]											
	E_{ox2}	E_{ox1}	**+1/0**				**0/–1**				$\Delta E_{1/2}$[e]	E_{red1}	E_{red2}
			E_{ox}	E_{red}	Δ[d]	$E_{1/2}$	E_{ox}	E_{red}	Δ[d]	$E_{1/2}$			
1[b]		1400	817	505	312	661	327	6	321	167	494	–1440	
2[b]		1370	826	493	333	660	333	–9	342	162	498	–1560	
3[c]	1860		778	575	203	677	265	107	158	186	491		–1720
4[c]	1800		730	550	190	640	276	103	173	190	450	–1550	
5[c]	1770	1540	718	551	167	635	230	83	147	157	478	–1410	
6[c]	1730	1540	707	537	170	622	229	77	152	153	467	–1550	

[a] Condition: scan rate 100 mV/s, N_2, mv vs Ag/AgCl/CH_3CN, 296 K. [b] Measured in 1,2-dimethoxyethane. [c] Measured in dichloromethane. [d] Separation between E_{ox} and E_{red}. [e] mV vs Ag/AgCl/CH_3CN. [e] Separation between $E_{1/2}$ (+1/0)–$E_{1/2}$ (0/–1).

Thermogravimetric Analyses.

In order to examine the thermolabilities of the axially coordinated acetonitrile molecules of **1** and **2**, the thermogravimetric (TG) measurements have been carried out. The TG diagrams of both complexes are given in Figure 9. Rapid weight loss of 14.2 (**1**) and 9.0 (**2**) % take place up to 520 K for two compounds. The liberation of two acetonitrile ligands accounts for this weight loss for **1** (13.1 %) and **2** (8.4 %) (eq. (2)). However, above this temperature, the complexes gradually lost the weight indication the thermal decomposition.

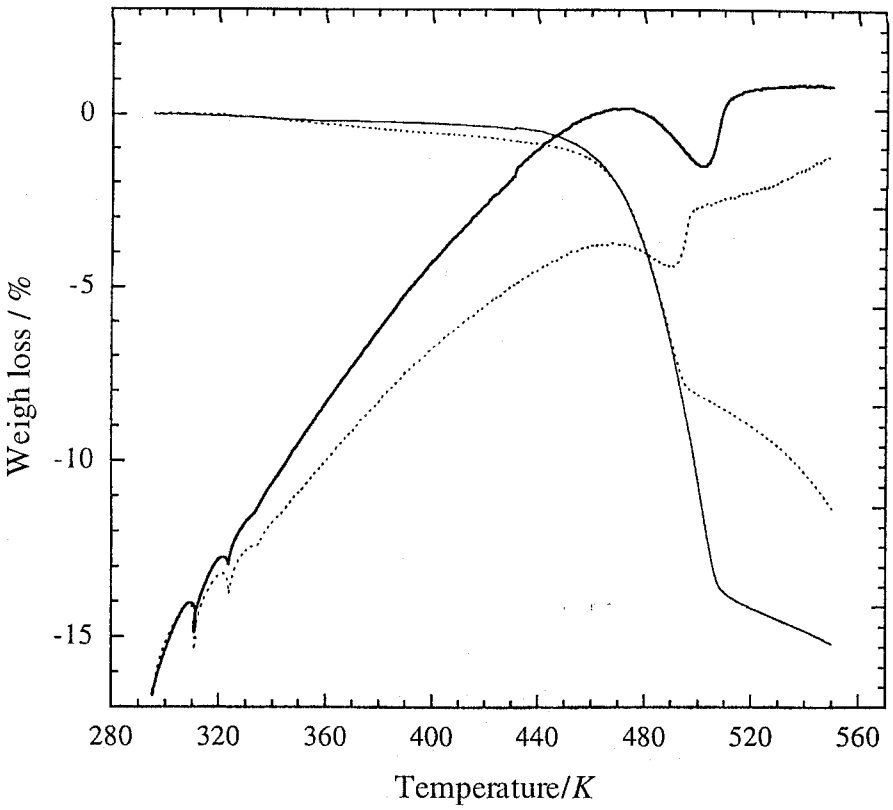

Figure 9. Thermogravimetric data for **1** (–) and **2** (···).

$$Cr^{III}(X_4SQ)(X_4Cat)(CH_3CN)_2 \xrightarrow{2CH_3CN} Cr^{III}(X_4SQ)(X_4Cat) \qquad (2)$$

Temperature Dependence of Magnetic Susceptibilities.

Figure 10 shows temperature dependence of $\chi_M T$ for all the complexes. At 300 K, the values are in the range of 0.934–1.12 emu·K·mol^{-1} close to the theoretical value of 1.00 emu·K·mol^{-1} expected for an S = 1 spin (g = 2.00).[8] The S = 1 ground state could be attributed to the intramolecular antifferomagnetic interactions between the S = 3/2 spin on the Cr(III) ion and S = 1/2 spin on the SQ ligand. No temperature dependence of $\chi_M T$ was observed in the region of 50–300 K. Therefore it must be concluded that the coupling is strongly antiferromagnetic with a ground state S = 1 and no exited state thermally populated. These results are similar to the mono-semiquinonate complexes [Cr^{III}(tren)(3,6-DTBSQ)](PF_6)$_2$ (tren = tris(2-aminoethyl)amine)[5(b)] for which the lower limit of the isotropic coupling constant

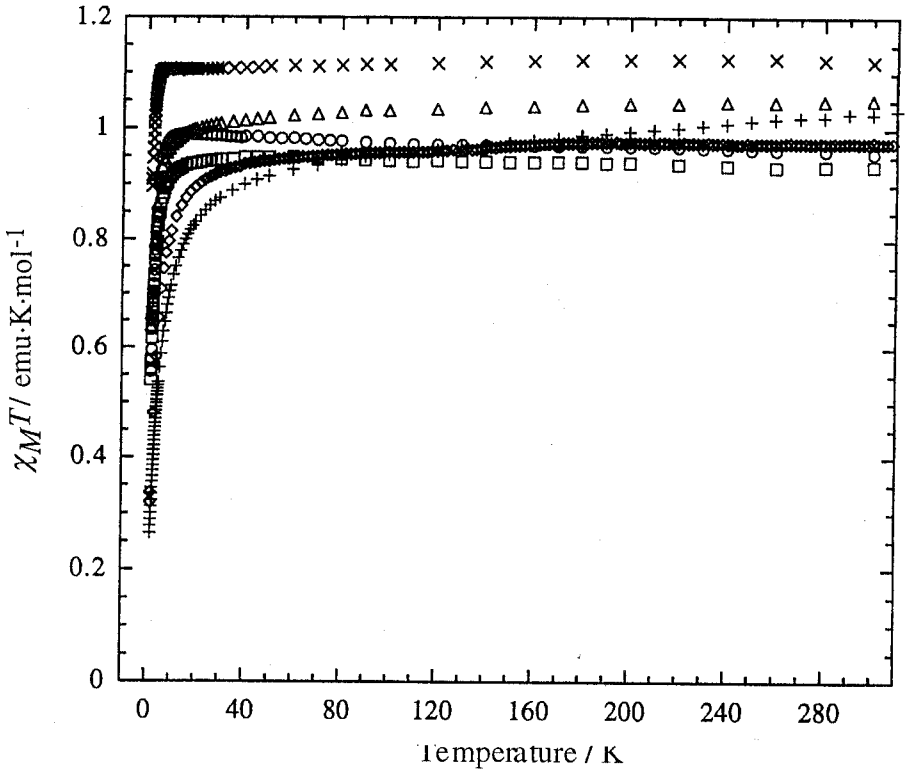

Figure 10. The plots of the temperature dependence of $\chi_m T$ of (a) **1** (O), (b) **2** (□), (c) **3** (◇), (d) **4** (×), (e) **5** (+), and (f) **6** (△) measured under the field of 1 T.

J is estimated to be larger than 350 cm^{-1} ($\boldsymbol{H} = 2J \cdot S_{Cr} \cdot S_{SQ}$). In the region of approximately 50–300 K, $\chi_M T$ values exhibit temperature independent behavior, whereas below 50 K, rapid decreases were observed. The decreasings of $\chi_M T$ values suggest the intermolecular antiferromagnetic interactions between the neighboring complexes. These intermolecular magnetic interactions are attributable to the stacking interaction between the adjacent complex molecules.

Solvent-induced Valence Tautomerism of $Cr^{III}(X_4SQ)_3$

Reaction of the tris(*o*-semiquinonate) complexes, $Cr^{III}(X_4SQ)_3 \cdot 4C_6H_6$, with acetonitrile lead to a rapid formation of dark purple solids of **1** and **2**. Only one report has been reported about the ligand exchange reaction of $Cr^{III}(Cl_4SQ)_3$ by Buchanan et al..[6] They carried out the exchange reaction of $Cr^{III}(SQ)_3$ complexes with bpy, however, only small quantities of bpy products could be detected. In general the octahedral Cr^{III} (d^3) ion is quite inert toward the

ligand exchange reaction, while chemically one-electron oxidized $[Cr^{III}(BQ)(SQ)_2]^+$ complex shows more rapid ligand exchange by bpy, which is accelerated by the weak coordination ability of the BQ ligand (eq. (3)). However, in the present case, the reaction proceeds without oxidation.

$$Cr^{III}(Cl_4SQ)_3 \xrightarrow{-e^-} [Cr^{III}(Cl_4BQ)(Cl_4SQ)_2]^+ \xrightarrow[Cl_4BQ]{bpy} [Cr^{III}(Cl_4SQ)(Cl_4Cat)(bpy)](\mathbf{3}) \qquad (3)$$

To investigate the observed conversion, the electronic absorption spectra of $Cr^{III}(Cl_4SQ)_3$ were determined in non-polar solvents dichloromethane, carbondisulfide, and cyclohesane, and polar-solvents, acetonitrile and acetone. Figure 11 shows these spectra together with the spectrum of **1** measured in 1,2-dimethoxyethane. As discussed in Chapter 1, the spectra obtained for the low dielectric constant solvents carbondisulfide, cyclohexane were found to be similar to the result obtained with dichloromethane. In these solvents, no absorption band was

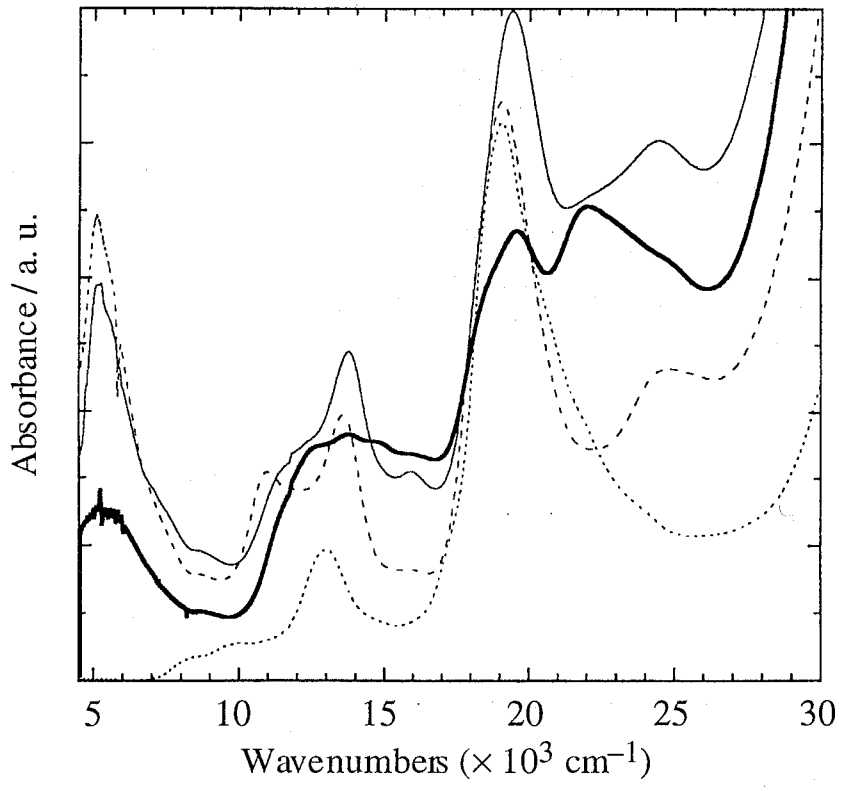

Figure 11. Electronic absorption spectra of $Cr^{III}(Cl_4SQ)_3$ measured in dichloromethane (····), acetonitrile (–), and acetone (—) and that of **1** in 1,2-dimethoxyethane (---). The spectra of $Cr^{III}(Cl_4SQ)_3$ in carbondisulfide and cyclohexane are similar to that of dichloromethane (Chapter 1).

observed in the region higher than 7000 cm^{-1}. On the other hand, the dissolution of $Cr^{III}(Cl_4SQ)_3$ in acetonitrile and acetone leads to increasings of the absorption intensities in the region of 4000–10000 cm^{-1}. As described above, complex **1** shows the IVCT band in this region derived from the ligand-based mixed-valence state. These spectral features indicate the dissolution of $Cr^{III}(Cl_4SQ)_3$ complex in the polar solvents causes a formation of the mixed-valence species. This fact indicates that the polarity of the solvents used is closely related with the intramolecular charge distribution of the complexes. The following reaction mechanism would be suggested to account for this conversion. Firstly, (i) the polarity of solvents induces the disproportionate charge distribution of $Cr^{III}(X_4SQ)_3$,

$$Cr^{III}(X_4SQ)_3 \rightleftarrows Cr^{III}(X_4BQ)(X_4SQ)(X_4Cat) \qquad (4)$$

where the valence tautomeric equilibrium between $Cr^{III}(Cl_4SQ)_3$ and a mixed-valence complex, $Cr^{III}(Cl_4BQ)(Cl_4SQ)(Cl_4Cat)$ occurs. Secondly, (ii) this equilibrium is immediately followed by the dissociation of the X_4BQ ligand which shows the weakest coordination ability to the metal ion among the three redox isomers, BQ, SQ, and Cat,

$$Cr^{III}(X_4BQ)(X_4SQ)(X_4Cat) \rightarrow Cr^{III}(X_4SQ)(X_4Cat) + X_4BQ \qquad (5)$$

If no chelate reagents such as bpy or TMphen in the solution, the acetonitrile molecules attack to the Cr^{III} ion to form complexes **1** and **2** (eq. (6a)). In fact, the red crystals were isolated from the filtrate, and shows infrared band at 1680 cm^{-1} assigned to the C=O stretching mode of Cl_4BQ.

$$Cr^{III}(X_4SQ)(X_4Cat) + 2CH_3CN \rightarrow \textit{trans}\text{-}Cr^{III}(X_4SQ)(X_4Cat)(CH_3CN)_2 \ (\mathbf{1} \text{ and } \mathbf{2}) \qquad (6a)$$

On the other hand, in the presence of the chelate reagents, *cis*-coordinated products should be formed followed by eq. (6b),

$$Cr^{III}(X_4SQ)(X_4Cat) + N\text{–}N \rightarrow \textit{cis}\text{-}Cr^{III}(X_4SQ)(X_4Cat)(N\text{–}N) \ (\mathbf{3}\text{–}\mathbf{6}) \qquad (6b)$$

The intramolecular electron transfers have been noted for the Co and Mn complexes induced

by temperature change.[1(b)-(c),18] On the other hand, Hendrickson et al. reported about the solvent dependent valence tautomeric equilibrium between $Fe^{II}(phenSQ)_2(N\text{-}N)$ and $Fe^{III}(phenSQ)(phenCat)(N\text{-}N)$ complexes[19] (eq. (7)),

$$Fe^{II}(phenSQ)_2(N\text{-}N) \rightleftarrows Fe^{III}(phenSQ)(phenCat)(N\text{-}N) \qquad (7)$$

where the equilibrium lies to the left in a low dielectric solvent, whereas in a high dielectric solvent the equilibrium is shifted to the right. This tendency is drastically changed in the present system that the high dielectric solvents favor the formation of heteloleptic mixed-valence complex. The difference between these two systems could be attributed to the difference of the metal ions. Namely, in the iron complexes, both of metal ion and ligands can change their valence states, while in the case of chromium complexes only the ligands could participate in the equilibrium due to the inertness of chromium (III) ion.

Conclusion

In this Chapter, the synthesis, crystal structures, and physical properties of mixed-valence bis(*o*-quinonate) chromium complexes were described. The complexes were synthesized by the conversion of $Cr^{III}(X_4SQ)_3$ in acetonitrile to the mixed-valence intermediate complex, $[Cr^{III}(X_4BQ)(X_4SQ)(X_4Cat)]$. The valence tautomerism of chromium complexes was made for the first time and proved to be useful for the synthesis of mixed-valence bis(*o*-quinonate) complexes. Interestingly, the observed conversion is based on the ligand-based redox activity of the chromium complexes.

References

(1) (a) Adams, D. M.; Hendrickson, D. N. *J. Am. Chem. Soc.* **1996**, *118*, 11515. (b) Adams, D. M.; Noodleman, L.; Hendrickson, D. N. *Inorg. Chem.* **1997**, *36*, 3966. (c) Jung, O. -S.; Pierpont, C. G. *J. Am. Chem. Soc.* **1994**, *116*, 2229.

(2) (a) Jung, O. -S.; Jo, D. H.; Lee, Y. -A.; J., C. B.; Pierpont, C. G. *Inorg. Chem.* **1997**, *36*, 19. (b) Jung, O. -S.; Jo, D. W.; Lee, Y. -A.; Chae, H. K.; Sohn, Y. S. *Bull. Chem. Soc. Jpn.* **1996**, *69*, 2211. (c) Jung, O. -S.; Jo, D. H.; Lee, Y. -A.; Sohn, Y. -S.; Pierpont, C. G. *Angew. Chem., Int. Ed. Engl.* **1996**, *35*, 1694. (d) Jung, O. -S.; Pierpont, C. G. *Inorg. Chem.* **1994**, *33*, 2227.

(3) Downs, H. H.; Buchanan, R. M.; Pierpont, C. G. *Inorg. Chem.* **1979**, *18*, 1736.

(4) Buchanan, R. M.; Kessel, S. L.; Downs, H. H.; Pierpont, C. G.; Hendrickson, D. N. *J. Am. Chem. Soc.* **1978**, *100*, 7894.

(5) (a) Benelli, C.; Dei, A.; Gatteschi, D.; Güdel, H. U.; Pardi, D. *Inorg. Chem.* **1989**, *28*, 3089. (b) Wheeler, D. E.; McCusker, J. K. *Inorg. Chem.* **1998**, *37*, 2296. (c) Rodrigues, J. H.; Wheeler, D. E.; McCusker, J. K. *J. Am. Chem. Soc.* **1998**, *120*, 12051.

(6) Buchanan, R. M.; Claflin, J.; Pierpont, C. G. *Inorg. Chem.* **1983**, *22*, 2552.

(7) Attia, A. S.; Pierpont, C. G. *Inorg. Chem.* **1998**, *37*, 3051.

(8) Kahn, O. *Molecular Magnetism*; VCH: New York, 1993.

(9) Jacobson, R. A. *REQABA Empirical Absorption Correction Version 1.1-03101998:* Molecular Structure Corp.: The Woodlands, TX, 1996–1998.

(10) Altomare, A.; Burla, M. C.; Camalli, M.; Cascarano, M.; Giacovazzo, C.; Guagliardi, A.; Pilidori, G. *J. Appl. Crystallogr.* **1994**, *27*, 435.

(11) Beurskens, P. T.; Admiraal, G.; Beurskens, G.; Bosman, W. P.; de Gelder, R.; Israel, R.; Smits, J. M. M. , The DIRDIF-94 program system, Technical Report of the Crystallography Laboratory; University of Nijmegen: Nijmegen, The Netherlands, 1994.

(12) *teXsan: Crystal Structure Analysis Package*; Molecular Structure Corporation: The Woodlands, TX, 1985, 1992.

(13) (a) Attia, A. S.; Bhattacharya, S.; Pierpont, C. G. *Inorg. Chem.* **1995**, *34*, 4427. (b)

Attia, A. S.; Pierpont, C. G. *Inorg. Chem.* **1995**, *34*, 1172.

(14) (a) Raymond, K. N.; Isied, S. S.; Brown, L. D.; Fronczek, F. R.; Nibert, J. H. *J. Am. Chem. Soc.* **1976**, *98*, 1767. (b) Sofen, S. R.; Ware, D. C.; Cooper, S. R.; Raymond, K. N. *Inorg. Chem.* **1979**, *18*, 234.

(15) Buchanan, R. M.; Pierpont, C. G. *J. Am. Chem. Soc.* **1980**, *102*, 4951.

(16) Hush, N. S. *Coord. Chem. Rev.* **1985**, *64*, 135.

(17) Creutz, C.; Taube, H. *J. Am. Chem. Soc.* **1973**, *95*, 1086.

(18) Attia, A. S.; Jung, O. -S.; Pierpont, C. G. *Inorg. Chim. Acta* **1994**, *226*, 91.

(19) Lynch, M. W.; Valentine, M.; Hendrickson, D. N. *J. Am. Chem. Soc.* **1982**, *104*, 6982.

Chapter 6

Synthesis, Structures, and Physicochemical Properties of Diruthenium Complexes of Tetrachlorocatecholate with $Ru^{3+}(\mu\text{-}OR)_2Ru^{3+}$ and $Ru^{3.5+}(\mu\text{-}OR)_2Ru^{3.5+}$ Cores (R = CH_3 and C_2H_5)

Abstract

Metal-metal bonded $Ru^{3+}(\mu\text{-}OR)_2Ru^{3+}$ (R = CH_3 and CH_3CH_2) and $Ru^{3.5+}(\mu\text{-}OR)Ru^{3.5+}$ complexes with tetrachlorocatecholate (Cl_4Cat) have been synthesized in the corresponding alcohol, MeOH and EtOH, from an unsupported complex, $Na_3[Ru_2(Cl_4Cat)_4(THF)]\cdot 3H_2O\cdot 7THF$ (**1**).

$[Ph_4P]_2[Ru_2(Cl_4Cat)_4(\mu\text{-}OMe)_2Na_2(MeOH)_6]$ (**2**)
$[Na(dibenzo\text{-}18\text{-}crown\text{-}6)(H_2O)(MeOH)]_2[Ru_2(Cl_4Cat)_4(\mu\text{-}OMe)_2Na_2(MeOH)_6]$ (**3**)
$[Na(benzo\text{-}15\text{-}crown\text{-}5)_2][Ru_2(Cl_4Cat)_4(\mu\text{-}OMe)_2Na_2(MeOH)_6]$ (**4**)
$[Na(benzo\text{-}15\text{-}crown\text{-}5)(H_2O)][Ru_2(Cl_4Cat)_4(\mu\text{-}OMe)_2Na_2(EtOH)_2(H_2O)_2(MeOH)_2]$ ·(benzo-15-crown-5) (**5**)
$(Ph_4P)_2[Ru_2(Cl_4Cat)_4(\mu\text{-}OEt)_2Na_2(EtOH)_2(H_2O)_2]$ (**6**)
$(Ph_4P)[Ru_2(Cl_4Cat)_4(\mu\text{-}OEt)_2Na_2(EtOH)_6]$ (**7**)

In the alcohol solvent, both $Ru^{3+}(\mu\text{-}OR)_2Ru^{3+}$ and $Ru^{3.5+}(\mu\text{-}OR)_2Ru^{3.5+}$ species are in equilibrium, and an addition of a counter cation gives rise to selective isolation as a stable species. Ph_4PCl and dibenzo-18-crown-6-ether afford homovalent species, **2** and **3**, respectively, while benzo-15-crown-5-ether provides a mixed-valent species, **4**. Furthermore, the air-oxidation of **1** in MeOH/EtOH (1 : 1 v/v) containing benzo-15-crown-5-ether provides a complex **5**. Similarly a $Ru^{3.5+}(\mu\text{-}OEt)_2Ru^{3.5+}$ species **7** forms in EtOH and a selective formation of a $Ru^{3+}(\mu\text{-}OEt)_2Ru^{3+}$ species **6** is found in the presence of pyrazine or 2,5-dimethylpyrazine.

The crystal structures of these complexes, except for **2** and **7**, have been determined by X-ray crystallography, and the spectroscopic and magnetic measurements have been carried out. The longer Ru–Ru bonds are found in the $Ru^{3+}(\mu\text{-}OR)_2Ru^{3+}$ species (2.606(1) and 2.628(2) Å for **3** and **6**, respectively) compare with those of 2.5260(6) Å and 2.514(2) Å for $Ru^{3.5+}(\mu$-

$OMe)_2Ru^{3.5+}$ species, **4** and **5**, respectively. These structural features, magnetic data, and ESR spectra show electronic configuration of $\sigma^2\pi^2\delta^{*2}\delta^2\pi^{*2}$ and $\sigma^2\pi^2\delta^{*2}\delta^2\pi^{*1}$ for $Ru^{3+}(\mu\text{-}OR)_2Ru^{3+}$ and $Ru^{3.5+}(\mu\text{-}OR)_2Ru^{3.5+}$, respectively. The cyclic voltammetry in DMF affords characteristic two reversible and two quasi-reversible redox waves; the electrochemical features of the $Ru^{3+}(\mu\text{-}OR)_2Ru^{3+}$ (**2**, **3**, and **6**) and the $Ru^{3.5+}(\mu\text{-}OR)_2Ru^{3.5+}$ (**4** and **7**) species are similar to each other, indicating that all the species are electrochemically stable.

Complex **5** forms a one-dimensional chain by hydrogen bonds between the waters and free crown-ether oxygen atoms ($O(H_2O)\cdots O(ether)$ = 2.91–3.04 Å). The isolation of

$[Ph_4P][Ru(Cl_4Cat)_2(L)_2]^-$ (L = pyrazine; **8**)
$[Ph_4P][Ru(Cl_4Cat)_2(L)_2]^-$ (L = 2,5-dimethylpyrazine; **9**)

revealed the selective isolation of **6** from solution containing pyrazine, where **8** or **9** is a main species in such solution and these are in equilibrium with the $Ru^{3+}(\mu\text{-}OEt)_2Ru^{3+}$ species. UV-Vis spectral variation by ethanolysis demonstrated the selective conversion from complex **9** to the $Ru^{3+}(\mu\text{-}OEt)_2Ru^{3+}$ species without an oxidation to the $Ru^{3.5+}(\mu\text{-}OEt)_2Ru^{3.5+}$ species.

Introduction

Dinuclear ruthenium complexes with oxo- (μ-O)[1] hydroxo- (μ-OH),[2] and alkoxo- (μ-OR) bridges[3] are of substantial interest in understanding the redox chemistry of polynuclear ruthenium cores because of not only the variety of geometric and electronic structures but also the catalytic reactivity for oxidation of water and organic substrates. A series of mono-oxo-bridged diruthenium complexes (A) with 2,2'-bipyridine (bpy) have been synthesized and their catalytic mechanism for the oxidation of water has been studied.[1(a)-(c),4] Regarding di-μ-oxo (B) and di-hydroxo (C) diruthenium cores, several instances have been obtained by using the anionic tripod ligand, $[\eta^5\text{-}C_5H_5)Co\{(CH_3O)_2P{=}O\}_3]^-$, where the homovalent $Ru^{3+}(\mu\text{-}OH)_2Ru^{3+}$ species of type (C) to $Ru^{4+}(\mu\text{-}O)_2Ru^{4+}$ and $Ru^{5+}(\mu\text{-}O)_2Ru^{5+}$ of type (B) were structurally characterized.[1(b),2]

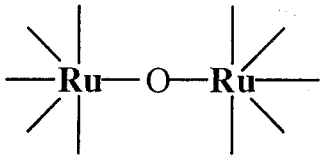

(A)

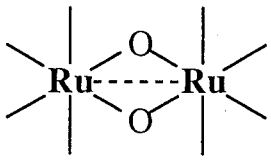

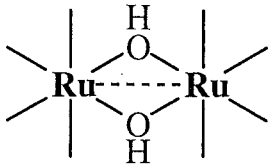

(B) **(C)**

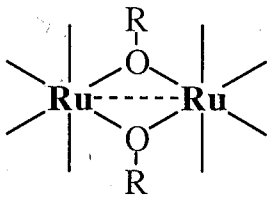

(D)

The isolation and characterization of each oxidation state in successive redox steps are necessary to understand and expand the diruthenium chemistry. However, forms of type (B) and (C) tend to change between themselves depending on the solution conditions such as pH and oxidation states of ruthenium ions, making the $Ru(\mu\text{-}O)_2Ru$ core chemistry complicated. In this context, the main focus is made on a type (D). Up to date only one sort of $Ru^{2+}(\mu\text{-}OR)_2Ru^{2+}$ complex (R = CH_3 and CH_3CH_2) has been reported.[3] Recently, unsupported diruthenium complex with tetrachlorocatecholate (Cl_4Cat), $Na_3[Ru_2(Cl_4Cat)_4(THF)]\cdot 3H_2O\cdot 7THF$ (**1**), and its one-electron oxidized complex, $Na_2[Ru_2(Cl_4Cat)_4(THF)_2]\cdot 3H_2O\cdot 3THF$ have synthesized by our group.[5] In this Chapter, the synthesis of a series of type (D) cores from complex **1** will be presented.

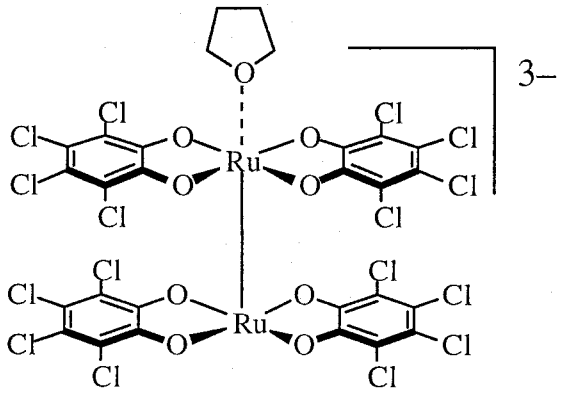

1

The oxidation products of **1** in MeOH and EtOH can be obtained by the use of sodium-crown ether complex and phosphonium cations as corresponding $Ru^{3+}(\mu\text{-}OR)_2Ru^{3+}$ and $Ru^{3.5+}(\mu\text{-}OR)_2Ru^{3.5+}$ complexes; $Ru^{3+}(\mu\text{-}OMe)_2Ru^{3+}$ species, $[A]_2[Ru_2(Cl_4Cat)_4(\mu\text{-}OMe)_2Na_2(MeOH)_6]$ ($[A]^+ = Ph_4P^+$; (**2**), $[Na(dibenzo\text{-}18\text{-}crown\text{-}6)(H_2O)(MeOH)]^+$; (**3**)), $Ru^{3.5+}(\mu\text{-}OMe)_2Ru^{3.5+}$ species, $[Na(benzo\text{-}15\text{-}crown\text{-}5)_2][Ru_2(Cl_4Cat)_4(\mu\text{-}OMe)_2Na_2(MeOH)_6]$ (**4**) and $[Na(benzo\text{-}15\text{-}crown\text{-}5)(H_2O)][Ru_2(Cl_4Cat)_4(\mu\text{-}OMe)_2Na_2(EtOH)_2(H_2O)_2(MeOH)_2]$ ·(benzo-15-crown-5) (**5**), $Ru^{3+}(\mu\text{-}OEt)_2Ru^{3+}$ species, $(Ph_4P)_2[Ru_2(Cl_4Cat)_4(\mu\text{-}$

$OEt)_2Na_2(EtOH)_2(H_2O)_2]$ (**6**) and $Ru^{3.5+}(\mu\text{-}OEt)_2Ru^{3.5+}$ species, $(Ph_4P)[Ru_2(Cl_4Cat)_4(\mu\text{-}OEt)_2Na_2(EtOH)_6]$ (**7**). This Chapter describes their synthetic reaction, structural characterization, and physico-chemical properties together with the characterization of the mononuclear ruthenium complexes, $(Ph_4P)[trans\text{-}Ru(Cl_4Cat)_2(L)_2]$ (L = pyrazine; **8**, 2,5-dimethylpyrazine; **9**).

Experimental Section

Materials.

All chemicals used for the synthesis were reagent grade. The solvents, MeOH, acetonitrile, and DMF, for the spectroscopic measurements were purified by a distillation under a dry nitrogen atmosphere. $Na_3[Ru_2(Cl_4Cat)_4(THF)]\cdot 3H_2O\cdot 7THF$ (**1**) was synthesized by the literature method.[5] All the synthesis was carried out under the atmosphere.

Preparation of the Complexes.

$[Ph_4P]_2[Ru_2(Cl_4Cat)_4(\mu\text{-}OMe)_2Na_2(MeOH)_6]$ (2) Complex **2** can be synthesized by the following two manors; (A): A MeOH solution (40 ml) of **1** (200 mg, 0.140 mmol) was stirred for an hour, then the violet solution changed to the dark blue one. After stirring a solid of Ph_4PCl (160 mg, 0.43 mmol) was added, and the solution was stirred further for five minutes and filtered. The filtrate was stand in air for two–three days to form dark brown prismatic crystals of **2**. They were collected by suction filtration, washed with a minimum amount of 2-propanol and dried in vacuo. (B): A MeOH solution (40 ml) of **1** (200 mg, 0.140 mmol) was stirred for half an hour and then added a solid of Ph_4PCl (160 mg, 0.430 mmol). The solution was filtered to remove an insoluble solid and the filtrate was stirred for two hours. During this time, the brown microcrystals precipitated from dark blue solution. They were collected by suction filtration, washed with a minimum amount of 2-propanol and dried in vacuo. Found: C, 44.32; H, 3.07. $C_{80}H_{70}C_{116}Na_2O_{16}P_2Ru_2$ requires C, 44.38; H, 3.26. λ_{max} (ε/$M^{-1}\cdot cm^{-1}$) in acetonitrile: 474 (10300) nm. IR (KBr): ν(C–O), 1258 and ν(C=C), 1436 cm^{-1}. Diamagnetic.

$[Na(dibenzo\text{-}18\text{-}crown\text{-}6)(H_2O)(MeOH)]_2[Ru_2(Cl_4Cat)_4(\mu\text{-}OMe)_2Na_2(MeOH)_6]$ (3)

Complex **3** can be synthesized by the following two manors. The single-crystal for X-ray crystallographic analysis was prepared by the method A; (A): A MeOH solution (40 ml) of **1** (200 mg, 0.140 mmol) was stirred for an hour, where the violet solution changed to the dark blue one. After stirring a solid of dibenzo-18-crown-6-ether (180 mg, 0.500 mmol) was added, and the solution was stirred further for ten minutes. In this time, an excess amount of dibenzo-18-crown-6-ether remained as a white solid in solution. The mixture was filtered to

remove an excess of dibenzo-18-crown-6-ether and the filtrate was allowed to stand for two–three days to form brown prismatic crystals of **3**. This single crystal was suitable for X-ray crystallographic analysis. (B): A MeOH solution (40 ml) of **1** (200 mg, 0.140 mmol) was stirred under air for half an hour and then added a solid of dibenzo-18-crown-6-ether (160 mg, 0.440 mmol). After stirring for ten minutes, the solution was filtered to remove an insoluble solid (free dibenzo-18-crown-6-ether) and the filtration was stirred for two hours. During this time, the bright brown microcrystals precipitated from dark blue solution. They were collected by suction filtration, washed with a minimum amount of 2-propanol and dried in vacuo. Found: C, 37.46; H, 3.13. $C_{74}H_{90}Cl_{16}Na_4O_{32}Ru_2$ requires C, 37.77; H, 3.86. λ_{max} (ε/$M^{-1}\cdot cm^{-1}$) in acetonitrile: 470 (12600) nm. IR (KBr): ν(C–O), 1254 and ν(C=C), 1435 cm^{-1}. Diamagnetic.

[Na(benzo-15-crown-5)$_2$][Ru$_2$(Cl$_4$Cat)$_4$(μ-OMe)$_2$Na$_2$(MeOH)$_6$] (4) A MeOH solution (40 ml) of **1** (200 mg, 0.140 mmol) was stirred for an hour. After stirring a solid of benzo-15-crown-5-ether (120 mg, 0.450 mmol) was added, and the solution was stirred further for five minutes and then filtered. The filtrate was stand in air for two–three days to form dark blue prismatic crystals of **4**. This single crystal was suitable for X-ray crystallographic analysis. They were collected by suction filtration, washed with a minimum amount of 2-propanol and dried in vacuo. Found: C, 34.62; H, 2.75. $C_{60}H_{70}C_{116}Na_3O_{26}Ru_2$ requires C, 35.23; H, 3.45. λ_{max} (ε/$M^{-1}\cdot cm^{-1}$) in acetonitrile: 575 (12800), 765 (sh, 6900), 1450 (2500) nm. IR (KBr): ν(C–O), 1255 and ν(C=C), 1422 cm^{-1}. μ_{eff}: 1.71 (1.9 K) and 2.04 μB (300 K).

[Na(benzo-15-crown-5)(H$_2$O)][Ru$_2$(Cl$_4$Cat)$_2$(μ-OMe)$_2$Na$_2$(EtOH)$_2$(H$_2$O)$_2$(MeOH)$_2$]·(benzo-15-crown-5) (5) A MeOH solution (30 ml) of **1** (200 mg, 0.140 mmol) was stirred for an hour. After stirring a solid of benzo-15-crown-5-ether (150 mg, 0.560 mmol) was added, and the solution was stirred further for five min. To this MeOH solution was added EtOH of 30 ml and then filtered. The filtrate was stand for two–three days to form dark blue prismatic crystals of **5**. This single crystal was suitable for X-ray crystallographic

analysis. They were collected by suction filtration, washed with a minimum amount of 2-propanol and dried in vacuo. Found: C, 35.31; H, 3.62. $C_{60}H_{72}Cl_{16}Na_3O_{27}Ru_2$ requires C, 34.92; H, 3.52. IR (KBr): ν(C–O), 1255 and ν(C=C), 1423 cm^{-1}. μ_{eff}: 1.75 (1.9 K) and 2.02 (300 K) μB.

$(Ph_4P)_2[Ru_2(Cl_4Cat)_4(\mu\text{-}OEt)_2Na_2(EtOH)_2(H_2O)_2]$ (6) A EtOH solution (30 ml) of **1** (200 mg, 0.140 mmol) was stirred for an hour. Then, an excess amount of pyrazine on solid (50 mg, 0.62 mmol) was added into this solution. The solution changed to the greenish blue, and this solution was stirred for an hour. A solid of Ph_4PCl (160 mg, 0.430 mmol) was added, and the solution was stirred further for five minutes and then filtered. The filtrate was stand for two–three days to form dark blue prismatic crystals of **6**. This single crystal was suitable for X-ray crystallographic analysis. They were collected by suction filtration, washed with a minimum amount of 2-propanol and dried in vacuo. The use of 2,5-dimethylpyrazine (70 mg, 0.65 mmol) instead of pyrazine also afforded a crystalline sample of **6**. Found: C, 44.03; H, 3.21. $C_{80}H_{70}Cl_{16}Na_2O_{16}P_2Ru_2$ requires C, 44.38; H, 3.26. λ_{max} (ε/$M^{-1}\cdot cm^{-1}$) in acetonitrile: 472 (12500) nm. IR (KBr): ν(C–O), 1257 and ν(C=C), 1435 cm^{-1}. Diamagnetic.

$(Ph_4P)[Ru_2(Cl_4Cat)_4(\mu\text{-}OEt)_2Na_2(EtOH)_6]$ (7) A EtOH solution (30 ml) of **1** (200 mg, 0.140 mmol) was stirred for an hour. Ph_4PCl (160 mg, 0.430 mmol) was added, and the solution was stirred further for five minutes and then filtered. The filtrate was stand for two–three days to form dark blue prismatic crystals of **7**. They were collected by suction filtration, washed with a minimum amount of 2-propanol and dried in vacuo. Found: C, 40.39; H, 3.14. $C_{64}H_{66}Cl_{16}Na_2O_{16}P_1Ru_2$ requires C, 39.67; H, 3.43. λ_{max} (ε/$M^{-1}\cdot cm^{-1}$) in acetonitrile: 575 (10500), 765 (sh, ~6000), 1400 (sh, ~2000) nm. IR (KBr): ν(C–O), 1255 and ν(C=C), 1422 cm^{-1}. μ_{eff}: 1.30 (1.9 K) and 1.72 (300 K) μB.

$[Ph_4P][Ru(Cl_4Cat)_2(pyrazine)_2]$ (8) A MeOH solution (30 ml) of **1** (200 mg, 0.140 mmol) was stirred for half an hour. Excess of pyrazine (150 mg, 1.86 mmol) was added into

this solution, and this mixture was stirred further for 1 hour. Then, a solid of Ph_4PCl (160 mg, 0.430 mmol) was added, and the solution was stirred further for five minutes. The solution was filtered and the filtrate was stand for two–three days to form dark blue prismatic crystals of **8**. This single crystal was suitable for X-ray crystallographic analysis. They were collected by filtration, washed with a minimum amount of 2-propanol and dried in vacuo. This sample does not dissolve in dichloromethane, benzene, toluene, so spectroscopic and electrochemical studies in solution could not be measured (in coordination solvents such as DMF, acetonitrile, THF, the fundamental structure of **8** does not maintain because of the replacement of axial ligand). λ_{max} (ε/$M^{-1}\cdot cm^{-1}$) in EtOH solution of **1** under air containing an excess pyrazine: 390 (sh, 9500), 480 (8700), 775 (14000) nm. IR (KBr): ν(C–O), 1258 and ν(C=C), 1434 cm^{-1}.

$[Ph_4P][Ru(Cl_4Cat)_2(2,5\text{-dimethylpyrazine})_2]$ (9) This complex was prepared in the same manner as **8**, except that 2,5-dimethylpyrazine (200 mg, 1.85 mmol) was used instead of pyrazine. This sample dissolves slightly in dichloromethane. UV-Vis (λ_{max}/nm in dichloromethane): 390, 470, 780. λ_{max} (ε/$M^{-1}\cdot cm^{-1}$) in EtOH solution of **1** under air containing an excess 2,5-dimethylpyrazine: 390 (sh, 9500), 480 (8700), 775 (14000) nm. IR (KBr): ν(C–O), 1257, ν(C=C), 1436 cm^{-1}.

Physical Measurements.

Infrared spectra were measured on KBr disks with Perkinelmer System 2000 FT-IR spectrophotometer. UV-Vis-near-IR spectra were recorded with Hewlettpackard 8452A Diode array spectrophotometer and Hitachi U-3500 spectrophotometer. General magnetic susceptibility data were measured over the temperature range from 2.0 to 300 K using an MPMS5 SQUID susceptometer (Quantum Design, Inc.) interfaced with an HP Vectra computer system, where the applied magnetic fields were 1 T. The samples for magnetic measurements were ground to powder in order to avoid an effect of the anisotropy from crystal orientation. Corrections were applied for diamagnetism using Pascal's constants[6] and for aluminum foil and vinyl capsule wrapping samples. Effective magnetic moments were calculated by the equation

$\mu_{eff} = 2.828\chi_M T/2$, where χ_M is the magnetic susceptibility per formula unit. Cyclic voltammograms were recorded in DMF (0.1 M tetrabuthylammonium perchlorate $(NBu_4)ClO_4$ as a supporting electrolyte) under a nitrogen atmosphere with BAS 100B/W(CV-50W). At the beginning of measurements, CVs of DMF and dichloromethane containing only supporting electrolyte were measured. To this solution were added the complexes (1 mM for **2–4**, **6** and **7**, 0.1 mM for **9**) and measured with a unit of carbon working-electrode, Pt counter-electrode, and Ag/AgCl reference electrode.

X-ray Data Collection, Reduction, and Structure Determination.

Single crystals of **3–6**, **8**, and **9** were prepared by the each method described in the synthetic procedure. Each single crystal for the crystallographic analysis was cut from thin plate crystal and mounted on a glass rod. All the measurements were made on a Rigaku mercury CCD diffractometer with graphite monochromated Mo Kα radiation ($\lambda = 0.71069$ Å). The data were collected at a temperature of 173 ± 1 K. Empirical absorption correction using the program REQABA[7] was performed for all the data. The structures were solved by direct methods[8] and expanded using Fourier techniques.[9] Except for complex **5**, the non-hydrogen atoms were refined anisotropically, while hydrogen atoms were refined isotropically. The refinement of all atoms for **5** was done with isotropically because of luck of the reflections. Full-matrix least-squares refinements were based on the observed reflections 4226 (**3**), 14345 (**4**), 4248 (**5**), 3899 (**6**), 8458 (**8**), and 3727 (**9**) ($I > 3.00\sigma(I)$, except ($I > 2.00\sigma(I)$) for **5**), where the unweighted and weighted agreement factors of $R = \Sigma||Fo|-|Fc||/\Sigma|Fo|$ and $R_w = [\Sigma w(|Fo|-|Fc|)_2/\Sigma w|Fo|^2]^{1/2}$ were used. The weighting scheme was based on counting statistics. Plots of $\Sigma w(|Fo|-|Fc|)^2$ versus $|Fo|$, reflection order in data collection, $\sin\theta/\lambda$ and various classes of indices showed no unusual trends. Neutral atomic scattering factors were taken from Cromer and Waber.[10] Anomalous dispersion effects were included in F_{calcd}; the values $\Delta f'$ and $\Delta f''$ were those of Creagh and McAuley.[11] The values for the mass attenuation coefficients are those of Creagh and Hubbel.[12] All calculations were performed using the teXsan crystallographic

software package of Molecular Structure Corporation.[13] Although X-ray crystallographic analyses were performed at low temperature, the fragility of the crystals and the existence of disordering made it difficult to improve the quality of the X-ray crystallographic analysis for **4** and **6**. For complex **5**, luck of the reflections and isotropical refinement made it difficult to improve the quality of the X-ray crystallographic analysis. The crystal data and details of the structure determinations for **3-6** and **8** and **9** are summarized in Table 1.

Table 1. Crystallographic and Refinement Data for **3-6**

	3	**4**	**5**	**6**
Formula	$C_{74}H_{90}O_{32}Cl_{16}$	$C_{61}H_{74}O_{27}Cl_{16}$	$C_{60}H_{72}O_{27}Cl_{16}$	$C_{80}H_{70}O_{16}Cl_{16}$
	Ru_2Na_4	Ru_2Na_3	Ru_2Na_3	$Ru_2P_2Na_2$
Formula weight	2350.84	2077.60	2063.57	2164.74
Color	brown	dark blue	blue	dark blue
Crystal system	monoclinic	triclinic	orthorhombic	monoclinic
Space group	*C2/m*	$P\bar{1}$	$Cmc2_1$	*P21/n*
a, Å	19.511(3)	12.657(1)	21.6069(3)	12.9343(8)
b, Å	18.803(2)	16.5820(5)	15.769(1)	26.275(2)
c, Å	14.1254(3)	20.887(2)	24.4792(4)	15.3341(5)
α, deg		76.303(2)		
β, deg	111.0893(5)	87.1994(8)		114.004(1)
γ, deg		80.4219(7)		
Z	2	2	4	2
V, Å^3	4835.1(8)	4199.3(5)	8340.7(7)	4760.6(4)
ρ, g/cm^3	1.615	1.643	1.643	1.510
μ, cm^{-1}	8.49	9.56	9.63	8.67
T, K	173 ± 1	173 ± 1	173 ± 1	173 ± 1
λ (Mo Kα), Å	0.71069	0.71069	0.71069	0.71069
No. observations	4226	14345	4248[a]	3899
No. parameters	303	982	230	532
Refls./para ratio	13.9	14.6	18.5	7.33
GOF	0.95	1.64	2.09	1.27
R, R_w[b]	0.045, 0.083	0.061, 0.087	0.098, 0.103	0.088, 0.110

[a] $I > 2.00\sigma(I)$. [b] $R = \Sigma||F_0|-|F_0||/\Sigma|F_0|$, $R_w = [\Sigma(|F_0|-|F_0|)^2/\Sigma w|F_0|^2)]^{1/2}$.

Table 1 (continue). Crystallographic and Refinement Data for **8** and **9**

	8	**9**
Formula	$C_{46}H_{32}N_4O_6Cl_8$	$C_{50}H_{44}N_4O_6Cl_8$
Formula weight	1152.45	1212.59
Color	dark blue	dark blue
Crystal system	monoclinic	monoclinic
Space group	*P*21/*c*	*P*21/*n*
a, Å	13.529(1)	17.874(2)
b, Å	12.0061(9)	13.565(1)
c, Å	30.1766(5)	21.841(1)
α, deg		
β, deg	100.7506(4)	97.663(2)
γ, deg		
Z	4	4
V, Å^3	4815.5(5)	5248.5(8)
ρ, g/cm^3	1.589	1.534
μ, cm^{-1}	8.55	7.88
T, K	173 ± 1	173 ± 1
λ (Mo Kα), Å	0.71069	0.71069
No. reflections	8458	3727
No. parameters	598	634
Refls./para ratio	14.1	5.88
GOF	1.24	1.32
R, R_w[a]	0.047, 0.069	0.075, 0.074

[a] $R = \Sigma||F_0|-|F_0||/\Sigma|F_0|$, $R_w = [\Sigma(|F_0|-|F_0|)^2/\Sigma w|F_0|^2)]^{1/2}$.

Results and Discussion

Synthesis and Isolation.

The air-oxidation reaction of **1** in alcohols affords corresponding $Ru^{3+}(\mu\text{-}OR)_2Ru^{3+}$ and $Ru^{3.5+}(\mu\text{-}OR)_2Ru^{3.5+}$ species by the alcoholysis. Many of them were isolated as crystalline forms with the aid of counter cations. The equilibrium between the $Ru^{3+}(\mu\text{-}OMe)_2Ru^{3+}$ and $Ru^{3.5+}(\mu\text{-}OMe)_2Ru^{3.5+}$ species is established in MeOH and either of those species, which is more stabilized by forming an ion pair with the characteristic counter cation, is isolated selectively as a crystalline solid. An addition of Ph_4PCl affords a $Ru^{3+}(\mu\text{-}OMe)_2Ru^{3+}$ species, **2**, in which two Ph_4P^+ cations are involved. Sodium-crown-ether complexes sometimes become a good counter cation for anionic assembly complexes, so the selective isolation of each species by using several crown-ether molecules was studied ; an addition of dibenzo-18-crown-6-ether affords a $Ru^{3+}(\mu\text{-}OMe)_2Ru^{3+}$ species of **3**, which contains [Na(dibenzo-18-crown-6)(H_2O)(Me-

Scheme 1

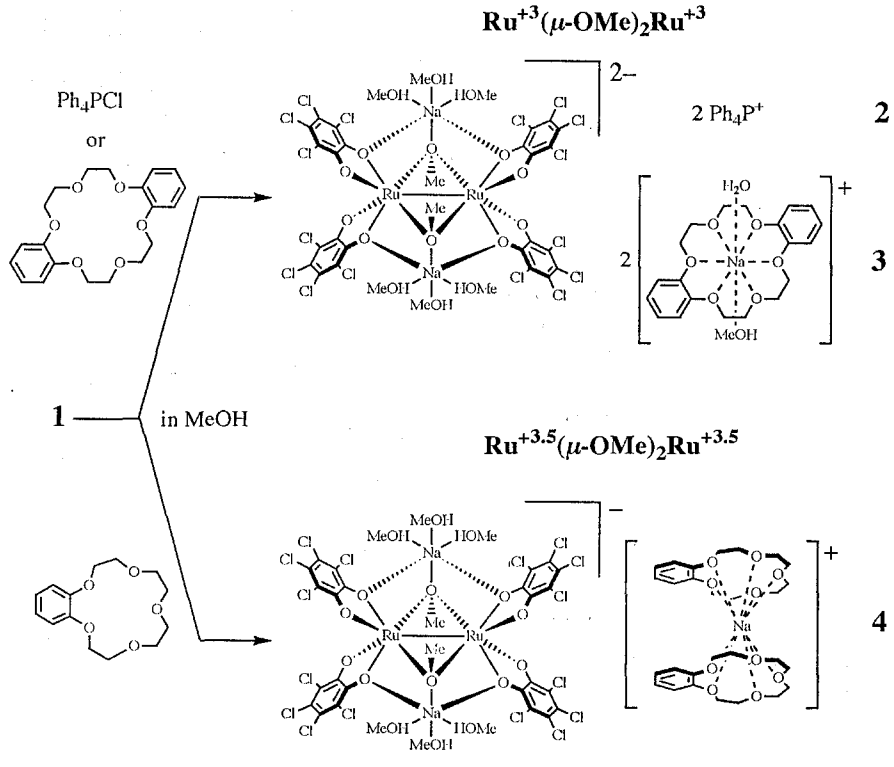

Scheme 2

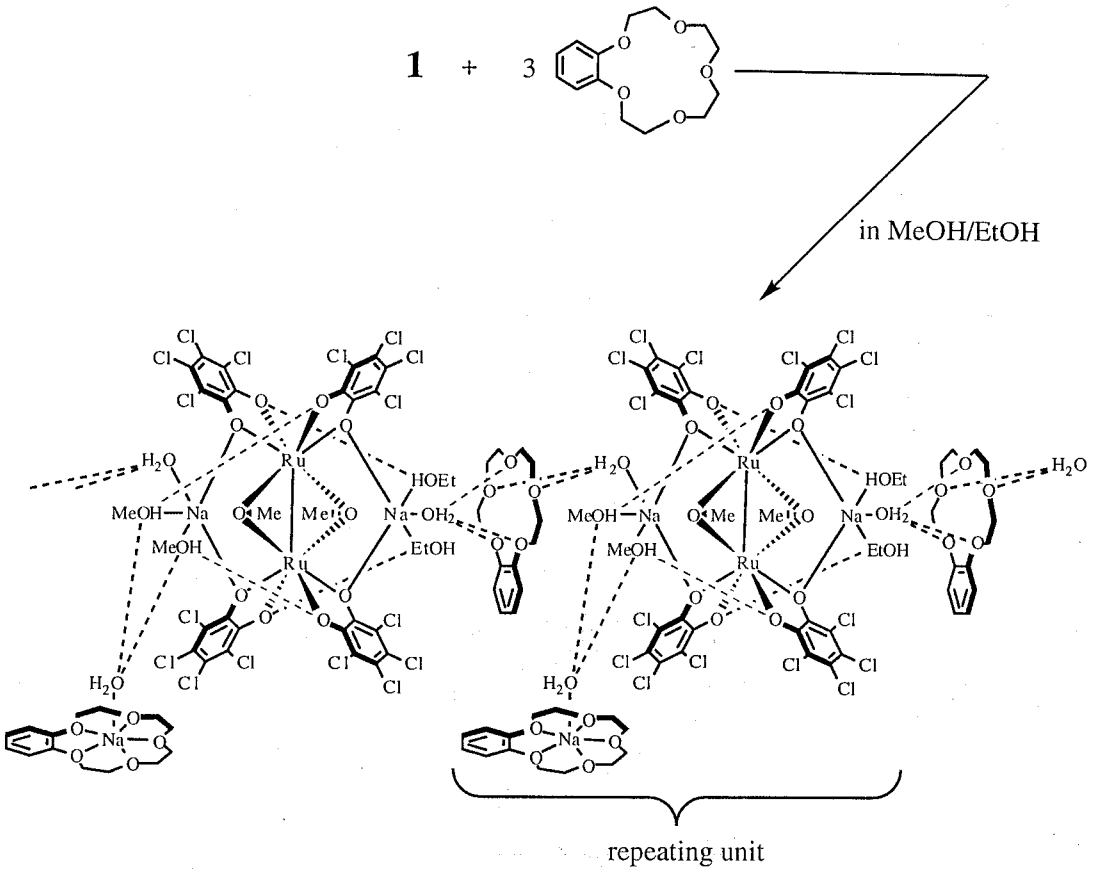

5

-OH)]$^+$ counter cation. The choice of benzo-15-crown-5-ether affords a $Ru^{3.5+}(\mu\text{-}OMe)_2Ru^{3.5+}$ species of **4** contains [Na(benzo-15-crown-5)$_2$]$^+$ counter cation (Scheme 1). In a mixed solution of MeOH/EtOH a $Ru^{3.5+}(\mu\text{-}OMe)_2Ru^{3.5+}$ species, **5**, is obtained as a salt with [Na(benzo-15-crown-5)(H_2O)]$^+$ as well as **4** (Scheme 2). Remarkable structural aspect of **5** is that free benzo-15-crown-5-ether molecule is contained in crystal unit, which forms a 1-D hydrogen bonded chain with $Ru^{3.5+}(\mu\text{-}OMe)_2Ru^{3.5+}$ moieties (see structural description).

On the other hand, in EtOH, an addition of Ph_4PCl affords a $Ru^{3.5+}(\mu\text{-}OEt)_2Ru^{3.5+}$ species, **7**, as a salt of with Ph_4P^+ cation. The selective isolation of the $Ru^{3+}(\mu\text{-}OMe)_2Ru^{3+}$ species of **6** is successful when pyrazine or 2,5-dimethylpyrazine (more than 2 equiv. per Ru) exists in the solution (Scheme 3).

Scheme 3

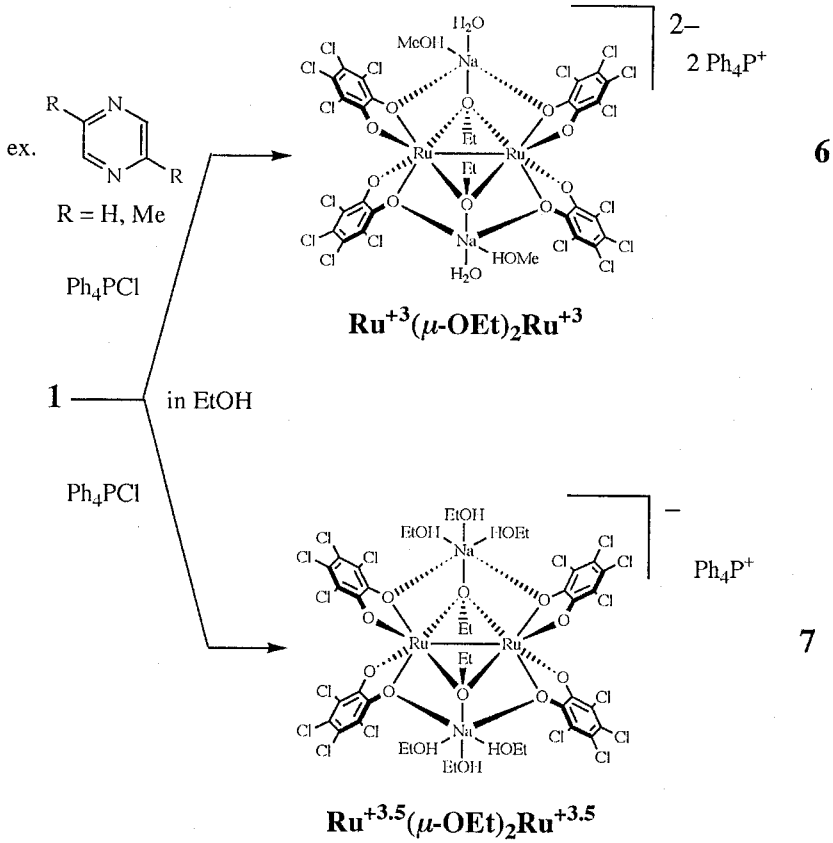

Crystal Structure of the Complexes.

Complex 3 An ORTEP drawing of the anionic moiety of **3** is depicted in Figure 1(a). Selected bond distances and angles are listed in Table 2. The formulated molecule consists of an anionic cluster and two Na^+-dibenzo-18-crown-6-ether cations. Complex shows two molecules in a unit cell, and the anionic moieties having a *C*2 axis through the Ru–Ru bond and a mirror plane lying on the OMe ligands, sodium ions, and two MeOH molecules coordinated to Na(1). The anionic moiety consists of two ruthenium ions bridged by two OMe ligands and two sodium ions, forming a Na_2Ru_2 cluster core. Each ruthenium ion has distorted octahedral coordination geometry, where two $Cl_4C_6O_2$ ligands and two OMe ligands coordinate to each ruthenium ion in a *cis*-fashion. All the $Cl_4C_6O_2$ ligands exhibit a catecholate form with an average C–O distance of 1.3285 Å. The $Ru–O_{Cl4Cat}$ bond distance is split into two groups, with a value of 2.016(4) Å for the bonds *trans* to the OMe ligands and 2.066(3) Å for the *trans* to other Cl_4Cat ligands. This trend is also found in complexes **4–6** where the former Ru–O bond distances are shorter by 0.024-0.05 Å than those of latter. For the OMe ligands, the

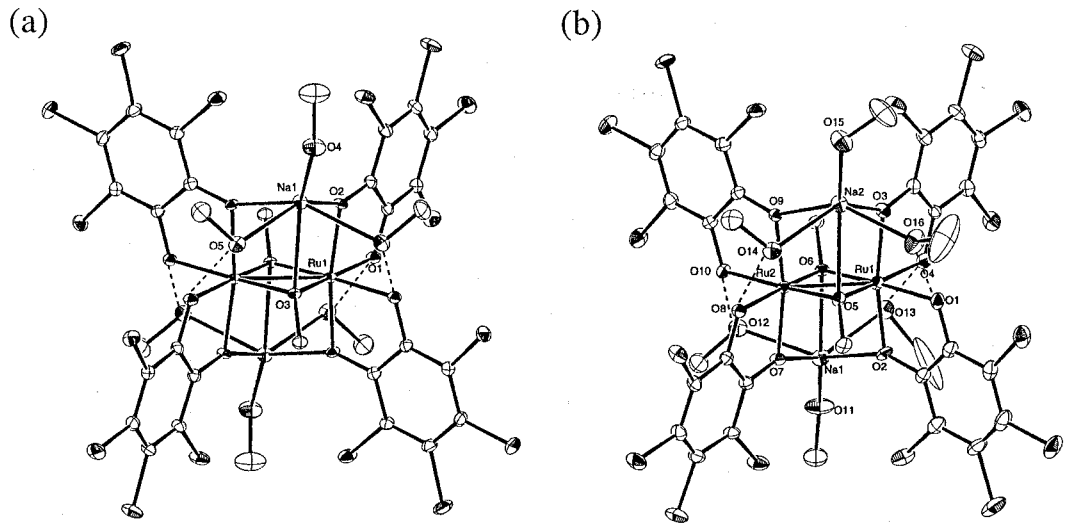

Figure 1. ORTEP drawings of anionic moieties of complexes (a) **3** and (b) **4**. The dashed lines denote hydrogen bonds.

Table 2. Relevant Bond Distances (Å) and Angles (°) for complex **3** with the Estimated Standard Deviations in Parentheses

Ru(1)–O(1)	2.016(4)	Na(1)–O(2)	2.308(4)
Ru(1)–O(2)	2.066(3)	Na(1)–O(3)	2.586(6)
Ru(1)–O(3)	2.035(4)	Na(1)–O(4)	2.372(7)
Ru(1)–Ru(1)*	2.606(1)	Na(1)–O(5)	2.506(4)
O(1)–Ru(1)–O(1)**	87.8(2)	O(2)–Ru(1)–O(2)**	170.4(2)
O(1)–Ru(1)–O(2)	83.2(1)	O(2)–Ru(1)–O(3)	91.7(2)
O(1)–Ru(1)–O(2)**	89.9(1)	O(2)–Ru(1)–O(3)*	94.4(2)
O(1)–Ru(1)–O(3)	172.0(1)	O(3)–Ru(1)–O(3)*	100.4(2)
O(1)–Ru(1)–O(3)*	86.1(1)	Ru(1)–O(3)–Ru(1)*	79.6(2)
Hydrogen Bonds			
O(1)···O(5)	2.730(5)		

bond distance of Ru(1)–O(3) is 2.035(4) Å and the bond angles are found to be 79.6(2)° and 100.4(2)° for Ru(1)–O(3)–Ru(1') and O(3)–Ru(1)–O(3'), respectively. The Ru–Ru bond distance is 2.606(1) Å, which is compatible with that of **6** and $Ru^{3+}(\mu\text{-}OH)_2Ru^{3+}$ complexes reported previously,[2,14] while slightly longer than that of $Ru^{3.5+}(\mu\text{-}OMe)_2Ru^{3.5+}$ species, **4** and **5** (*vide infra*). Each sodium ion has O_6 coordination environment including two oxygen atoms of

catecholates, three oxygen atoms of MeOH molecules, and one oxygen atom of OMe ligand. The overall bridging feature is assumed with Na_2Ru_2-double cuboidal cluster (Figures 1(a) and 2(a)), where the Na–catecholate and Na–OMe bonds constitute a part of cuboidal skeleton with the bond distances of 2.308(4) and 2.586(6) Å for Na(1)–O(2) and Na(1)–O(3), respectively. Two of three MeOH molecules coordinating to each sodium ion form an intramolecular hydrogen bond with catecholate oxygen atoms(O(1)···O(5) is 2.730(5) Å).

Complex 4 ORTEP drawing of the anionic moiety of **4** is depicted in Figure 1(b). Selected bond distances and angles are given in Table 3. Complex crystallized in triclinic space group $P\bar{1}$, and two formulated molecules exist in a unit cell (Z = 2). The structural feature of an anionic moiety is similar to that of **3**, consisting of two ruthenium ions bridged by the two OMe ligands and two sodium ions, forming a Na_2Ru_2-double cuboidal cluster (Figure 2(b)). Two of the three MeOH molecules coordinating to each sodium ion form an intramolecular hydrogen bond with the oxygen atoms of $Cl_4C_6O_2$ ligands (O(1)···O(16) = 2.878(6) Å, O(4)···O(13) = 2.763(6) Å, O(8)···O(14) = 2.777(5) Å, O(10)···O(12) = 2.756 Å; dashed line in Figure 1b). The $Cl_4C_6O_2$ ligands are characteristic of catecholate with an average C–O distance of 1.343 Å. The $Ru–O_{Cl4Cat}$ distances shows two types of average bond distances, 2.000(4) Å for Ru(1)–O(1) and Ru(1)-O(4) bonds *trans* to the OMe ligands and 2.024(4) Å for Ru(1)–O(2) and Ru(1)–O(3) bonds *trans* to other Cl_4Cat ligands. The bridging part is constructed with the Ru–O bond distance of 2.017(3) , 2.024(4), 2.016(4), and 2.018(3) Å for Ru(1)–O(5), Ru(1)–O(6), Ru(2)–O(5), and Ru(2)–O(6), respectively, and the bond angles of 77.5(1)°, 77.4(1)°, 102.4(1), and 102.7(1)° for Ru(1)–O(5)–Ru(2), Ru(1)–O(6)–Ru(2), O(5)–Ru(1)–O(6), and O(5)–Ru(2)–O(6), respectively. The average $Ru–O_{alkoxo}$ distance of **4** is 2.019 Å shorter than 2.035 Å found for **3** (Δ = 0.016 Å). The cuboidal skeleton is constituted with the $Ru–O_{OMe}$, $Ru-O_{Cl4Cat}$, and $Na–O_{Cl4Cat}$ bonds with the bond distances of 2.398(4), 2.554(4), 2.377(4), 2.371(4), 2.689(4), and 2.401(4) Å for Na(1)–O(2), Na(1)–O(6), Na(1)–O(7), Na(2)–O(3), Na(2)–O(5), and Na(2)–O(9), respectively. The difference in the diruthenium cores between **3** and **4** occurs in the Ru–Ru bond; the bond distance of **4** is 2.5260(6) Å which is compatible with that of $Ru^{3.5+}(\mu\text{-}OH)_2Ru^{3.5+}$ complexes,[2] while is slightly shorter than that of **3** (Δ = 0.08 Å)

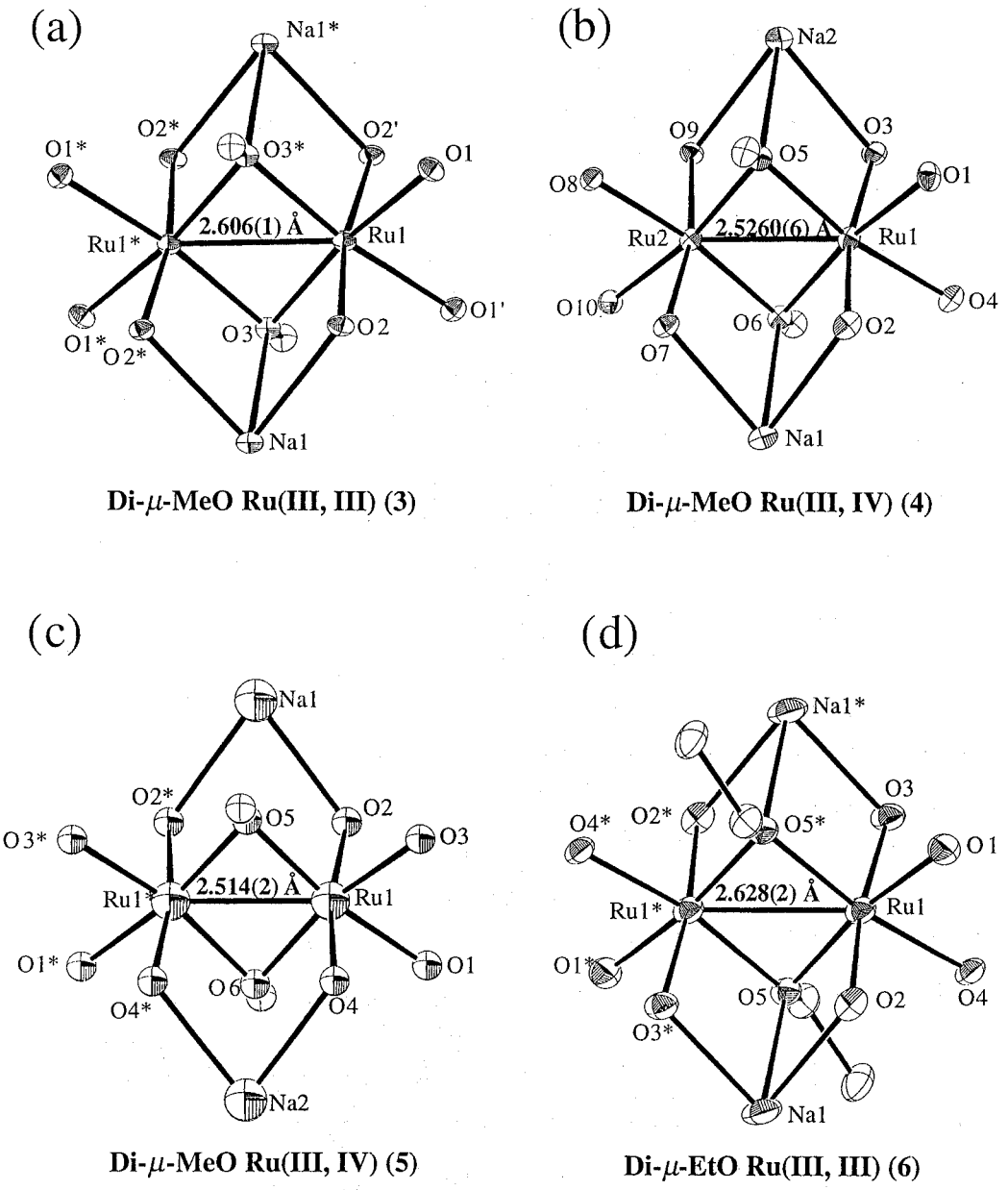

Figure 2. Coordination geometries of Na_2Ru_2 cluster cores in (a) **3**, (b) **4**, (c) **5**, and (d) **6**, where **3** and **6** are $Ru^{3+}(\mu\text{-OR})_2Ru^{3+}$ species and **4** and **5** are $Ru^{3.5+}(\mu\text{-OMe})_2Ru^{3.5+}$ species.

(Figure 2). The electronic configurations for $Ru^{3+}(\mu\text{-OR})_2Ru^{3+}$ and $Ru^{3.5+}(\mu\text{-OR})_2Ru^{3.5+}$ cores are interpreted to be $\sigma^2\pi^2\delta^{*2}\delta^2\pi^{*2}$ and $\sigma^2\pi^2\delta^{*2}\delta^2\pi^{*1}$, respectively. Similarly, the bond order of 1.0 ($\sigma^2\pi^2\delta^{*2}\delta^2\pi^{*2}$) and 1.5 ($\sigma^2\pi^2\delta^{*2}\delta^2\pi^{*1}$) could be assigned for **3** and **4**, respectively.

Table 3. Relevant Bond Distances (Å) and Angles (°) for complex **4** with the Estimated Standard Deviations in Parentheses

Ru(1)–O(1)	2.001(4)	Na(1)–O(2)	2.398(4)
Ru(1)–O(2)	2.028(3)	Na(1)–O(6)	2.554(4)
Ru(1)–O(3)	2.020(3)	Na(1)–O(7)	2.377(4)
Ru(1)–O(4)	1.999(3)	Na(1)–O(11)	2.338(5)
Ru(1)–O(5)	2.017(3)	Na(1)–O(12)	2.458(5)
Ru(1)–O(6)	2.024(4)	Na(1)–O(13)	2.536(4)
Ru(2)–O(5)	2.016(4)	Na(2)–O(3)	2.371(4)
Ru(2)–O(6)	2.018(3)	Na(2)–O(5)	2.689(4)
Ru(2)–O(7)	2.031(3)	Na(2)–O(9)	2.401(4)
Ru(2)–O(8)	1.998(3)	Na(2)–O(14)	2.531(4)
Ru(2)–O(9)	2.032(3)	Na(2)–O(15)	2.323(5)
Ru(2)–O(10)	1.990(4)	Na(2)–O(16)	2.358(5)
Ru(1)–Ru(2)	2.5260(6)		
O(1)–Ru(1)–O(2)	83.4(2)	O(5)–Ru(2)–O(6)	102.7(1)
O(1)–Ru(1)–O(3)	90.1(1)	O(5)–Ru(2)–O(7)	96.6(1)
O(1)–Ru(1)–O(4)	87.7(1)	O(5)–Ru(2)–O(8)	84.5(1)
O(1)–Ru(1)–O(5)	84.9(1)	O(5)–Ru(2)–O(9)	90.2(1)
O(1)–Ru(1)–O(6)	170.8(1)	O(5)–Ru(2)–O(10)	170.4(1)
O(2)–Ru(1)–O(3)	169.7(1)	O(6)–Ru(2)–O(7)	90.1(1)
O(2)–Ru(1)–O(4)	88.2(1)	O(6)–Ru(2)–O(8)	170.7(1)
O(2)–Ru(1)–O(5)	97.7(1)	O(6)–Ru(2)–O(9)	96.5(1)
O(2)–Ru(1)–O(6)	90.1(1)	O(6)–Ru(2)–O(10)	85.1(1)
O(3)–Ru(1)–O(4)	83.5(1)	O(7)–Ru(2)–O(8)	83.2(1)
O(3)–Ru(1)–O(5)	89.6(1)	O(7)–Ru(2)–O(9)	169.3(1)
O(3)–Ru(1)–O(6)	95.4(1)	O(7)–Ru(2)–O(10)	88.8(1)
O(4)–Ru(1)–O(5)	169.9(1)	O(8)–Ru(2)–O(9)	89.2(1)
O(4)–Ru(1)–O(6)	85.6(1)	O(8)–Ru(2)–O(10)	88.3(1)
O(5)–Ru(1)–O(6)	102.4(1)	O(9)–Ru(2)–O(10)	83.4(1)
		Ru(1)–O(5)–Ru(2)	77.5(1)
		Ru(1)–O(6)–Ru(2)	77.4(1)
	Hydrogen Bonds		
O(1)···O(16)	2.878(6)	O(4)···O(13)	2.763(6)
O(8)···O(14)	2.777(5)	O(10)···O(12)	2.756(5)

Complex 5 ORTEP drawing of the anionic moiety of **5** is depicted in Figure 3 with the atom numbering scheme. Selected bond distances and angles are given in Table 4. Complex **5** crystallized in orthorhombic space group *Cmc*21 with a *C*2 symmetrical axis through the Ru–Ru bond and a mirror symmetrical plane through the midpoint of Na_2Ru_2 cluster and crown-ether moieties (free molecule and Na-crown-ether cation) (Z = 4). The quinone ligands are typically catecholate type with an average C–O distance of 1.34 Å. The trend of $Ru–O_{Cl4Cat}$ distances found in complexes **3** and **4** is also observed; the shorter average bonds distance 2.00(1) Å for the bonds *trans* to the OMe ligands (Ru(1)–O(1) and Ru(1)–O(3)) and 2.03(1) Å for *trans* to other Cl_4Cat ligands (Ru(1)–O(2) and Ru(1)–O(4)). The cluster moiety consists of a ruthenium dinuclear trianion, $[(Cl_4Cat)_2Ru^{3.5+}(\mu\text{-}OMe)_2Ru^{3.5+}(Cl_4Cat)_2]^{3-}$, and two sodium cations, where one water and two MeOH or two EtOH molecules coordinate to the sodium ions. The oxygen atoms of OMe ligands do not coordinated to sodium ions, being μ_2-bridging mode dissimilar to μ_3-bridging mode in **3** and **4** (Figure 2(c)). The MeOH and EtOH molecules coordinated to the sodium ions show intramolecular hydrogen bond with catecholate oxygen

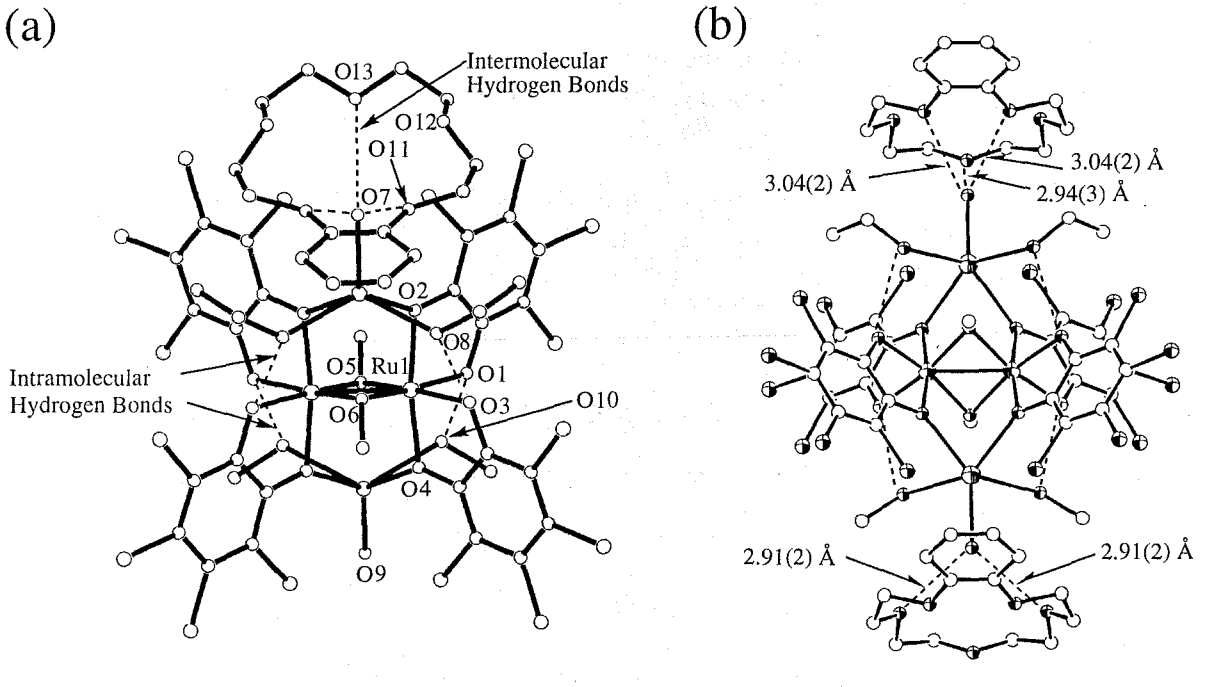

Figure 3 (a) Perspective view of Na_2Ru_2 mono-anionic cluster and free benzo-15-crown-5-ether molecule of **5**. (b) Hydrogen bonds between Na_2Ru_2 anionic cluster and free benzo-15-crown-5-ether molecules. The hydrogen bond distances are shown in the Figure.

Table 4. Relevant Bond Distances (Å), Hydrogen Bond Distances (Å), and Angles (°) for **5** with the Estimated Standard Deviations in Parentheses

Ru(1)–O(1)	2.00(1)	Na(1)–O(2)	2.42(1)
Ru(1)–O(2)	2.03(1)	Na(1)–O(7)	2.36(2)
Ru(1)–O(3)	1.99(1)	Na(1)–O(8)	2.43(1)
Ru(1)–O(4)	2.021(10)	Na(2)–O(4)	2.37(1)
Ru(1)–O(5)	2.00(1)	Na(2)–O(9)	2.31(2)
Ru(1)–O(6)	2.02(1)	Na(2)–O(10)	2.62(1)
Ru(1)–Ru(1)*	2.514(2)		
O(1)–Ru(1)–O(2)	83.6(4)	O(3)–Ru(1)–O(4)	83.2(4)
O(1)–Ru(1)–O(3)	85.5(4)	O(3)–Ru(1)–O(5)	87.1(4)
O(1)–Ru(1)–O(4)	89.6(4)	O(3)–Ru(1)–O(6)	169.0(4)
O(1)–Ru(1)–O(5)	170.4(4)	O(4)–Ru(1)–O(5)	95.7(5)
O(1)–Ru(1)–O(6)	85.4(4)	O(4)–Ru(1)–O(6)	90.5(5)
O(2)–Ru(1)–O(3)	90.3(4)	O(5)–Ru(1)–O(6)	102.5(3)
O(2)–Ru(1)–O(4)	171.0(4)	Ru(1)–O(5)–Ru(1)*	77.9(5)
O(2)–Ru(1)–O(5)	90.1(5)	Ru(1)–O(6)–Ru(1)*	77.0(6)
O(2)–Ru(1)–O(6)	94.9(5)		
	Intramolecular Hydrogen Bonds		
O(1)···O(10)	2.80(2)	O(3)···O(8)	2.84(2)
	Intermolecular Hydrogen Bonds		
O(7) ··· O(11)	3.04(2)	O(7) ··· O(13)	2.94(3)
O(9) ··· O(12)	2.91(2)		

atoms, the bond distances being for 2.80(2) and 2.84(2) Å for O(1)···O(10) and O(3)···O(8), respectively (Figure 3). The structural feature of the dinuclear trianion is similar to those of **3** and **4**; for each ruthenium ion, two Cl_4Cat ligands and two OMe ligands coordinate in a *cis*-fashion. The OMe ligands exhibit the Ru–O bond distances of 2.00(1) and 2.02(1) Å for Ru(1)–O(5) and Ru(1)–O(6), respectively, and the bond angles of 77.9(5)°, 77.0(6)°, and 102.5(3)° for Ru(1)–O(5)–Ru(1'), Ru(1)–O(6)–Ru(1'), and O(5)–Ru(1)–O(6), respectively. The Ru–Ru bond distance is 2.514(2) Å (Figure 2), close to that of **4** (2.5260(6) Å).

Interestingly, complex **5** forms a one-dimensional chain along the *b*-axis based on

intermolecular hydrogen bonding interaction between the coordinated water and the crown-ether oxygen atoms in (2, 3)-folding mode. Hydrogen bonding link is depicted in Figure 3(b) and the crystal packing is given in Figure 4. Three hydrogen bond distances of O(water)···O(ether) are 2.91(2), 2.94(3), and 3.04(2) Å. As mentioned above, the OMe ligands of **5** is μ_2-bridging mode, while other complexes have μ_3-bridging mode (Figure 2). The intermolecular hydrogen bonds lead to a separation of Na atoms from OMe oxygen atoms.

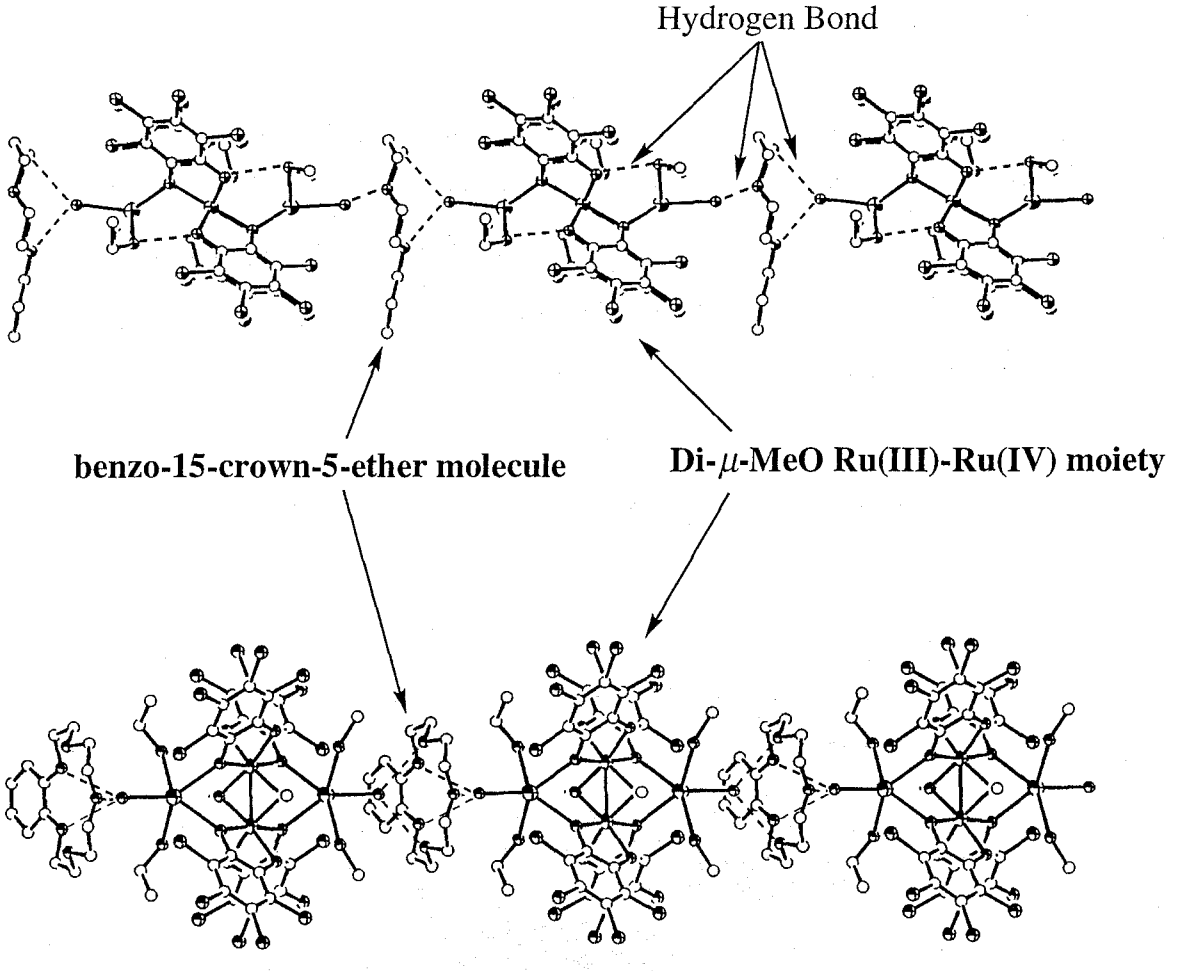

Figure 4. Hydrogen bonded one-dimensional chain of **5** running along the *b*-axis.

Complex 6 ORTEP drawing of the anionic moiety in complex **6** is depicted in Figure 5. Selected bond distances and angles are given in Table 5. Complex **6** crystallized in monoclinic space group *P*21/*n* with an inversion center at the midpoint of Ru–Ru bond, existing two formulated molecules in a unit cell (Z = 2). The structure of the dianionic moiety consists of two ruthenium ions bridged by two OEt ligands and two sodium ions, forming Na_2Ru_2 anionic

core (Figure 2(d)) similar to those of **3** and **4**. Each ruthenium ion is assumed to be pseudooctahedral coordination geometry, where the two $Cl_4C_6O_2$ ligands and two OEt ligands coordinate in *cis*-fashion. The bridging part is constructed with the Ru–O bond distances of 2.041(8) and 2.030(9) Å for Ru(1)–O(5) and Ru(1)–O(5'), respectively, and the bond angles 80.4(3)° and 99.6(3)° for Ru(1)–O(5)–Ru(1') and O(5)–Ru(1)–O(5'), respectively. The Ru–Ru bond distance of **6** is 2.628(2) Å which is comparable with 2.606(1) Å of **3**, while slightly longer than those of **4** (2.5260(6) Å) and **5** (2.514(2) Å) (Figure 2). The structural data and diamagnetic properties (*vide infra*) of **6** demonstrate that the electronic configuration in the Ru–Ru bond is $\sigma^2\pi^2\delta^{*2}\delta^2\pi^{*2}$ as well as that of **3**. The $Cl_4C_6O_2$ ligands coordinate to the ruthenium ion with the shorter bonds of 2.01(1) and 2.018(7) Å for Ru(1)–O(1) and Ru(1)–O(4), respectively, and the longer bonds of 2.043(9) and 2.071(9) Å for Ru(1)–O(2) and Ru(1)–O(3), respectively. The average C–O bond distance is 1.33 Å which is consistent with that of catecholate. Each sodium ion is coordinated to two catecholate oxygen atoms, one EtOH, one water, and OEt oxygen atoms. The overall bridging feature is assumed with Na_2Ru_2 double cuboidal cluster (Figure 2), where the Na-catecholate and Na–OEt bonds constitute a part of

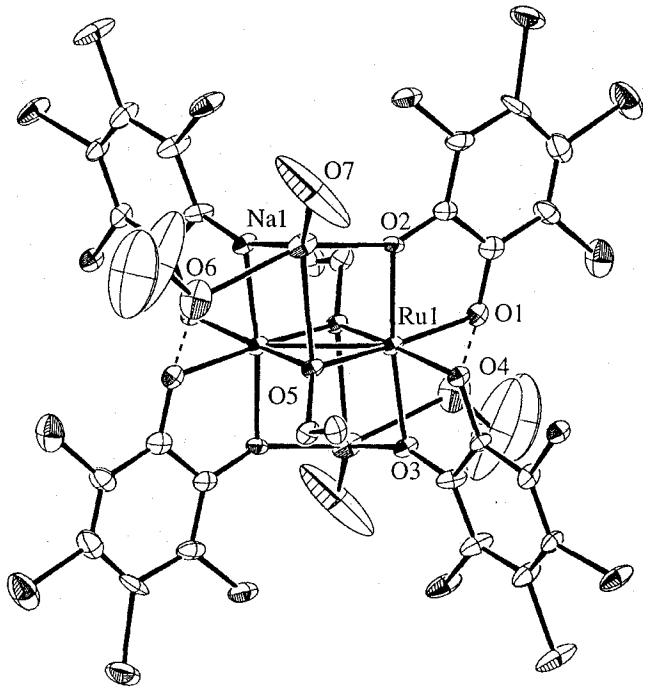

Figure 5. ORTEP drawing of Na_2Ru_2 di-anionic cluster of **6**.

Table 5. Relevant Bond Distances (Å) and Angles (°) for **6** with the Estimated Standard Deviations in Parentheses

Ru(1)–O(1)	2.01(1)	Na(1)–O(2)	2.30(1)
Ru(1)–O(2)	2.043(9)	Na(1)*–O(3)	2.230(10)
Ru(1)–O(3)	2.071(9)	Na(1)–O(5)	2.52(1)
Ru(1)–O(4)	2.018(7)	Na(1)–O(6)	2.42(2)
Ru(1)–O(5)	2.030(9)	Na(1)–O(7)	2.63(6)
Ru(1)–O(5)*	2.041(8)		
Ru(1)–Ru(1)*	2.628(2)		
O(1)–Ru(1)–O(2)	83.4(5)	O(3)–Ru(1)–O(4)	83.0(3)
O(1)–Ru(1)–O(3)	91.0(4)	O(3)–Ru(1)–O(5)	95.3(4)
O(1)–Ru(1)–O(4)	86.7(4)	O(3)–Ru(1)–O(5)*	89.8(3)
O(1)–Ru(1)–O(5)	171.1(4)	O(4)–Ru(1)–O(5)	87.8(3)
O(1)–Ru(1)–O(5)*	86.7(4)	O(4)–Ru(1)–O(5)*	170.1(4)
O(2)–Ru(1)–O(3)	172.5(4)	O(5)–Ru(1)–O(5)*	99.6(3)
O(2)–Ru(1)–O(4)	91.8(3)	Ru(1)–O(5)–Ru(1)*	80.4(3)
O(2)–Ru(1)–O(5)	89.8(4)		
O(2)–Ru(1)–O(5)*	94.8(3)		
	Hydrogen Bond		
O(1)···O(6)	2.84(2)		

cuboidal skeleton with the bond distances of 2.30(1), 2.230(10), and 2.52(1) Å for Na(1)–O(2), Na(1)–O(3) , and Na(1)–O(5), respectively. The EtOH molecules coordinating to sodium ions form intramolecular hydrogen bonds with catecholate oxygen atoms (O(1)···O(6) is 2.84(2) Å; dashed line in Figure 1(a).

Spectral Characterization of 2–4, 6, and 7.

Figure 6 shows UV-Vis spectra of complexes **3**, **4**, **6**, and **7** in acetonitrile under a dry nitrogen. The spectrum of **2** is essentially identical to that of **3**. The observed absorption parameters are summarized in Table 6. For complexes **2** and **3**, the absorption bands at 474 nm (ε = 12600 $M^{-1}\cdot cm^{-1}$) and 470 nm (ε = 12600 $M^{-1}\cdot cm^{-1}$), respectively, are assigned to a catecholate to Ru charge transfer (LMCT) band. No other absorption bands are observed in

longer wavelength region. For complex **4**, three characteristic absorption bands at 575 (ε = 12800 $M^{-1}\cdot cm^{-1}$), 765 (ε = 6900 $M^{-1}\cdot cm^{-1}$), and 1400 nm (ε = 2500 $M^{-1}\cdot cm^{-1}$) are observed, in which the former two bands are assigned to catecholate to Ru LMCT bands. A broad, weak absorption band at 1400 nm is observed only in the $Ru^{3.5+}(\mu\text{-}OR)_2Ru^{3.5+}$ complexes of **4** and **7** (*vide infra*). Complex $[Ru_2(dtne)(\mu\text{-}O)_2(\mu\text{-}CO_3)]PF_6\cdot 5H_2O$ (dtne = 1,2-bis(1,4,7-triazacyclononan-1-yl)ethane) having a $Ru^{3.5+}(\mu\text{-}O)_2Ru^{3.5+}$ core, reported by Wieghardt et al., shows a similar broad absorption band at 1224 nm (ε = 406 $M^{-1}\cdot cm^{-1}$).[14] In addition the electrochemically generated $[Ru^{2.5+}(bpy)_2(\mu\text{-}OMe)_2Ru^{2.5+}(bpy)_2]^{3+}$ cation also shows the absorption band at 1750 nm (ε = 5000 $M^{-1}\cdot cm^{-1}$) which was not detected in homovalent complexes, $[Ru^{2+}(bpy)_2(\mu\text{-}OMe)_2Ru^{2+}(bpy)_2]^{2+}$ and $[Ru^{3+}(bpy)_2(\mu\text{-}OMe)_2Ru^{3+}(bpy)_2]^{4+}$.[15(b)]

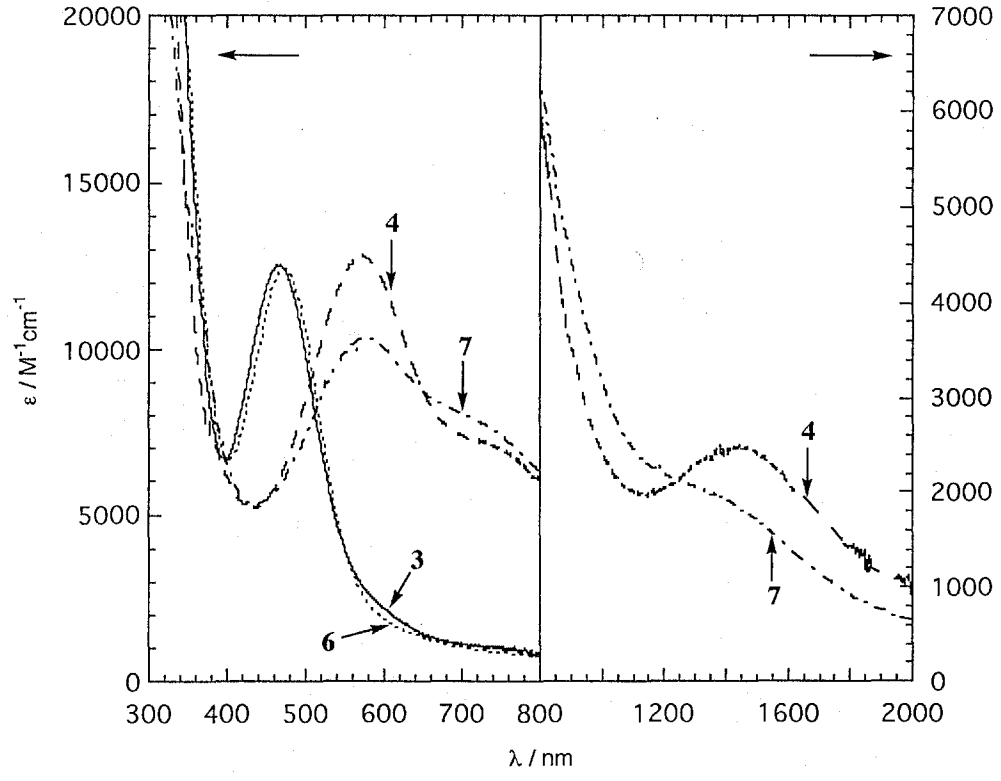

Figure 6. The electronic spectra of the $Ru^{3+}(\mu\text{-}OMe)_2Ru^{3+}$ species, **3**, the $Ru^{3.5+}(\mu\text{-}OMe)_2Ru^{3.5+}$ species, **4**, the $Ru^{3+}(\mu\text{-}OEt)_2Ru^{3+}$ species, **6**, and the $Ru^{3.5+}(\mu\text{-}OEt)_2Ru^{3.5+}$ species, **7**, in acetonitrile under a dry nitrogen.

Ward et al. assigned this absorption band to a π-π* transition, which is associated with orbitals fully electron delocalized over $Ru_2(\mu\text{-OMe})_2$ core (class-III characteristic), rather than the intervalence charge-transfer (IVCT) of the valence-localized $Ru^{2.5+}(\mu\text{-OMe})_2Ru^{2.5+}$ core (class-II characteristic). Analogously the assignment such as π-π* transition could be made for the lower energy absorption bands of the present mixed-valence $Ru^{3.5+}(\mu\text{-OR})_2Ru^{3.5+}$ cores. The spectral features of **6** and **7** are essentially identical to those of **3** and **4**, respectively.

Infrared Spectra.

The *o*-quinone ligand in metal complexes has been well characterized by infrared spectroscopy, in particular, the C–O stretching frequencies being characteristic of the oxidation state. In all of the complexes **2**–**7**, the bands are observed near 1250 cm^{-1} and 1420 cm^{-1} indicative of catecholate form (Table 6). If the semiquinonate species exists, the C–O stretching appears in the region of 1400–1500 cm^{-1}.[15f] All the *o*-quinone ligands are catecholate form, and

Table 6. Infrared and Electronic Spectral parameters, Magnetic Moments, and *g*-Values Detected from ESR Measurements for **2**–**7**

complex	ν(C–O), ν(C–C), cm^{-1}	λ_{max}, nm ($\varepsilon = M^{-1}\cdot cm^{-1}$ in acetonitrile)
2	1258, 1436	474 (10300)
3	1254, 1435	470 (12600)
4	1255, 1422	575 (12800), 765 (sh, 6900), 1450 (sh, 2500)
5	1255, 1423	
6	1257, 1435	472 (12500)
7	1255, 1422	575 (10500), 765 (sh, 6000), 1400 (sh, 2000)

complex	magnetic moments, μB	*g*-value at 77 K
2	diamagnetic	–
3	diamagnetic	–
4	1.71 (1.9 K), 2.04 (300 K)	2.54, 2.01, 1.80
5	1.75 (1.9 K), 2.02 (300 K)	2.57, 1.90, 1.73
6	diamagnetic	–
7	1.30 (1.9 K), 1.72 (300 K)	2.43, 2.04, 1.86

therefore, the valence of ruthenium ions is $Ru^{3+}(\mu\text{-}OR)_2Ru^{3+}$ and $Ru^{3.5+}(\mu\text{-}OR)_2Ru^{3.5+}$ for **2**, **3**, and **6** and **4**, **5**, and **7**, respectively, compatible with the results obtained from the structural aspects.

Magnetic and ESR Studies.

The magnetic and ESR data for complexes **2**–**7** are summarized in Table 6. Complexes **2**, **3**, and **6** are exactly diamagnetic. For complex **4**, the magnetic moments between 2.04 and 1.71 μB at 300 and 1.9 K, respectively, per dinuclear unit. These results clearly demonstrate a S = 1/2 ground state, which is compatible with the ESR spectrum of a powdered sample recorded at 77 K as shown in Figure 7(a). The ESR signal displays rhombic signals with g_1 = 2.54, g_2 = 2.01, and g_3 = 1.80, which is consistent with those of $Ru^{3.5+}(\mu\text{-}O)_2Ru^{3.5+}$ complexes having Ru–Ru bond reported previously.[14] The magnetic behavior for **5** is essentially the same as that of **4**, demonstrating the S = 1/2 ground state (1.75 (1.9 K) and 2.02 μB (300 K)), and no apparent interaction was detected through the hydrogen bonds. ESR spectrum of a powder sample of **5** is shown in Figure 7(b), in which the signal pattern is more complicated than that of **4**, but similar in rhombic pattern. The magnetic behavior for **7** is essentially the same as those of **4** and **5**. For complex **7**, the effective magnetic moment is 1.30 (2 K) and 1.72 (300 K) μB, respectively. The value of μ_{eff} at room temperature is slightly smaller than the values observed for **4** and **5** and the previously reported values (1.9–2.70 μB).[2,14] This is because the presence of a small amount of $Ru^{3+}(\mu\text{-}OEt)_2Ru^{3+}$ diamagnetic species could cause a slight deviation from the expected one. The g-values are also consistent with the results from S = 1/2 ground state for $Ru^{3.5+}(\mu\text{-}OMe)_2Ru^{3.5+}$ species, where rhombic signals with g values at g_1 = 2.43, g_2 = 2.04, and g_3 = 1.86 were observed (Figure 7(c)). These magnetic data, in addition to structural characterization, well demonstrate the electronic configurations $\sigma^2\pi^2\delta^{*2}\delta^2\pi^{*2}$ and $\sigma^2\pi^2\delta^{*2}\delta^2\pi^{*1}$ for $Ru^{3+}(\mu\text{-}OR)_2Ru^{3+}$ and $Ru^{3.5+}(\mu\text{-}OR)_2Ru^{3.5+}$, respectively, where the former is diamagnetic and the latter is paramagnetic having S = 1/2 ground state. The electronic

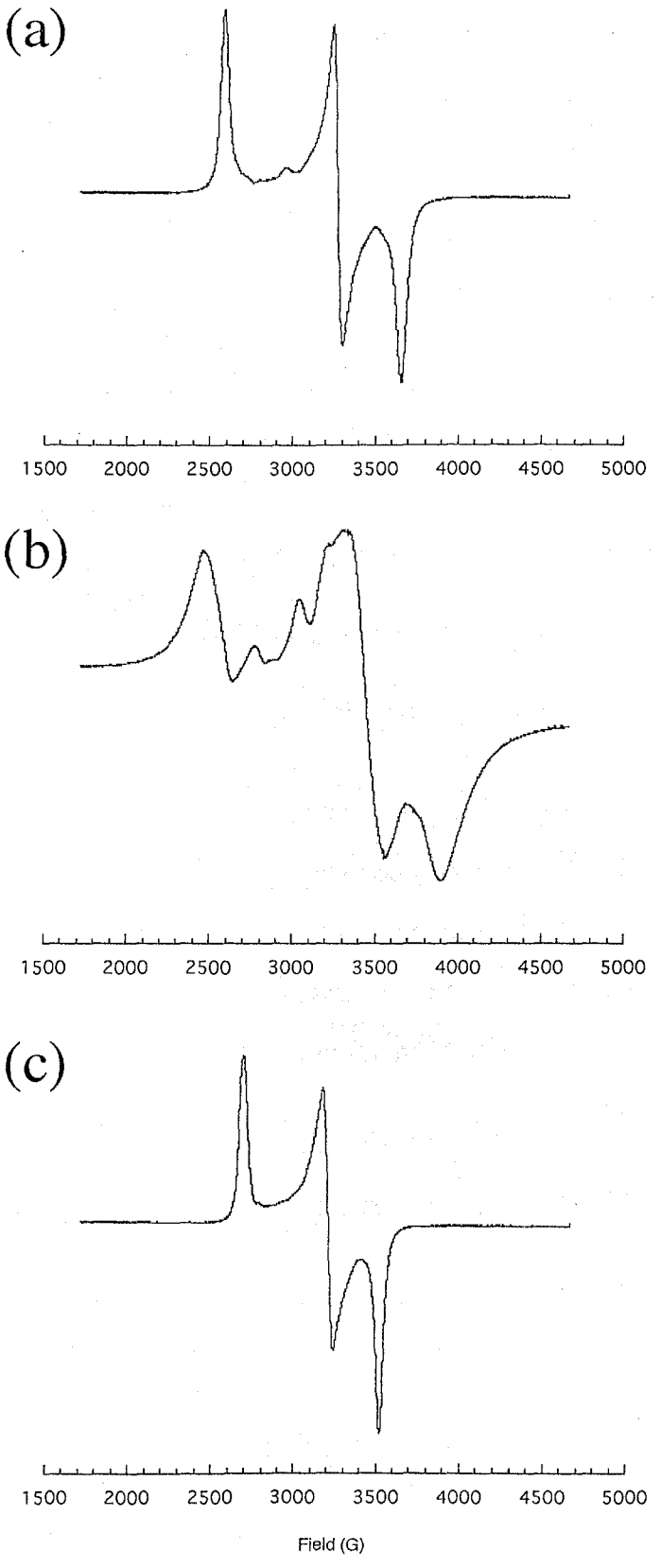

Figure 7. ESR spectra of powder samples of the $Ru^{3.5+}(\mu\text{-}OMe)_2Ru^{3.5+}$ species, (a) **4** and (b) **5**, and the $Ru^{3.5+}(\mu\text{-}OEt)_2Ru^{3.5+}$ species, (c) **7** which were measured at 77 K (microwave frequency, 9.194 GHz; power, 8.03 mW for **4**, microwave frequency, 9.196 GHz; power, 8.02 mW for **5**, and microwave frequency, 9.192 GHz; power, 8.03 mW for **7**).

configuration in di-μ-bridging core having metal-metal bond has been minutely investigated by Hoffmann[16] and Cotton.[17] The electronic configuration for the $Ru^{3+}(\mu\text{-}OH)_2Ru^{3+}$ complex, $[(L_{OMe})(CH_3CN)Ru^{3+}(\mu\text{-}OH)_2Ru^{3+}(NCCH_3)(L_{OMe})][CF_3SO_3]_2$ (L_{OMe} = $[(\eta^5\text{-}C_5H_5)Co\{(CH_3O)_2P{=}O\}_3]^-$), was predicted to be $\sigma^2\pi^2\delta^{*2}\delta^2\sigma^{*2}$ by Labinger and Bercaw et al.,[2] where the energy level of σ^* varies depending upon the geometry of cluster cores.[16] However, the electronic configurations for $Ru^{3+}(\mu\text{-}OR)_2Ru^{3+}$ (**2**, **3**, and **6**) and $Ru^{3.5+}(\mu\text{-}OR)_2Ru^{3.5+}$ (**4** and **7**) complexes are predicted as $\sigma^2\pi^2\delta^{*2}\delta^2\pi^{*2}$ and $\sigma^2\pi^2\delta^{*2}\delta^2\pi^{*1}$, respectively, according to structural aspects (Ru–Ru bond and $Ru\text{–}O_{alkoxo}$ bond distances) together with their spectral and magnetic data.

Cyclic Voltammetry.

Cyclic voltammetries for **2**–**4**, **6**, and **7** were performed in DMF solution in a potential range of –2.0–1.0 V vs Ag/AgCl reference electrode. Figure 8 shows the cyclic voltamograms for **3**, **4**, **6** and **7**. The features of voltamograms for these complexes are essentially identical; two reversible and two quasi-reversible redox waves clearly observed, where each redox wave is assigned to one-electron process. The quasi-reversible wave at $E_{1/2}$ = –1.58 V arises from $Ru^{3+}(\mu\text{-}OR)_2Ru^{3+}/Ru^{2.5+}(\mu\text{-}OR)_2Ru^{2.5+}$ redox couple. The reversible waves at $E_{1/2}$ = –0.21 V and +0.04 V are associated to $Ru^{3.5+}(\mu\text{-}OR)_2Ru^{3.5+}/Ru^{3+}(\mu\text{-}OR)_2Ru^{3+}$ and $Ru^{4+}(\mu\text{-}OR)_2Ru^{4+}/Ru^{3.5+}(\mu\text{-}OR)_2Ru^{3.5+}$ couple, respectively. The redox potential of $Ru^{3.5+}(\mu\text{-}OR)_2Ru^{3.5+}/Ru^{3+}(\mu\text{-}OR)_2Ru^{3+}$ is relatively lower, actually, the complexes **2**, **3**, and **6** are oxidized gradually in solution (DMF and acetonitrile) under the atmosphere. The quasi-reversible wave at $E_{1/2}$ = +0.86 V is assigned to $Ru^{4.5+}(\mu\text{-}OR)_2Ru^{4.5+}/Ru^{4+}(\mu\text{-}OR)_2Ru^{4+}$. The similar redox behavior in the these complexes indicates that the substituents of the bridging ligands exert no significant effect on the electronic states of the complexes.

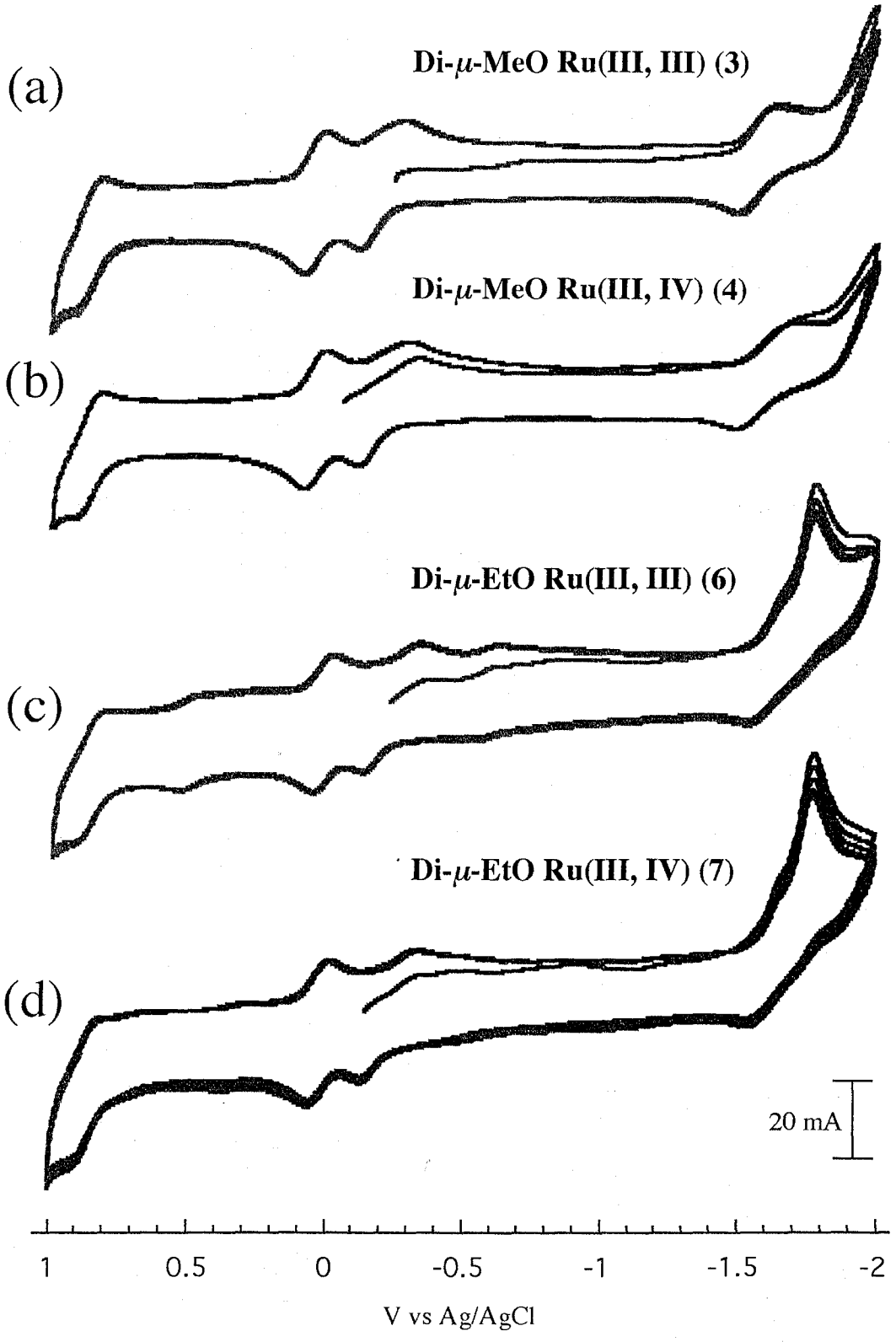

Figure 8. Cyclic voltamograms of (a) the $Ru^{3+}(\mu\text{-}OMe)_2Ru^{3+}$ species, **3**, and (b) the $Ru^{3.5+}(\mu\text{-}OMe)_2Ru^{3.5+}$ species, **4**, (c) the $Ru^{3+}(\mu\text{-}OEt)_2Ru^{3+}$ species, **6**, and (d) $Ru^{3.5+}(\mu\text{-}OEt)_2Ru^{3.5+}$ species, **7**, in DMF. The several small redox waves are may be due to the decomposition of Ph_4P^+.

Spectral Investigation of Oxidation and Methanolysis of 1.

The oxidation of **1** in MeOH under the atmosphere leads to $Ru^{3+}(\mu\text{-}OMe)_2Ru^{3+}$ and $Ru^{3.5+}(\mu\text{-}OMe)_2Ru^{3.5+}$ species. Figure 9 shows the time course of UV-Vis spectra of **1** in MeOH under the atmosphere for a day. Firstly, the absorption bands at 480 and 710 nm are observed in MeOH under a dry nitrogen. This spectrum is accounted for by the formation of axially MeOH-coordinated species, $[Ru_2(Cl_4Cat)_4(MeOH)_2]^{3-}$ (**1'**). The absorption band for **1'** does not cross the isosbestic points during the period of oxidation, because it may be due to the rapid oxidation of **1'** to the $Ru^{3+}(\mu\text{-}OMe)_2Ru^{3+}$ species under the atmosphere. The absorption band at 480 nm changed continuously to the band near 590 nm. These two bands are ascribed to the LMCT bands of **2–4**, respectively. In addition, the observation of isosbestic points at 380 and 537 nm clearly exhibits that the two species, $Ru^{3+}(\mu\text{-}OMe)_2Ru^{3+}$ and $Ru^{3.5+}(\mu\text{-}OMe)_2Ru^{3.5+}$ are in equilibrium.

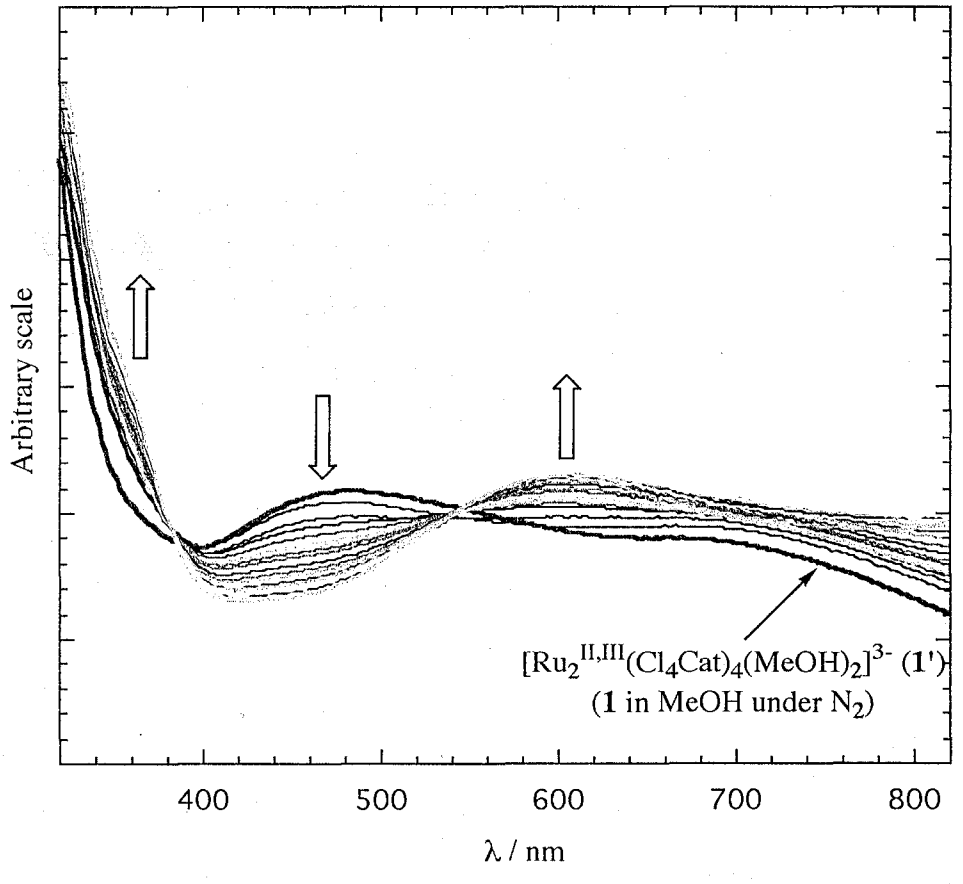

Figure 9. The variation of UV-Vis spectra of **1** in MeOH under the atmosphere.

Spectral Investigation for Formation of 6 and 7.

In EtOH, both $Ru^{3+}(\mu\text{-}OEt)_2Ru^{3+}$ and $Ru^{3.5+}(\mu\text{-}OEt)_2Ru^{3.5+}$ species are formed by the oxidation and ethanolysis of **1**. The UV-Vis spectrum for **1** shows an absorption maximum at 535 nm in EtOH under a dry nitrogen ($[Ru_2(Cl_4Cat)_4(EtOH)_2]^{3-}$ (**1''**)). The spectral change by air-oxidation was monitored as shown in Figure 10. Firstly, the initial absorption intensity increased slightly and a new absorption band was observed near 500 nm as a shoulder (inside of Figure 10), which shift finally to 585 nm with isosbestic points at 455 and 558 nm. The absorption bands at 500 and 585 nm correspond to LMCT bands of **6** (472 nm) and **7** (575 nm), respectively. Such spectral variation indicates a continuous conversion from **1''** to **6** and finally to **7** by the air-oxidation and structural modification due to the ethanolysis. The addition of Ph_4PCl as a counter cation gives rise to the isolation of $Ru^{3.5+}(\mu\text{-}OEt)_2Ru^{3.5+}$ species **7**, which is the final product of the oxidation reaction.

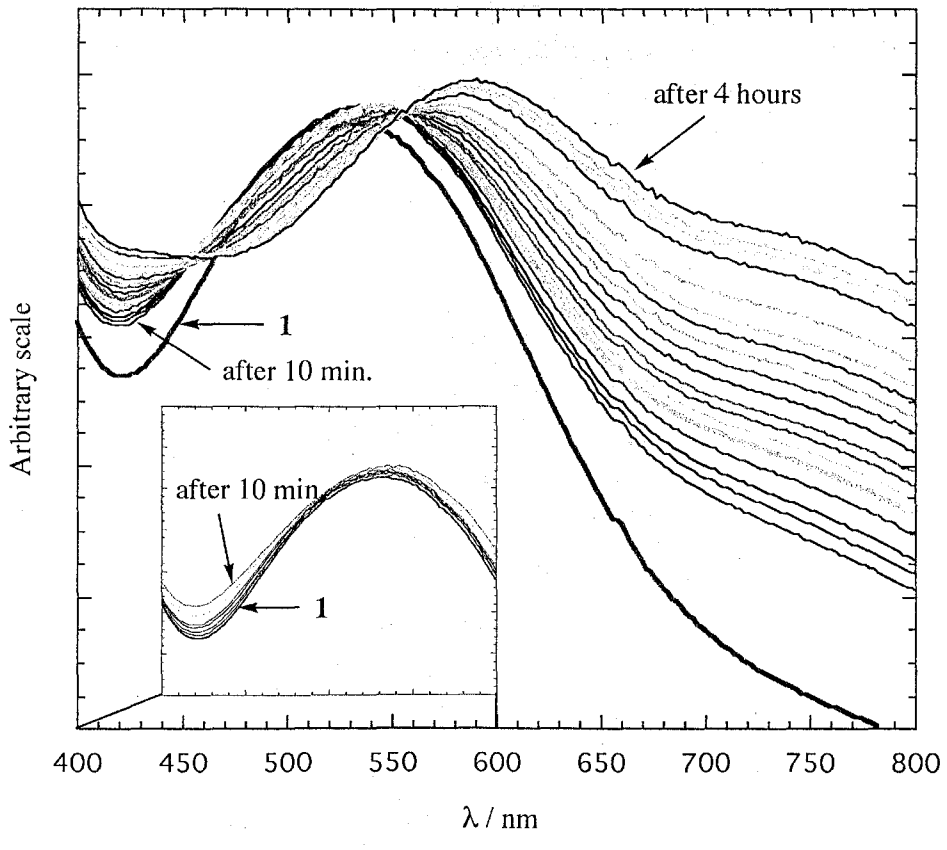

Figure 10. Spectral variation of **1** in EtOH under the atmosphere. (inside figure): the variation for initial 10 min.

On the other hand, the air-oxidation reaction in the presence of pyrazine (or 2,5-dimethylpyrazine) afforded the $Ru^{3+}(\mu\text{-}OEt)_2Ru^{3+}$ species of **6** as a solid. The addition of an excess of pyrazine (or 2,5-dimethylpyrazine) (4 equiv. per Ru) to the EtOH solution of **1** under the atmosphere causes a large shift of the band at 535 nm to 780 nm, which is attributable to the formation of $[Ru(Cl_4Cat)_2(L)_2]^-$ (L = pyrazine; **8**, 2,5-dimethylpyrazine; **9**) as shown in Figure 11. Complexes **8** and **9** were characterized by X-ray crystallographic analysis (*vide infra*). To confirm the selective conversion from **8** or **9** to the $Ru^{3+}(\mu\text{-}OEt)_2Ru^{3+}$ species by ethanolysis, UV-Vis spectral variation was observed when EtOH was added to a dichloromethane solution of **9** under the atmosphere (EtOH : CH_2Cl_2 = 1 : 5 v/v) (Figure 12); the absorption bands at 775 and 600 nm, which are assigned to LMCT and ILCT (inter-ligand charge transfer) bands of **9**, respectively, decrease and instead, the absorption band at 475 nm increases with an isosbestic point at 517 nm, where the absorption peak at 475 nm corresponds to LMCT band of **6** (472 nm). After two hours, the final spectrum similar to that of **6** was obtained. On this basis, it was concluded that equilibrium exists between the $[Ru(Cl_4Cat)_2(L)_2]^-$ (**8** and **9**) and the $Ru^{3+}(\mu\text{-}$

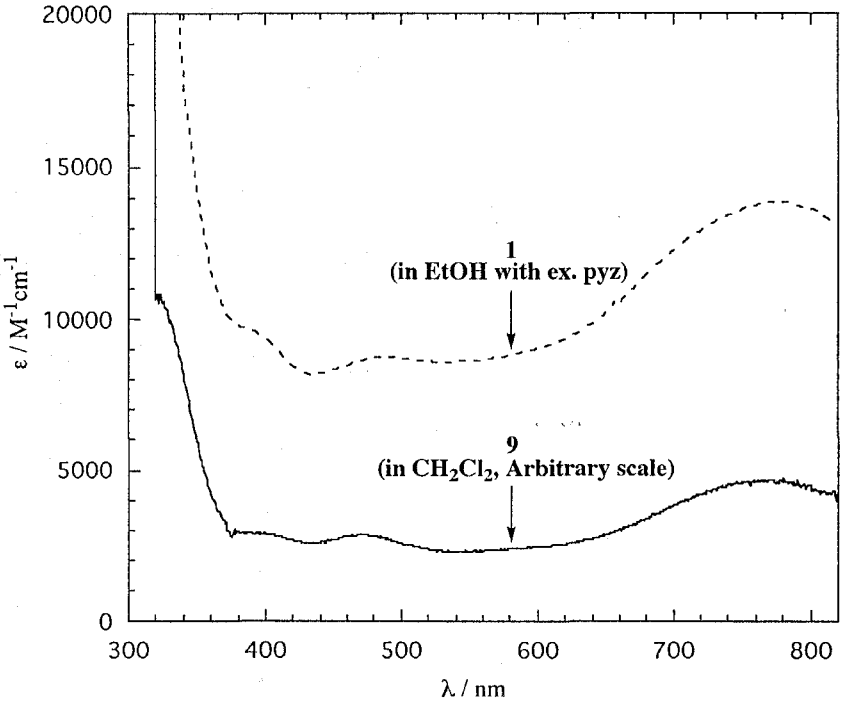

Figure 11. UV-Vis spectra of **9** (–) in dichloromethane (under a dry nitrogen), and the spectrum of EtOH solution of **1** containing an excess of pyrazine under the atmosphere, exhibiting of the formation of **8** (···).

$OEt)_2Ru^{3+}$ (**6**) species. The presence of pyrazine derivatives suppresses the further oxidation to the $Ru^{3.5+}(\mu\text{-}OEt)_2Ru^{3.5+}$ (**7**) species. Therefore the addition of pyrazine or 2,5-dimethylpyrazine is relevant for the selective isolation of the $Ru^{3+}(\mu\text{-}OEt)_2Ru^{3+}$ species (Scheme 4).

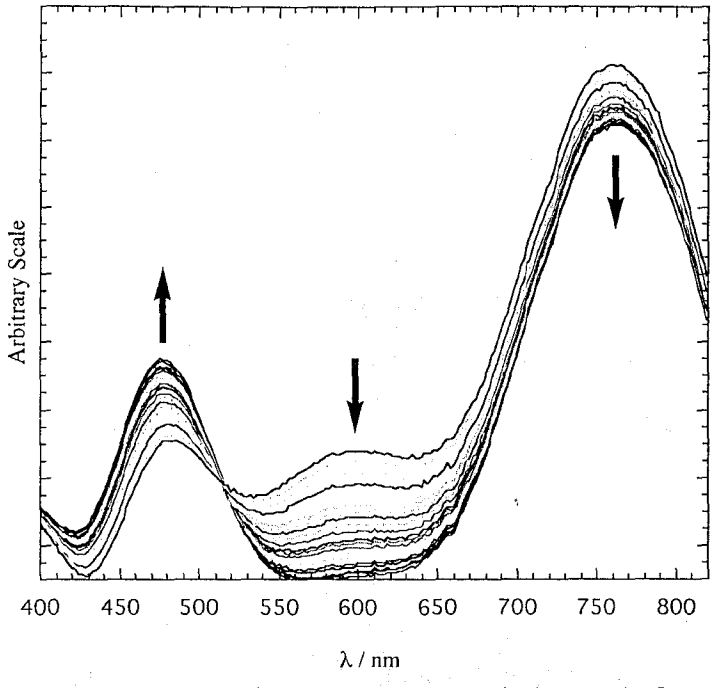

Figure 12. Spectral variation of dichloromethane solution of **9** containing EtOH (CH_2Cl_2:EtOH = 5:1 v/v) under the atmosphere. It was recorded for two hours, and then maintained as such.

Scheme 4

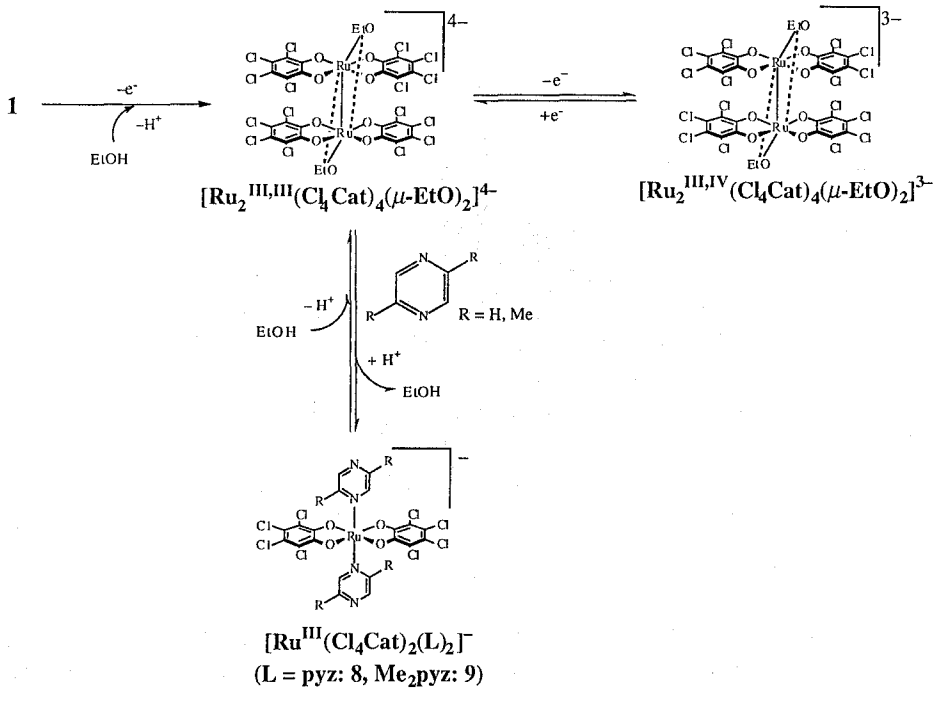

Crystal Structures of 8 and 9.

The isolation of single crystals of **8** and **9** in EtOH is relatively difficult because of preferential crystallization of **6**. Then, the single crystals were prepared in MeOH with an excess of pyrazine or 2,5-dimethylpyrazine (more than 6 eqiv. per Ru), respectively. The structural features of both complexes are essentially similar. Since two independent mononuclear anions are included in asymmetrical unit and both molecules are structurally similar to each other. ORTEP drawings of only one of them are depicted in Figure 13. Selected bond distances and angles of **8** and **9** are given in Table 7. In complexes **8** and **9**, two pyrazine or 2,5-dimethylpyrazine molecules coordinate axially to a ruthenium ion with the bond distances of 2.056(3) and 2.065(3) Å for Ru(1)–N(1) and Ru(2)–N(3), respectively, for **8** and

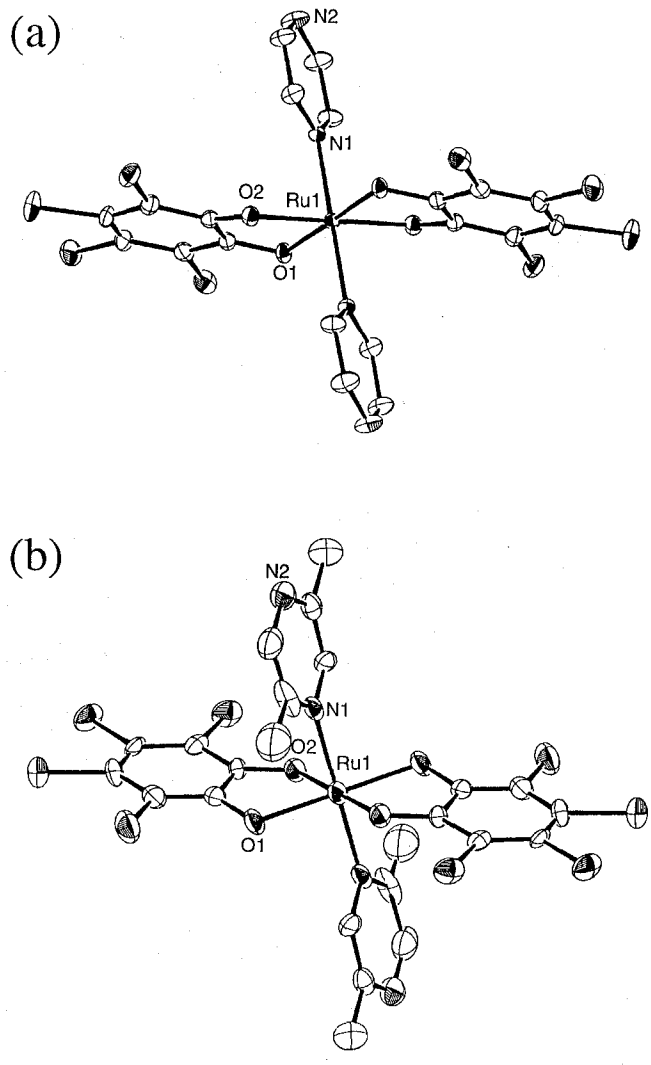

Figure 13. ORTEP drawings of the monoanionic moieties of (a) **8** and (b) **9**.

Table 7. Relevant Bond Distances (Å) and Angles (°) for **8** and **9** with the Estimated Standard Deviations in Parentheses

8		**9**	
Ru(1)–O(1)	2.026(3)	Ru(1)–O(1)	2.032(8)
Ru(1)–O(2)	2.020(2)	Ru(1)–O(2)	2.022(8)
Ru(1)–N(1)	2.056(3)	Ru(1)–N(1)	2.10(1)
Ru(2)–O(3)	2.013(3)	Ru(2)–O(3)	1.998(8)
Ru(2)–O(4)	2.035(2)	Ru(2)–O(4)	2.030(7)
Ru(2)–N(3)	2.065(3)	Ru(2)–N(3)	2.04(1)
O(1)–Ru(1)–O(2)	81.47(10)	O(1)–Ru(1)–O(2)	80.5(3)
O(1)–Ru(1)–N(1)	90.6(1)	O(1)–Ru(1)–N(1)	88.5(4)
O(2)–Ru(1)–N(1)	86.2(1)	O(2)–Ru(1)–N(1)	88.2(4)
O(3)–Ru(2)–O(4)	98.6(1)	O(3)–Ru(2)–O(4)	98.9(3)
O(3)–Ru(2)–N(3)	89.3(1)	O(3)–Ru(2)–N(3)	86.0(4)
O(4)–Ru(2)–N(3)	89.3(1)	O(4)–Ru(2)–N(3)	91.4(4)

2.10(1) and 2.04(1) Å for Ru(1)–N(1) and Ru(2)–N(3), respectively, for **9**. The average bond distances of Ru–O are 2.024 (**8**) and 2.021 (**9**) Å, respectively, and those of C–O bond distances are 1.327 (**8**) and 1.325 (**9**) Å, respectively. The observed C–O bond distances are reasonable for a structural character of catecholate, which exhibits that the valence of ruthenium ion is +3.

General Properties of 8 and 9.

The CV for **9** was successfully recorded in dichloromethane, but for **8** failed due to the low solubility and the occurrence of decomposition of complex. For complex **9**, two reversible redox waves, $E_{1/2}$ = +0.24 and –0.93 V (vs Ag/AgCl), were observed. The redox couple at +0.24 V was assigned to the [Ru^{3+}/Ru^{4+}] couple (reversible one-electron transfer) and suggests that $[Ru(Cl_4Cat)_2(2,5\text{-}Me_2pyz)_2]^-$ is stable in Ru^{3+} valence state under the atmosphere. The redox potential $E_{1/2}$ = –0.93 V (reversible one-electron transfer) was assigned to the couple of [Ru^{2+}/Ru^{3+}].

The infrared spectra for **8** and **9** also showed the characteristic frequencies for catecholate, where the frequencies at 1258 and 1434 cm^{-1} for **8** and at 1257 and 1436 cm^{-1} for **9** were

observed leading the valence of ruthenium ion of Ru^{3+} in both complexes. These results are compatible with the above mentioned structural data.

Conclusion

In summary, a series of new edge-sharing bioctahedral $Ru^{3+}(\mu\text{-}OR)_2Ru^{3+}$ and $Ru^{3.5+}(\mu\text{-}OR)_2Ru^{3.5+}$ (R = CH_3 and CH_3CH_2) complexes of tetrachlorochatecholate have been synthesized and structurally and physicochemically characterized. The complexes described are the first example of the $Ru^{3+}(\mu\text{-}OR)_2Ru^{3+}$ and $Ru^{3.5+}(\mu\text{-}OR)_2Ru^{3.5+}$ complexes having metal-metal bond in our knowledge.

Crown-ether molecules take an important role for the isolation of labile molecules and intermediates, thus promoting supramolecular complexation.[18] The molecular recognition by the formation of hydrogen bond affords various specific oligomeric and polymeric molecular assemblies in solid state arrangement. Namely, the alkaline metal-crown-ether cations behave not only as a cation for ionic complexation but also as a crystallization agent by its nature of supramolecular linker. Complexes **3–5** were selectively isolated by their packing effects. In addition, complex **5** was concomitantly obtained as a novel hydrogen bonded assembly involving a $Ru^{3.5+}(\mu\text{-}OMe)_2Ru^{3.5+}$-Na cluster molecule and free benzo-15-crown-5-ether molecule. The addition of pyrazine or 2,5-dimethylpyrazine promotes selective isolation of $Ru^{3+}(\mu\text{-}OEt)_2Ru^{3+}$ species. Finally, the metal complexes adducted with *o*-quinone ligands are available as a building block to construct the multi-nuclear and multi-dimensional complexes. Because the *o*-quinone ligands afford not only various geometric coordination modes but also electronic transfer modes between metal ions and ligands.[15]

References

(1) (a) Gilbert, J. A.; Eggleston, D. S.; Murphy, Jr., W. R.; Geselowitz, D. A.; Gersten, S. W.; Hodgson, D. J.; Meyer, T. J. *J. Am. Chem. Soc.* **1985**, 107, 3855. (b) Schoonover, J. R.; Ni, J.; Roecher, L.; White, P. S.; Meyer, T. J. *Inorg. Chem.* **1996**, 35, 5885. (c) Phelps, D. W.; Kahn, E. M.; Hadgson, D. J. *Inorg. Chem.* **1975**, 10, 2486. (d) Masuda, H.; Taga, T.; Osaki, K.; Sugimoto, H.; Mori, M.; Ogoshi, H. *Bull. Chem. Soc. Jpn.* **1982**, 55, 3887. (e) Masuda, H.; Taga, T.; Osaki, K.; Sugimoto, H.; Mori, M.; Ogoshi, H. *J. Am. Chem. Soc.* **1981**, 103. 2199. (f) Schneider, R.; Weyhermüller, T.; Wieghardt, K. *Inorg. Chem.* **1993**, 32, 4925. (g) Mathieson, A. McL.; Mellor, D. P.; Stephenson, N. C. *Acta Crystallogr.* **1952**, 5, 185. (h) Deloume, J. P.; Faure, R.; Thomas-David, G. *Acta Crystallogr., Sect. B: Struct. Crystallogr. Cryst. Chem.* **1979**, B35, 558. (i) Neubold, P.; Della Vedova, B. S. P. C.; Wieghardt, K.; Nuber, B.; Weiss, J. *Inorg. Chem.* **1990**, 29, 3355. (j) Power, J. M.; Evertz, K.; Henling, L.; Marsh, R.; Schaefer, W. P.; Labinger, J. A.; Bercaw, J. E. *Inorg. Chem.* **1990**, 29, 5058.

(2) Kelson, E. P.; Henling, L. M.; Schaefer, W. P.; Labinger, J. A.; Bercaw, J. E. *Inorg. Chem.* **1993**, 32, 2863.

(3) (a) Bardwell, D.; Jeffery, J. C.; Joulié, L.; Ward, M. D. *J. Chem. Soc. Dalton Trans.* **1993**, 2255. (b) Bardwell, D.; Horsburgh, L.; Jeffery, J. C.; Joulié, L.; Ward, M. D.; Webster, I.; Yellowlees, L. J. *J. Chem. Soc. Dalton Trans.* **1996**, 2527.

(4) (a) Weaver, T. R.; Meyer, T. J.; Adeyemi, S.; Brown, G. M.; Eckberg, R. P.; Hatfield, W. E.; Johnson, E. C.; Murray, R. W.; Untereker, D. *J. Am. Chem. Soc.* **1975**, 97. 3039. (b) Ikeda, M.; Shimizu, K.; Sato, G. P. *Bull. Chem. Soc. Jpn.* **1982**, 55, 797. (c) Doppelt, P.; Meyer, T. J. *Inorg. Chem.* **1987**, 26, 2027. (d) Geselowitz, D.; Meyer, T. J. *Inorg. Chem.* **1990**, 29, 3894. (e) Hurst, J. K.; Zhou, J.; Lei, Y. *Inorg. Chem.* **1992**, 31, 1010. (f) Lei, Y.; Hurst, J. K. *Inorg. Chem.* **1994**, 33, 4460. (g) Lei, Y.; Hurst, J. K. *Inorg. Chimi. Acta* **1994**, 226, 179 and references therein.

(5) Kondo, M.; Hamatani, M.; Kitagawa, S.; Pierpont, C. G.; Unoura, K. *J. Am. Chem. Soc.* **1998**, 120, 455.

(6) Boudreaux, E. A.; Mulay, L. N. *Theory and Applications of Molecular Paramagnetism*, John Wiley and Sons: New York, 1976; pp 491-495.

(7) Jacobson, R. A. *REQABA Empirical Absorption Correction Version 1.1-03101998:* Molecular Structure Corp.: The Woodlands, TX, 1996–1998.

(8) (a) SIR92: Altomare, A.; Burla, M. C.; Camalli, M.; Cascarano, M.; Giacovazzo, C.; Guagliardi, A.; Polidori, G. *J. Appl. Cryst.* **1994**, 27, 435. (b) PATTY: Beurskens, P. T.; Admiraal, G.; Beurskens, G.; Bosman, W. P.; Garcia-Granda, S.; Gould, R. O.; Smits, J. M. M.; Smykalla, C. (1992).

(9) DIRDIF94: Beurskens, P. T.; Admiraal, G.; Beurskens, G.; Bosman, W. P.; de Gelder, R.; Israel, R.; Smits, J. M. M. (1994). The DIRDIF program system, Technical Report of the Crystallography Laboratory, University of Nijmegen, The Netherlands.

(10) Cromer, D. T.; Waber, J. T. *International Tables for Crystallography* Vol IV, The Kynoch Press, Birmingham, England, Table 2.2A (1974).

(11) Creagh, D. C.; McAuley, W. J. *International Tables for Crystallography* Vol C, (Wilson, A. J. C., Ed.), Kluwer Academic Publishers, Boston, Table 4.2.6.8, pp 219-222 (1992).

(12) Creagh, D. C.; Hubbell, J. H. *International Tables for Crystallography* Vol C, (Wilson, A. J. C., Ed.), Kluwer Academic Publishers, Boston, Table 4.2.4.3, pp 200-206 (1992).

(13) teXsan: Crystal Structure Analysis Package, Molecular Structure Corporation (1985 and 1992)

(14) Geilenkirchen, A.; Neubold, P.; Schneider, R.; Wieghardt, K.; Flörke, U.; Haupt, H. -J. ; Nuber, B. *J. Chem. Soc., Dalton Trans.* **1994**, 457.

(15) (a) Bhattacharya, S.; Boone, S. R.; Fox, G. A.; Pierpont. C. G. *J. Am. Chem. Soc.* **1990**, 112, 1088. (b) Bhattacharya, S.; Pierpont, C. G. *Inorg. Chem.* **1994**, 33, 6038. (c) Bhattacharya, S.; Pierpont, C. G. *Inorg. Chem.* **1991**, 30, 1511. (d) Haga, M.; Dodsworth, E. S.; Lever, A. B. P.; Boone, S. R.; Pierpont, C. G. *J. Am. Chem. Soc.* **1986**, 108, 7413. (e) Boone, S. R.; Pierpont, C. G. *Inorg. Chem.* **1987**, 26, 1769. (f) Lever, A. B. P.; Auburn, P. R.; Dodsworth, E. S.; Haga, M.; Liu, W.; Melnik, M.; Nevin, A. *J. Am. Chem. Soc.* **1988**, 110, 8076. (g) Haga, M.; Dodsworth, E. S.; Lever, A. B. P. *Inorg. Chem.* **1986**, 25, 447. (h) Auburn, P. R.; Dodsworth, E. S.; Haga, M.; Liu, W.; Nevin, W. A.;

Lever, A. B. P. *Inorg. Chem.* **1991**, 30, 3502. (i) Masui, H.; Lever, A. B. P.; Auburn, P. R. *Inorg. Chem.* **1991**, 30, 2402. (j) Boone, S. R.; Pierpont, C. G. *Polyhedron* **1990**, 9, 2267.

(16) Shaik, S.; Hoffmann, R.; Fisel, C. R.; Summervill, R. H. *J. Am. Chem. Soc.* **1980**, 102, 4555.

(17) (a) Cotton, F. A. *Polyhedron* **1987**, 6, 667. (b) Cotton, F. A.; Walton, R. A. *Multiple Bonds Between Metal Atoms*, 2nd ed., Clarendon Press, Oxford (1993).

(18) Lehn, J. -M. *Supramolecular Chemistry*; VCH: Weinheim, 1995.

List of Publications

Chapter 1 X-ray Crystal Structures and Two-dimensional π···π Stacking Interaction of $Cr^{III}(X_4SQ)_3 \cdot 4C_6H_6$ (X = Cl and Br)
Chang, H. -C. and Kitagawa, S.
Mol. Cryst. Liq. Cryst. **2001**, in press.

Chapter 2 Synthesis, X-ray Crystallographic Structures, and Properties of Chromium Complexes with Semiquinonate and Catecholate
Chang, H. -C.; Ishii, T.; Kondo, M.; Kitagawa, S.
J. Chem. Soc, Dalton Trans. **1999**, 2467-2576.

Structural, Spectroscopic, and Magnetic Properties of Charge-transfer Complex, $(TMTSF)[Cr(Cl_4SQ)_2(Cl_4Cat)] \cdot 1/2CH_2Cl_2$
Chang, H. -C.; Kitagawa, S.; Kondo, M.; Ishii, T.
Mol. Cryst. Liq. Cryst. **1999**, 335, 183-192.

Chapter 3 New Mixed-valence Supramolecular Assemblies of Redox Isomers, $(BEDT\text{-}TTF)_3[Cr^{III}(Cl_4SQ)_2(Cl_4Cat)][Cr^{III}(Cl_4SQ)(Cl_4Cat)_2]$
Chang, H. -C. and Kitagawa, S.
to be submitted to *Angew. Chemie. Int. Ed.*

Chapter 4 New Molecular Assemblies of Redox Isomers, $[Cr^{III}(X_4SQ)_{3-n}(X_4Cat)_n]^{-n}$ (X = Cl, Br; n = 0, 1, and 2) with Metallocenium Cations, $[M^{III}Cp_2]^+$ (M = Co and Fe); X-ray Crystal Structures and Physical Properties
Chang, H. -C.; Miyasaka, H.; Kitagawa, S.
Inorg. Chem. **2001**, 40,146.

Chapter 5 Synthesis of Ligand-based Mixed-valence $Cr^{III}(X_4SQ)(X_4Cat)(L)_n$ (X = Cl and Br, n = 1 or 2) Complexes via Solvent-induced Valence Tautomeric Conversion of $Cr^{III}(X_4SQ)_3$
Chang, H. -C.; Mochizuki, K.; Kitagawa, S.
to be submitted

Chapter 6 Synthesis, Structures, and Physicochemical Properties of Diruthenium Compounds of Tetrachlorocatecholate with $Ru^{3+}(\mu\text{-}OR)_2Ru^{3+}$ and $Ru^{3.5+}(\mu\text{-}OR)_2Ru^{3.5+}$ Cores (R = CH_3 and C_2H_5)
Miyasaka, H.; Chang, H. -C.; Mochizuki, K.; Kitagawa, S.
to be submitted to *Inorg. Chem.*

List of Other Publications

(1) New Coordination Networks Constructed from *N*-(4-pyridyl)isonicotinamide
Kondo, M.; Asami, N.; Chang, H. -C.; Kitagawa, S.
Crystal Engineering **1999**, 2, 115-122.

(2) Hydrogen-Bond Network of Dimeric Copper Complex of Vanillic Acid (HVA), $[Cu(VA)_2(H_2O)]_2$
Zhu, L.; Kitagawa, S.; Chang, H. -C.; Miyasaka, H.
Mol. Cryst. Liq. Cryst. **2000**, 97-102.

List of Presentations

(1) Synthesis and Characterization of Novel Hybrid System $Cr(C_6O_2X_4)_3$ (X = Cl and Br)/TTF derivatives
Chang, H. -C.; Kondo, M.; Kawata, S.; Matsuzaka, H.; Kitagawa, S.
72th Annual Meeting of Chemical Society of Japan, Tokyo, March 1997.

(2) Crystal Structure and Properties of CT Compounds of Chromium Complexes with Semiquinonate Ligands
Chang, H. -C.; Kondo, M.; Kitagawa, S.
47th Symposium on Coordination Chemistry of Japan, Morioka, September 1997.
(Poster presentation)

(3) Synthesis and Properties of Charge-transfer Compounds of 1,2-Dioxolene Transition Metal Complexes and TTF Derivatives
Chang, H. -C.; Kondo, M.; Kawata, S.; Matsuzaka, H.; Kitagawa, S.
Symposium on Molecular Structures, Nagoya, October 1997.

(4) Crystal structures and properties of CT compounds of transition metal complexes and TTF derivatives with various spin states
Kitagwa, S.; Chang, H. -C.; Umeya, M.; Kondo, M.; Matsuzaka, H.
Symposium on Molecular Structures, Nagoya, October 1997.
(Poster presentation)

(5) Magnetic Properties of Charge-transfer Compounds of 1,2-dioxolene Complexes and TTF Derivatives
Chang, H. -C.; Kondo, M.; Ishii, T.; Kitagawa, S.
73th Annual Meeting of Chemical Society of Japan, Kyoto, March 1998.

(6) Synthesis and Properties of Charge-transfer Compounds Derived from First Transition Metal Semiquinonate Complexes and TTF derivatives
Chang, H. -C.; Kondo, M.; Kitagawa, S.; Ishii, T.; Matsuzaka, H.
48th Symposium on Coordination Chemistry of Japan, Kochi, September 1998.

(7) Magnetic Properties of $(BEDT\text{-}TTF)_3[Cr(Cl_4C_6O_2)_3]_3$ Compound and Its Derivatives
Kitagawa, S.; Chang, H. -C.; Kondo, M.; Ishii, T.; Matsuzaka, H.
International Conference of Molecular Magnetism, France, September 1998.
(Poster presentation)

(8) Molecular Assemblages of Chromium Complexes with Mixed-valence Semiquinonate/ Catecholate Ligands
Chang, H. -C.; Miyasaka, H.; Ishii, T.; Kitagawa, S.
49th Symposium on Coordination Chemistry of Japan, Sapporo, September 1999.

(9) Structures, Spectroscopic, and Magnetic Properties of Charge-Transfer Compounds with $[Cr(X_4SQ)_m(X_4Cat)_{3-m}]^{-(3-m)}$ (X = Cl, Br; m = 1 or 2) Anions.
Chang, H. -C. and Kitagawa, S.
International Symposium, Molecular Design and Functionalities of Assembled Metal Complexes, Kyoto, November 1999
(Poster presentation)

(10) Synthesis and Properties of Novel Chromium Complexes with Mix-charged Ligands Semiquinonate/Catecholate
Chang, H. -C. and Kitagawa, S.
78th Annual Meeting of Chemical Society of Japan, Chiba, March 2000
(Poster presentation)

(11) Molecular Assemblages of Transition Metal Complexes with Mixed-valence Semiquinonate/Catecholate Ligands
Chang, H. -C.; Nishida, N.; Mochizuki, K.; Kitagawa, S.
50th Symposium on Coordination Chemistry of Japan, Kusatsu, September 2000

List of Other Presentations

(1) Synthesis and Crystal Structure of Novel Ligand-unsupported Dinuclear Ruthenium Complex $Na_3[Ru_2(3,5\text{-di-}tert\text{-butylcatcholate})_4]$ (2)
Chang, H. -C.; Miyasaka, H.; Mochizuki, K.; Kitagawa, S.
78th Annual Meeting of Chemical Society of Japan, Chiba, March 2000